THE UNIVERSITY
of EDINBURGH

Development of an integrated computational tool for modelling structural frames in fire considering local effects

LIMING JIANG

Doctor of Philosophy

The University of Edinburgh

2016

Declaration

The research detailed in this thesis has been completed solely by Liming Jiang at the University of Edinburgh under the supervision of Professor Asif Usmani and Prof. Yong Lu. Where other sources are quoted, full references are given. This work has not been submitted for any other degree or professional qualification.

Liming Jiang

The University of Edinburgh, 2016

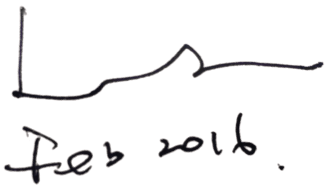

Abstract

In terms of developing knowledge to enable more effective use of performance based engineering (PBE), one of the key limitations is the lack of an easy to use integrated computational tool that is also robust and comprehensive enough to enable automated modelling of more realistic fire scenarios, i.e., the structural response to localised or travelling fires. The main objective of this thesis is to establish such an integrated computational tool, which shall be based on the OpenSees software framework and facilitated by specially developed approaches to achieve higher efficiency of the integrated analysis. This includes the analysis of heat transfer from the fire to structural members, as well as the analysis of structural response to elevated temperatures during the fire.

In this thesis, the research begins with the investigation of the feasibility of dimensional reduction for heat transfer analyses of structural members subjected to localised fire action (SFPE and Eurocode 1 fire models), which can be numerically represented by a linear or exponential correlation between incident heat flux and radial distance. Accurate estimates of the error induced by dimensional reduction are presented under strongly varying localised heat fluxes that represent the most non-uniform fire conditions in a building compartment. It is shown that beams and slabs can be adequately modelled with a lower

dimensional heat transfer analysis for ordinary building fires. Using this approach, the complexity of heat transfer modelling and the required computing resource and user effort can both be significantly reduced, especially in cases where structural members are subjected to localised fire action.

Thermo-mechanical simulations are presented to address the behaviour of structural members subjected to localised fire action, for which a **ThermalActionWrapper** is developed to approximate the temperature distribution from a mixed-order interpolation between sections (beam) or locations (slab). For concrete slabs subjected to localised fire, MITC4 based shell elements are used to account for material and geometric nonlinearities.

An integrated simulation environment is developed, which is designed to be a computational tool that requires limited input but provides a comprehensive solution to the problem of simulating large structural frame and sub-frame response under realistic fire scenarios. A considerable amount of code has been written to create and operate the building model, and to process the heat fluxes from the design fires to the structure and the consequential structural response to the evolution of temperatures within it.

Parametric studies have been performed to investigate the computational performance of the newly developed elements in modelling beams and slabs subjected to different cases of localised fire action. The results suggest that 3 to 6 force-based beam elements can adequately describe the localised response however more elements are required for quadratic distribution of incident heat flux and higher temperatures, which is due to the degradation of material strength that governs the accuracy especially when the members are heavily loaded. For slabs exposed

to localised fires, centre fires are found to produce greater deflections than corner fires, while lateral restraints applied to the slabs may also lead to higher deflections.

A small-scale three dimensional structural frame is modelled as a demonstration of the tool, tested against a number of localised fire scenarios. The global behaviour of the structure with the local effects induced by the fire action and partially damaged fire protection are investigated. Severe damage can be found in the members exposed to a single whole compartment fire, in contrast with the relatively small deflections that are observed when a fully protected column is engulfed by a localised fire. However if the passive fire protection is partially damaged, collapse may occur in the column as a result of load magnification because of the redistribution.

To the author's knowledge this is the first piece of research that has been able to develop a practically feasible approach to enable efficient coupled computation of the response of structural frames to realistic fire scenarios on a freely available open source software platform. Currently this kind of analysis can only be carried out by just two or three large consulting firms because of the prohibitive commitment of analyst time and effort and to a lesser extent the need for significant computing resources. The work of this thesis will contribute enormously towards making high-end performance based engineering of structural fire resistance a much more practical proposition for small and medium size structural consultancies. Furthermore, the choice of OpenSees, which is a very well respected software framework for simulating structural response to earthquakes naturally enables this work to be extended to the simulating the multi-hazard structural

resistance, such as in the event of a fire following an earthquake which may have locally damaged passive fire protection.

Publications

Journal papers J. Jiang, **L.M. Jiang**, P. Kotsovinos, J. Zhang, A. Usmani. OpenSees Software Architecture for the Analysis of Structures in Fire. Journal of Computing in Civil Engineering, 2015, 29(1).

Conference papers

A. Usmani, Y.Q. Jiang, J. Jiang, **L.M. Jiang**, S. Welch. Adapting OpenSees to simulate bridge structures in fire, in Proceedings of the 6th International Conference on Bridge Maintenance, Safety and Management, 2012, pp. 315-319.

L.M. Jiang, Y.Q. Jiang, J.Jiang, A. Usmani, S.W. Chen. An OpenSees-based integrated tool for modelling structures in realistic design fires, in Proceeding of the 8th International Conference on Structures in Fire, 2014, pp. 987-994.

S.W. Chen, **L.M. Jiang**, A. Usmani, G.Q. Li. Experimental and numerical studies on damage mechanisms in cementitious coatings on structural steel members, in Proceeding of the 8th International Conference on Structures in Fire, 2014, pp. 1251-1258.

L.M. Jiang, D. Xu, P. Kamath, A. Usmani. OpenSees-based integrated tool for modelling structures in fire, in Proceeding of the 1st International Conference on Fire and Blast, 2015, pp. 556-565.

Acknowledgements

It has been a wonderful journey in Edinburgh for the past four years. During my PhD study, Prof. Asif Usmani always impressed me in his great wisdom and endless energy. Special thanks to Prof. Yong Lu, Prof. Luke Bisby, Prof. Michael Rotter, Dr Stephen Welch and other staffs for the inspirations they offered in conversations. I would like to express my gratitude to Prof. Suwen Chen from Tongji University as my mentor guiding me through all the obstacles. I want to thank all my colleagues in Fire Group and friends in IIE. Such an international environment made life full of passion and joy, and I believe the friendship would continue to bring us these good things in the future.

Thanks to my family for their understanding and support in my life, and to all the friends I met in Shanghai and Edinburgh.

The research presented in this thesis is jointly funded by the China Scholarship Council and The University of Edinburgh who are gratefully acknowledged. People who ever worked with OpenSees or gave suggestions are gratefully acknowledged as well, for the community of Open Source Development and the spirit of sharing and collaboration.

Contents

List of Tables

List of Figures

Chapter 1

Introduction

1.1 Background to the project

In modern design of structures, quantification of performance over the useful life of a structure including its resistance to natural and man-made hazards is becoming ever more important. Improved quantification of structural performance should enable better and informed decision making involving all stakeholders and therefore promote a safe, secure, sustainable and resilient built environment. This thesis is concerned specifically with the issue of structural fire safety, which is normally referred as the performance of building structures under fire exposure.

The traditional fire safety strategy for steel-framed buildings has been to protect all steel members with insulating materials. Meanwhile, the design guidance in accordance with regulatory codes is primarily based on the performance of isolated structural members in Standard Fire tests. The recent decades of research, particularly after Cardington tests, have suggested that it may be too conservative

to protect all steel beams and columns in a fire, as this underestimates the remaining load bearing capacity provided by composite floor slab in a steel framed composite building. On the other hand, traditional design approaches may even be unsafe in certain circumstances as no effort is made to quantify the actual global response of the structure under realistic fire scenarios.

A trend of using performance-based design methodologies has begun to emerge in the field of structural fire safety engineering, because of the improved understanding generated from research and relaxation of regulatory constraints. To take full advantage of this trend structural engineers must develop a better understanding of the global behaviour of structures under common fire scenarios, such as standard and parametric fires, and ideally also localised and travelling fires for buildings with large open-plan interior spaces. Conventionally, the thermal response of structures subjected to non-uniform heating has been ignored in the previous studies, which was considered adequate since post-flashover fires are assumed to be more or less spatially uniform in terms of the gas temperature. Such a uniformity was questioned by Stern-Gottfried et al. (2010b) when reviewing the test data obtained from the fire tests in compartments. This led to the 'Travelling fire' methodology (Stern-Gottfried and Rein, 2012a,b) as a novel concept to account for the non-uniform heating in large open-plan compartments. Localised fires also generate non-uniform heating in large spaces without continuous distributed fuel, which implies that fire spread is unlikely to take place, such as a vehicle fire in a parking building, or a lorry fire underneath a bridge.

In general, two types of computer programs are available for simulating structural behaviours in fire: research-oriented and for commercial use. The former, such as SAFIR, VULCAN, and ADAPTIC have been developed to address specific

computational structural engineering problems (such as structural response to fire or earthquake loading). All of the aforementioned software have grown out of the university based research groups and therefore have inherent limitations because of a limited number of users and a vanishingly small team of developers. The continued development of such software is academic-research driven and highly prone to the risk of losing valuable development work when team members leave the research group. Commercial software packages such as ABAQUS, ANSYS and DIANA are used by researchers and industry across the world. However limited access to source codes; lack of transparency of the computational framework; and the high cost of purchase and maintenance are major limitations.

In 1997, an open source software framework, Open System for Earthquake Engineering Simulation(OpenSees) was developed at the University of California, Berkeley by McKenna (1997). It was initially designed to simulate non-linear response of structural frames under seismic excitations. OpenSees has an object-oriented architecture and is written in C++. Object-oriented capabilities enable structural engineers to focus on modelling objects that also have their own attributes and functions rather than just data. Major attributes such as elements, materials, analysis procedures, and solution algorithms are designed as individual objects and they can be added into the framework freely by anyone anywhere [3]. Meanwhile, an active group of OpenSees experts moderate the framework using a version control system, Subversion. This way of developing a community based software tool has been successful in attracting the researchers from across the globe to contribute their piece of code to the original framework and help make it more capable, robust and bug-free.

In 2009, OpenSees was adopted at the University of Edinburgh to conduct

further development for structural fire analysis. Significant contributions in terms of heat transfer and fire modules have been made to the framework in developing the Thermal version of OpenSees (Jiang, 2012b). Temperature dependent formulations have been incorporated for basic element types, beam element and shell elements to account for the thermal effects (Usmani et al., 2012; Jiang et al., 2014). The material library of the original framework has also been updated by adding new temperature dependent material models for steel and concrete based on Eurocodes (CEN, 2004, 2005).

1.2 Aims of this research

The main objective of this project is to develop a computational tool which could perform coupled analysis of structures in fire with particular emphasis placed on the local effects induced by non-uniform heating. Unlike the commercial finite element packages, this analysis is expected to be performed in an highly integrated environment which automatically implements the idealised fire models and applies this fire action to structures. The objectives of this research are as follows:

- Provide a quantitative assessment of the feasibility of dimensionally reduced heat transfer analysis for idealised non-uniform fire models in order to enable significantly faster computation of large whole frame simulations.
- Develop and validate a finite element solution strategy to analyse structural members and structural frames subjected to spatially non-uniform heating.
- Develop an integrated computational tool for modelling structural behaviour in realistic fire scenarios.

- Investigate the thermal and structural responses of a steel-framed structure subjected to localised fire exposure along with partially damaged fire protection, with a view to enabling multi-hazard computations (such as fire following an earthquake or blast).

1.3 Outline of thesis chapters

Chapter 2

An overview of modelling structures in fire

A literature review of modelling 'structures in fire' is presented, which begins with the discussion on the evolution of design fire models. It is followed by a review of the behaviour of steel and composite structures in fire. The last section of this chapter describes the previous development work on OpenSees carried out at the University of Edinburgh.

Chapter 3

Dimensional reduction of heat transfer analysis for structural members subjected to localised fire action

A quantitative assessment of discrepancies caused by dimensionally reduced heat transfer analyses is investigated when it is implemented for beams and slabs subjected to localised fire action. It is followed by an approach developed for rapid estimation of heat transfer from idealised non-uniform fires to structural members using polynomial interpolation.

Chapter 4

Strategies for modelling structural members subjected to localised heating effects

Elements are adapted and developed for considering localised heating effects. Steel beams subjected to localised fire action are modelled using displacement or force based beam-column elements featuring non-uniform heating. Shell elements with geometric and material nonlinearities are used to model the concrete slabs heated by localised fires.

Chapter 5

An OpenSees-based and integrated tool for modelling structures in fires

Development in OpenSees for modelling 'structures in fire' is described in detail. An integrated computational environment is developed within the OpenSees framework to simplify the process of coupled modelling.

Chapter 6

Modelling beams and slabs subjected to localised fire action

Numerical studies are presented to check the performance of beam-column elements and shell element, which are extensively tested against analytical, experimental and numerical results using ABAQUS.

Chapter 7

Coupled analysis for evaluating the structural performance considering localised effects

Based on a generic model representing a 2×2×2 composite steel frame, the

thermal and structural responses induced by localised fire action are investigated taking into account partial damage to passive fire protection.

Chapter 8

Conclusions and future work

A summary of the results and conclusions of the work is presented in this thesis. Suggestions for future work are provided.

Chapter 2

An overview of modelling structures in fire

2.1 Introduction

This chapter reviews the modelling of structures in fires from a perspective of *performance based structural engineering* (PBSE) for fire resistance. Historically the design and construction of buildings were performed as satisfying a list of requirements in the codes, which is conventionally termed as the prescriptive design approach due to its 'prescriptive' specifications. Codes rely on empirical rules that have been developed and adopted over a long period of design and construction for resisting specified combinations of loading, allowing for a simple procedure during the design process and facilitating oversight by the regulatory authorities. Nevertheless, in the practice of structural engineering, the limitations of using the prescriptive approach emerges as the options available to the design

team are rather restricted and often the actual structural response to the loading is not predictable in terms of its performance. It can be uneconomical due to the redundancy of the generally uniform consideration, or partially over-estimated with respect to the performance in the context of unusual structure or complicated loading cases.

The performance-based design approach is applied widely in the field of structural engineering especially in the case of complex and exceptional loading conditions. The essence of this approach has been quite concisely defined by Gibson (1982) as:

"The performance approach is the practice of thinking and working in terms of ends rather than means. It is concerned with what a building or a building product is required to do and not with prescribing how it is to be constructed."

Here, the ends of a design are typically related to the safety of the occupants when the structure is subjected to extremes of loading and its in-service performance under routine loading conditions (CEN, 2002b). This chapter will exclusively discuss the use of the PBSE approach to the structural performance and behaviour under fire action, as this is the major concern of this thesis and represents an important extreme loading case that structures are designed to resist through modelling and analyses. The first section of this literature review will focus on the modelling of fire exposure, beginning with a an general overview of enclosure fires followed by different conceptual fire models representing pre- and post-flashover fires. Heat transfer from fire to structural members is then discussed, including a summary of available numerical tools for Structural heat transfer analysis. The second section is dedicated to review the behaviour of steel and composite structures under fire conditions, with emphasis placed on steel

members, reinforced concrete slabs and composite floor systems. The Cardington fire tests as a milestone in structural fire engineering are briefly described in this context. Localised effects induced by partial damage to fire protection is discussed with respect to recent developments, such as the studies of damage mechanism of cementitious coatings and the fire performance of composite beams and steel columns with parts of fire protection deliberately removed. Modelling 'Structures in fire' with an Open System for Earthquake Engineering Simulation (OpenSees) (McKenna, 1997; Usmani et al., 2012) is reviewed in the last section. Fire and heat transfer modules developed in OpenSees are presented with the main algorithmic formulations. Beam-column and shell elements for thermo-mechanical analyses are presented highlighting key aspects as well as formulations.

2.2 Modelling of fire exposure

This section reviews the modelling of fire exposure, beginning with fire behaviour in compartments. A number of methodologies for describing pre-flashover and post-flashover fires are briefly mentioned. Models such as the standard fire and parametric fires (CEN, 2002a) are reviewed in the category of post-flashover fires, while for pre-flashover or localised fires Eurocode 1 (EN1991-1-2) (CEN, 2002a) and SFPE (Lattimer, 2002) correlations are presented. The theory of heat transfer from fire to structural members is reviewed, which is followed by a summary of available numerical tools for conducting heat transfer analyses.

2.2.1 Behaviour of enclosure fires

Normally the development of an enclosure fire is considered to occur in three stages: (1) fire growth after ignition; (2) fully developed fire; (3) decay stage as the fuel is gradually depleted. In the first stage, the size of the fire increases which may spread to its vicinity. Although the average temperature during the growth stage is low, locally high temperatures may exist as a result of direct interaction with the fire plume. As the combustible material is burning, large quantities of smoke may fill the fire compartment. The mixture of hot gas and smoke layer could accelerate the burning by spontaneous ignition of combustibles away from the point of origin of the fire, which leads to a fully developed fire after a rapid spread of combustion within the enclosure. Such a transition from stage 1 to stage 2 is known as "flashover" which usually occurs over a short duration of time. It is at this stage that the fire becomes a severe threat to the occupants and the structure. After flashover, the fire enters a relatively steady state and begins to consume a large amount of fuel. The post-flashover fire can be categorised as fuel controlled or ventilation controlled, which has been discussed in detail in Drysdale's book (2011b). During this stage, the temperature of gas-air mixture is reckoned as uniformly distributed in the compartment, and can reach values in excess of 1100^oC (Drysdale, 2011b).

2.2.2 Travelling fires

The homogeneous temperature assumption for post-flashover compartment fires was questioned in the work presented by Stern-Gottfried et al. (2010b). A series of statistical analyses were performed which suggested a considerable non-uniformity

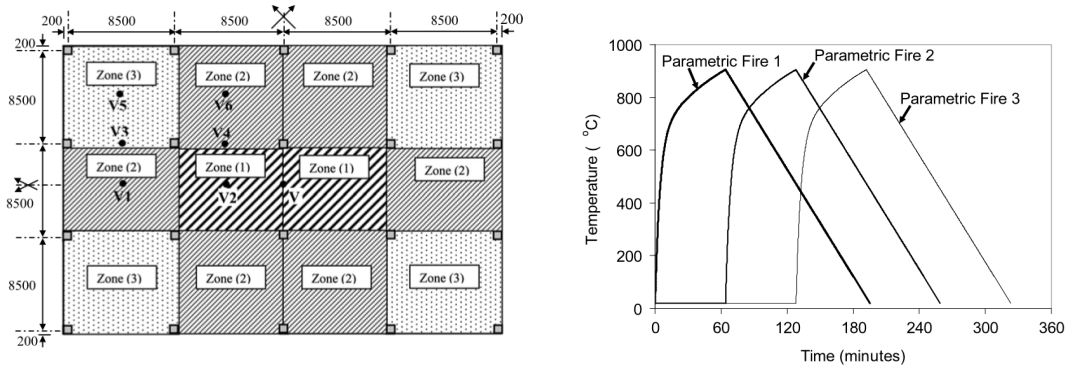

(a) Compartment dived into zone (b) Ignition-delayed parametric fire curves

Figure 2.1: Travelling fire model based on zones and parametric fire cures (Ellobody and Bailey, 2011)

in the temperature field of real post flashover fires. Although a spatially uniform temperature is still widely used and may be appropriate for small compartments, a number of published works published by Bailey et al. (1996a), Röben et al. (2010), Ellobody and Bailey (2011) and Stern-Gottfried (2011); Stern-Gottfried and Rein (2012a,b) have explored alternative models to describe the 'travelling' nature of compartment fires. For example, Ellobody and Bailey (2011) divided a compartment into a number of zones for which the parametric curves with different ignition times are used in order to represent the travelling motion of fires. This modelling approach is shown in Figure 2.1.

A more comprehensive methodology for horizontally travelling fires have been established by Rein and Stern-Gottfried (2010a; 2011; 2012a; 2012b), which represents travelling fires more realistically by considering key aspects of fire dynamics in large enclosures. As shown in Figure 2.2, the whole fire environment is horizontally divided into two regions (Stern-Gottfried and Rein, 2012a), which are termed as "near field" and "far field". The near field temperature is normally approximated with a constant value (e.g. 1200^oC) while the far field temperature

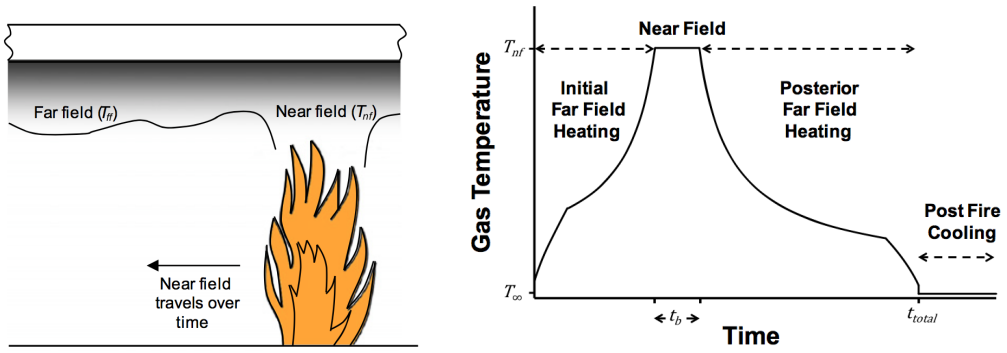

(a) Illustration of travelling fire

(b) Time-temperature curve

Figure 2.2: Illustration of travelling fire model (Stern-Gottfried and Rein, 2012a)

distribution follows an empirical correlation, which is adapted from Alpert's ceiling jet model (Evans, 1995).

For vertically travelling fires, an idealised global time delay was introduced by Röben et al. (2010) to represent the fire spread between floors, while time-temperature relationship at each floor is described by an generalised exponential curve (Flint, 2005). A similar time-delay was used in the work (Usmani et al., 2009) which developed a simple method for assessing tall building safety in major fires, where a strong floor mechanism as well as a weak floor mechanism were identified for the collapse of tall buildings. This vertically travelling fire scheme was later used with a 2D model of WTC tower to investigate the travelling effects (Kotsovinos et al., 2013). The work assumed a time sequence for the vertically travelling fire over multiple floors. For each floor, a parametric fire curve associated with a constant inter-floor time delay Δt_{delay} was assigned in order to ideally illustrate the 'travelling' nature.

It is noticed that neither the horizontal traveling fire model nor the vertical traveling fire model can accurately describe the evolution of gas temperature field

in a real building, where the distribution of fuel load and ventilation condition lead to significant uncertainty. Meanwhile, it should be pointed out that the travelling patterns introduced to these fire models are extremely idealised. However, there is an increasing consensus on using more realistic non-uniform fires compared to traditional models employing uniform gas temperature assumption. These more realistic descriptions will enable a full-period assessment to the fire resisting performance of structures, which is the key pursuit of performance based fire safety engineering.

2.2.3 Localised fires

The concept 'travelling fires' was introduced to address the non-homogenous characteristics of post-flashover compartment fires. However, in some circumstances, a fuel controlled fire may remain in the pre-flashover stage when the fuel distribution is extremely localised so that it is unlikely to cause the spread of fire (CEN, 1999). Such fire scenarios may be found in parking buildings (Zhao and Kruppa, 2002), airports, metro stations, atriums, and bridges (Garlock et al., 2012; Alos-Moya et al., 2014), where significant spatial variation of heat fluxes or temperatures are found suggesting that uniform fire exposure in such cases is unrealistic. Early efforts for characterising localised fires were reported in the work (You and Faeth, 1979; Kokkala, 1991; Hasemi et al., 1997) where heat fluxes received from fire plumes impinging on the ceiling were measured. In 1990s, a series of tests (Wakamatsu and Hasemi, 1988; Hasemi et al., 1996; Pchelintsev et al., 1997; Wakamatsu et al., 2003) were reported to investigate the heating mechanism of building components (steel beam underneath a ceiling) exposed to a localised fire and also conducted numerical modelling. They then proposed a

framework to estimate the incident heat fluxes at the ceiling level and at the surfaces of an I-section beam underneath the ceiling. The heat flux was suggested to be correlated to the radial distance from fire origin; the heat release rate; the nominal dimension of the fire source; and the ceiling height to the source (Pchelintsev et al., 1997). The same framework is adopted in Eurocode 1 with modified correlations based on the localised fire tests and validation work presented in the report (CEN, 1999). According to Eurocode 1, the heat flux distribution in a localised fire model is only valid when the fire plume impinges on the ceiling, while for small fires Alpert ceiling Jet flow model (Evans, 1995) may be applied.

Note the above mentioned localised fire models are only appropriate to be used in an unconfined space as any hot gas or smoke layer developed in confined cases is not included. According to the report (CEN, 1999) which concerns itself with design rules for steel structures subjected to natural fires in large compartment, temperatures predicted by the Hasemi model are higher in the vicinity of fire source and lower at the far ends, when compared to the natural fire test results. This is due to an accumulation of hot gases and smokes in the upper zone of the confined compartment. Therefore a combined model can be introduced to include the hot smoke layer (CEN, 1999), which is illustrated in Figure 2.3. The spatially uniform model accounts for the exposure to an upper zone of hot smoke(Cadorin and Franssen, 2003; Cadorin et al., 2003). This hot smoke temperature may be calculated according to equations given by Thomas (1963) and Hinkley (1986) as mentioned in Wang's book (2003).

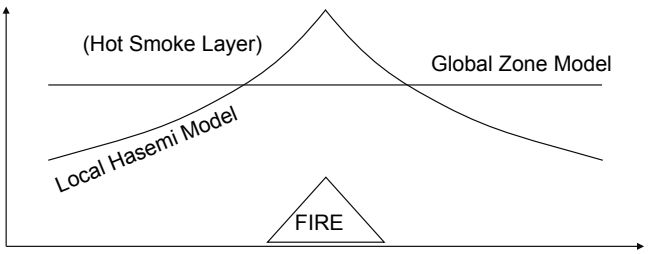

Figure 2.3: Consideration of smoke layer in localised heating scenario (CEN, 1999)

2.2.4 t-squared fires

After the ignition of fuel, the rate of heat release is obviously not constant. It is found that the rates of development of many fires can be approximated as a parabolic growth, such that the heat release rate is proportional to the time squared, which is referred to as a 't-squared fire' (Drysdale, 2011b). There are usually four different levels of fire growth, being denoted as ultra-fast, fast, medium, and slow growth, as depicted in Figure 2.4, where the heat release rate Q is given by:

$$Q = (t/k)^2 \tag{2.1}$$

in the above formulation t is the time elapse after ignition (s), and k is a growth constant ($\mathrm{s{\cdot}MW^{-0.5}}$) (Buchanan, 2001). An alternative description of t-squared fire is expressed with a fire intensity coefficient α (Drysdale, 2011b), of a unit $\mathrm{MW{\cdot}s^{-2}}$:

$$Q = \alpha t^2 \tag{2.2}$$

Both the parameters α and k represent the rate of fire growth, which can be found in books written by 2.1 with the corresponding fire scenarios.

When estimating the heat release rate (HRR) using the t-squared fire model, it is noticed that the heating effect may be negligible as the structural members

are not directly exposed to fires at the early stage. Hence a possible approach here is ignoring the heat transfer until the localised fire develops to impinge on the structural members, then an increasing HRR can be applied to localised fire models.

Table 2.1: Fire growth rates for t-squared fires (Buchanan, 2001; Drysdale, 2011b)

Fire growth rate	k (s·MW$^{-0.5}$)	α(MW·s^{-2})	Typical scenario
Slow	600	0.00293	Densely packed paper products
Medium	300	0.0117	Traditional mattress, individual furniture items with small amount of plastci
Fast	150	0.0466	PU mattress, PE pallets, some upholstered furniture
Ultra-fast	75	0.1874	High-rack storage, High-stacked PE rigid foam

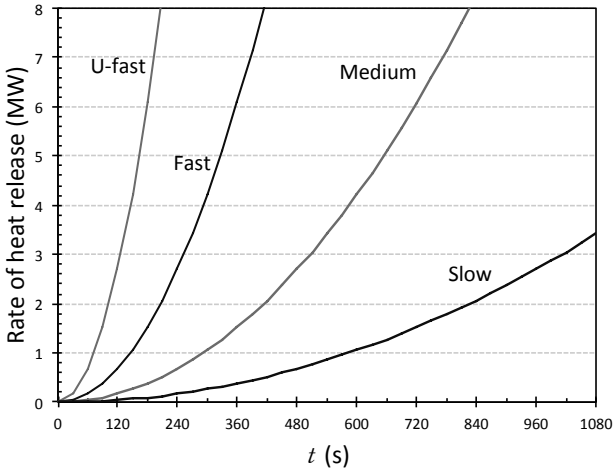

Figure 2.4: Fire growth described in t-squared fire models (Buchanan, 2001)

2.2.5 Mathematical models of fire

In the history of structural fire safety engineering, mathematical models were pursued to predict the fire action, which are usually represented by gas temperature for spatially uniform models, and by spatial distribution of heat fluxes for localised fire models.

•Standard fire

standard time-temperature curve (CEN, 2002a) has played a significant role in testing the performance of structural members in fires, such as the work presented in (Wickström, 1985; Han et al., 2002). The commonly used standard fire curve is assumed to represent the worst case for compartment fires, where the gas temperature is assumed uniform in the enclosure, following a time-temperature relationship as below:

$$T_g = 20 + 345log(8t + 1) \tag{2.3}$$

where t is the standard fire exposure time in minutes, and $T_g(^oC)$ is the gas temperature in the fire compartment. This standard curve has been widely used in the construction industry to determine the fire resistance of a given structural member or assembly based on time to failure in a furnace, often based on an arbitrary failure criterion. The drawback of such a time-temperature curve is the fire load such as heat release rate or ventilation conditions.

•Parametric fires

Eurocode 1 (CEN, 2002a) gives an equation to determine the compartment gas temperature based on a combination of fuel load, ventilation openings and wall lining materials. During the heating phase, the time-temperature relationship is

given as:

$$T_g = 20 + 1325(1 - 0.324e^{-0.2t^*} - 0.204e^{-1.7t^*} - 0.427e^{-19t^*} \tag{2.4}$$

where t^* is given as:

$$t^* = t \cdot \Gamma \tag{2.5}$$

where t is the fire duration in hours, and Γ represents the effect of ventilation and enclosure properties. The maximum temperature of the heating phase is related to the fuel load in the compartment, which experiences a linear cooling phase afterwards. Details of the parametric fire model can be found in the Eurocode.

•Eurocode 1 Localised fire model

In Eurocode 1, a localised fire model is defined as a simplified natural fire model. The unconfined flame height of a localised fire L_f is given by Equation (2.6).

$$L_f = -1.02D + 0.0148Q^{2/5} \tag{2.6}$$

where D is the diameter of the fire [m], and Q is the heat release rate (HRR) of the fire. When L_f is greater than the ceiling height it suggests that the fire plume is impinging on the ceiling. It is then necessary to account for the horizontal length of the flame (L_C) from the stagnation point along the ceiling, as determined in the following equation,

$$L_C = 2.9H_C(Q^*_{H_C})^{0.33} - H_C \tag{2.7}$$

where H_C is the height from fire source to the ceiling, and $Q^*_{H_C}$ is the non-dimensional HRR that is given by:

$$Q^*_{H_C} = Q/(\rho_\infty C_p T_\infty \sqrt{g} H_C^{2.5}) \tag{2.8}$$

where ρ_∞ and T_∞ are the density and temperature of ambient air ($\mathrm{kg{\cdot}m^{-3}}$), respectively. The specific heat of air is C_P ($\mathrm{J{\cdot}kg^{-1}{\cdot}K^{-1}}$), and g is the gravitational acceleration ($\mathrm{m{\cdot}s^{-2}}$).

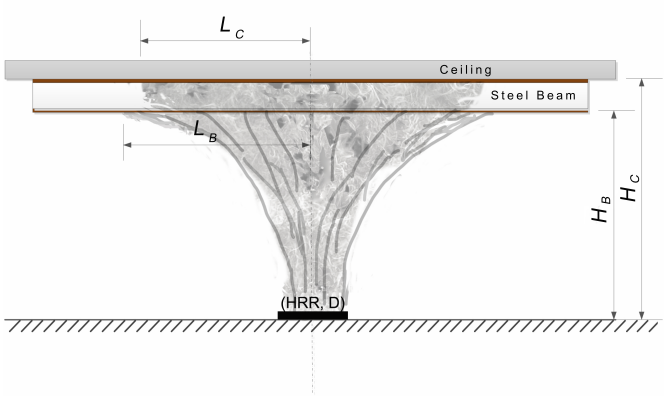

Figure 2.5: Localised fire impinging on a beam underneath the ceiling

To quantitatively describe the correlation between the localised heat flux and the radial distance to the stagnation point (r), it is a common approach to use a dimensionless parameter (y_C), as defined in Equation (2.9).

$$y_C = \frac{r + H_C + z'}{L_C + H_C + z'} \tag{2.9}$$

where z' is a correction value given by the equations as below, using the conception of virtual fire source depth (Wakamatsu and Hasemi, 1988).

$$z' = 2.4D(Q^{*2/5}_D - Q^{*2/3}_D), \text{ when } Q^*_D < 1.0 \tag{2.10a}$$

$$z' = 2.4D(1.0 - Q_D^{*2/5}), \text{ when } Q_D^* \geq 1.0 \tag{2.10b}$$

where Q_D^* terms another non-dimensional rate of heat release which is defined the same as in Equation (2.8), except H_C is replaced by D.

In Eurocode 1, the localised heat flux $\dot{h}$(kW) is correlated to the parameter y_c as:

$$q'' = 100, \text{ when } y_C \leq 0.30; \tag{2.11a}$$

$$q'' = (136.3 - 121y_C), \text{ when } 0.30 < y_C \leq 1.0; \tag{2.11b}$$

$$q'' = 15y_C^{-3.7}, \text{ when } y_C \geq 1.0 \tag{2.11c}$$

According to Eurocode 1,the net heat flux $\dot{h}_{net}$ received by the fire exposed surface of the structural member is modified as:

$$\dot{h}_{net} = \dot{h} - \alpha_c \cdot (\Theta_m - 20) - \Phi \cdot \epsilon_m \cdot \epsilon_f \cdot \sigma \cdot [(\Theta_m + 273)^4 - (293)^4] \tag{2.12}$$

This accounts for the correction of the heat transfer by convection and radiation (Hasemi et al., 1996), which is due to the temperature difference between the structural member and the heat flux gauge, as it is usually cooled by water to maintain the initial lab temperature (taken as 20^oC by Eurocode 1). In Equation (2.12), α_c is the convective heat transfer coefficient, and Θ_m is the temperature of the structural surface; Φ and σ are the configuration factors (set to 1 if the shadow effect is ignored) and Stefan Boltzmann constant ($= 5.67 \times 10^8 W/m^2/K^4$) respectively, ϵ_m is the emissivity of the structural surface and ϵ_f is the emissivity of fire.

•SFPE Localised fire model

When a steel beam is located underneath the ceiling the shielding effect of the beam flanges may become significant, especially when the localised fire is relatively small in terms of the HRR of the fire source. As mentioned earlier, correlations suggested by Wakamatsu et al. (2003) are adopted in the SFPE handbook (Lattimer, 2002) that define the heat flux with reference to the various parts of the beam. Heat fluxes along the lower flange are affected by the flame tip length underneath the beam (L_B) while heat fluxes to other surfaces are related to the flame tip length underneath the ceiling (L_C). Here L_B and L_C are similarly calculated as L_c in Equation (2.7), but with modified coefficients to consider the beam,

$$L_B = 2.3H_B(Q^*_{H_B})^{0.3} - H_B \tag{2.13a}$$

$$L_C = 2.9H_C(Q^*_{H_C})^{0.4} - H_C \tag{2.13b}$$

where H_B is the distance from fire source to the bottom face of the beam, and $Q^*_{H_B}$ is the non-dimensional HRR revised for beam, which can be also defined in the form of Equation (2.8) with the H_C replaced by H_B.

According to the suggested correlations, the highest heat flux occurs at the downward face of the lower flange, which is estimated as:

$$q'' = 518.8e^{-3.7y_B} \tag{2.14}$$

The upward face of the lower flange and the web may have heat flux expressed as:

$$q'' = 148.1e^{-2.75y_C} \tag{2.15}$$

Meanwhile, heat flux at the downward face of the upper flange is represented by:

$$q'' = 100.5e^{-2.85y_C} \tag{2.16}$$

where y_B is the normalised parameter for beam bottom as parameter y_C defined in Equation (2.9), nevertheless, L_C and H_C should be replaced by L_B and beam height H_B respectively. H_B represents the distance from the fire source to the bottom face of the beam, as illustrated in Figure 2.5.

2.2.6 Heat transfer from fire to structure

There are three basic mechanisms of heat transfer, which are conduction, convection and radiation. Inside the structural members, heat conduction occurs as a flow of heat from high temperature regions to low temperature regions (Drysdale, 2011a). The basic equation is the Fourier's law to represent a one-dimensional heat conduction, which is given by:

$$q'' = -k\frac{dT}{dx} \tag{2.17}$$

where dT represents the temperature difference across an infinitesimal distance dx, and q'' is the rate of heat transfer across the distance. In the equation k, the thermal conductivity, is temperature dependent for most building materials. The heat exchanges between a structural member and fire or ambient air are primarily through convection and radiation. Convection occurs when a solid is surrounded by a dynamic fluid, with a empirical relationship known as the Newton's law of cooling:

$$q'' = h\Delta T \tag{2.18}$$

where h is the convective heat transfer coefficient, and ΔT represents the temperature difference between the solid surface and surrounding fluid. h is highly dependent on the characteristics of the thermal system, which is determined through a comprehensive study. However, some typical coefficients of convection are assumed when the commonly accepted fire models are used, according to Eurocode 1. A more scientific discussion of the coefficient can be found from Drysdale's book (2011a). As indicated earlier, thermal radiation contributes a considerable portion of the heat flux when a structural member is exposed to the flame or hot smoke layer. With the introduction of the concept of 'grey body', the total radiation emitted by a unit area of grey surface (denoted as E) can be given by the Stefan-Boltzmann equation:

$$E = \varepsilon \sigma T^4 \tag{2.19}$$

where ε is the emissivity of the grey surface which is equal to its absorptivity according to Kirchhoff's law (Wang, 2003). The resulting heat flow by radiation between the flame and a structural member can be given by:

$$q'' = \Phi \varepsilon_r \sigma (T_f^4 - T_m^4) \tag{2.20}$$

where T_f is the absolute temperature of the fire flame (K), and T_m is the absolute temperature of structural member. Φ is known as the configuration factor, while ε_r represents the resultant emissivity.

Heat absorption of the material itself is taken into account in the transient form of the heat conduction equation, which is expressed as a second order equation:

$$\rho C_p \frac{\partial T}{\partial t} = \nabla (k \nabla T) \tag{2.21}$$

where ρ is the density of member material, and C_p is the specific heat capacity. A valid solution to the above governing equation requires boundary conditions, which could be given in different forms:

initial condition for the domain:

$$T(t_0) = T_0, \quad in \quad \Omega \tag{2.22}$$

Dirichlet condition given over one part of the boundary:

$$T(t) = T_b, \quad on \quad \Gamma_T \tag{2.23}$$

Neumann boundary condition given as heat fluxes over the remaining part of boundary:

$$-k\nabla T = \overline{q}, \quad on \quad \Gamma_q \tag{2.24}$$

in the above expression, $\overline{q}$ can be decomposed as:

$$\overline{q} = q_c + q_r + q_{pr} \tag{2.25}$$

where q_c represents the convective component of heat flux, and q_r is the radiant heat flux. q_{pr} is the prescribed heat flux which is usually from a heat resource with a known incident heat flux.

Regarding heat transfer in structural members, thermal properties of building materials such as concrete and steel are of great importance when solving the transient heat conduction equation. For steel, the density is usually adopted as 7850 kg/m^3 and remains constant regardless of the increase in temperature. However, temperature dependencies exist for the thermal conductivity and specific

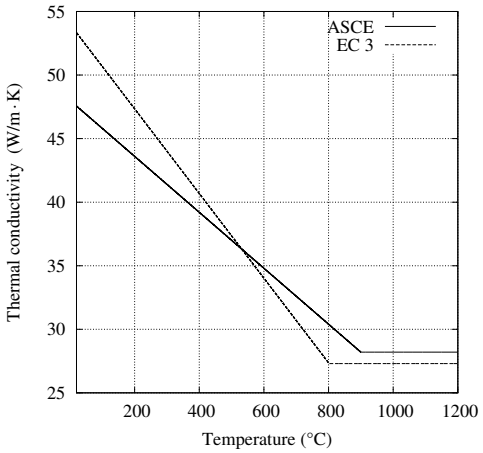

(a) Thermal conductivity

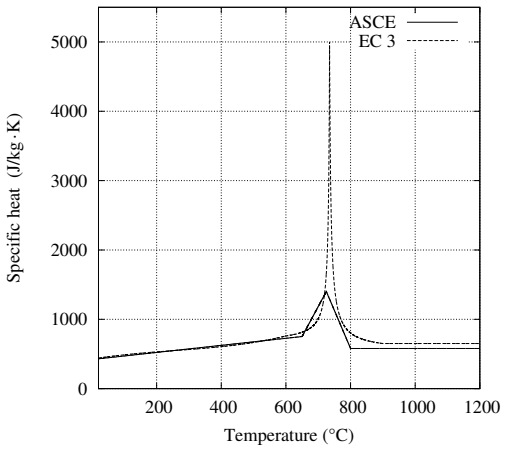

(b) Specific heat

Figure 2.6: Thermal properties of carbon steel (Jiang, 2012b)

heat. Empirical models are provided in Eurocode 3 (EN-1993-1-2) (CEN, 2004) and the ASCE manual (Lie and Others, 1992), as plotted in Figure 2.6. Thermal conductivity decreases with temperature in both models and reaches constant values when the temperature exceeds 800^oC in Eurocode 3 and 900^oC in the ASCE model, respectively. The specific heat of carbon steel gradually increases with temperature up to 750^oC, which is followed by an abrupt jump due to the phase transformation of steel from a ferrite-pearlite to austenitic microstructure.

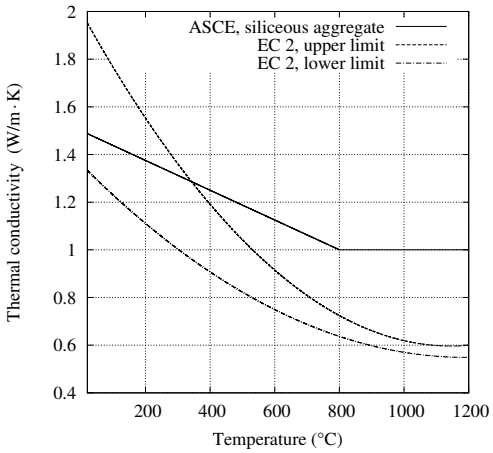

(a) Thermal conductivity

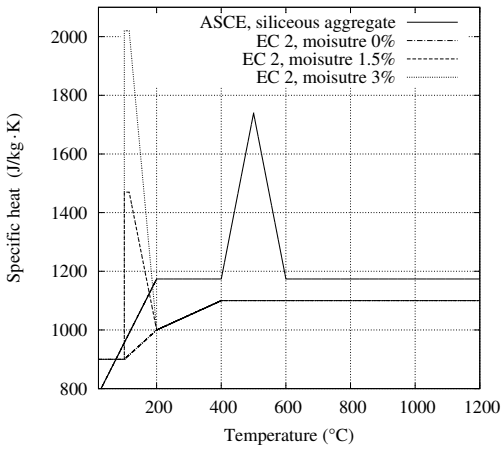

(b) Specific heat

Figure 2.7: Thermal properties of normal weight concrete (Jiang, 2012b)

Empirical models for concrete materials are commonly used according to Eurocode 2 (EN-1992-1-2) (CEN, 2005) and the ASCE manual (Lie and Others, 1992). Figure 2.7 depicts the variations of thermal properties of normal weight concrete. The thermal conductivity is usually chosen between the lower limit and the upper limit. The specific heat of a concrete material is related to its moisture content, as the evaporation consumes heat.

2.2.7 Computational tools for thermal analysis of structures in fire

For heat transfer analysis with simplified fire models, a number of well-known computer programs were developed and utilised in the research field, which include TASEF (Wickström, 1980), TEMPCALC (IFSD, 1987), FIRES-T3 (Iding et al., 1977) and SAFIR (Franssen, 2005). Also an adaptive heat transfer program HADAPT (Huang and Usmani, 1994) was used for heat transfer analysis of the composite slab (Lamont et al., 2001). Numerical solutions can also be obtained using general-purpose commercial finite element analysis packages such as ANSYS (ANSYS, 2009) and ABAQUS (ABAQUS, 2002). The solution strategy in all these programs is fundamentally similar, therefore the availability of idealised fire models and the user-friendliness of the software are the main influencing factors in making a choice between them.

For heat transfer analyses considering localised fire action, Franssen et al. (2007) suggested that three dimensional (3D) thermal response could be approximated through lower dimensional analyses if the Eurocode 1 localised model is used. The key limitation of this work is that a quantitative measure of temperature errors have thus caused was not been determined. Instead of using two dimensional (2D) representation, Jeffers and Sotelino (2009) developed a fibre based heat transfer element for modelling the thermal response of beam-type members. Furthermore, a shell heat transfer element was also developed by Jeffers (2013) which discretises the temperature field into 2D layers that were coupled by a finite difference approximation of the transverse heat flux. In this thesis, the author adopts a methodology proposed by Franssen et al. (2007) to approximate 3D response with a number of 2D or 1D heat transfer analyses. A quantitative investigation

is presented in Chapter 3 in order to estimate the errors caused by dimensionally reduced analyses.

2.3 Behaviour of steel and composite structures in fire

The traditional fire safety strategy for steel framed composite buildings has been to apply protection to all the steel members preventing the steel from reaching too high a temperature for a specified fire resistance time (Bailey and Moore, 2000b). An alternative approach was proposed in the first ever fire design code BS5950:part8 (BSI, 1990), which adopts a limiting temperature method based on the level of utilisation (load ratio) and material partial safety factor. Eurocode 3 and Eurocode 4 adopted a similar but more comprehensive strategy, the development of design codes provides a more solid scientific foundation for the fire safety of steel framed structures. However, it is suspected that the traditional code based approaches may be too conservative as they require full fire protection for all structural members. On the other hand, traditional approaches may even be unsafe as the global behaviour of a structure is not addressed at all. Based on the investigations carried out after the Broadgate fire (Newman, 1991), it was proposed that the behaviour of real buildings in fire should be assessed on the basis of treating the structure as a framework of interacting connected elements rather than a collection of isolated elements, which had always been the implication of the traditional approach. This stimulated a rapid advance of knowledge and understanding of the real behaviour of steel and composite structures in fire, which was not achieved until the ground-breaking Cardington fire tests (British

Steel, 1998, 1999; Usmani, 2000; Lennon, 2003). Numerous research articles were published based on output from the full-scale tests, as well as more fundamental work (Elghazouli and Izzuddin, 2000; Usmani et al., 2001; Foster et al., 2004) conducted to understand the observed behaviour in the Cardington tests.

These full scale tests were conducted in an eight-storey steel framed structure built by the Building Research Establishment (BRE) at its Cardington Large Building Test Facility. It was designed and constructed to resemble a typical modern city centre office structure. The structural design was carried out to BS5950, and also compiled with Eurocode 3 and Eurocode 4 according to the report (British Steel, 1999). The structure was designed as a braced frame with cross bracings in chosen frame locations in both directions, while the beams were designed as simply-supported acting compositely with the floor slab through shear studs. A general view of the test building is presented in Figure 2.8, which covered an plan area of 21m $\times$ 45m with an overall height of 33m. The plan layout of this framed structure is illustrated in Figure 2.9. Two programmes of tests were sponsored by British Steel (BS)/European Coal and Steel Community(ECSC) and BRE, involving six different tests carried out at Cardington from January 1995 to September 1996. A summary of these tests is presented in Table 2.2.

In this section, an overview of recent development towards understanding the behaviour of steel members in fire is presented, as well as the progress that has been made regarding the behaviour of concrete slabs under fire conditions. Composite floor system as an assembly of steel grillage and concrete slab with steel deck and reinforcement is reviewed with respect to its in-fire behaviour. The effect of fire protection is looked up on with reference to partial damage and the consequent structural behaviour in fire.

Figure 2.8: General view of test building (British Steel, 1999)

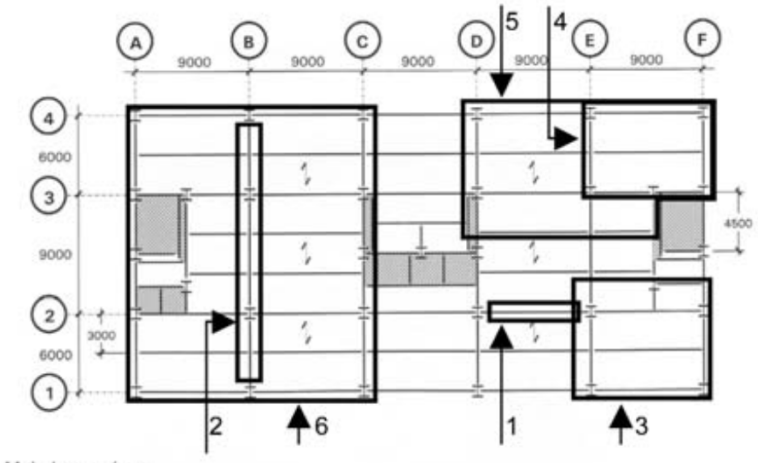

Figure 2.9: General plan of test building (British Steel, 1999)

Table 2.2: Summary of Cardington fire tests (Bailey, 1999)

Test date	Sponsor	Description	Floor area(m^2)	Location
Jan 1995	British Steel	Restrained beam	24	Level 7
Apr 1995	British Steel	Plane frame	53	Level 4
Oct 1995	BRE	1st Corner	54	Level 2
Nov 1995	British Steel	2nd Corner	76	Level 1
Apr 1996	BRE	Large compartment	340	Level 2
Sep 1996	British Steel	Large compartment (office)	136	Level 1

2.3.1 Material properties at elevated temperature

Led by elevated temperature, material degradation and thermal expansion of steel and concrete are considered in this thesis, while the creep effect (Bažant, 2001) and concrete spalling (Mindeguia et al., 2010) are not included in the analyses. The estimation of thermal expansion in steel and concrete members may follow the Eurocodes provisions (CEN, 2004, 2005), which can be illustrated with Figure 2.10.

At elevated temperature, steel may experience softening and strength loss. Reduction factors suggested in Eurocode 3 (CEN, 2005) are commonly applied to account for reduction in elastic stiffness and yield strength of steel, allowing for a smooth transition from linear elasticity to plastic plateau. The normalised stress-strain curves at specific temperatures are plotted in Figure 2.11. The stress and strain relationship for steel reinforcement is similarly defined in Eurocode 2 (CEN, 2004), but with different reduction factors. Compressive strain induced stress in siliceous concrete may be assumed to develop in accordance to Figure 2.12 at specific temperatures. The generic reduction factors associated with compressive

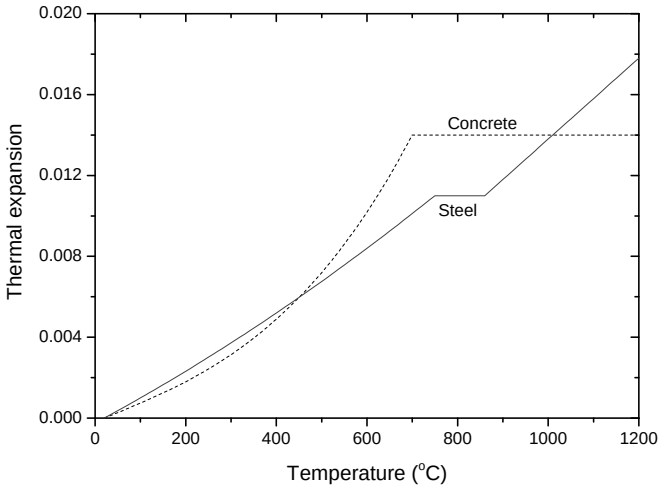

Figure 2.10: Thermal expansion strain in siliceous concrete and steel (CEN, 2004, 2005)

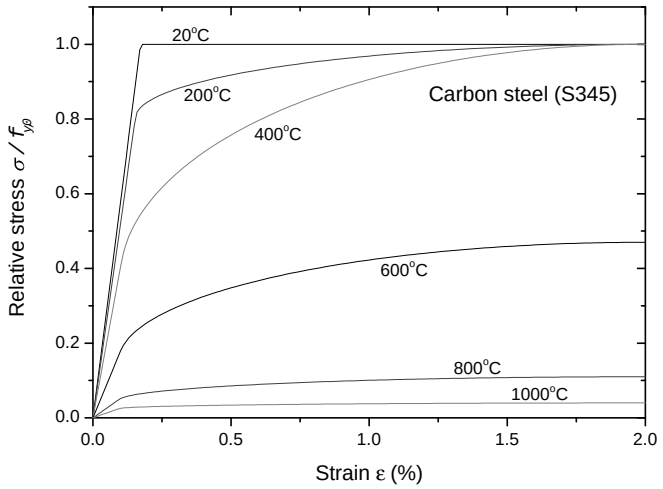

Figure 2.11: Strain-stress curves of carbon steel at elevated temperature (CEN, 2005)

strength and the temperature dependent strain limits from Eurocode 2 depend upon the the aggregate used in the concrete (siliceous or calcareous). Tensile strength of concrete is usually modelled as linear elastic followed by an exponential decay to account for its tensile contribution in tension regions. Reduction factors can be also found in Eurocode 2 to degrade the tensile strength.

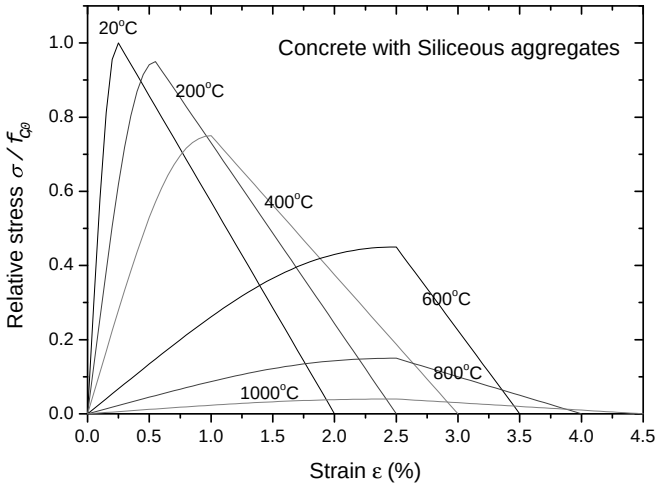

Figure 2.12: Strain-stress curves of siliceous concrete at elevated temperature (CEN, 2004)

2.3.2 Steel framed members in fire

Steel columns under compression should be designed against global buckling, cross-sectional yield and local buckling. The restraint effects imposed by adjacent structural members to thermal expansion become substantial when columns are subjected to fire. Beams in fire also experience significant restraint effects, both during the heating and expansion phase and the cooling phase where a catenary mechanism may develop after large deflections occur in the beam. As most beams in steel frame structures are laterally restrained by the composite floor system, lateral torsional buckling rarely occurs, however long span cellular steel beams supporting composite floors are highly susceptible to distortional buckling (Nadjai et al., 2007) in normal structures. Moreover, globally evaluating the behaviour of a steel structure in fire has become a major concern as different failure mechanisms have been explored in recent decades.

The **global buckling** of unprotected steel columns were experimentally and

numerically investigated by Huang and Tan (2007), and Tan et al. (2007) with emphasis placed on the second order effects. A Rankine approach proposed by Toh et al. (2000) and an analytical study by Huang and Tan (2003) were developed to estimate the global buckling of retrained columns. **Local buckling** is more commonly seen in thin walled steel members, where the effective width method is still applied in the practical design considering fire exposure (Couto et al., 2014). Regarding the behaviour of steel beams in fire, Usmani et al. (2001) drew the attention from the traditional material degradation to some fundamental effects including thermal expansion and bowing under restrained boundaries. Axial restraint was found beneficial after large deflections had developed, which was proven by the experimental work (Liu and Davies, 2001; Liu et al., 2002) and the following numerical study (Yin and Wang, 2004). This effect was recognised as the **catenary action** of steel beam in fire and a simplified hand calculation method was developed to evaluate the load bearing contribution by Yin and Wang (2005b,a). It has been noticed that this beneficial effect can be even enhanced in a composite slab system due to the membrane action of concrete slab, which significantly improves its performance in resisting fire exposure. Researches exploring this area are presented later in this section.

When beams and columns are investigated in the context of a complete structure, different mechanisms induced by fire exposure may be found. Shepherd and Burgess (2011) investigated the restraint effect on columns with a 2D plane frame model. The heated columns were seen to "hang" from the restraining spring after buckling because of load redistribution towards the adjacent structure. It was found that a progressive buckling mechanism may occur if adjacent columns were also heated. Kodur and Dwaikat (2009) used a 3D subframe to investigate the beam-column behaviour under different fire conditions, where high temperature

creep was found to be important and the fire scenario played a significant role in determining the response of restrained steel beams. Large frame models were used in the work by Liew et al. (1998), where uniform fires were localised in compartments and fire spread was considered based on Bailey's work(1996a). The proposed analysis demonstrated the consideration of the simultaneous effects of axial force, bending moments and thermal expansion. Large frame models subjected to multiple floor fires were modelled by Flint et al. (2007), based on the collapse of WTC towers (Sivaraj, 2005; Kotsovinos and Usmani, 2013). Two mechanisms of generic tall building collapse initiated by fire were identified as the weak floor and the strong floor mechanism (Usmani et al., 2003; Lange et al., 2012), which led to flexural failure initiated at different locations of the tall building frames leading to global instability. A simple method was developed by Usmani et al. (2009) to evaluate the structural resistance to multiple floor failure induced by fires. Although this thesis will mostly focus on localised fire scenarios, the research on multi-compartment (floor) fires could enlighten the understanding of structural response when a localised fire bursts in an open plan building as more adjacent members are involved.

Non-uniform heating was numerically studied by Yin and Wang (2003) for evaluating LTB resistance of steel I-beams, where only temperature gradients across the beam section were discussed. A simply supported steel beam subjected to localised fire action was modelled by Jeffers's new fibre based heat transfer element (Jeffers and Sotelino, 2009). Thermo-mechanical analyses were performed in ABAQUS to observe the failure time (approximately 520s for a 1MW fire) while a uniformly distributed load was imposed on the beam (Jeffers and Sotelino, 2012). A similar investigation was seen in the work conducted by Zhang et al. (2013), in which ANSYS (ANSYS, 2009) was chosen to run heat transfer and structural

analyses of an axially restrained steel beam subjected to the SFPE localised fire. A lower failure temperature (454^oC) was reported for the localised heating compared to standard fire exposure (514^oC). In addition to the beam analyses, heat transfer to a steel column from a localised fire was investigated by Sjöström et al. (2012). Temperature variation was measured along the column height, which showed that the maximum appears at the bottom area near the burner. However, the fire burned around the column in the test without ceiling confinement, which leads to lower temperatures in the top part of the column. A column surrounded by localised fire action was modelled by Fang et al. (2011) using ADAPTIC (Izzuddin, 1990), where a grillage of beams was employed to represent the concrete slab in a car parking building and the temperature distribution along the column is taken as uniform. The work suggested that the occurrence of overall collapse is dependent on the floor configuration, location of fire, loading level, column size and number of ambient floors above the fire affected floor.

2.3.3 Reinforced concrete slabs in fire

A traditional design approach for estimating the load carrying capacity of reinforced concrete slabs at ambient temperature is the Yield line analysis (Johansen, 1962). However, this plastic bending theory significantly underestimates the ultimate performance of concrete slabs (with or without composite floor) under fire conditions, as observed in the Cardington fire tests. This led to an exploration of the unique load carrying mechanism for slabs in fire, which is now understood as **tensile membrane action** (Wang, 1997; Bailey, 2001; Huang et al., 2003a). Different researchers have attempted to model and explain this mechanism using different approaches. Among them, Wang (1997) may be the first who described

the tensile membrane action in reinforced concrete slabs with large fire-induced deflections. Cracks extending over the depth of concrete redistributed the load to steel reinforcement mesh which is anchored by the outer compressive ring near the edges(Figure 2.13). Bailey et al. (2000) carried out a series of slab tests in which a small area of steel deck was artificially removed. These ambient tests demonstrated the existence of compressive ring which was a conceptual mechanism before. Based on the tests, a design method (Bailey, 2001) was derived to predict the membrane behaviour of simply supported concrete slabs. The method was later refined with a more accurate estimate of the in-plane stress distribution(Bailey and Toh, 2007a), which was learned from the 44 small scale slab tests at ambient and elevated temperatures (Bailey and Toh, 2007b). Modelling membrane action also attracted other researcher's interests. For example, Huang et al. (2003b,a) developed a layered nine-node shell element (Yu and Huang, 2008) in VULCAN (Bailey et al., 1996b; Bailey, 1995) which were validated against the results from slab tests at ambient and elevated temperatures. A recent implementation of this element was to model the slab behaviour within a concrete structure, where concrete spalling was considered in a few analyses (Huang, 2010). The membrane mechanism was also explored in Edinburgh University(Gillie et al., 2004; Usmani and Cameron, 2004) using ABAQUS (ABAQUS, 2002), with findings such as that a lower placed steel mesh may increase the slabs ability to accommodate large deflections, and a large increase in moment capacity was found in the slabs with in-plane membrane compression due to the temperature induced thermal expansion. With emphasis on the effect of large deflection and differed from the Yield line approach, a design method was proposed by Cameron and Usmani (2005b,a) to determine the membrane capacity of laterally restrained composite floor slabs in fire. The method revised the energy calculation for slabs in fire, and was used to

calculate the the ultimate load capacity for any given thermal input. Notably, the research platform at Edinburgh was recently extended to OpenSees (McKenna, 1997; Usmani et al., 2012), in which development was carried out by Jiang et al. (2014) to model concrete slabs in fire. A group of researchers (Lim et al., 2004) also employed SAFIR (Franssen, 2005) as a numerical tool to model the fire behaviour of two-way reinforced concrete slabs, which were experimentally tested by Lim and Wade at Canterbury(Lim and Wade, 2002).

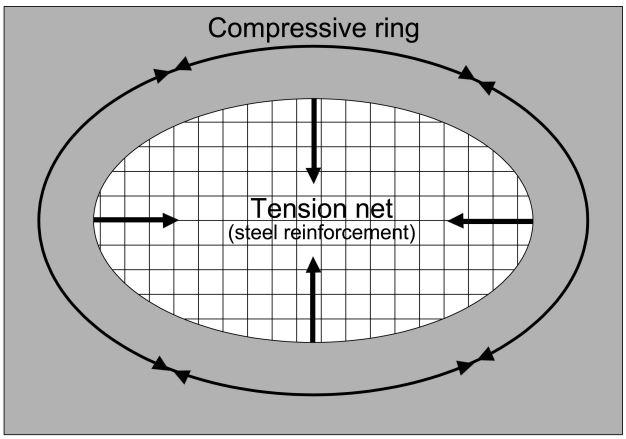

Figure 2.13: Mechanism of tensile membrane action in a simply supported slab (Wang, 1997)

Few references could be found discussing concrete slabs under localised fire action. Nonetheless, with respect to heat transfer from localised fire to slab, Jeffers (2013) has published a layered shell element to model the thermal response which showed a great potential in saving computational cost. A dimensionally reduced scheme for heat transfer analysis of concrete slabs is developed in this thesis to provide temperature histories induced by spatially non-uniform fire action. The slab behaviour will be analysed using modified shell elements formulated using a multi-layer section, which will be presented in Chapter 6 of this thesis.

2.3.4 Composite floor system in fire

Composite floor systems are widely used in the practical construction of steel and composite structures, with a typical form as shown in Figure 2.14, which usually consists of a trapezoidal or re-entrant steel deck and a concrete slab reinforced by steel mesh, and being placed on a grillage of steel beams with shear studs to provide resistance against the slip (Bailey, 2003).

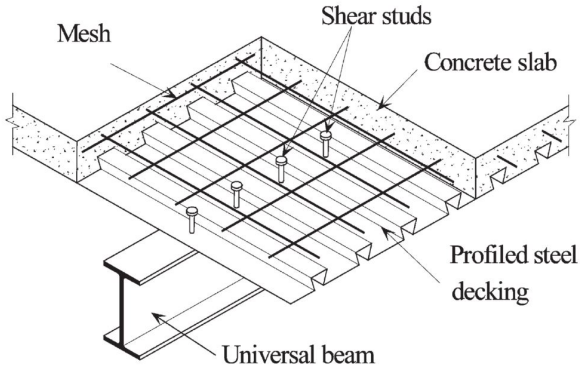

Figure 2.14: Typical composite floor (Bailey, 2003)

In the past two decades, most of the work involving the behaviour of composite floor systems in fire were based on the Cardington fire tests. The official reports released by British Steel (merged to Corus and now Tata Steel) (British Steel, 1998, 1999; Lennon, 2003), BRE (BRE, 2005), and University of Edinburgh (PIT project) (Usmani, 2000) summarise the remarkable findings. Meanwhile, significant additional effort at many other institutions was devoted to understand the observed behaviours.

An early attempt of modelling the British Steel Restrained Beam Test was reported by Bailey et al. (1996b) with linear shell elements introduced into INSTAF (El-Zanaty et al., 1980; Saab, 1990) which is the predecessor of VULCAN(Bailey

et al., 1996b; Bailey, 1995; Huang et al., 1999). Concrete ribs were ignored in that model, but with semi-rigid connections included to account for beam-column joints. A similar approach was later used by Bailey (1998) to model the BRE Corner Test, with comparison between the software predicted displacements and the measured data from the test while the prediction was found higher than the tested results. The two BRE tests (BRE Corner Test and BRE Large Compartment Test) were modelled by Bailey (1999) with conclusions such as: structural behaviour was different and better than estimated by standard fire tests; steel beams should be conservatively assumed as pinned to columns in a fire design. Especially, the beam performance was found to benefit greatly from the composite slab, which was suspected to be caused by tensile membrane action. Based on the observations of the damage from the Cardington fire tests, a new design method for composite floors in fire was proposed by Bailey and Moore (2000a,b). The method used a simple energy approach to calculate the load-carrying capacity of a composite floor system, with consideration of tensile membrane behaviour. Further discussions upon this design method and tensile membrane action were seen in Bailey's publications(2003; 2004), where the necessity of beam fire protection was questioned.

Numerical modelling of the Cardington fire tests was systematically carried out at the University of Edinburgh. Lamont et al. (2001) performed heat transfer analyses using HADAPT (Huang and Usmani, 1994) to estimate the temperature profiles of composite slabs. The existence of the metal deck and evaporation of moisture were included in the model, as well as an interface element to account for the interfacial heat conduction. A slight overestimation was seen from the numerical results in comparison to the test captured data. The thermo-mechanical analysis of BS Restrained Beam Test was carried out by Sanad et al.

(2000c) using ABAQUS (ABAQUS, 2002). The finite element model was built up using beam elements and the temperature was increased linearly from ambient to the maximum value for each member. The work confirmed that the structural response was governed by the thermal effects of restrained expansion and bowing. The effect of thermal gradients and mean temperatures of the slabs in the British Steel restrained beam test were investigated by Sanad et al. (2000a,b). The scheme for modelling composite slabs in ABAQUS with FEAST (Liu, 1996) enhanced shell elements was discussed by Gillie et al. (2001b) and applied to analyse the Restrained Beam test(Gillie et al., 2001a), where the conclusions were made as the floor deflections and forces are dominated by the effects of the thermal expansion rather than material degradation or gravity loading. The British Steel Corner Test was later modelled by Gillie et al. (2002) using the same techniques. The analysis revealed that large curvatures and deflections were caused by incompatible thermal expansions in steel beam and concrete slab. Tensile membrane action was found in the analysis and believed to be an important load-carrying mechanism at large deflections. The most recent work in modelling composite floors in fire (Jiang and Usmani, 2013; Jiang et al., 2014) was reported at Edinburgh, where OpenSees was adopted as the computational platform. A few benchmark tests were carried out to validate the performance of the Total Lagrangian shell element, which was further validated by modelling the Cardington Restrained Beam Test and Corner Tests.

The two BRE fire tests (BRE Corner Test and BRE Large Compartment Test) were also independently analysed by Wang (2000) using a finite element program developed by Wang and Moore (1995). Membrane action in the floor slab was reproduced by the analysis. Based on the findings from the Cardington tests, Wang and Kodur (2000) suggested that unprotected steel beams in steel framed

buildings may be acceptable and emphasised the necessity of protecting steel columns. The Restrained Beam Test and the Corner Test were numerically modelled by Izzuddin (1990) using ADAPTIC, using a grillage representation of the composite floor. The analysis suggested that an early buckling of the floor system may occur due to thermal expansion and tensile membrane action could be used to carry the load when large deflections developed in the slab. Furthermore, they concluded that for a large compartment (Corner Test), material degradation and initial gravity loading played more pronounced roles. These findings were seen to be summarised in the publication by Izzuddin and Moore (2002). Following this, using the layered shell element developed by Huang et al. (2000a) in VULCAN, the Cardington British Steel Corner Test and BRE Large Compartment Test were modelled (Huang et al., 2000b, 2003a). An excellent performance was shown in modelling composite slabs with the layered shell element, with the typical phenomena such as large deflections and membrane action highlighted.

As analyses were conducted to model and analyse the behaviours observed in the Cardington tests, many technical advances in numerical models were witnessed in the past decades. Compared to the grillage representations used by Izzuddin (1990) and Sanad et al. (2000c), composite slabs were relatively more accurately modelled using shell elements by Bailey et al. (1996b) which however ignored the ribs and did not account for geometrical nonlinearity. This was advanced to an orthogonal shell element with layered sections (Huang et al., 2000a), which included the concrete ribs using an effective stiffness approach. Furthermore, concrete slabs and steel beams could be assembled with connections, as the model defined by Huang et al. (2000b). This proposed model well represents

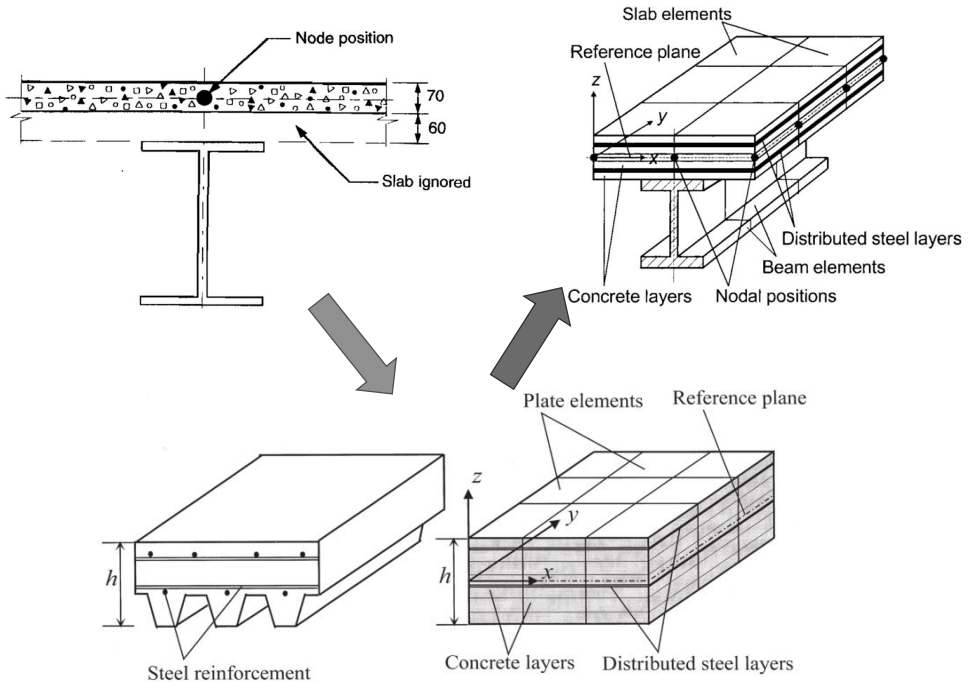

Figure 2.15: Advances for modelling composite floor system in VULCAN (Bailey et al., 1996b; Huang et al., 2000a,b)

the composite floor system, and has been implemented in modelling Cardington tests with satisfactory performance (Huang et al., 2000b, 2003a).

2.3.5 The effect of partial fire protection

The observations from the Cardington tests suggested possible as a fire protection strategy that beams could be left unprotected (Wang and Kodur, 2000). Nevertheless, it was agreed that columns should be properly protected against fire exposure. There are many different approaches to protect the steel members, among them the passive protection systems could be concrete encasement, board systems, spray-applied fire resistive material (SFRM), intumescent paints, water

filling, and flame shields (Buchanan, 2001). In this thesis, SFRM protection (cementitious fire-resistant coating) is primarily chosen for investigation with respect to the localised effects. SFRM is widely used in the practice because of its advantages, such as low density, low thermal conductivity (around 0.1 W/m/K), low cost and non-toxic emissions in fire. However, SFRM has very low strength and ductility, and is therefore prone to damage (Chen et al., 2010; Dwaikat et al., 2011; Leo Braxtan and Pessiki, 2011). In terms of its thermal properties, Kodur and Shakya (2013) reported the test results of three typical types of SFRMs and temperature dependencies were found in thermal conductivity, specific heat, thermal strain and mass loss. When applying SFRM to steel plate, its mechanical performance has been tested by attaching it to small scale steel plates under monotonic axial loadings (Chen et al., 2015) or pure bending moments (Chen and Jiang, 2015). A quantitative measure of the steel strains or curvatures corresponding to the occurrence of cracking was addressed in the work, where finite element models based on the Cohesive Zone Model (CZM) (de Borst et al., 2004a) for SFRM-steel interface were used to investigate the damage mechanisms of SFRM coatings, and cracking pattern including interfacial cracks and transverse cracks was notably identified. A similar series of tests (Leo Braxtan and Pessiki, 2011) were reported, where the SFRM covered steel plates are subjected to tensile yielding. For modelling the SFRM damage, CZM and dynamic analysis were employed by Dwaikat and Kodur (2011) to describe the debonding and fracture in SFRM layers, which suggested that CZM based model can be a valid tool for describing the partial damage of SFRM.

When evaluating the fire performance of steel members with damaged fire protection, composite beams were investigated by Wang (1998) using artificially generated partial protections, which covered the lower flange and left three

quarters of web and upper flange of the steel beam unprotected. It was expected that the remaining stiffness in the concrete slab could carry the load in cooperation with the protected lower flange. It is noticed that the partial removal of fire protection is identical along the beam length, which implies a temperature gradient over the depth of the section if uniform fire model is applied. Similar type of tests were conducted by Dwaikat et al. (2011), who removed different parts of protection such as flange edges, middle flange surfaces along the column height. Thermal gradients were formed in the beam due to partial removal of fire protection, which led to considerable bending-moments developing in the columns and a plastic yielding failure. A few 2.7m high columns were tested with different lengths (7% or 14% column height) of fire protection removed near the ends (Wang and Li, 2009). It was found that the column failure occurring in the unprotected parts was highly correlated to the degree of partial damage.

2.3.6 Computational tools for thermo-mechanical analysis of structures in fire

A very brief review of the existing computational tools available for modelling structural behaviour in fires is presented in this section. Despite the historical existence of many specially developed tools as mentioned in textbooks (Wang, 2003; Buchanan, 2001), the most commonly used programs in this century may be the general purpose commercial packages such as ABAQUS (ABAQUS, 2002), ANSYS (ANSYS, 2009), DIANA (TNO, 2011)), and the Structural specialised tools such as ADAPTIC (Izzuddin, 1990), SAFIR(Franssen, 2005),VULCAN (Bailey et al., 1996b; Bailey, 1995; Huang et al., 1999), OpenSees Thermal (McKenna, 1997; Usmani et al., 2012). For commercial packages, integrated

analysis coupled with FDS have been reported by Zhao et al. (2007), although lack of structural material library and inconvenience of building structural models maybe the major obstacle in using general purpose commercial packages. **ADPATIC** was developed by Izzuddin (1990) during his PhD study, initially driven by the needs of nonlinear analysis tools to deal with extreme static and dynamic loadings in offshore engineering, which was further developed over time to include the capability of modelling structures subjected to earthquake, fire or blast loading (Song et al., 2000; Izzuddin et al., 2000). Steel frames and concrete slabs could be modelled using ADPATIC with temperature histories calculated using other softwares. Features such as automatic mesh refinement and dynamic analysis capability make the software outstanding. **SAFIR** is known as a computer program specialised in analysis of structures in fires, and was developed by Franssen (2005). A relatively rich library of elements for structural analysis have been developed in addition to the capability of heat transfer analysis (Mason, 1999). It is noticed recently that a FDS-SAFIR interface was developed to perform integrated analysis (Tondini et al., 2012), which allows weak coupling (Welch et al., 2008) between analyses of fire development, heat transfer and thermo-mechanical response. **VULCAN** is a well known software for modelling fire related structural behaviour, developed from the finite element frame analysis program INSTAF (El-Zanaty et al., 1980; Saab, 1990). A decent amount of development has been carried out in the past decades, such as 3D analysis capability added by Najjar and Burgess (1996), shell elements and semi-rigid connections introduced by Bailey et al. (1996b); Bailey (1995), and the recent advance in modelling composite slabs delivered by Huang et al. (2000a, 2003b,a). The limitation of VULCAN is the lack of thermal analysis capability, as the input of heat transfer results has to be obtained from other specialised software or

calculations. Commercial finite element packages are also available for modelling structures in fire, and have been discussed previously in this chapter. The key drawback of commercial packages is their black box environment inhibiting further development, which makes it very tedious to perform specialised analyses such as modelling structures subjected to localised (Pchelintsev et al., 1997; CEN, 2002a) or travelling fires (Stern-Gottfried and Rein, 2012b,a).

OpenSees has now become a powerful research tool not only for earthquake engineering simulation as its original objective indicates (McKenna, 1997), but also for 'structures in fire' modelling (Jiang et al., 2011; Usmani et al., 2012; Jiang and Usmani, 2013; Jiang et al., 2014). Although considerably more validation work should be conducted to prove the robustness of modelling structural fire behaviour with this software, its development continues apace from heat transfer analysis (Jiang et al., 2011) to frame analysis (Jiang and Usmani, 2013), and shell analysis (Jiang et al., 2014). In addition to development of the essential structures-in-fire modelling capabilities a significantly more ambitious project is currently underway. The aim is to create a highly integrated computational framework which can sequentially perform coupled thermal and structural analyses of large and realistic structural frames under equally realistic fire scenarios. The development of this integrated computational environment is covered in Chapter 5 of this thesis.

2.4 Simulating 'structures in fire' using OpenSees

In 1997, an open source software framework later named as OpenSees was developed at the University of California, Berkeley by McKenna (1997). It was initially designed to simulate non-linear response of structural frames under

seismic excitations. OpenSees has an object-oriented architecture and is written in C++. Object-oriented capabilities enable structural engineers to focus on modelling objects that also have their own attributes and functions rather than just data. Major attributes such as elements, materials, analysis procedures, and solution algorithms are designed as individual objects and they can be added into the framework freely by anyone anywhere (Usmani et al., 2012). An active group of OpenSees experts moderate the framework using a version control system, Subversion (Pilato, 2004). This attracts researchers from across the globe to contribute their piece of code to the original framework and help make it more robust and bug-free.

In 2009, OpenSees was adopted at the University of Edinburgh to further develop it to perform structural fire analysis. Significant contributions in terms of heat transfer and fire modules have been made to the framework in developing the Thermal version of OpenSees (Jiang et al., 2011; Jiang, 2012b). Temperature dependent formulations have been incorporated for basic element types, beam element and shell elements to account for the thermal effects (Jiang, 2012a; Jiang and Usmani, 2013; Jiang et al., 2015). The material library of the original framework has also been updated by adding new temperature dependant material models for steel and concrete based on Eurocodes (CEN, 2002a, 2004, 2005). Development of OpenSees Thermal is an ongoing project which will be introduced in Chapter 5.

2.4.1 Fire modelling and heat transfer analysis

A thermal analysis framework was developed within OpenSees originally by Jiang (2012b) as a part of his PhD work . A fire module which contains a range of widely used empirical fire models was created to quantify the fire imposed boundary conditions, together with a heat transfer module developed to address non-linear heat conduction in structural members using the finite element method.

The governing equation of heat conduction in solids was introduced in Equations. (2.21)-(2.25). Based on the *Galerkin Weighted Residual Method*, a weak form can be derived for a finite element after discretisation of the domain, which may be expressed as:

$$\int_{\Omega^e} \left[W \rho c_p \frac{\partial T}{\partial t} + k_x \frac{\partial W}{\partial x}\frac{\partial T}{\partial x} + k_y \frac{\partial W}{\partial y}\frac{\partial T}{\partial y} + k_z \frac{\partial W}{\partial z}\frac{\partial T}{\partial z} \right] d\Omega - \oint_{\Gamma_q^e} W \overline{q}\, d\Gamma = 0 \tag{2.26}$$

where W is the weighting function. A matrix form of the governing equation can be written for an element in the form of an ordinary differential with respect to the time variable:

$$\mathbf{C}^e \dot{\mathbf{T}}^e + \mathbf{K}^e \mathbf{T}^e = \mathbf{Q}^e \tag{2.27}$$

By assembling the elemental matrices and vectors and discretising the time variable using finite difference method, the global system of equations can be written as:

$$\mathbf{C}_{n+1} \dot{\mathbf{T}}_{n+1} + \mathbf{K}_{n+1} \mathbf{T}_{n+1} = \mathbf{Q}_{n+1} \tag{2.28}$$

$$\dot{\mathbf{T}}_{n+1} = \frac{1}{\alpha \Delta t} \left[\mathbf{T}_{n+1} - \mathbf{T}_n - (1-\alpha)\Delta t \dot{\mathbf{T}}_n \right] \tag{2.29}$$

A predictor-corrector algorithm with Newton iteration method was adopted in

the heat transfer module, which can be summarised as:

$$\text{Solution predictor(given} \quad \mathbf{T}_n \,,\, \dot{\mathbf{T}}_n \,,\, ir = 0)$$

$$\mathbf{T}^{ir}_{n+1} = \tilde{\mathbf{T}}_{n+1} = \mathbf{T}_n + \Delta t(1-\alpha)\dot{\mathbf{T}}_n \tag{2.30}$$

$$\dot{\mathbf{T}}^{ir}_{n+1} = \tilde{\dot{\mathbf{T}}}_{n+1} = 0 \tag{2.31}$$

$$\text{Solution corrector (iterating until converged)}$$

$$\mathbf{M}^{*ir}_{n+1}\Delta\mathbf{T}^{ir}_{n+1} = -\mathbf{R}^{ir}_{n+1} \tag{2.32}$$

$$\mathbf{T}^{ir+1}_{n+1} = \mathbf{T}^{ir}_{n+1} + \Delta\mathbf{T}^{ir}_{n+1} \tag{2.33}$$

$$\dot{\mathbf{T}}^{ir+1}_{n+1} = \frac{1}{\alpha\Delta t}(\mathbf{T}^{ir+1}_{n+1} - \tilde{\mathbf{T}}_{n+1}) \tag{2.34}$$

$$ir = ir + 1 \tag{2.35}$$

where $\mathbf{M}^{*ir}_{n+1}$ is the tangent matrix which counts the parts led by specific heat, thermal conductivity and boundary heat flux (convection and radiation), as expressed in the following equation: $\mathbf{M}^{*ir}_{n+1} = \frac{1}{\alpha\Delta t}\mathbf{C}(\mathbf{T}^{ir}_{n+1}, t_{n+1}) + \mathbf{K}(\mathbf{T}^{ir}_{n+1}, t_{n+1}) + \mathbf{M}^{q}(\mathbf{T}^{ir}_{n+1}, t_{n+1})$. The residual (likewise unbalanced force) is evaluated as

$$\mathbf{R}^{ir}_{n+1} = \mathbf{C}(\mathbf{T}^{ir}_{n+1}, t_{n+1})\dot{\mathbf{T}}^{ir}_{n+1} + \mathbf{K}(\mathbf{T}^{ir}_{n+1}, t_{n+1})\mathbf{T}^{ir}_{n+1} - \mathbf{Q}(\mathbf{T}^{ir}_{n+1}, t_{n+1}) \tag{2.36}$$

The implementation of heat transfer analysis in OpenSees was delivered via a number of classes: e.g. **HeatTransferDomain**, **HeatTransferAnalysis**, **HeatTransferElement**, **HeatTransferMaterial**, **HeatFluxBC** and **BoundaryPattern**, etc. These new classes were organised with a similar hierarchy as adopted in the original OpenSees, while finite element model components were stored in the central storage class **HeatTransferDomain**. The state-of-art heat transfer and fire modules will be discussed in Chapter 5.

2.4.2 Geometrical and material nonlinearities

OpenSees was initially developed to model the nonlinear behaviour of structures (Scott et al., 2008a). In structural analyses, nonlinearities are primarily introduced when structural materials are loaded beyond their elastic limit (material nonlinearity); and when the assumption that the structural geometry remains unchanged after loading is no longer valid (geometrically nonlinear behaviour, such as second-order effects) (Wriggers, 2008).

• **Geometrical nonlinearity**

The kinematic descriptions of geometrically nonlinear finite element analysis are mostly referred to as: *Total Lagrangian* (TL), *Updated Lagrangian* (UL), and *Corotational* (CR). For a *Total Lagrangian* description, the FEM equations are formulated with respect to a fixed reference configuration which is not changed throughout the analysis. Often this is the initial configuration assumed by the structure, but in special cases it could be an artificial base configuration that is not actually assumed by the structure. An *Updated Lagrangian* scheme formulates the FEM equations with reference to the last accepted solution (converged step). The reference configuration is updated during the analysis, however, the base configuration remains fixed (Felippa, 2000). As an element is formulated with a *Corotatinal* (CR) description (Crisfield, 1991), the reference configuration is split into base and corotated, where the elemental strains and stresses are calculated from the corotated to the current configuration. This kinematic description is suitable for the analyses with small strains and arbitrarily large finite motions, while the TL description is recommended for nonlinear elastic analysis and the UL description is applicable in nonlinear analysis involving plasticity (Felippa, 2000).

In OpenSees, geometrical nonlinearity is realised in beam elements using different geometrical transformation schemes, such as the P-delta transformation which ignores the change of element length and the Corotational transformation (A linear transformation is available for geometrically linear analysis). For shell analysis, different shell elements are developed for geometrically nonlinear analysis. Currently, Total Lagrangian and Updated Lagrangian descriptions have been used for formulating shell elements at ambient temperature in OpenSees (Lu et al., 2015). For thermo-mechanical analyses, a shell element (Jiang and Usmani, 2013; Jiang et al., 2014) based on TL formulation was developed to model concrete slabs. However, this element cannot utilise multi-layer section and is only suitable for uniform thermal action. In this thesis, a multilayer shell element with updated Lagrangian formulation will be introduced and implemented in the analyses involving localised fire action.

• **Material nonlinearity**

For beam-column elements, there are two different approaches to address the material nonlinearity, which are concentrated plasticity and distributed plasticity. The former is usually in the form of beam elements with plastic hinges (Powell and Chen, 1986) or inelastic zones (Coleman and Spacone, 2001; Scott and Fenves, 2006), while the latter is typically implemented using displacement based (DB) or force based (FB) beam elements (Spacone et al., 1996a; Scott et al., 2004), and in conjunction with fibre section model (Taucer et al., 1991; Spacone et al., 1996b; Spacone, 1996). The beam elements with distributed plasticity were adopted to model the beams and columns subjected to fires within OpenSees, considering the location of plastic zone due to fire exposure is arbitrary along the beam and both displacement and force based formulation could produce satisfactory results. Plasticity is thereby distributed to sections which are corresponding to

the numerical integration points, each of them being discretised into a number of fibres. Furthermore, each fibre is assigned with a uniaxial material model, e.g. steel and concrete materials according to the Eurocodes (CEN, 2004, 2005).

For shell elements in OpenSees, material nonlinearity is achieved with a layered section and multi-axial material models. Jiang and Usmani (2013) used a **MembranePlateFiberSectionThermal** with interface to thermal action which was modified from the previously existing **MembranePlateFiberSection** class . However, the section class developed only allows a single material (e.g., concrete) to be assigned, which suggests that an additional thin shell was necessary to be defined to account for the steel reinforcement. FE Models presented in the papers (Jiang and Usmani, 2013; Jiang et al., 2014) adopted an Drucker-Prager material for concrete, along with an variation of Drucker-Prager material for smeared steel shell. Here the variation refers to the removal of hydrostatic Stress part which leads to a Von-Mises type material (J2 plasticity) (Ibrahimbegovic, 2009). Note temperature dependent properties such as material degradation and thermal expansion were included in both the Drucker-Prager type materials.

It is known that a classic Drucker-Prager criterion can be expressed in the following form, with parameters corresponding to OpenSees model:

$$f = \sqrt{2J_2} + \rho I_1 - \sqrt{\frac{2}{3}}\sigma_Y \leqslant 0 \tag{2.37}$$

where J_2 is the second invariant of the deviatoric part of the Cauchy stress, and I_1 is the first invariant of the Cauchy stress. The term ρ is the frictional parameter, while σ_Y is the so-called yield stress which is neither the tensile nor the compressive yielding strength, but as a factor which defines the yield surface. Parameters σ_Y and ρ can be obtained by an uniaxial fitting for the concrete

material:

$$\sigma_Y = 2\left(\frac{\sigma_c \sigma_t}{\sigma_c + \sigma_t}\right); \tag{2.38}$$

$$\rho = \frac{2}{\sqrt{3}}\left(\frac{\sigma_c - \sigma_t}{\sigma_c + \sigma_t}\right); \tag{2.39}$$

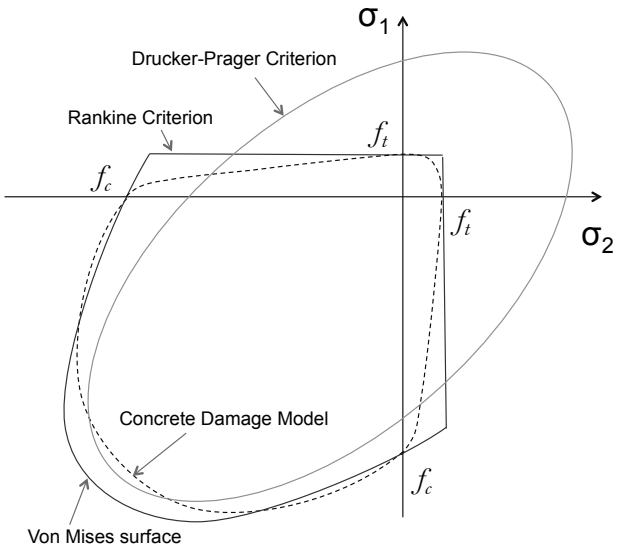

Figure 2.16: Different material models for concrete in 2D plane stress

There exist many other models for concrete which address the unique behaviour of the material such as shown in Figure 2.16 using a plane stress description. A plane stress model in SAFIR which employs a Mises surface combined with a Rankine criterion was used by Talamona (2005) to model concrete slabs in fire. A *Concrete Damaged Plasticity* model (Loret and Prevost, 1986; Lubliner et al., 1989) is widely used in ABAQUS (ABAQUS, 2002), while a few discrete or smeared cracking models for concrete (Hillerborg et al., 1976; de Borst et al., 2004b; Moes et al., 1999) have been used for simulating cracks in concrete. In OpenSees, choices for multi-axial concrete models are rather limited, especially in terms of the models with accessible source code. At ambient temperature, a *Damage2P* model (similar to ABAQUS *Concrete Damaged Plasticity* model) as

well as a plane stress concrete model are reckoned to be more sophisticated models. However, currently the source code is not available for further development.

2.4.3 Thermo-mechanical analyses of beam and columns

Currently there is a rich collection of beam elements in OpenSees that are capable of representing the behaviour of structural members. To model beams and columns in fire, displacement based beam elements in OpenSees were initially chosen to construct finite element models to deal with thermal action (Usmani et al., 2012). A 2D displacement based beam-column element was modified by adding interfaces to elevated temperature and time-variant behaviour, which was achieved using a fibre based beam section (**FiberBeamSection2D**) and several uniaxial materials (**Steel01Thermal**, **Steel02Thermal**,**Concrete02Thermal**) with temperature dependent properties included. To address the geometrical nonlinearity, a corotational transformation is used for beam-column analyses. Moreover, a few different aspects about the beam-column element implementation in OpenSees are discussed in the following review.

• **Corotational transformation**

The corotational theory (Crisfield, 1991) is an approach which decomposes the beam displacements as a combination of rigid body motion and strain-inducing local displacements. This enables the separation of material nonlinearity from the nonlinear geometric response of a frame beam element(Scott and Filippou, 2007).

In the transformation, as shown in Figure 2.17, the displacements of a beam element can be denoted with a vector $\mathbf{p}_g$ in the context of the global coordinate

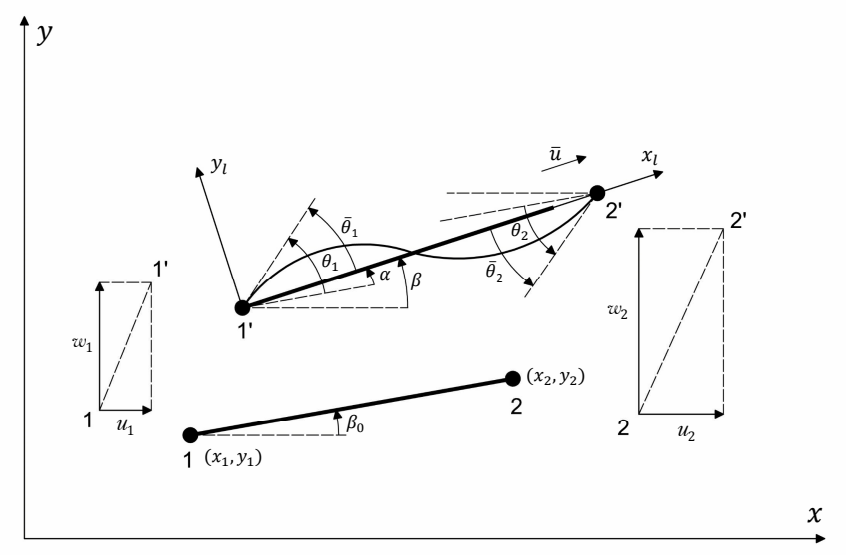

Figure 2.17: Reference and corotational configuration of a typical beam element

system.

$$\mathbf{p}_g = [u_1, w_1, \theta_1, u_2, w_2, \theta_2]^T \tag{2.40}$$

By removing the rigid body displacement modes, the local displacements of the beam element can be derived as:

$$\mathbf{p}_l = \begin{bmatrix} \overline{u} \\ \overline{\theta}_1 \\ \overline{\theta}_2 \end{bmatrix} = \begin{bmatrix} l_n - l_0 \\ \theta_1 - \alpha \\ \theta_2 - \alpha \end{bmatrix} \tag{2.41}$$

where $\overline{u}$, $\overline{\theta_1}$, and $\overline{\theta_2}$ are the longitudinal deformation, beam end rotations of the element in its current local system, respectively. θ_1 and θ_1 are the beam end rotations in the global system, while l_n and l_0 denote the current and initial

lengths of the element, which can be calculated as below:

$$l_0 = \sqrt{(x_2 - x_1)^2 + (y_2 - y_1)^2} \tag{2.42}$$

$$l_n = \sqrt{(x_2 + u_2 - x_1 - u_1)^2 + (y_2 + w_2 - y_1 - w_1)^2} \tag{2.43}$$

and α denotes the rotation of the rigid body:

$$\alpha = \beta - \beta_0 \tag{2.44}$$

in the above equation, β and β_0 are the initial and current angles of the element from the x-axis, respectively, which can be calculated from the corresponding coordinates of the beam end nodes. A detailed description of the Co-rotational formulation can be found from Battini's report (2002).

• **Fibre based section**

A fibre based section has been widely used in beam-column analyses (Taucer et al., 1991; Ceresa et al., 2007; Scott et al., 2008a), where the member section is discretised into a number of fibres with uniaxial materials assigned, as shown in Figure 2.18. In OpenSees, a **FibreBeamSection2D** was first developed to account for the thermally induced deformation (Usmani et al., 2012). Later the 3D beam sections were modified to enable 3D beam-column analyses (Jiang and Usmani, 2013). A no-slip condition is assumed to exist between fibres (Monti and Spacone, 2000) in the current fibre sections based on the plane section remains plane assumption as Euler-Bernoulli beam theory is applicable after removing the rigid-body motion.

For a section located at x in the local coordinate system, the total flexural strain

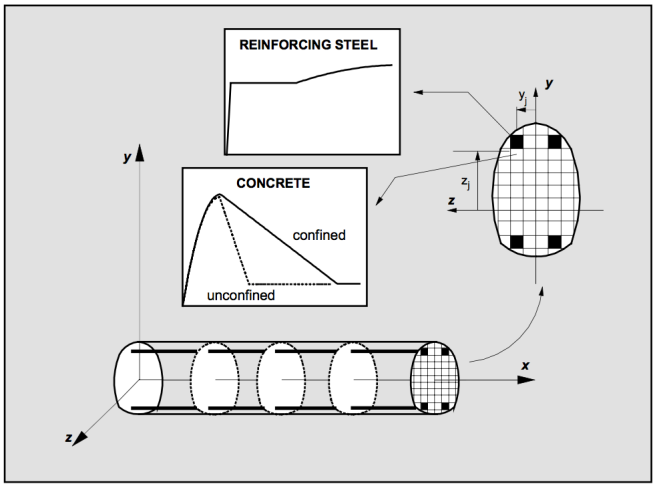

Figure 2.18: Beam section subdivided into fibres (Taucer et al., 1991)

ε_t of a fibre located at (y, z) is derived as:

$$\varepsilon_t = \begin{bmatrix} 1 & -y & z \end{bmatrix} \begin{bmatrix} \varepsilon_0 \\ \phi_z \\ \phi_y \end{bmatrix} = I(y,z)\mathbf{d}(x) \tag{2.45}$$

For a 2D beam element, the strain calculation yields to the following expression:

$$\varepsilon_t = \begin{bmatrix} 1 & -y \end{bmatrix} \begin{bmatrix} \varepsilon_0 \\ \phi_z \end{bmatrix} = I(y)\mathbf{d}(x) \tag{2.46}$$

In the above expression, ε_0 is the normal (longitudinal) strain at the centroid of the section, while ϕ_z and ϕ_y represent the curvature about local y and z axis at the section, respectively. The geometric vector is denoted as a multiplier $I(y, z)$ or $I(y)$, and $d(x)$ wraps the section deformation.

Furthermore, the thermal elongation of the fibre should be taken into account if its temperature is elevated. The thermal strain ε_{th} is given by the material model

assigned to the fibre, and updated in each load step for thermal action. As the fibre's total strain is calculated, the mechanical strain ε_m then can be computed by cancelling the thermal strain from it:

$$\varepsilon_m = \varepsilon_t - \varepsilon_{th} \tag{2.47}$$

Here for simplifying the expression, the following discussion would be presented for a 2D beam, which is usually deployed to solve the uniaxial bending problem. In accordance with the virtual work principle, calculating the the section stiffness $k(x)$ would follow the integration:

$$\mathbf{k}(x) = \int_{A(x)} I^T(y) E(x,y) I(y) dA \tag{2.48}$$

where E(x,y) is the tangent material modulus. The above expression of section stiffness can be reshaped as assembling the stiffness contribution from all the fibres:

$$\mathbf{k}(x) = \begin{bmatrix} \sum \left(E_{fi} \cdot A_{fi} \right) & -\sum \left(E_{fi} \cdot A_{fi} \cdot y_{fi} \right) \\ -\sum \left(E_{fi} \cdot A_{fi} \right) & \sum \left(E_{fi} \cdot A_{fi} \cdot y_{fi}^2 \right) \end{bmatrix} \tag{2.49}$$

where E_{fi} and A_{fi} are the stiffness and the area of each fibre, respectively. $E_{fi} \cdot A_{fi}$ marks the longitudinal modulus of the fibre, and y_{fi} indicates the lever arm of the contribution.

• Displacement based VS. force based formulation

For beam-column elements formulated using distributed plasticity, there are commonly two different methods to determine the state of element. One is based on interpolation functions for the elemental displacements and referred to as the displacement-based formulation (stiffness method), while the other is based on

interpolation of the internal forces and known as the force-based formulation (flexibility method) (Spacone et al., 1996b; Spacone, 1996).

If a beam-column element is formulated using displacement interpolation, linear Lagrangian shape functions are usually adopted to obtain the generic axial displacements, and cubic Hermitian polynomials are adopted for transverse displacements. Note this interpolation scheme leads to a strain field which consists of a constant axial strain along the neutral axis and a linearly distributed curvature along the length. For an arbitrary section of the element, the relationship between section deformation and force increments in vector notation can be given as:

$$\Delta \mathbf{D}(x) = \mathbf{k}(x)\Delta \mathbf{d}(x) = \mathbf{k}(x)\ \mathbf{B}(x)\Delta \mathbf{q} \tag{2.50}$$

where $\mathbf{d}(x)$ and $D(x)$ denote the deformation and force vectors of a section, respectively. A Δ ahead of the terms indicates the increments of the corresponding quantities. $\mathbf{B}(x)$ represents the displacement interpolation functions for section deformation, which contains first and second derivatives of the displacement shape functions (Neuenhofer and Filippou, 1997). The stiffness matrix of an arbitrary section is denoted as $\mathbf{k}$. Thus at the element level, the governing equations are given as:

$$\mathbf{K}\Delta \mathbf{q} = \mathbf{R} \tag{2.51}$$

where $\mathbf{R}$ is the residual force, $\mathbf{K}$ is the element stiffness, given as:

$$\mathbf{K} = \int_0^L \mathbf{B}^T(x)\mathbf{k}(x)\mathbf{B}(x)\mathbf{d}(x) \tag{2.52}$$

If force based interpolation is adopted to formulate a beam-column element, interpolation functions are applied to the force field, which assumes a constant axial

force and linearly distributed bending moments along the length. Section deformation is then obtained as the section force is given. In OpenSees, since the global solution is based on nodal displacements, the force-based element is formulated in a mixed way (Spacone et al., 1996a; Alemdar and White, 2005), which receives trial displacements to initialise the state determination. Therefore nodal forces are first calculated in the element using the trial displacements, which is followed by another interpolation to obtain section forces. Considering that a numerical integral of section deformation may not match the trial displacements, a Newton type iteration is therefore used to obtain the section response. An incremental description of section force-deformation relationship based on flexibility method can be given as:

$$\Delta \mathbf{d}(x) = \mathbf{f}(x)\Delta \mathbf{D}(x) = \mathbf{f}(x)\mathbf{b}(x)\mathbf{Q}(x) \tag{2.53}$$

where $\mathbf{f}(x)$ in the above equation represents the section flexibility, and $\mathbf{Q}(x)$ the resisting force of the element. Force interpolation functions are embedded in the matrix $\mathbf{b}(x)$. The elemental equilibrium equation is similar to Equation (2.51) but with $\mathbf{K}$ replaced by $\mathbf{F}^{-1}$, in which $\mathbf{F}$ is the flexibility matrix:

$$\mathbf{F} = \int_0^L \mathbf{b}^T(x)\mathbf{f}(x)\mathbf{b}(x)\mathbf{d}(x) \tag{2.54}$$

The earlier development(Usmani et al., 2012) for beams and columns in fire was carried out using displacement based beam-column elements (Scott et al., 2008a). This was appropriate in practice as a longitudinally uniform distribution of the temperatures was assumed (Usmani et al., 2012; Jiang et al., 2015). The benefits of force-based approach were understood when localised fire action was considered in modelling beams columns in fire. With force based formulation, the beam-column element is able to describe a non-uniform distribution of section

deformation along the length, and the elemental force equilibrium is still satisfied. The implementation of beam-column elements for non-uniform thermal action will be discussed in Chapter 4 of this thesis.

2.4.4 Thermo-mechanical analysis of floor slabs

As reviewed earlier, it is necessary to include concrete slabs when modelling the steel and composite structures in fire. The theory of mixed interpolation technique was introduced by Bathe and Bolourchi (1980) and discussed in terms of implementation by Bucalem and Bathe (1997). For thin shells, a formulation based on the discrete-kirchhoff approach was also mentioned in the paper (Jürgen Bathe et al., 1983) which ignored the shear deformation through thickness for simplicity. In OpenSees, Jiang adapted the **ShellMITC4** element to consider thermally induced behaviour (Jiang, 2012b), and applied the modified element to model a composite floor system in fire (Jiang et al., 2014). Here a brief review on formulating MITC4 type shell element is presented. The element consists of four nodes, using isoparametric bilinear shape functions, as shown in Figure 2.19.

• Generic displacement

Each node connected to the shell element possesses 6 degrees of freedom, including 3 translational displacements and 3 rotations:

$$u_i = \{\mu_i, \nu_i, \omega_i, \theta_{xi}, \theta_{y_i}, \theta_{zi}\}^T \tag{2.55}$$

The classic Reissner-Mindlin plate hypothesis is employed to describe the generic

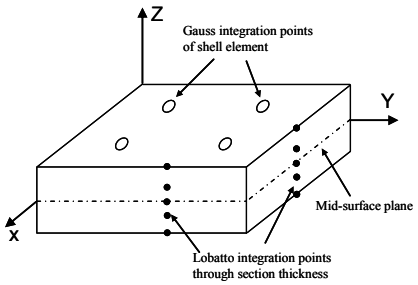

(a) Integration scheme of shell element

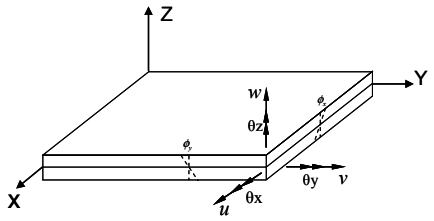

(b) Nodal degrees of freedom

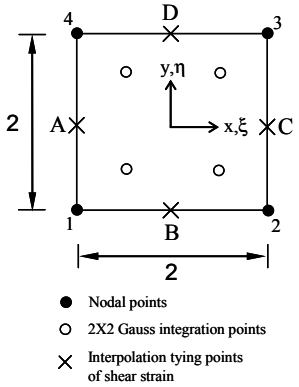

(c) Geometry of 2×2 element

Figure 2.19: Geometry of a four-node shell element in the x,y plane (Jiang, 2012a)

displacement inside the shell element,

$$\mu(x, y, z) = \mu^0(x, y) - z\theta_x^0(x, y) \tag{2.56a}$$

$$\nu(x, y, z) = \nu^0(x, y) - z\theta_y^0(x, y) \tag{2.56b}$$

$$\omega(x, y, z) = \omega^0(x, y) \tag{2.56c}$$

◦ Isoparametric shape functions

Bilinear shape functions are adopted for deriving the generic coordinates at the

mid-surface from the nodal coordinates:

$$x = \sum_{i=1}^{4} N_i x_i \tag{2.57a}$$

$$y = \sum_{i=1}^{4} N_i y_i \tag{2.57b}$$

where N_i repreenting the bilinear shape functions are normally given as:

$$N_1 = \frac{(1-\xi)(1-\eta)}{4} \tag{2.58a}$$

$$N_2 = \frac{(1+\xi)(1-\eta)}{4} \tag{2.58b}$$

$$N_3 = \frac{(1+\xi)(1+\eta)}{4} \tag{2.58c}$$

$$N_4 = \frac{(1-\xi)(1+\eta)}{4} \tag{2.58d}$$

Isoparametric concept was used in applying the same shape function to interpolate the generic in-plane displacements from the nodal displacement tensor:

$$u^0 = \sum_{i=1}^{4} N_i u_i^0 \tag{2.59}$$

∘ MITC shear strain replacement

The simplified expression of Green's strain for shell elements is normally given as:

$$\varepsilon = \left\{ \begin{array}{c} \varepsilon_x \\ \varepsilon_y \\ \gamma_{xy} \\ \gamma_{xz} \\ \gamma_{yz} \end{array} \right\} = \left\{ \begin{array}{c} u_{,x} + \frac{1}{2}(w_{,x}^2) \\ v_{,y} + \frac{1}{2}(w_{,y}^2) \\ u_{,y} + v_{,x} + w_{,x} w_{,y} \\ u_{,z} + w_{,x} \\ v_{,z} + w_{,y} \end{array} \right\} \tag{2.60}$$

where the subscripts denote the derivative with respect to x or y.

The MITC approach features the replacement of shear strains to avoid the shear locking (Bathe and Bolourchi, 1980; Bucalem and Bathe, 1997). Instead of directly deriving them from the generic displacement, the transverse shear strains are suggested to be interpolated from the physical shear strains: $\gamma_{\eta z}^{A}$,$\gamma_{\xi z}^{B}$,$\gamma_{\eta z}^{C}$,$\gamma_{\xi z}^{D}$. The locations of A, B, C, D have been shown in Figure 2.19, and the corresponding strains can be obtained according to the Equation (2.60).

$$\gamma = \left\{ \begin{array}{c} \gamma_{\xi z} \\ \gamma_{\eta z} \end{array} \right\} = \frac{1}{2} \left\{ \begin{array}{c} (1-\eta)\gamma_{\xi z}^{B} + (1+\eta)\gamma_{\xi z}^{D} \\ (1-\xi)\gamma_{\eta z}^{A} + (1+\xi)\gamma_{\eta z}^{C} \end{array} \right\} \tag{2.61}$$

◦ Governing equation

The governing equation of MITC4 shell element is sought to be derived from the potential energy, which can be established in the following form:

$$\Pi = \frac{1}{2}\int_{V} \varepsilon^{T}\sigma dV + \frac{1}{2}\int_{V} k_{\theta}(\omega - \theta_{z})^{2} dV - \int_{V} u^{T} f dV \tag{2.62}$$

where the first term on the right-hand represents the strain energy, in which σ is the stress vector. The second term represents the strain energy corresponding to the drilling degrees of freedom.

$$\int_{V} d\mathbf{B}^{T}\sigma dV + (\int_{V} \mathbf{B}^{T}\mathbf{D}\mathbf{B} dV)du + (\int_{V} \mathbf{B}_{dr}^{T}\mathbf{k}_{\theta}\mathbf{B}^{dr}]dV)du = d\{\mathbf{F}\} \tag{2.63}$$

where $\{F\} = \int_{V} f dV$ is the equivalent elemental load. The governing equation

can be rearranged in the form as:

$$(\mathbf{K}_M + \mathbf{K}_\sigma + \mathbf{K}_D)d\mathbf{u} = \mathbf{K}_T d\{\mathbf{F}\} \tag{2.64}$$

where $\mathbf{K}_M$ is referred to the material matrix; $\mathbf{K}_\sigma$ is the representation of the geometric matrix; $\mathbf{K}_D$ accounts for the drilling stiffness. These components comprise the tangent stiffness matrix $\mathbf{K}_T$, and can be correspondingly derived from the Equation (2.63) and written as:

$$\mathbf{K}_M = \int_V \mathbf{B}^T \mathbf{D}\mathbf{B} dV \tag{2.65a}$$

$$\mathbf{K}_D = \int_V \mathbf{B}_{dr}^T \mathbf{k}_\theta \mathbf{B}_{dr}] dV \tag{2.65b}$$

$$\int_V d\mathbf{B}^T \sigma dV = \mathbf{K}_\sigma du \tag{2.65c}$$

2.5 Concluding remarks

This chapter has reviewed the recent advances in describing fire behaviour and structural response to fire, as well as the numerical approaches developed for modelling such issues. Concluding remarks based on the literature review are made as follows:

- It has been suggested by recent researches that it is necessary to consider the spatial difference of gas temperature field in large compartment fires, which turns out to be more necessary in the cases of localised fires that can never develop to flashover stage. There has been a significant amount of work aiming to propose reasonable numerical descriptions for fires, which include the localised fire and travelling fire models. Although these models

are developed based on many assumptions, it is considered to be more realistic compared to the traditional uniform gas temperature models from a performance based point of view.

- This thesis will mostly discuss the structural response to different idealised non-uniform fires, which can be defined according to Eurocode or SFPE hand book as reviewed in this chapter, allowing for non-uniform spatial distribution of incident heat fluxes. Theses fire models will be implemented in OpenSees and automatically applied as boundary conditions for heat transfer analyses.

- Conventionally, a three-dimensional heat transfer model is employed to perform heat transfer analysis for structural members subjected to localised fires, which consumes significant amount of computational resources and increases the complexity of interacting with the structural model. An alternative approach is using 2D models which has been proposed, but with little quantitative investigation. Therefore it is necessary to quantitatively discuss the feasibility of implementing dimensionally reduced heat transfer analyses for beams and slabs involving localised fire action, which will provide a guidance to economically and efficiently performing heat transfer analysis.

- Steel beams and slabs in uniform fires have been extensively studied, with numerous findings in understanding their thermo-mechanical responses. Attention has also been paid to the whole frame structural behaviour in fire. Investigations of the load bearing mechanism of composite structures in fire are inspired by Cardington fire tests and have been numerically and experimentally conducted, which identified that the membrane action of

composite slab systems experiencing large deflections could significantly improve the ultimate fire resisting performance. Concerns are also raised towards the effect of non-uniform heating, which may be caused by localised fire action or partial damage of fire protection. In order to model structural responses to non-uniform heating, finite element solutions need to be adapted while further development should be carried out in OpenSees. Displacement based and force based beam elements should be employed to model the steel or reinforced concrete beams, where modifications are necessary to be made to account for non-uniform total strain distribution. For slabs subjected to localised fire action, shell elements based on MITC techniques and layered shell sections should be developed.

- The complexities of modelling structures in fire as a coupled problem include the implementation of non-uniform fire models, different model scales for heat transfer and thermo-mechanical analysis, and the data communication from fire modelling to heat transfer analysis to thermo-mechanical analysis. To overcome these obstacles, an integrated computational environment could substantially simplify the modelling process and would be favoured by structural engineers who design buildings against fires. Such a tool shall be designed to minimise user input and able to automate interaction between different modules. In this thesis, the final part of work will be integrating different modules and providing an OpenSees based computational modelling tool, as well as a few example cases to demonstrate the usage of this tool.

Chapter 3

Dimensional reduction of heat transfer analysis for structural members subjected to localised fire action

3.1 Introduction

The commonly used assumption of uniform gas temperature in the compartment is very convenient from the point of view of simple and efficient modelling of heat transfer into the solid boundaries of the compartment and the structural members. The uniform temperature assumption allows the problem of heat transfer to be reduced from a 3D problem to a 2D problem for beams on ceilings and for any columns; and only a one dimensional (1D) problem for floor and ceiling slabs and

for walls. However for spatially non-uniform and localised fires a full-blown 3D analysis seems to be unavoidable. This is not only computationally expensive but also makes the problem much more tedious for the analyst in terms of setting up full 3D models and meshing and therefore discourages the use of more realistic fires and performance based engineering solutions. To overcome this problem some researchers proposed alternative solutions, for example, it is suggested by Franssen et al. (2007) that a series of 2D analyses performed at various locations along the length could adequately describe the thermal response of a steel beam subjected to a localised fire. This idea could potentially also be extended to the heat transfer analysis of concrete slabs and walls, where a series of 1D analyses over the area of the slab/wall may be adequate as the temperature gradients parallel to the surface of the wall are likely to be much lower than the temperature gradients normal to the surface even for localised heat fluxes (hence heat transfer normal to the surface should remain dominant). Heat transfer and structural analyses are presented by Jeffers and Sotelino (2009, 2012); Jeffers (2013), which increased the computational efficiency and also reduced the model setting up time. This approach however requires a significant time investment into programming beam and shell type heat transfer elements in existing software. This chapter attempts to investigate whether this effort is absolutely necessary, or the original suggestion of a simplified approach of dimensional reduction (Franssen et al., 2007) is adequate for most realistic fire scenarios expected in compartments of modern buildings.

Meanwhile, an integrated computational tool as mentioned before is to be developed for researchers to run large structural model under a large range realistic fire scenarios thereby producing greater insights into the nature of the fire hazard in buildings and the resilience of modern architecture and structural

systems to it. The natural progression beyond this would involve using this efficient tool to explicitly account for uncertainties by integrating a probabilistic analysis layer (this already exists within the OpenSees framework). To bring this vision to fruition it is essential to investigate the feasibility of dimensional reduction for heat transfer analysis in structures subjected to realistic fires.

As the structural members are discussed with exposure to localised fire action, fire protection has not been taken into account yet. For a fireproof material protected member, temperature rise caused by localised fire action is certainly lower than bare members. In the work presented by Franssen et al. (2007), a few steel plates (5-40 mm thick steel plates protected with a 20 mm thick fireproof layer) submitted to discontinuous heat flux exposure were considered to be protected by a hypothetical product. During the exposure, steel temperatures showed a smooth transition from the heated zone to the unheated zone, where the maximum of temperature could only reach approximately 420^oC after two hours of exposure to the standard fire. However, more concerns have been raised for the structural members with partial fire protection, which could be deliberately designed as the partially protected composite beam (Wang, 1998), or caused by partial loss due to the impact loading or large deformation in the member (Dai et al., 2009; Wang and Li, 2009). For the partially unprotected surface which absorbs heat from a fire, localised response would be inevitable.

The key aim of this chapter is to accurately estimate the error induced by dimensional reduction under highly varying localised heat fluxes representative of the most non-uniform fire conditions in a building compartment, excluding hydrocarbon or jet fires. Firstly two 2D blocks (concrete and steel) are applied with a number of idealised distribution patterns of input heat fluxes. The 1D

and 2D temperature results are compared and analysed to help identify the key aspects that cause errors after applying dimensional reduction to heat transfer analysis. Using the same approach, the effect of partial damage to passive fire protection is discussed with a conclusion that dimensional reduction scheme may be only used for uniform fires. Furthermore, temperature errors between full-blown 3D and dimensionally reduced (2D or 1D) analyses for beams and slabs are presented, where localised fire models according to Eurocode and SFPE handbook are applied. This is followed by the discussion about a fast estimation through rationally interpolating heat transfer results at several selected sections. By doing so the computational cost for performing heat transfer analysis to localised fire action could be further reduced although with little compromise in accuracy. The whole implementation then enables a fast but comprehensive evaluation of the fire safety of a structure. A rich collection of fire scenarios (localised fires) could be quickly checked with respect to the full structural response, which is ultimately preferred from the perspective of performance based design.

3.2 Localised fire Action

3.2.1 Localised fire models

Localised fire models in Eurocode 1 and SFPE hand book have been reviewed in Chapter 2. The Eurocode 1 model implies that the localised heat flux distribution is dependent upon the HRR, the burner dimensions and the ceiling height. In Figure3.1 the variation of the heat flux has been plotted against distance from the centre of fire for a range of fire loads represented by the HRR Q and the diameter

D of the burner for a ceiling height of 3.0m. Based on this plot the heat flux is increasingly linearly correlated to the radial distance to fire origin as the heat release rate increases. It is also worth noting that the heat flux plateaus at 100 kW/m^2 according to Eurocode 1.

Similarly, heat flux distributions derived from SFPE fire model can be plotted in terms of different parts of beam member. As presented in Figure 3.2, the localised fire is located underneath a 0.3m deep beam, while the ceiling height is set as 3.0 m. The rate of heat release from the fire source has been assumed as 1 MW, with a diameter as 0.5 m. It is observed that the ceiling and downward face of lower flange receive higher external heat fluxes than the rest parts of beam near the fire origin, whereas at the far end the upper face of lower flange and the web are impacted by slightly higher heat fluxes compared to the downward face of lower flange.

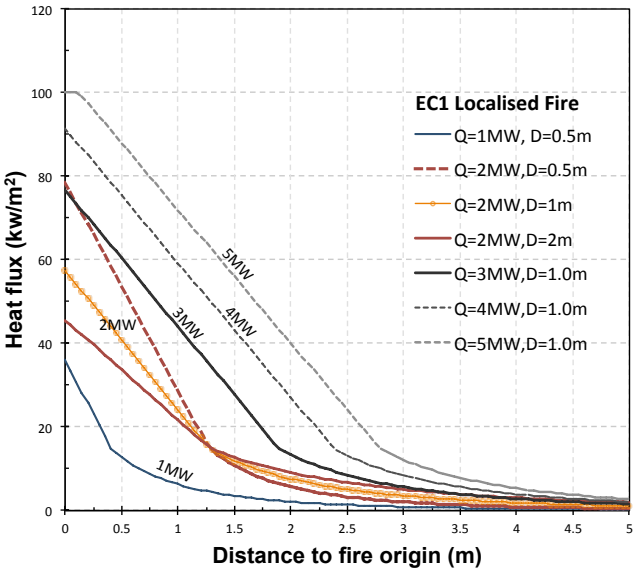

Figure 3.1: Localised heat flux based on EC1 localised fire model

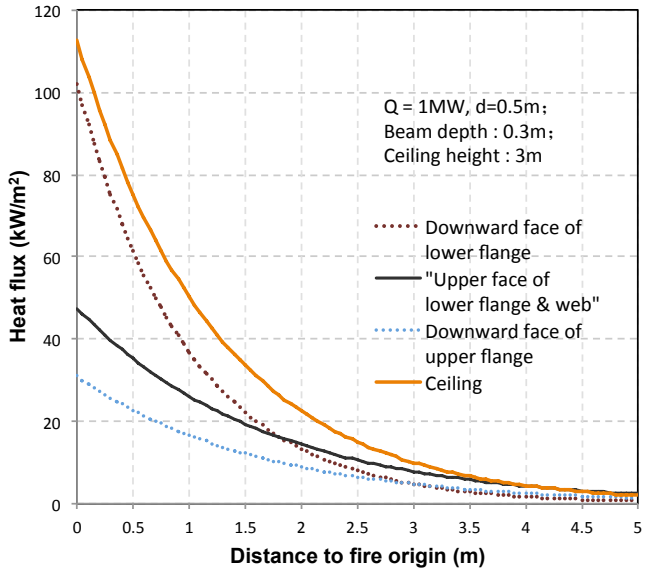

Figure 3.2: Localised heat flux based on SFPE localised fire model

3.2.2 Idealisation of localised heat fluxes

The representations of localised fires can potentially be generalised as a combination of one or more idealised correlations (for example see Figure 3.3) of localised heat flux and distance from fire origin. When an idealised flux distribution varies sharply along the length of a structural member, the influence of conduction within the body of the structural member perpendicular to the incident flux on the surface may become significant. To investigate this quantitatively we use a two dimensional (2D) rectangular block as an idealisation of a structural member and subject it to a set of idealised distributions of localised heat fluxes. The idealised distributions chosen are based on the distributions recommended by SFPE and Eurocode 1 and are tabulated in Table A.1 and plotted in Figure 3.3.

The idealised distributions showing a linear and exponential decay (similar to SFPE model) represent the most common heat flux variations in recommended

Table 3.1: Expressions of artificially localised heat flux correlation

Pattern	**Heat flux** $q''(x)$ (kW/m^2)
Linear	$100 - 50x$
Bilinear	$100 - 100 < x - 1 >$
Exponential	$100e^{-4x}$
Quadratic_0.25	$25x^2 - 100x + 100$
Quadratic_0.75	$-25x^2 + 100$

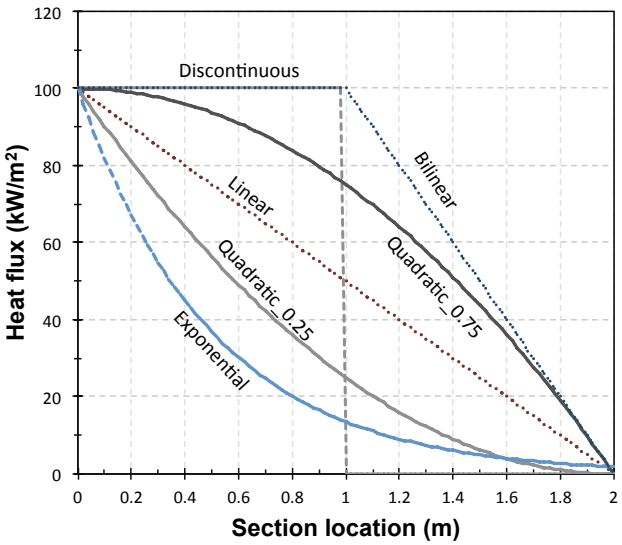

Figure 3.3: Idealised heat-flux distributions

localised fire models. A discontinuous or discontinuous heat flux distribution will be used as an extreme limiting case. In addition to the previous three cases, two quadratic distributions will also be used to ensure that a full range of possible heat flux distributions is accounted for and that the conclusions from the study are robust.

3.3 Study of heat transfer in a 2D rectangular block subjected to a localised fire

It is an intuitive assumption that localised fires should require a full 3D heat transfer analysis for accurate resolution of temperatures in structural members. However, the premise of this chapter is that the error introduced by using 2D or 1D (where appropriate) models may be adequate in the context of most building fires of practical interest. As mentioned earlier a 2D rectangular block will be used to represent a structural member which will be subjected to the idealised heat fluxes identified in the previous section in order to quantify the magnitudes of error introduced by dimensional reduction.

Two rectangular blocks representing concrete and steel structural members are shown in the Figure 3.4. The steel block, representing the flange or web of a steel beam, is assumed to experience fire exposure on a single face from the localised heat flux and with no heat loss at the unexposed surfaces. The concrete block also experiences one-sided fire exposure but it is assumed to lose heat through convection and radiation to the ambient air from both the upper and lower faces.

Both blocks are 2 m long. The depth or thickness of the concrete block is 100 mm and that of the steel block is 10mm. The material properties for the steel block are defined as Eurocode 3 (CEN, 2005) corresponding to carbon steel, while concrete has been defined according to Eurocode 2 (CEN, 2004) for normal weight siliceous concrete with zero moisture ratio. To investigate the error caused by dimensional reduction, the results from 2D heat transfer analyses of the blocks are compared with 1D analyses at various section locations along the length of the block. The

error is normalised as,

$$\eta = (\Theta_{1D} - \Theta_{2D})/\Theta_{2D} \tag{3.1}$$

Using the above models, the feasibility of dimensional reduction will be investigated for a range of heat flux patterns, material properties and duration of the exposure.

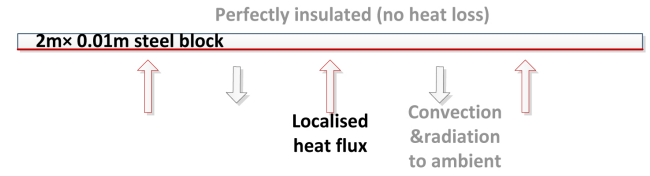

(a) Steel block

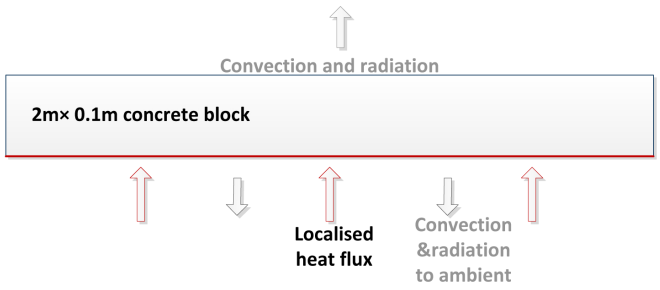

(b) concrete block

Figure 3.4: Configuration of 2D blocks investigating effect of localised heat flux

3.3.1 Application of ideally localised heat fluxes

Equation (2.12) represents a universal approach for estimating the net heat flux received at the surface of a solid and will be used to analyse the steel and concrete block models described above. The convective heat transfer co-efficient is set to $35W/m^2/K$ based on Eurocode 1 and the resultant emissivity is set to 0.7 for both concrete and steel based on Eurocodes 2 and 3 respectively. For the

unexposed face of the concrete block the convective heat transfer co-efficient is fixed to $4W/m^2/K$ as Eurocode1 suggests when radiation is taken into account independently. The heat transfer analyses are carried out for an exposure of 30 minutes (1800s) using a constant time step of 30 seconds. The reason for restricting exposure time to 30 minutes is that steady state is approached even for the extreme case of the discontinuous flux distribution, as shown in Figure 3.6. Furthermore, it is practically unlikely for a localised fire to burn at a single location in compartment for over 30 minutes. It usually develops into flashover or begins to decay over this period of time (Drysdale, 2011b).

3.3.2 Aspects influencing the heat transfer results

There have been several aspects discussed as they are potentially influencing the heat transfer results, which include the time effect addressing the duration of fire exposure, thermal conductivity of material as the major factor driving the heat conduction, and the choice of finite element tools using for heat transfer analysis.

∘ *Time effect*

The contour plots of the temperature profile after a 30 minute exposure to a number of localised heat fluxes are presented in Figure 3.5. The upper slender plots represent the steel block and the lower fatter plots represent the concrete block. As expected, the discontinuous flux produces the most abrupt transition of temperatures while the blocks subjected to linear and exponential distributions of incident heat flux produces much smother transitions. The heated region in the concrete block is concentrated close to the exposed face, again according to expectations, with a significant thermal gradient establishing through the depth for the member.

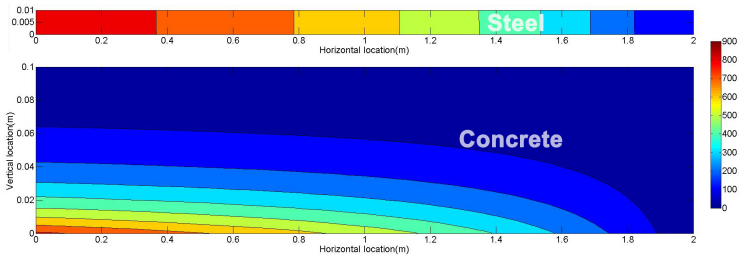

(a) Linear

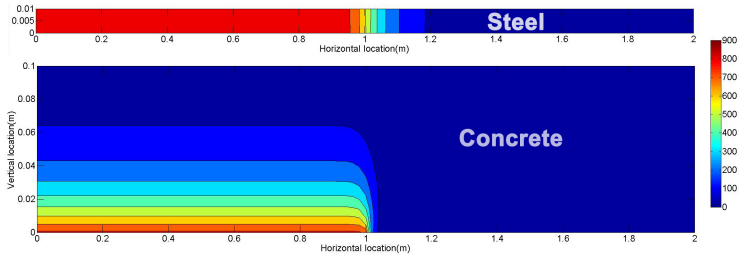

(b) Discontinuous

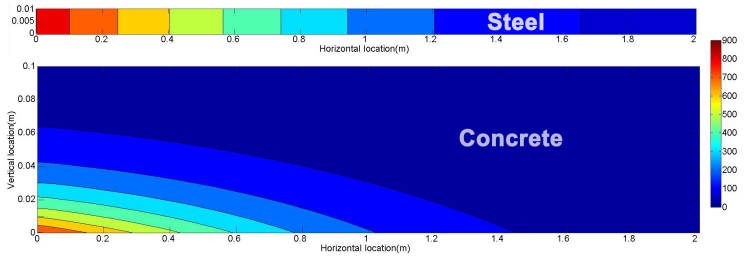

(c) Exponential

Figure 3.5: Thermal response to the Idealised heat flux input

∘ *Thermal conductivity*

Figure 3.6 shows the transition from the hot left portion of the steel block to the cool right portion (when exposed to the discontinuous heat flux) and reflects the heat conduction in the longitudinal direction, which depends upon the thermal conductivity of the material in that direction. A simple numerical test is performed by varying the thermal conductivity in order to understand the effect of this parameter. The simulated transitions are illustrated in Figure 3.7,

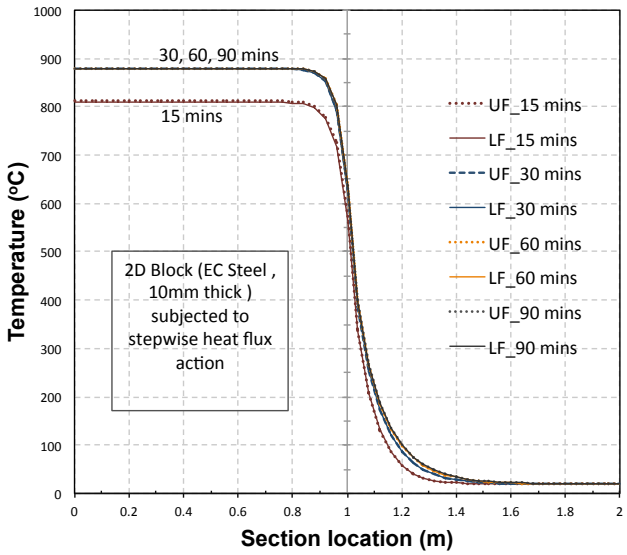

Figure 3.6: Time effect in the HT analyses with discontinuous heat flux action

from where it can be observed that the discontinuous distribution is smoothed-out considerably as the thermal conductivity is increased to values nearly ten times that of carbon steel. The inset plot inside Figure 3.7 shows the normalised temperature difference, which can be used as a measure of the reliability of dimensional reduction, and will be used frequently in the following sections. In this case the plot shows that in the vicinity of the discontinuity, 1D analyses will certainly fail to simulate the temperature distributions.

◦ *Choices of FE Software*

Heat transfer analyses presented in this chapter are conducted using OpenSees. The heat transfer module developed in OpenSees has undergone validation against analytical solutions as well as experimental results (Jiang et al., 2011; Jiang, 2012b). For this chapter, an OpenSees analysis is compared with an Abaqus analysis of heat transfer in a concrete block subjected to localised heat flux exposure, as presented in Figure 3.8. The comparison is also based on the 2D concrete block, and linear and exponential heat flux distributions are

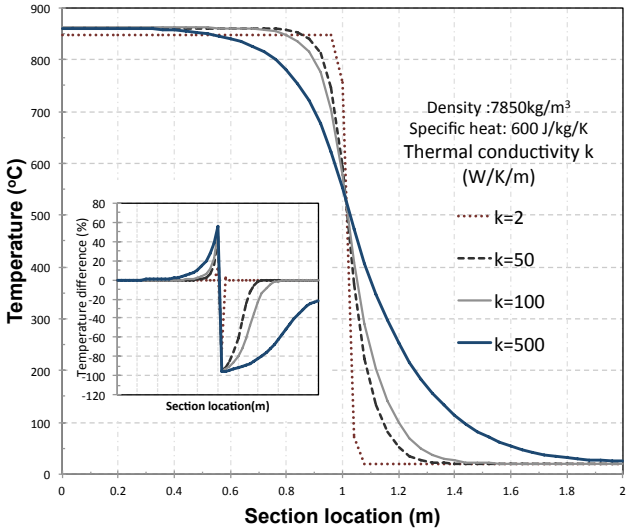

Figure 3.7: The effect of thermal conductivity in the HT analyses with discontinuous heat flux action

applied respectively. The results show that the two softwares produces identical temperature distribution.

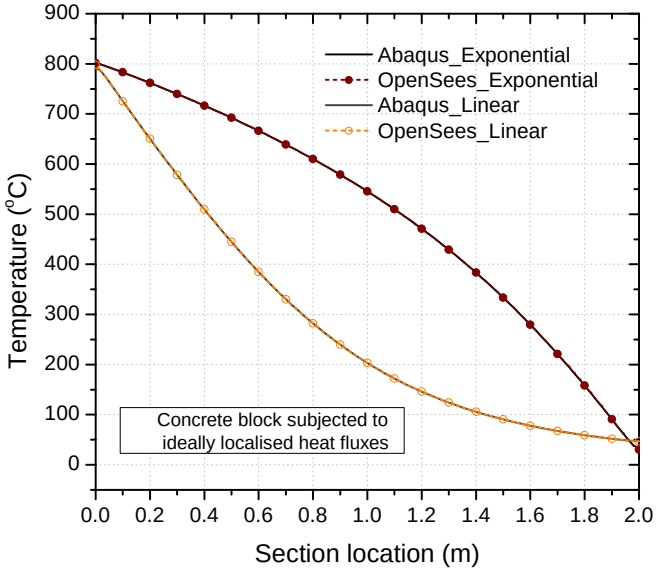

Figure 3.8: Heat transfer analyses conducted with different FE softwares

3.3.3 Analysis of the heat transfer results from the simple model

The normalised errors, as defined in Equation (3.1), are plotted for the steel block subjected to various heat flux patterns as shown in Figure 3.9. The discontinuous heat flux produces the greatest errors as expected compared to the 2D analysis, however this is an artificial situation and cannot really occur in practice. Nevertheless, it is interesting to note that even for this extreme situation the error on the hotter left hand side rapidly decays to being negligible, while the error on the right hand side does not have practical significance as the temperatures are too low. The next highest error occurs for the quadratic_0.75 case at the right hand end of the block. This higher magnitude of error at the right hand end also occurs for all the other distributions. The lowest error at the end is produced by the exponential curve, as the heat flux is much lower close to the end because of the nature of the distribution. It can therefore be concluded that error in the 1D analysis temperature distributions is only significant near the tails of the localised distributions chosen, where the temperatures are too low to be significant from a design perspective.

The normalised errors are also examined for concrete block. The errors at the top surface of the concrete block are plotted in Figure 3.10 while those at the bottom surface are presented in Figure 3.11. The greatest error appears in the case of the discontinuous distribution. It is also apparent that the rest of the distributions all produce an error at the right hand end as observed from the response of the steel block, and this effect is more severe at the bottom surface. Even though the highest value of normalised error is approximately 50% in case of quadratic_0.75, it wouldn't be of much practical significance as the temperature in the region is

low (around 40^oC), moreover the end errors are highly localised in the cool region of the block.

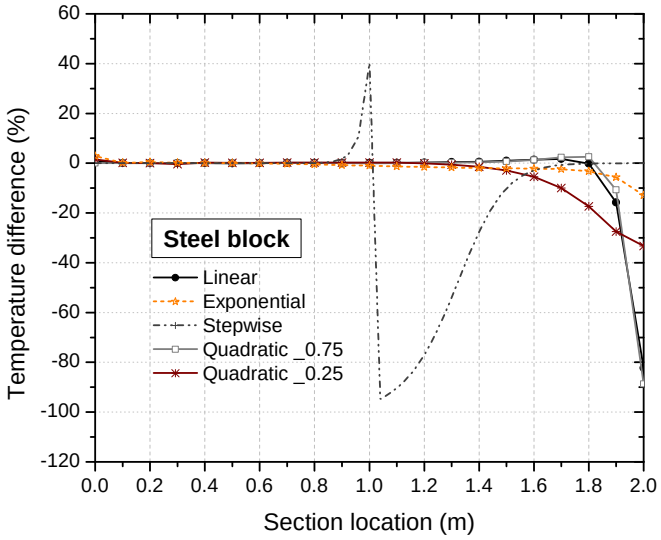

Figure 3.9: 1D/2D temperature difference in the steel block

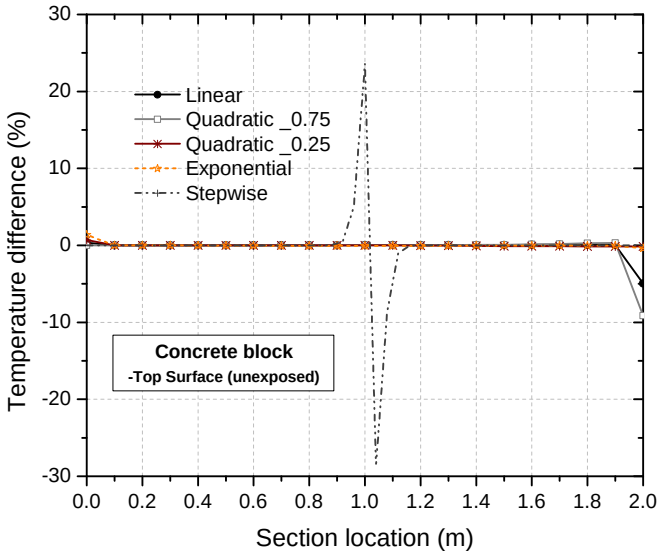

Figure 3.10: 1D/2D temperature difference at the top face of the concrete block

An explicit cause to the error between 1D and 2D results is the unbalanced heat conduction along the length of blocks (longitudinal direction). Here the intensity of heat flow has been visualised with Figure 3.12, which shows the

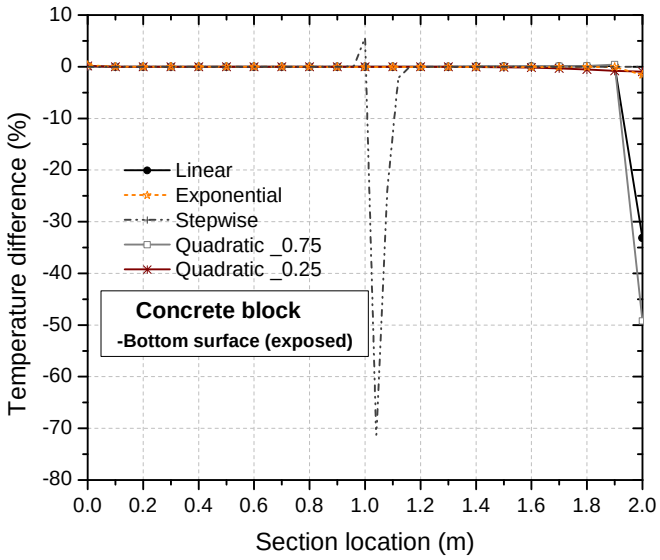

Figure 3.11: 1D/2D temperature difference at the bottom face of the concrete block

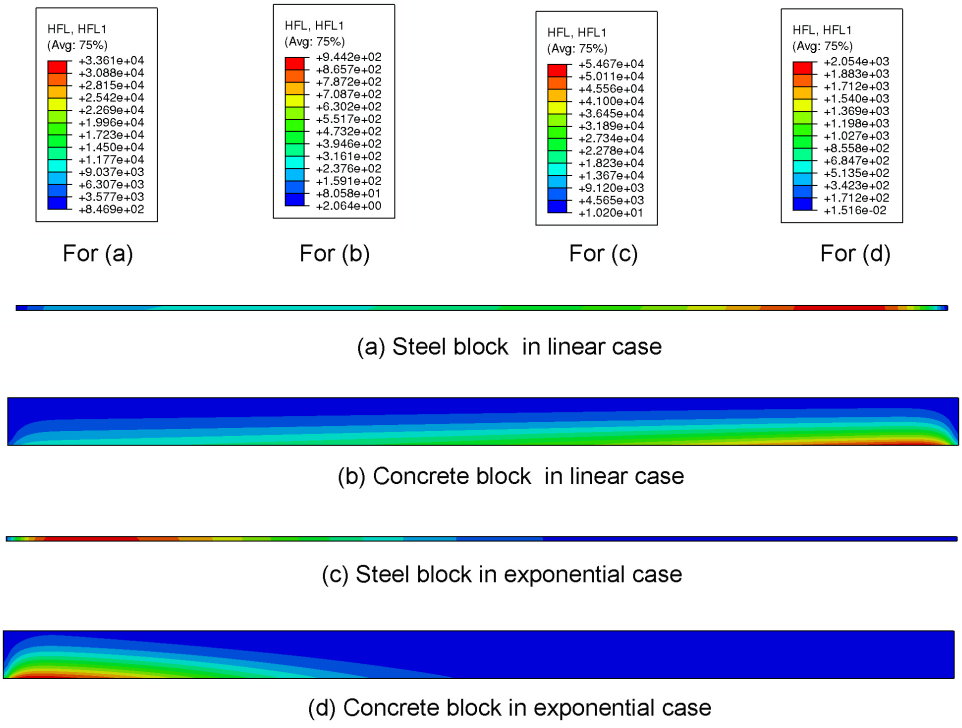

Figure 3.12: Heat transfer analyses conducted with different FE softwares

internal heat fluxes along the length (HFL1) of the steel or concrete block when linearly or exponentially distributed heat fluxes are applied, respectively. The plots are extracted from ABAQUS as an output from the validation analyses earlier mentioned. In the case of linear pattern, the along-length heat flux reaches its peak near the cool end of the block, and then rapidly dropping to zero as it hits the insulated boundary condition. Thus for each sampling section (1D) of the 2D block, it receives higher heat flux input but with lower heat flux streaming out, which leads to an underestimated temperature result from 1D section analysis compared to the 2D result. In contrast to the linear case, the maximum of along-length heat flux appears near the left end of the block when exponential pattern is applied. This is driven by the dramatic decay of external heat flux input. The internal heat flux starts from zero at the edge and increases to the peak value $5.467 \times 10^4 W/m^2$ in the steel block, which is 60% higher than the linear case ($3.361 \times 10^4 W/m^2$). However, the relatively high heat flux (indicating slightly high temperature error) could not lead to large normalised error because of a much higher base temperature at the hot zone. An extra finding from Figure 3.12 is about the concrete blocks, which have shown similar patterns of heat flux distribution as steel blocks but with considerably lower values, as a product of lower thermal conductivity.

3.4 Study of heat transfer considering the effect of passive fire protection

3.4.1 Thermal properties of SFRM

Here the passive fire protection is assumed to be a thermal barrier of specified thickness, such as a Spray-applied Fire Resistive Material (SFRM). As a type of passive fire protection, SFRM has been widely used to insulate the steel members from direct exposure to fire (Dwaikat and Kodur, 2011), with unique properties such as light weight and low thermal conductivity. However, as pointed out by Kodur and Shakya (2013), there is precious little public domain information available on the thermal properties of SFRM. The work reported by Franssen et al. (2007) adopted a hypothetical material to represent passive fire protection, of thermal conductivity $\lambda = 0.08W/m/K$, and volumetric heat capacity $c_p\rho = 0.08W/m/K$ (denoted as Franssen model). Wang and Li (2009) investigated the effect of partially damaged fire protection, using SFRM with thermal properties assigned as $\lambda = 0.05W/m/K$, density $\rho = 350kg/m^3$, and specific heat $c_p = 1100J/k/kg$ (denoted as YC SFRM model). In the paper by Kodur and Shakya (2013), three different SFRM materials (CAFCO-300, Carboline Type-5MD, and Tyfo WR-AFP) were selected to test for the thermal properties. By approximating the test results, a number of numerical descriptions for the material thermal conductivity, specific heat and other properties were reported.

The above models are hereby used in the heat transfer analyses performed to investigate the dependencies of thermal responses regarding SFRM thermal

properties. Similar to the previous analyses, 2D blocks are employed to conduct the analyses with single-side exposure to fire considered. The 2D block model consists of a 10 mm thick steel plate and a 20mm thick SFRM layer. Figure 3.13 illustrates the analysed temperature distributions using different SFRM models, where the steel plate is modelled as Eurocode 3 carbon steel, and a 15 minute fire is imposed using the standard fire curve. It is shown that constant thermal properties lead to a linear temperature distribution through the thickness of the coatings, whilst a range of nonlinear distributions are found when temperature dependent thermal properties are considered. Compared to these temperature dependent material models, the YC SFRM model is found as an appropriate representation of SFRM without considering temperature dependent thermal properties. However, it has to be noticed that this discussion is limited to exposure time and fire behaviours.

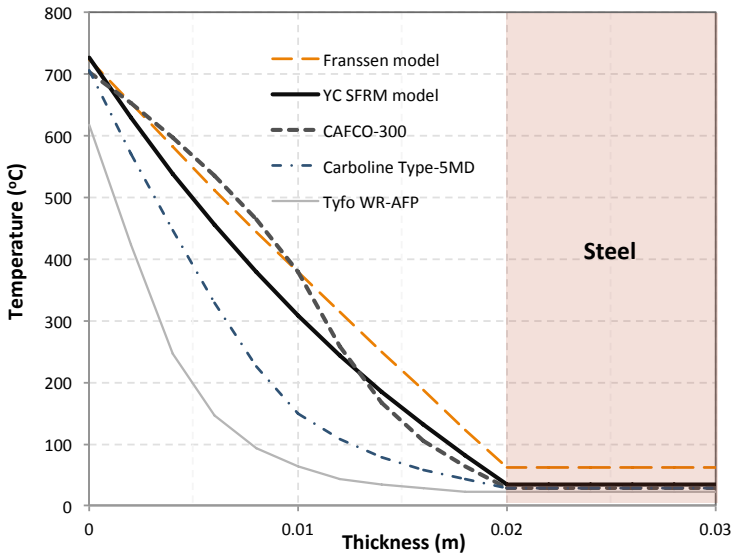

0

Figure 3.13: Thermal response of fully protected steel plate subjected to standard fire

3.4.2 SFRM protected steel block subjected to localised fire action

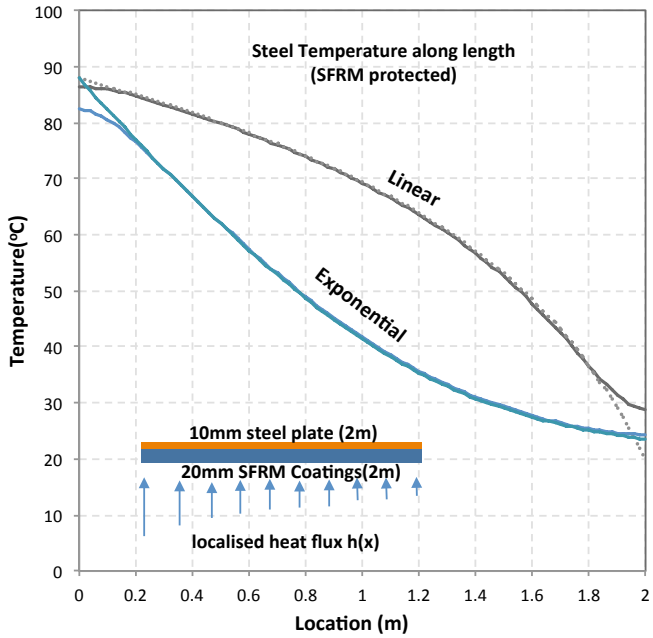

Figure 3.14: Thermal response of fully protected steel plate subjected to localised distributed heat fluxes

As demonstrated in Figure 3.13, temperature increase in SFRM coated steel plate can be significantly delayed by using passive fire protection. Unlike the uniform fire action implied by the Standard Fire curve, localised fire action is applied underneath the SFRM coated steel plate as shown in Figure 3.14, where the thermal response has been examined with respect to the linear and exponential distribution of incident heat fluxes. After 30 minutes of localised heating, temperatures of steel plate are significantly lower compared to the previously conducted analyses on the unprotected steel block. Despite the inhibited thermal response, variation along the length is still observed. The dimensionally reduced heat transfer analyses are also performed at a number of sections (20 sections). As

depicted in Figure 3.14, the dimensionally reduced approach is able to predict the thermal response of the SFRM insulated steel block with an acceptable accuracy at most of the sections. For a linear decay of heat flux input, the largest error occurs at the right cool end as 30.6% (normalised). Moreover, the largest error for an exponential distribution of heat fluxes appears at the hot end (6.74%), with an accurate prediction in the region ranging from 0.2m to 2.0m. These end errors are caused by unbalanced heat flow from hot area to cool area near the ends, which are related to the gradient of heat flux decay.

3.4.3 Steel block under fire action with partially damaged fire protection

It has been observed and studied about the peeling off of SFRM coating due to large deformation of the steel plates (Dwaikat and Kodur, 2011; Chen and Jiang, 2015). To address the partial damage of SFRM protection, some research deliberately removed a block of SFRM coatings at the end of the member (Wang and Li, 2009). The damage mechanism is believed to be a combined result from the transverse (tensile) cracks and damaged bond contact caused by the high level interfacial stresses (Chen and Jiang, 2015).

Localised high temperatures are found near the unprotected surface, as shown in Figure 3.15. The 2 m long 10 mm thick steel block is partially covered by a 1.6 m $\times$ 20 mm thick SFRM layer, with 0.4m long region left unprotected. Heat transfer analyses are performed to model the thermal response of the steel block, with the fire placed underneath the plate. Uniform fire action represented by standard fire curve is first applied with various duration of exposure. Noted that

the left part of unprotected steel block is identical to the unprotected case. The temperatures start to decrease rapidly at the location of 0.3 m to the left end, and the downward gradient declines after entering in the protected region. In the large part of the area near the right hand end, temperatures are the same as 1D results of insulated steel block. For fire actions lasting for 15 mins, 30 mins, 60 mins, and 120 mins, the maximum temperatures in the unprotected region rise to 564^oC, 766^oC, 938^oC, and 1002^oC, respectively. In the protected region, the temperatures of insulated steel only reach 34^oC, 70^oC, 151^oC, and 302^oC for 15 mins, 30 mins, 60 mins, and 120 mins period of exposure. From the maximum to the minimum temperature, a transition area exists from 0.2 m to 1.2 m, which suggests that the dimensional reduction may not be appropriate to use,or requires a polynomial interpolation to approximate the temperature distribution.

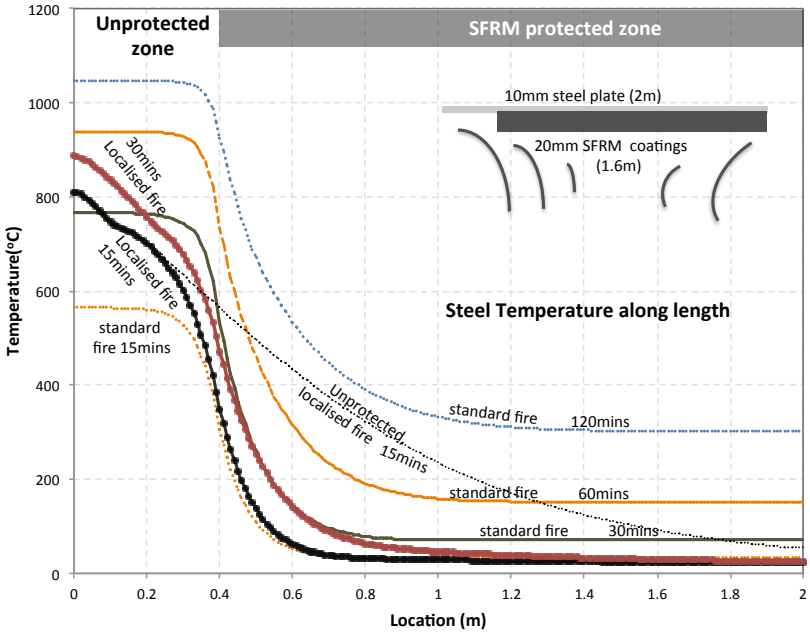

Figure 3.15: Thermal response of partially protected steel plate

In addition to the standard fire exposure, heat flux distributed in an exponential pattern (as used before) is applied to the partially protected steel block. The

temperature distribution has been presented in Figure 3.15, where the response to 15mins and 30mins have been illustrated. A dramatic decay is seen in the unprotected part which is a combined action of the localised heat flux and partial SFRM protection. Comparing with the thermal response of the totally unprotected steel block, the temperature profiles are identical from 0m to 0.2m, and then differ due to the heat conduction from intensely heated area to the protected part.

3.5 Comparison between dimensionally reduced and full 3D heat transfer analyses of structural members

3.5.1 2D sectional and full 3D analysis of steel beams in localised fires

In this section an unprotected hot-rolled steel I-beam is subjected to heat flux distributions from the most commonly used localised fire models discussed earlier in the paper. The beam is assumed to have a perfectly insulated top surface (top surface of the upper flange) while all the other faces of the beam section are subjected to the specified heat fluxes. The hypothetical boundary condition for the top surface represents a limiting case of heat exchange between the steel beam and the superstructure it supports. Perfect contact is assumed in the analysis of a steel and concrete composite beam discussed in Section 3.5.2, which allows free exchange of heat through the steel-concrete interface.

3.5.1.1 Steel beam subjected to an SFPE localised fire model

The SFPE correlations between heat flux and radial distance are proposed based on the tests done by Wakamatsu et al. (2003). In the test, a H-section (75mm × 150mm×6mm×6mm) steel beam is allocated underneath a 1.82m×3.64m rectangular flat ceiling, which is composed of two layers of 12 mm thick perlite boards. Different burner sources are used to heat the beam and the burner to ceiling distance varies. Heat fluxes received by different parts of the beam are monitored with heat flux gauges. Figure 3.16 plots the measured heat flux distribution at the downward face of upper flange in test 130-0.6, which is referred to the heat release rate of the burner as 130kW, and the distance between beam bottom to the fire origin as 0.6m. Since the SFPE model is an average estimate of the heat flux distribution in different localised fires, the discrepancies between them are not out of expectation.

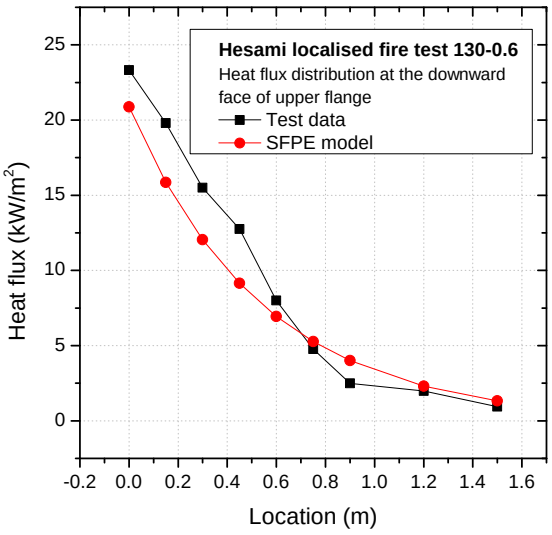

Figure 3.16: Localised heat flux measured in Hasemi test (Wakamatsu et al., 2003) compared with SFPE model

Figure 3.17 presented the lower flange temperature obtained from the test 130-0.6 and the heat transfer analyses corresponding to the test. The heat transfer analyses are performed as full-blown 3D and dimension reduced 2D as well, with localised fire action defined according to SFPE correlations, and the method to apply localised fire model is the same as earlier mentioned. Due to the inherited discrepancies from SFPE model compared to test capatured heat flux distribution, the analysed thermal response is slightly higher than the measured data. However, both 2D and 3D analyses are able to predict the similar result and successfully address the localised temperature profile along the beam.

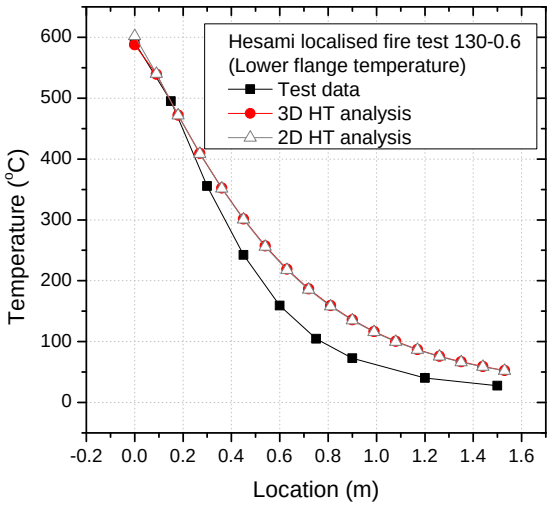

Figure 3.17: Temperature distribution from the test and numerical simulation

For a localised fire with low rate of heat release (HRR $<$ 2 MW), the SFPE correlation must be used for considering the various flame tip lengths on the beam assembly. A localised fire of HRR = 1MW and the fire source diameter of 0.5m is assumed. A number of beams of different cross sections are investigated to determine the effect of dimensional reduction from 3D to 2D. The distribution of normalised error in averaged flange and web temperatures along the beam length is presented in Figure 3.18, for a 305 $\times$ 127 $\times$ 42 universal beam. Symmetry

about the peak flux allows simplification of the analysis, therefore the left hand end of the beam heat transfer model has the highest temperatures and the right hand end is the coolest (consistent with the idealised flux distributions considered earlier). This time errors appear at both ends of the model as a result of the heat conduction along the beam length. The error is highest for the upper flange (1.2%) at the point of the peak incident flux and at the right hand end (4%), but neither of these errors are practically significant. Temperatures were recorded at five equidistant points along the beam as shown in Figure 3.19, from which it can be seen that the 2D and 3D analyses produce nearly identical distribution of temperatures.

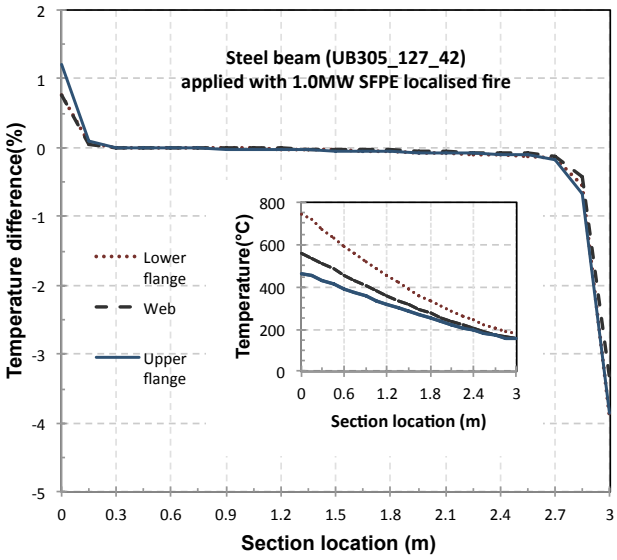

Figure 3.18: 2D/3D temperature difference in a steel beam subjected to SFPE localised fire

The above discussion is based on the consideration that fire develops to a steady state in a very short time after ignition, which ignores the period of fire growth. It is therefore necessary to review the accuracy of the heat transfer results after dimensional reduction as it may be affected by the variation of fire growth. Such a

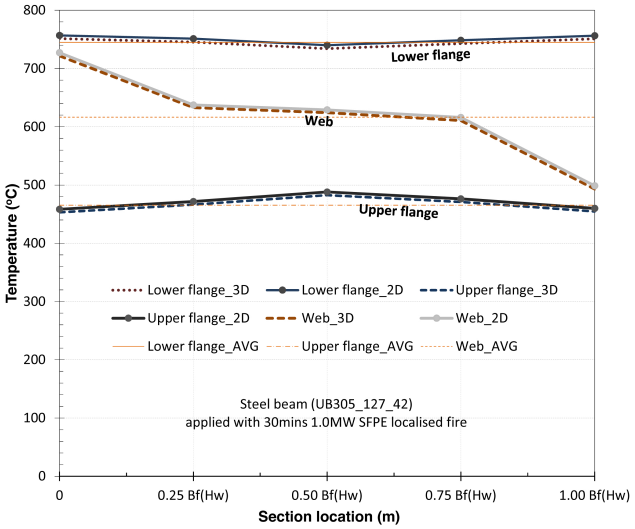

Figure 3.19: Temperature profile at the beam section above the localised fire origin

period after ignition is often characterised as a t-squared growth (Buchanan, 2001) and can be defined as Equation (2.1). Figure 3.20 presents the error measure for different speeds of fire growth, where the early stage of fire not impinging on the beam is not taken into accounted into the heat flux input to the member surface.

3.5.1.2 Steel beam subjected to Eurocode 1 localised fire model

When the heat release rate of the fire source exceeds 2MW, the variation of the flame tip length due to the shielding effect of the beam flange can be ignored. In this case the Eurocode 1 localised fire is appropriate for estimating the heat flux received by the exposed structural surfaces. A number of steel beams are subjected to the Eurocode 1 localised fire to examine the temperature difference between 2D and full 3D models at the selected section locations. The boundary conditions are identical to the analysis in the previous section and net heat flux

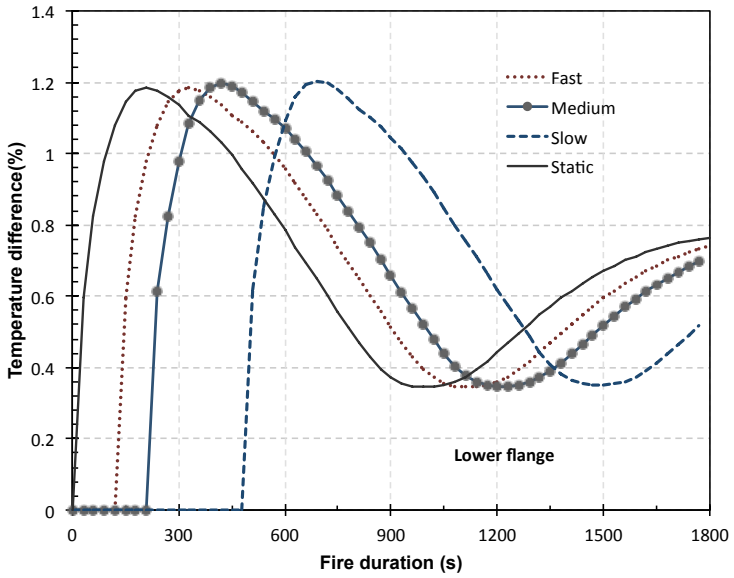

Figure 3.20: Error measure of the temperature difference when considering fire growth

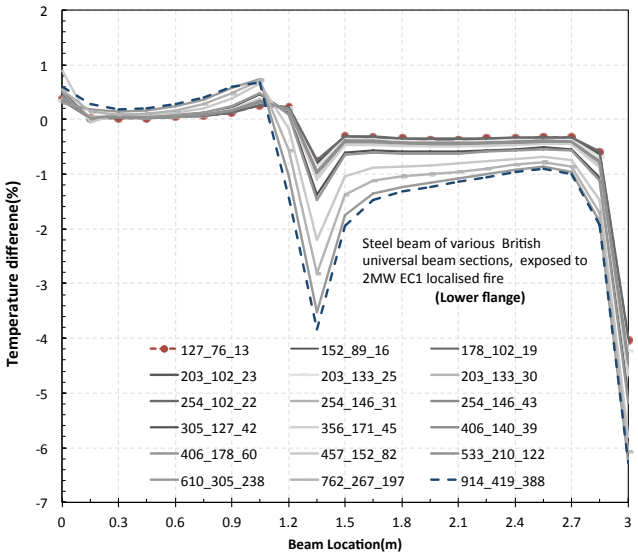

Figure 3.21: 2D/3D temperature difference at the lower flange of steel beams of various cross sections

is obtained based on Equation (2.12) as before. A wide range of British universal beam sections are examined using the normalised error in the average temperature

of the lower flange along the beam length as shown in Figure 3.21. The maximum error is again observed at the cooler end, approximately 5% in the most stocky section. In these models an additional area of discrepancy occurs in the middle of the model (between 1.2m and 1.5m). This is caused by the transition from a linear to an exponential distribution in the Eurocode 1 localised fire as its fire source has a 2MW rate of heat release and the diameter defined as 1m (The transition can be found from Figure 3.1). The largest error caused by the transition is approximately 1.9%, whilst at the hot end(mid-span of the beam) the normalised error is generally under 1.2% as seen in the previous section.

3.5.2 2D and 3D analyses of composite beams in localised fires

Complementary to the single beam analyses in the previous section, a composite beam is analysed here to examine the effect of heat transfer from the steel beam to a composite concrete slab. The interface between the steel and concrete is considered to be in perfect contact (a limiting case opposite to the a fully insulated top flange considered in the previous section). The assumed interface condition allows free heat exchange between the steel beam and concrete slab which behaves as a heat sink. During the exposure, the top surface of the concrete slab is treated as unexposed but with convection and radiation to the ambient air (heat transfer coefficients are adopted as previously mentioned). The composite beam has also been examined in terms of various British universal beam I sections, under a 30-minute exposure to a 2 MW Eurocode 1 localised fire. The concrete slab is assumed to be 100mm deep with a width of 600mm. Over the period of fire

exposure, the bottom face of the slab is exposed to the localised fire except for the area shielded by the steel beam.

3.5.2.1 Effect of concrete slab

As the slab absorbs the heat from the composite steel beam, the top flange has a significantly lower temperature than the bottom flange and the web. Heat transfer to the composite beam subjected to uniform gas temperatures has been studied in the referenced work (Lamont et al., 2001; Jiang, 2012b). Even in a localised fire, a similar temperature distribution can be observed. The temperature distributions in the the beam section UB305 $\times$ 127 $\times$ 42 is shown against the corresponding composite section in Figure 3.22. The bottom flange of the steel beam is relatively unaffected by the concrete slab, as a result, its temperature essentially reproduces the results obtained from the single steel beam analysis, in which the flanges (12.1mm) and the web (8mm) are all heated up to a similar temperature.

3.5.2.2 2D/3D temperature difference in composite beams

As the bottom flange and web of the steel beam is less affected by the heat transfer to the slab compared to the top flange the normalised error in the upper flange of the composite beam is plotted in Figure 3.23 along the beam length. The end effects and the discrepancy at the transition from linear to exponential are reflected in the plot as discussed earlier. The largest difference reaches 4.5% at the cool end of the beam for the 914 $\times$ 419 $\times$ 388 universal beam section, while the difference at the hot end does not exceed 1.2%.

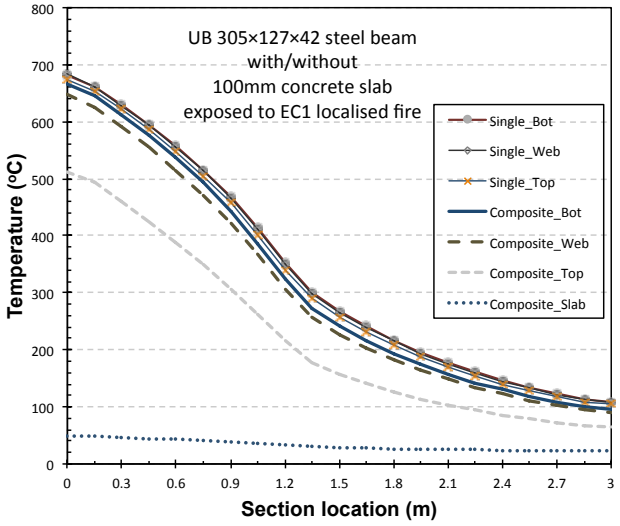

Figure 3.22: Temperature distribution in the single steel beam and corresponding composite beam

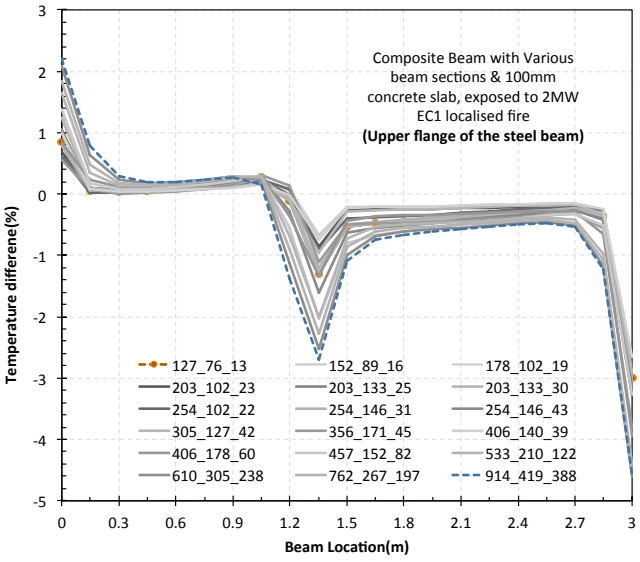

Figure 3.23: 2D/3D temperature difference at the upper flange of composite beams of various cross sections

3.5.3 1D heat transfer over the depth and full 3D analysis of concrete slabs in localised fires

Given the considerably low thermal conductivity of concrete, it may be adequate to determine the temperature evolution of slabs in localised fires simply by a series of 1D heat transfer analyses over the depth of the slab for a number of points over the exposed area. In this section a $3m \times 3m \times 0.1m$ concrete slab is analysed against a Eurocode 1 localised fire action exploiting symmetry on two sides (therefore one corner of the model is exposed to the peak heat flux). Similar to the previous models, the net heat flux is applied according to Equation (2.12) and the top surface of the slab loses heat by convection and radiation to the ambient air.

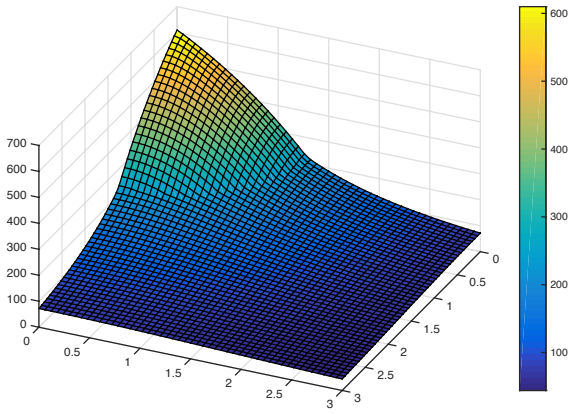

Figure 3.24: Thermal response of 0.1m thick concrete slab subjected to 2MW EC1 localised fire

Figure 3.24 shows the temperature distribution from the doubly symmetric 3D slab model as a result of the localised 2MW Eurocode 1 fire (D=1m). The plotted temperature profile shows the bottom surface temperatures. In order to examine the difference between the 3D simulation and 1D analyses, a number of points

are chosen along the diagonal joining the point of peak flux to the coolest point opposite. The temperatures and the normalised errors are plotted along the path for the bottom and top surfaces and the mid-depth of the slab, as shown in Figures 3.25 and 3.25(b).

The error plot shows a behaviour similar to that observed in the previous sections, small errors at the ends and at the transition from linear to exponential distribution. The absolute temperatures are practically identical from the 1D and 3D heat transfer analyses as clearly seen in Figure 3.25. The normalised error does not exceed 1.2%, which appears in the transition area and is negligible for practical purposes.

Figure 3.26 shows the thermal response of concrete slab to a smaller Eurocode 1 localised fire of 1MW HRR for a 1m diameter burner. This fire shows a more intense decay compared to the 2MW fire, causing an observable increase in normalised error at the corner, which climbs up to 3% at the top surface and the mid-depth layer. However, the difference at the bottom surface remains relatively low (around 1%).

3.6 Rapid estimation of thermal response of structure members

3.6.1 Polynomial interpolation for localised fire exposure

Through the investigation carried out in the previous sections, it has been found feasible to apply dimensional reduction for heat transfer analyses even for localised

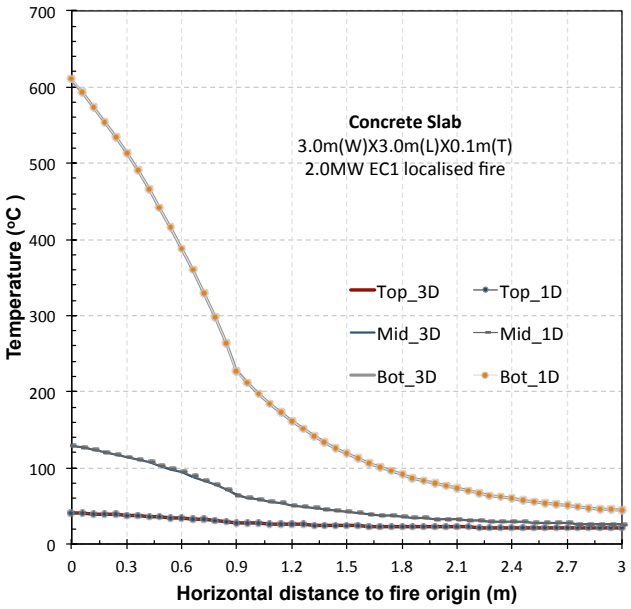

(a) Temperature in the slab along the diagonal path

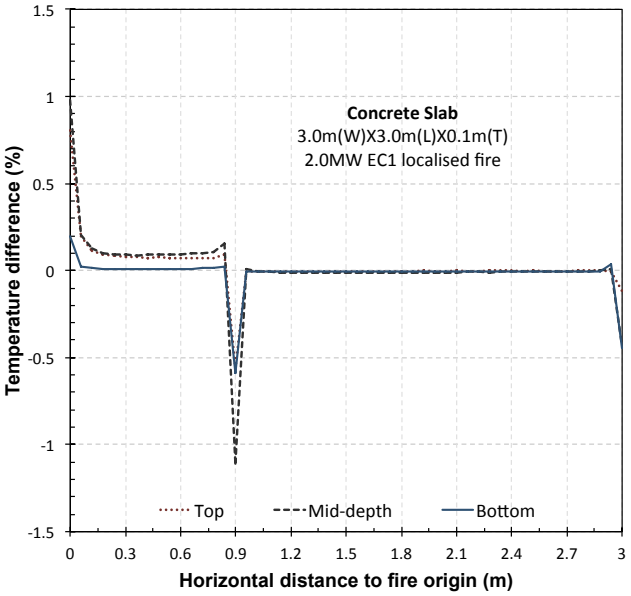

(b) 1D/3D temperature difference in the slab along the diagonal path

Figure 3.25: Concrete slab exposed to 2MW EC1 localised fire

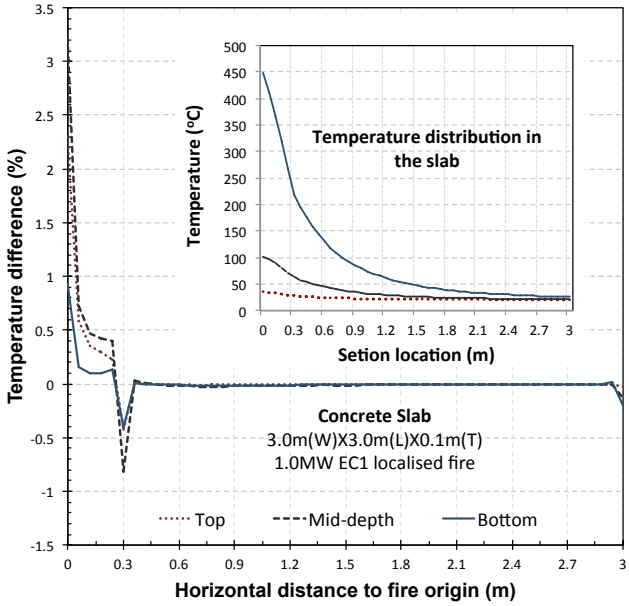

Figure 3.26: Temperature difference from 1D/3D analyses with 1MW EC1 local fire applied

fire action. It is demonstrated to be adequate to obtain temperature histories by only carrying out a number of 2D cross-sectional heat transfer analyses for beams, and 1D through-depth analyses for concrete slabs.

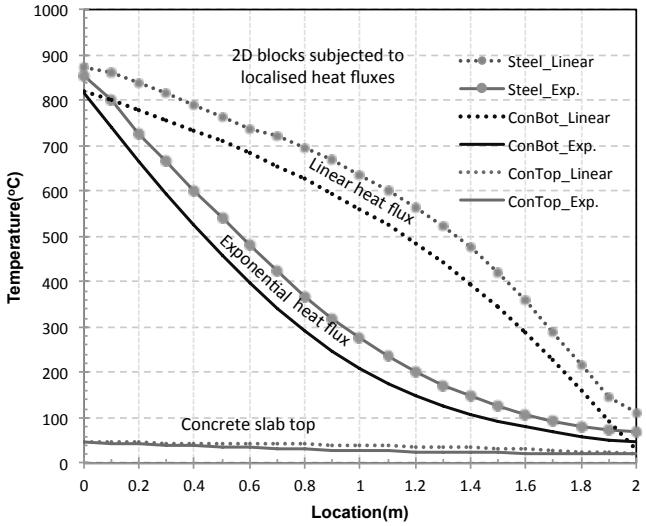

Figure 3.27: Temperature profile of steel beam subjected to SFPE Localised fire

The variation of thermal response is highly correlated to the distribution of heat fluxes received. It is desirable in computational modelling to use an empirical model to represent the real flux distribution along the exposed surfaces of structural members. For the localised fire models reviewed in Chapter 2, it is commonly accepted to use linear and exponential curves to approximate the heat flux distribution against the horizontal distance to the fire origin (Hasemi et al., 1996; CEN, 1999).

As shown in Figure 3.27, temperature distributions are derived from the heat transfer results in 2D blocks, which are subjected to linearly and exponentially distributed heat fluxes respectively. It is observable in the figure that exposure to a linearly decaying heat flux leads to a convex shaped distribution, whilst an exponential decay may leads to a concave distribution. Considering the practical models for localised fire action that are constructed with linear and exponential correlations, it is thus possible to apply a polynomial approximation for the thermal response to localised fire action. The ultimate goal of this approximation scheme is to significantly decrease the computational consumption in providing the temperature history for the sequentially conducted thermo-mechanical analysis.

3.6.2 Polynomial interpolation for quick estimation of thermal response to localised fire action

Three formulations of approximation have been applied to obtain the approximated thermal response, which have been shown in Figure 3.28. When a beam is exposed to heat fluxes with a linear or exponential distribution, a quadratic

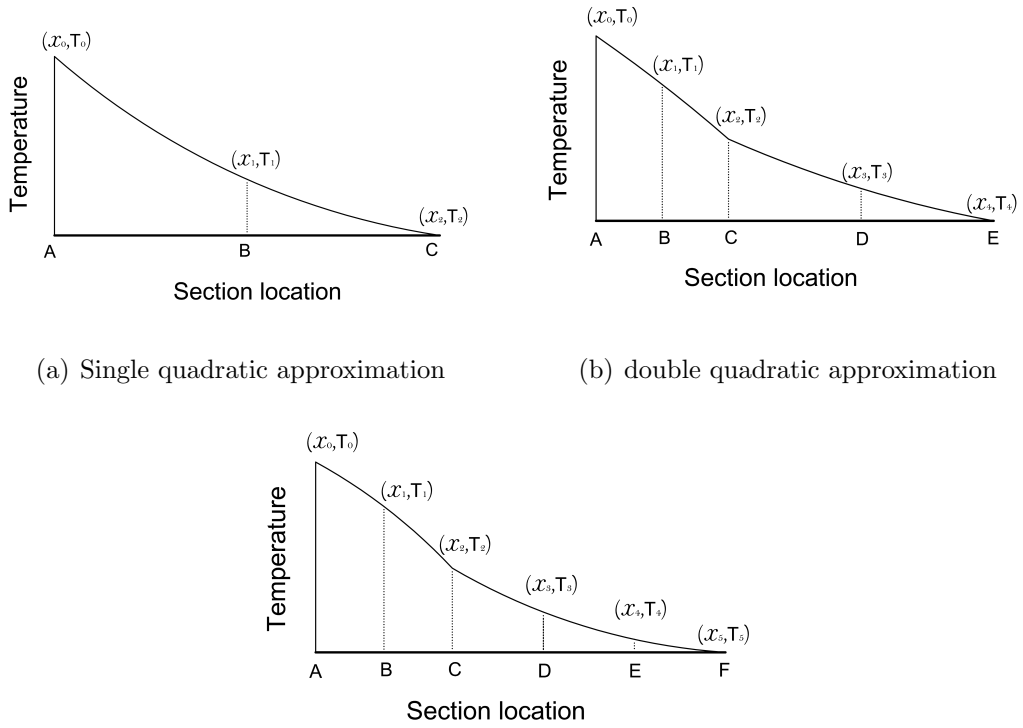

(a) Single quadratic approximation

(b) double quadratic approximation

(c) Mixed-order approximation

Figure 3.28: Different approximations to the thermal response induced by localised fire exposure

approximation is possibly adequate to describe the resultant temperature distribution. For an arbitrary section with local coordinate x, its corresponding temperature T is interpolated from the three given section responses, which are extracted from the dimensionally reduced heat transfer analyses. The interpolation is written as polynomials in the Lagrange form:

$$T = L_0 T_0 + L_1 T_1 + L_2 T_2 \tag{3.2}$$

where the $L_i(i = 0, 1, 2)$ are commonly referred to as *Lagrange basis functions* are :

$$L_0 = \frac{(x - x_1)(x - x_2)}{(x_0 - x_1)(x_0 - x_2)} \tag{3.3a}$$

$$L_1 = \frac{(x - x_0)(x - x_2)}{(x_1 - x_0)(x_1 - x_0)} \tag{3.3b}$$

$$L_2 = \frac{(x - x_0)(x - x_1)}{(x_2 - x_0)(x_2 - x_1)} \tag{3.3c}$$

When the localised fire action is modelled using the Eurocode 1 suggested expression, piecewise correlation between heat flux and radial distance should be applied, which consequently leads to a jump discontinuity at the linear-to-exponential transition. In such cases, the location of the jump continuity should be determined first, which may be taken as the same location of discontinuity of the heat flux distribution. Nevertheless, the heat flux near the fire source may plateau at $100kw/m^2$, which requires the extra calculation to determine the location where the decay starts and set the boundary of interpolation. For the linear-to-exponential heat flux exposure, the temperature at an arbitrary location can be interpolated with a double quadratic approximation as:

$$T = L_0T_0 + L_1T_1 + L_2T_2, when\ x_0 \leq x < x_2 \tag{3.4a}$$

$$T = L_2'T_2 + L_3T_3 + L_4T_4, when\ x_2 < x \leq x_3 \tag{3.4b}$$

Here L_2', L_3 and L_4 are the Lagrange basis functions defined for the second period, which can be similarly obtained as 3.3 by replacing the coordinates x_0, x_1, x_2 with x_2, x_3, x_4 in order.

In practical application of the above approximations, it has been found that higher

order interpolation may be needed for the exposure defined in the exponential piece of Eurocode 1 localised fire model. In such cases, the interpolated temperature may be given as:

$$T = L_0 T_0 + L_1 T_1 + L_2 T_2, when\ x_0 \leq x < x_2 \tag{3.5a}$$

$$T = L_2'' T_2 + L_3'' T_3 + L_4'' T_4 + L_5'' T_5, when\ x_2 < x \leq x_3 \tag{3.5b}$$

where L_i'' (i=2,3,4,5) represents the cubic basis functions, which can be expressed as:

$$L_i'' = \prod_{2 \leq j \leq 5}^{i \neq j} \frac{(x - x_j)}{(x_i - x_j)} \tag{3.6}$$

Such an interpolation scheme is not only applied in steel beams, but is also adequate for the concrete slabs. This is based on the distribution of heat flux assumed for localised fire action, which is cylindrical around the centre of fire source. Meanwhile, the thermal response of concrete slab in a localised fire is correlated to the incident heat flux that is received by the exposed surface. The interpolation scheme for the slab is shown in Figure 3.29.

Where interpolation is now performed between along longest path so the lowest and highest temperatures are both covered.

3.6.3 Accuracy of polynomial interpolation

3.6.3.1 Accuracy of polynomial interpolation for steel beams

In the previous section, 20 section analyses were performed to achieve a desirable accuracy of prediction when dimensional reduction of heat transfer analysis

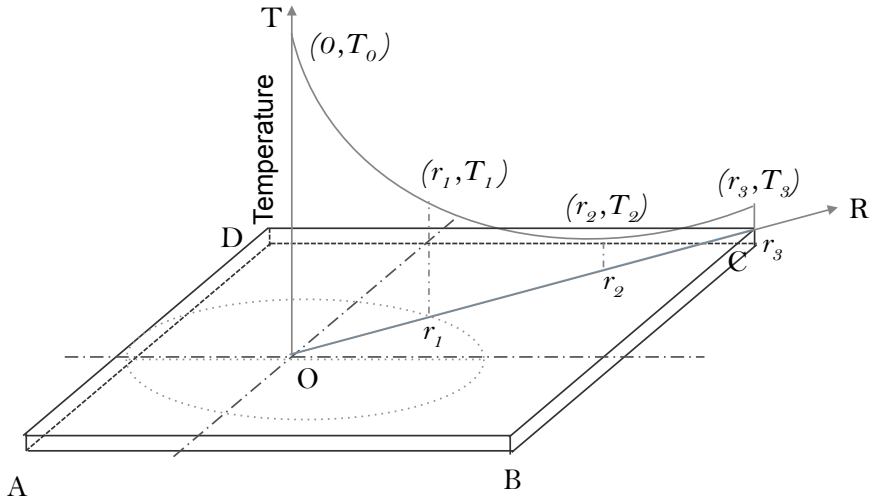

Figure 3.29: Temperature approximation for concrete slab subjected to Localised fire action

is applied. For beams exposed to SFPE type localised fire action, it has been observed that a single quadratic interpolation could provide a well fitted approximation. A steel beam with a $UB305 \times 127 \times 42$ section as studied previously is subjected to a 30 mins exposure defined as 1MW SFPE localised fire, which leads to a significant temperature gradient along the beam, as shown in Figure 3.31. Notice that the dash and dot curves plotted in the figure represent the temperature distribution interpolated with a single quadratic approximation. Temperature differences between quadratic interpolation and full 3D analysis has been presented in Figure 3.32 as a reference of accuracy, where the difference is normalised in a similar form as adopted previously (Equation 3.1). The temperature errors are also calculated over the distributions obtained from the 20-section results, which is an intuitive estimate used when a linear interpolation is applied between the adjacent sampling sections.

It should be noticed that there are the intrinsic errors between 2D and 3D results,

as a result of ignoring longitudinal heat flow. Therefore the temperature error at the ends of the flux profile are unavoidable but acceptable, because of the temperatures are the lowest at the end (where the maximum error measure appears). Excluding the ends, good accuracy can be found from the quadratic interpolation as the maximum error remains below 1.5%, which is perfectly acceptable in the field of structural engineering.

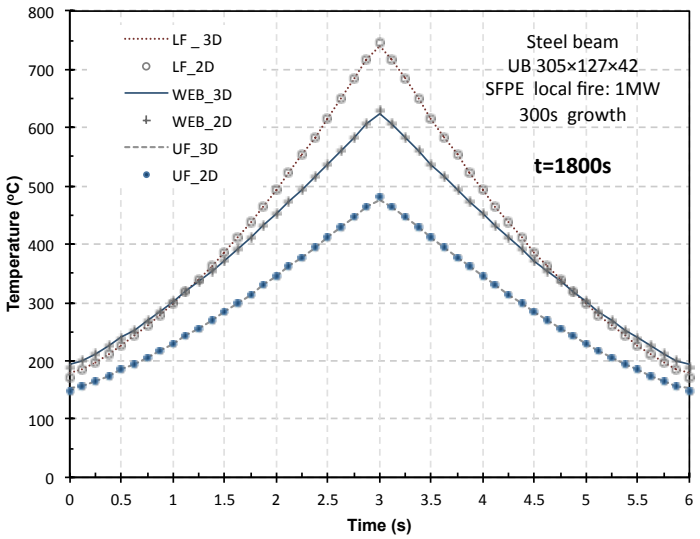

Figure 3.30: Non-uniform temperature profile of steel beam subjected to SFPE Localised fire

When a steel beam encounters fire action described using the Eurocode 1 localised fire model, the temperature distribution may be found piecewise. In this case, the location of the transition should be identified. For example, assuming the fire model is established as the one used in Section 3.5.1, with a HRR as 2MW, source diameter as 0.5m, and ceiling height as 3.0m, the transition should occur at a radial distance to the fire origin equal to 1.268m. In the zone where the radial distance is lower than 1.268m, the exposure is represented by a linear decay, whilst the rest is represented by an exponential decay. Thermal response to the

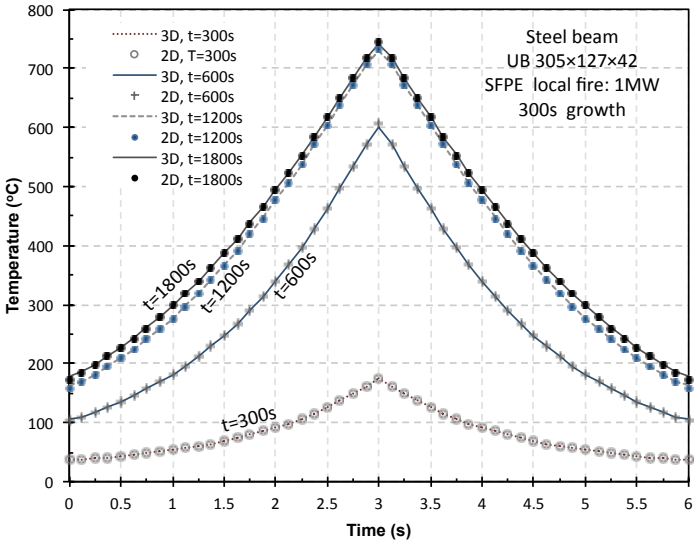

Figure 3.31: Temperature profiles obtained from 2D Interpolations and 3D analysis

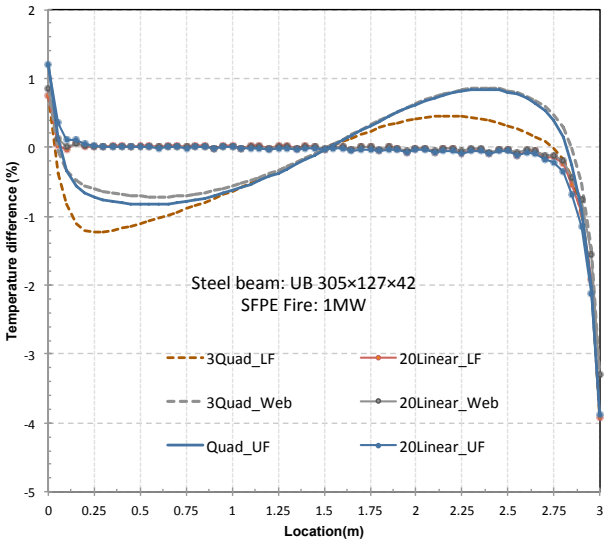

Figure 3.32: 2D Int. /3D Temperature difference of steel beam subjected to SFPE Localised fire

linear heat flux exposure may be obtained with a single quadratic interpolation, on the other hand, thermal response to the exponential portion can be either approximated by quadratic interpolation or cubic interpolation. Here these two

different interpolating schemes are denoted as double quadratic approximation and mixed approximation, respectively. The measures of accuracy have been shown in Figure 3.33, where A steel beam with a UB305 × 127 × 42 section is exposed to the earlier mentioned localised fire model.

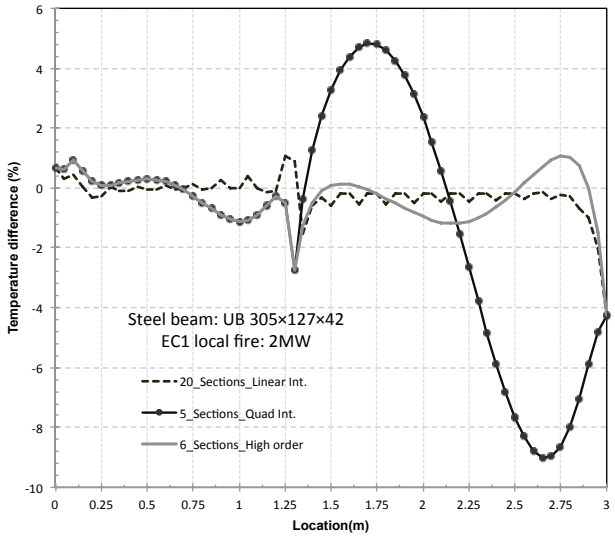

Figure 3.33: 2D Int. /3D Temperature difference of steel beam subjected to Eurocode 1 Localised fire

The temperature error predicted by quadratic interpolation in the left part of the beam is relatively low, when comparing with the errors formed at the beam ends or the errors produced by quadratic interpolation in the right hand part. The errors can be remarkably decreased from (-9%, 4.8%) to (-0.8%, 1.8%) if the cubic interpolation is applied.

3.6.3.2 Accuracy of polynomial interpolation for concrete slabs

A polynomial interpolation with respect to the radial distance has been performed to approximate the temperature distribution in concrete slabs subjected to

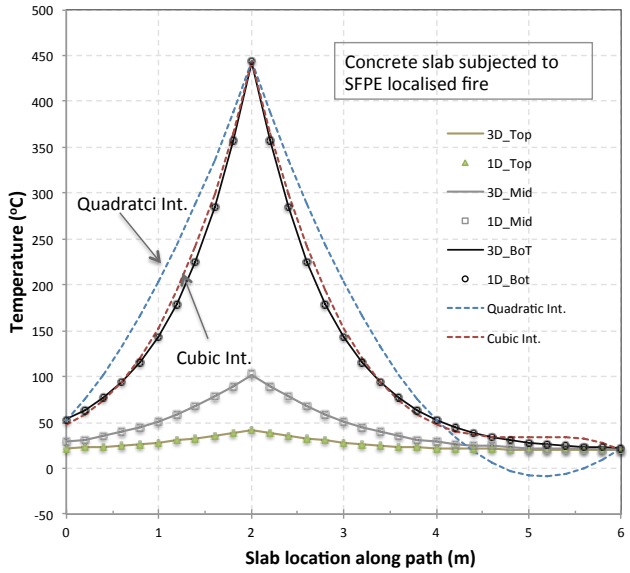

Figure 3.34: Temperature interpolation for slab subjected to localised fire action

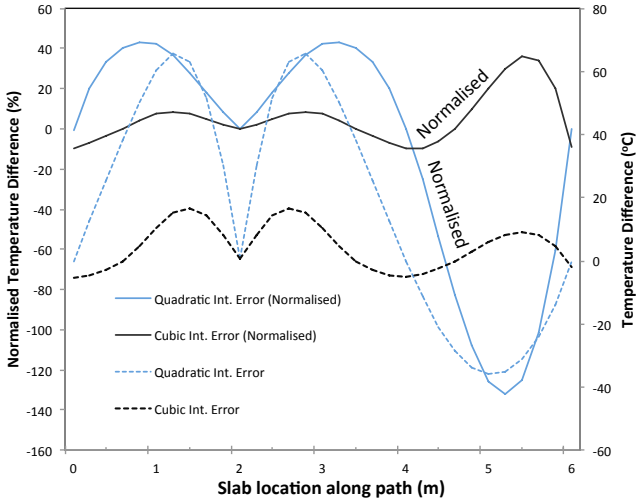

Figure 3.35: Temperature different between interpolation and 3D results at slab bottom subjected to localised fire action

localised fires. As previously shown in Figure 3.29, a localised fire defined in SFPE model is placed underneath the 6m×6m concrete slab of thickness 0.1m. The rate of heat release is assumed as 1MW, while the nominal diameter of the fire source is 1m. The modelling procedure is carried out with consistency to the

previous heat transfer analyses. Heat transfer results are plotted in Figure 3.34 along the diagonal path of the slab. A rapid decrease of temperature in the slab at the bottom surface can be observed, which is resulting from the exponential decay of the incident heat fluxes given in SFPE model, and particularly due to the low conductivity of the concrete compared to the temperature distribution of the steel beam. Through depth heat conduction is too low to sufficiently exchange with upper layers, which leads to a highly localised heating and challenges the feasibility of the interpolation scheme. As shown in Figure 3.34, Quadratic and cubic interpolations are performed to estimate the thermal response of the exposed surface, respectively. It is found that a quadratic interpolation may not be able to predict the temperature distribution with a decent accuracy. However, the refined scheme a cubic interpolation provides an acceptable estimation on the thermal response, although an over estimation is seen at the far end of the low temperatures.

The actual temperature differences between the polynomial interpolation and 3D results are given in Figure 3.35. The error in quadratic prediction could reach up to 65^oC around the peak temperature, whereas a lower error is seen when implementing a cubic interpolation (up to 20^oC). The normalised temperature differences are also presented in Figure 3.35, which suggests that a cubic interpolation is able to give an accurate enough prediction in the hot area which is more important in terms of structural fire safety. For the extreme fire scenarios with travelling and localised burning, thermal action may be defined on a number of nodes rather than using this developed scheme.

3.7 Conclusion

In this chapter, a set of comprehensive analyses have been carried out to determine the feasibility of dimensional reduction in heat transfer analysis for structural members subjected to localised fire action. The following conclusions can be drawn:

- Based upon the numerical study of 2D blocks of steel and concrete, it can be concluded that 1D heat transfer analysis over the block depth can adequately represent full 2D analysis except for the extreme scenarios of discontinuous heat flux distributions.

- For protected steel plates, dimensionally reduced heat transfer analyses are able to predict the real thermal response. Nevertheless, it is not appropriate to employ dimensional reduction when partial damage of fire protection occurs.

- No matter what assumptions are made for the heat exchange between the steel beam and composite concrete slab, the temperature error is practically negligible between heat transfer analyses over a number of 2D sections or full 3D analyses. This applies to both the commonly used localised fires, the SFPE localised fire model for HRR less than 2MW and Eurocode 1 localised fire model for larger localised fires.

- It appears adequate and reasonable to determine the temperature evolution of concrete slabs from a series of 1D analyses under localised fire, which should generally produce results practically identical to full 3D analyses.

- Based on the results of this work it is justifiable to use dimensional reduction

in all practical heat transfer analyses for structural members exposed to localised fire action. This finding is of major significance in the context of modelling large structures under all practical cases of realistic fire exposures, whether spatially uniform, localised or travelling fires. The reduction in computational cost and analyst effort in building computational models that can be achieved using this approach can potentially make the difference when engineer undertaking a large structural analysis for performance-based engineering of fire resistance or retreating to the unscientific prescriptive approach.

- A rapid estimation scheme using polynomial interpolations is proposed to approximate the non-uniform temperature distributions based on the results from the dimensionally reduced heat transfer analyses. The interpolation is implemented for beams and slabs subjected to localised fire action and further reduces the computational cost.

Chapter 4

Strategies for modelling structural members subjected to localised heating effects

4.1 Introduction

Discussion in the previous chapter has drawn a feasible and rapid approximation to the thermal response when localised fire action is considered. In this chapter, this will be implemented to determine the thermo-mechanical response of structural members subjected to localised fire action using beam and shell elements in OpenSees. Resulting from the non-uniform heating, a longitudinal variation of thermal elongation and localised material degradation should be considered in the beam element, which require modifications in terms of not just the thermal action, but also the formulation of elements. Displacement based and force based

beam elements are made available to analyse beams subjected to localised fires, which are incorporated with fibre based section and material models with temperature dependent material properties included. For modelling concrete slabs in OpenSees, geometric nonlinearity has been introduced into the shell element formulation with an updated Lagrangian description, which is initially proposed in the work completed by Lu et al. (2015). The linear and nonlinear shell elements are based on the Mixed Interpolation of Tensorial Component (MITC) technique (Bathe and Bolourchi, 1980; Bucalem and Bathe, 1997). A multi-layer plate fibre section is adopted to represent the concrete and the distributed steel reinforcement, which employs a plane stress model for concrete and uniaxial steel material for steel, with temperature dependant properties considered in accordance with Eurocodes (CEN, 2005, 2004). The theories and formulations of aforementioned beam and shell elements are addressed in this chapter.

4.2 Thermo-mechanical analysis for framed beams subjected to localised fire action

4.2.1 Implementation of beam-column element

Beam-column elements in OpenSees can be formulated as displacement based or force based. Beams subjected to fire action are first modelled in OpenSees with **DispBeamColumnThermal** elements, which have been validated in comprehensive work reported by Jiang et al. (2015). Force based approach (Taucer et al., 1991; Alemdar and White, 2005) was used for beams and columns in OpenSees

and implemented for fire scenario in ABAQUS by Jeffers and Sotelino (2012), with validation provided against experimental test data for uniform fire exposure.

To model the nonlinear behaviour of the beams, classical linear Euler-Bernoulli beam theory is expanded in conjunction with the corotational geometric transformation, which separates the element displacements as rigid body modes and local deformation. Moreover, a fibre model is used to discretise the beam section as a number of fibres with which the stiffness and resisting force can be determined for the section. During the analysis, an interpolation between the element displacements is performed for each section to gain the trial deformations, which is referred to as displacement based or stiffness based approach for beam-column elements. Alternatively, the element state can be determined by the trial forces that are interpolated over the element forces, which is referred to as the force based or flexibility oriented approach (Taucer et al., 1991). A diagram is presented in Figure 4.1 to describe the architecture of the framed beam-column elements and the communication between the aggregated components, which are:

1) **Fibre section** $\leftrightarrows$ **Fibre uniaxial material**. Each fibre possesses a uniaxial material model which receives the mechanical strain and temperature information from the section and returns the updated tangent modulus, stress, and thermal elongation. After collecting the material response from each fibre, the section stiffness matrix and the resisting force should be calculated by summing up the contribution of the fibres. This process is referred to as the **section state determination**.

2) **Beam element** $\leftrightarrows$ **Fibre section**, which involves the **element state determination** and addresses most of the development for localised (non-uniform) thermal action. It can be achieved either with a displacement interpolation or

force interpolation depending upon the element used. During the process, section force and deformation should be updated and determined as a result of incremental element displacement, followed by the formulation of elemental stiffness matrix and resultant forces calculated though the numerical integrations over section responses.

3) **Structure** $\leftrightarrows$ **Beam element**, which is referred to as the **structure state determination**, including geometric transformation and assembling stiffness matrices as well as the residual vectors;

Before discussing the various procedures for state determination, it is necessary to declare the subscripts that may be used in the following sections:

Load step i, which is used for applying thermal action, indicates the i-th step of thermo-mechanical analysis. For a realistic fire scenario, load step might be set as 30 seconds, which suggests the real duration of exposure as $k \times 30s$;

Iteration k, denotes the Newton-Raphson iteration, is performed at the structure level. During the k-th iteration, element state are updated to form the new residual force vectors and stiffness matrix, aiming to solve for the incremental displacements. This looped procedure continues until convergence is achieved, which is checked using specified principles.

Element iteration j, may only appear in the force based beam element, and is performed for determining the element state as a product of nodal displacements updated by iteration i.

Section si, also linked to the beam integration points, represents the si-th section

in a beam element, with which the numerical interpolation and integration are performed.

Fibre fi, the fi-th fibre in a fibre based section, which employs a uniaxial material model with contribution to the flexural resistance of the section.

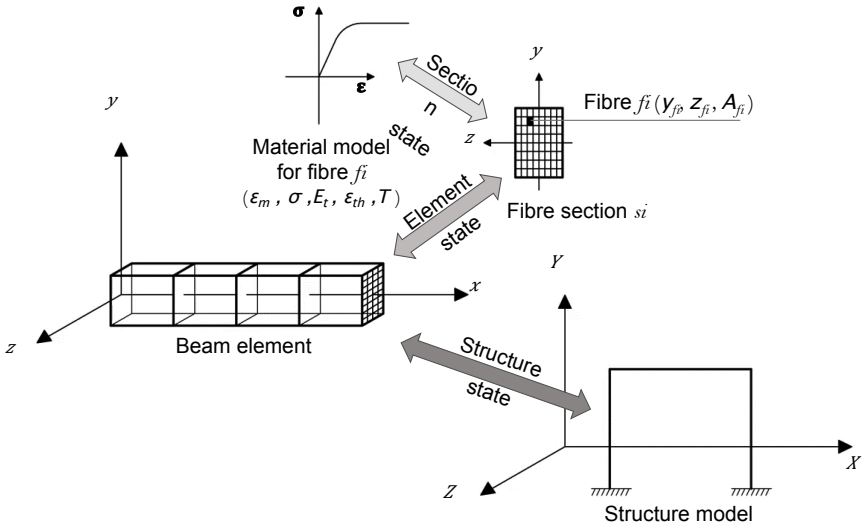

Figure 4.1: Thermo-mechanical analysis with displacement based beam element in OpenSees

4.2.1.1 Section state determination

The section state including the force **D** and deformation **d** is determined on the basis of fibre model, which subdivides the beam section as a finite number of longitudinal fibres. The calculation of fibre strains has been discussed in Chapter 2 and follows the Equations 2.46-2.47.

Thermal strain of the fibres are increased as a result of elevated temperature. Thus a thermally induced force shall be calculated out of the thermal elongation,

which is plugged into the first iteration for each load step to deal with the abrupt expansion. The thermal force $\mathbf{F}_{th}$ is calculated in an incremental form as ${F_{si}}^{i}$ and ${M_{si}}^{i}$ are the direct force prediction at the current ith step:

$$\mathbf{F}_{th}(x) = \begin{bmatrix} {F_{si}}^{i} - {F_{si}}^{i-1} \\ {M_{si}}^{i} - {M_{si}}^{i-1}) \end{bmatrix} \tag{4.1}$$

$$\begin{bmatrix} F_{si} \\ M_{si} \end{bmatrix} = \begin{bmatrix} \sum \Big(E_t \cdot \varepsilon_{th} \cdot A \Big) \\ -\sum \Big(E_t \cdot \varepsilon_{th} \cdot A \cdot y \Big) \end{bmatrix} \tag{4.2}$$

in the above expression, the ε_{th} represents the thermal elongation in a fibre, while E_t denotes its tangent modulus. The above process is illustrated with a flowchart presented in Figure 4.2.

4.2.1.2 Element state determination

For each new step of thermal action, the first iteration is executed to apply the thermally induced force $\mathbf{F}_{th}$. The calculated incremental displacement could neutralise a major portion of thermally induced deformation, although the material degradation shall be taken into account within the following iterations. With the calculated incremental displacements Δ_u, section deformation e_{si} could be estimated by means of displacement based formulation or force based formulation. The first one assumes a linear distribution of the rotation and a constant axial deformation, whereas an inverse calculation for section deformation can be

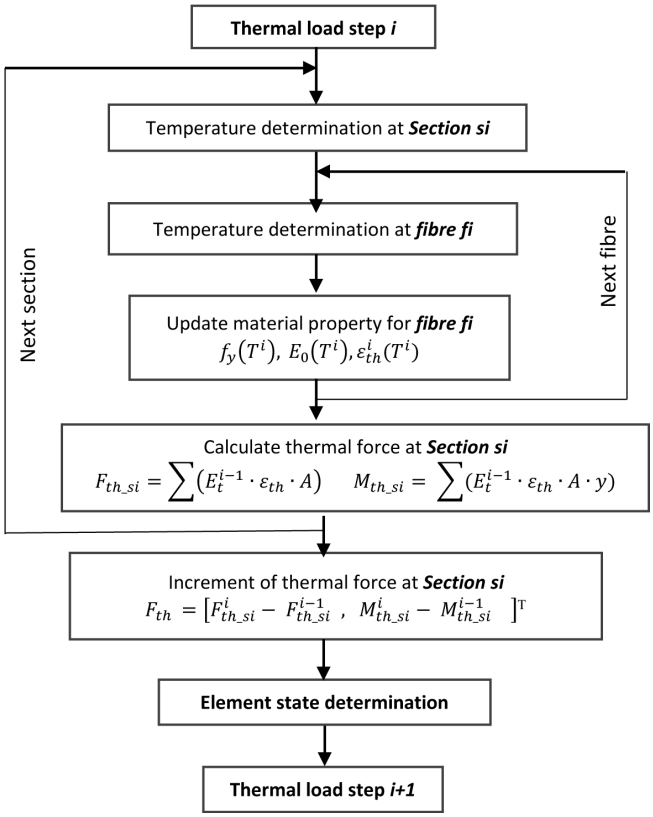

Figure 4.2: Calculation of thermal-induced force in fibre based section

performed in force based beam elements, based on the assumed linearly interpolated section force. The general process for thermo-mechanical beam analysis is presented in Figure 4.3.

◦ ***Element displacements and forces***

The prerequisite step to update the state of the element is to set up the trial displacements in the context of the local coordinate system, which is thereby corotationally transformed. Figure 4.4 is adapted from the one presented by Taucer et al. (1991), to explain the force and displacement variables involved in the beam elements, where $\overline{Q}, \overline{q}$ represent the corresponding nodal forces and displacements. After removing the rigid body modes, the nodal displacements yield two pairs of nodal rotations and one longitudinal displacement. A vector

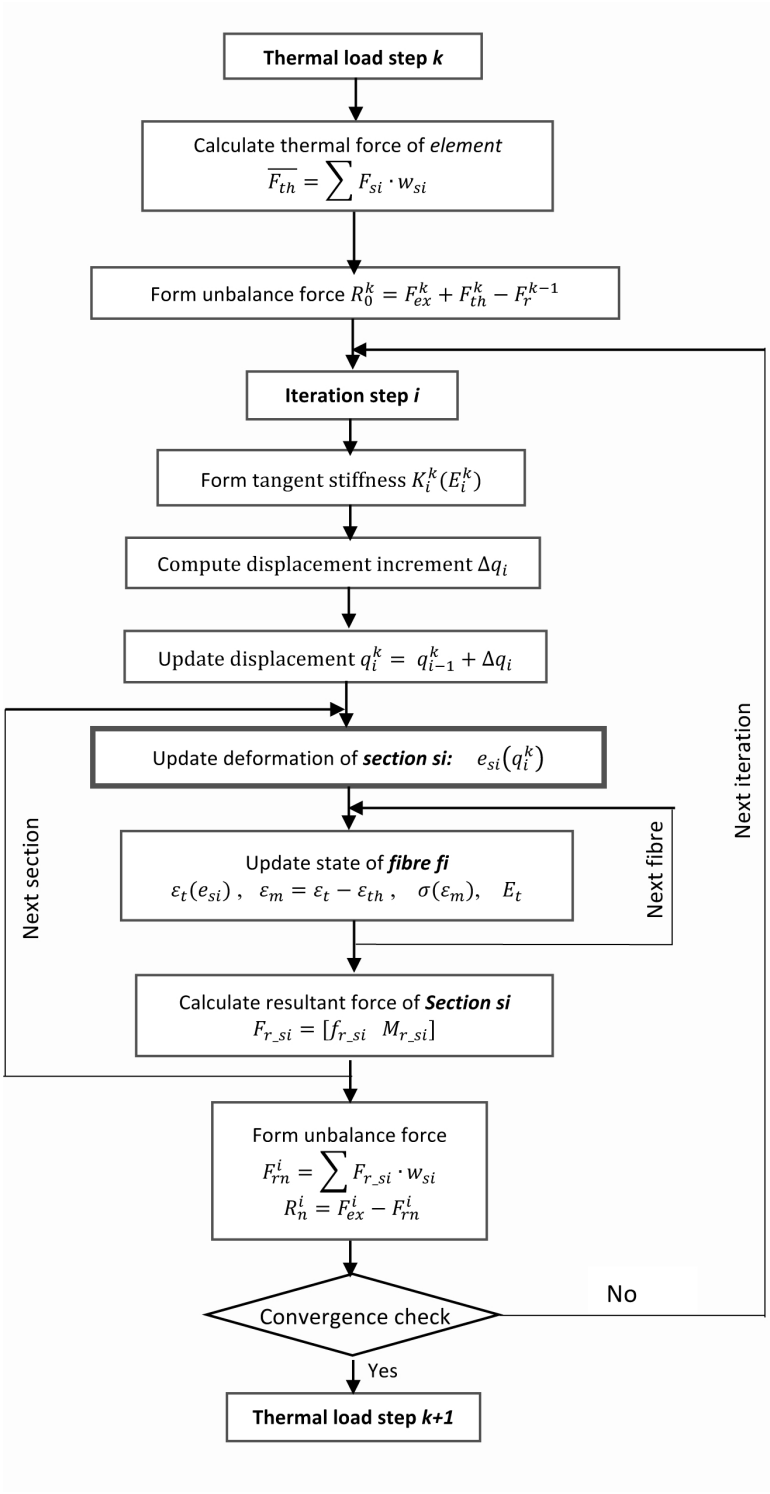

Figure 4.3: Thermo-mechanical analysis using beam-column elements in OpenSees

form **q** is written as:

$$\mathbf{q} = \{q_1 \quad q_2 \quad q_3 \quad q_4 \quad q_5\}^T \tag{4.3}$$

Correspondingly, the nodal forces can be denoted as a vector **Q**.

$$\mathbf{Q} = \{Q_1 \quad Q_2 \quad Q_3 \quad Q_4 \quad Q_5\}^T \tag{4.4}$$

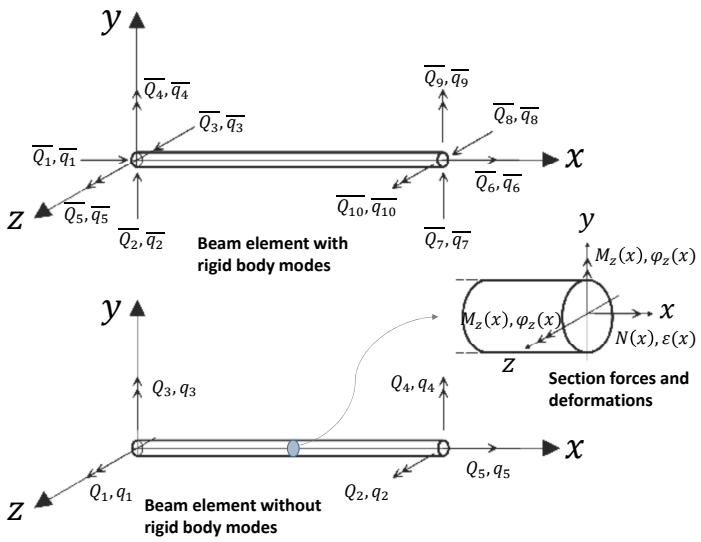

Figure 4.4: Generalized forces and deformations at the element and section level(adapted from (Taucer et al., 1991))

○ *Gauss-Lobatto quadrature*

The Gauss-Lobatto quadrature has been used in the evaluation of the integrals along the beam length. The numerical integration scheme counts the end contributions, and specifies the weights ω_{si} at the deterministic locations ξ_{si} ranging from -1 to 1 in a natural domain. It has been transformed for the beam implementation which defines the integration points at locations x_{si} in the element

domain [0,L], as defined in Equation 4.5 (Scott and Filippou, 2007).

$$x_{si} = (\xi_{si} + 1)/2 \tag{4.5a}$$

$$w_{si} = \omega_{si}/2 \tag{4.5b}$$

Using the above scheme, a integral along the beam length could be evaluated with m integration points:

$$\int_0^L g(x)\ dx = \frac{1}{L}\sum_{si=1}^{m}\Big(g(x_{si})\ w_{si}\Big) \tag{4.6}$$

◦ ***Displacement based beam Element state determination***

In a displacement based beam element, the section deformations are given as an interpolation between the nodal displacements without rigid body modes, which could be written as a vector.

Here for simplicity, a uniaxial bending problem is discussed, with local displacements denoted as:

$$\mathbf{q} = \{q_1 \quad q_2 \quad q_5\}^T \tag{4.7}$$

With the above nodal displacements, section deformations without consideration of non-uniform thermal action can be interpolated as:

$$\overline{\mathbf{d}}(x) = \left\{ \begin{array}{c} \overline{\varepsilon}(x) \\ \overline{\phi}(x) \end{array} \right\} = \mathbf{B}(x)\mathbf{q} \tag{4.8}$$

where $\mathbf{B}(x)$ is derived from the displacement interpolation function, and represents the relationship between the section deformation and nodal displacements.

$$\mathbf{B}(x) = \begin{bmatrix} 0 & 0 & \frac{1}{L} \\ \frac{1}{L}(6\xi - 4) & \frac{1}{L}(6\xi - 2) & 0 \end{bmatrix} \tag{4.9}$$

In the above expression, ξ known as a natural coordinate is given by (x/L). Since the longitudinal displacement at an arbitrary section is linearly interpolated, a constant strain is thereby assumed along the element. This principle remains valid even if the beam is heated by homogenous fire exposure, as the distribution of the total strain $\overline{\varepsilon}$ (mechanical strain plus thermal strain) remains uniform. However, the uniformity is violated in the localised heating regime, where the thermal strain (elongation) varies along the length. As shown in Figure 4.5, a compensation modifier to handle such a localised effect is introduced to refine the axial strain calculation:

$$\overline{\varepsilon}(x) = \frac{q_1}{L} + \overline{\varepsilon_{th}^{e}} - \overline{\varepsilon_{th}}(x) \tag{4.10}$$

where $\overline{\varepsilon_{th}^{e}}$ is the average thermal strain of the element, given as

$$\overline{\varepsilon_{th}^{e}} = \frac{1}{L}\int_0^L \overline{\varepsilon_{th}}(x) \cdot dx = \frac{1}{L}\sum(\varepsilon_{th}(x_{si}) \cdot w_{si}) \tag{4.11}$$

and $\overline{\varepsilon_{th}}$ reflects the average thermal strain of the section, calculated as an integral over the section area $A(x)$

$$\overline{\varepsilon_{th}}(x) = \frac{1}{A(x)}\int_{A(x)} \varepsilon_{th} \cdot dA = \frac{1}{A(x)}\sum(\varepsilon_{th}^{fi} \cdot A_{fi}) \tag{4.12}$$

The modification calculates the thermal strain part before setting up the trial deformations, and deliver the compensated axial total strain to overcome the

uniform total strain assumption. After receiving the modified axial strain, state determination could be performed for the fibre section. According to the classical principle of virtual displacement or minimum potential energy, the element stiffness matrix $\mathbf{K}_e$ is formed from the section stiffnesses using Gauss-Lobatto Quadrature :

$$\mathbf{K}_e = \int_0^L \mathbf{B}^T(x)\mathbf{k}(x)\mathbf{B}(x)\mathbf{d}(x) = L \cdot \sum \left(\mathbf{B}^T(x_{si}) \cdot \mathbf{k}(x_{si}) \cdot \mathbf{B}(x_{si}) \cdot w_{si}\right) \quad (4.13)$$

Similarly, the element resisting force $\mathbf{Q}_r$ is derived as

$$\mathbf{Q}_r = \int_0^L \mathbf{B}^T(x) \cdot \mathbf{D}(x) \cdot dx = L \cdot \sum \left(\mathbf{B}^T(x_{si}) \cdot \mathbf{D}(x_{si}) \cdot w_{si}\right) \quad (4.14)$$

in the above equations, $\mathbf{k}(x_{si})$ and $\mathbf{D}(x_{si})$ are the stiffness and resisting force of section si, respectively.

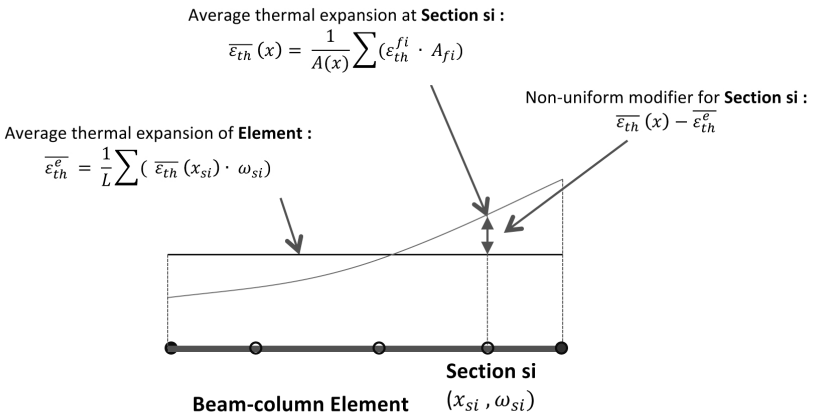

Figure 4.5: Thermo-mechanical analysis with displacement based beam element in OpenSees

◦ ***Force based beam element state determination***

Force based beam element applies the interpolation towards the nodal forces Q,

which is denoted as a vector shown as below for a 2D beam, and corresponding to the notations in Figure 4.4.

$$\mathbf{Q} = \{Q_1 \quad Q_2 \quad Q_5\}^T \tag{4.15}$$

The formulation of force based beam element follows the assumption that the bending moment distribution inside the element is linear, whilst the axial force distribution is constant. The interpolation to get the section forces N and M_z are given as:

$$\overline{\mathbf{D}}(x) = \left\{ \begin{array}{c} N(x) \\ \\ M_z(x) \end{array} \right\} = \mathbf{b}(x)\mathbf{Q} \tag{4.16}$$

where $\mathbf{b}(x)$ represents the interpolation function for section forces:

$$\mathbf{b}(x) = \left[\begin{array}{ccc} 0 & 0 & 1 \\ \\ \frac{x}{L} - 1 & \frac{x}{L} & 0 \end{array} \right] \tag{4.17}$$

Although a linear interpolation is applied at this stage for section moment, the resultant section forces are not distributed in a linear fashion, which is mainly accomplished by the internal iterations performed during the element state determination (Neuenhofer and Filippou, 1997; Scott et al., 2004). The element is known to be based on flexibility, which can be formed through integrating the section contributions:

$$\overline{\mathbf{F}} = \int_0^L \mathbf{b}^T(x) \cdot \mathbf{f}(x) \cdot \mathbf{b}(x) \cdot dx = L \cdot \sum \left(\mathbf{b}^T(x_{si}) \cdot \mathbf{f}(x_{si}) \cdot \mathbf{b}(x_{si}) \cdot w_{si} \right) \tag{4.18}$$

The section flexibility $f(x_{si})$ is given as a inverted form of stiffness matrix:

$$\mathbf{f}(x) = k^{-1}(x) \tag{4.19}$$

Obviously, the section deformation can be derived from the section force, and flexibility.

$$\mathbf{d}(x) = \mathbf{f}(x) \cdot \mathbf{D}(x) \tag{4.20}$$

As pointed out in (Taucer et al., 1991), nodal displacements can be extracted from the incremental solution to the structural response in each load step, i.e. $k-1$, which will be transformed into the local element system as the initialised input for determining the element state in load step k. Similar to the displacement based formulation, the first iteration $i = 1$ for a new step k is responsible to eliminate the effect of thermal induced forces. This is followed by the state update of an element and the state determination in iteration $i = 2$, with the solved incremental displacement $\Delta\mathbf{q}_{i=2}$, as well as the updated nodal displacement $\mathbf{q}_{i=2}$. Both of them have been geometrically transformed into the local coordinate system with the rigid body modes removed. By now, the element is ready to carry out the internal iterations that aim to approximate the real response to the prescribed displacement $\mathbf{q}$. During the iterations performed inside the beam element, the first iteration j=1 after applying new thermal action step k (which means global iteration $i = 2$) is modified to deal with the abruptly increased displacement induced by thermal expansion. The modification attempts to distribute the element deformation to the corresponding sections, which simply adopts the method used in displacement beam formulation as shown in Figure 4.5.

4.2.1.3 Structure state determination

After the element state has been determined, elemental stiffness matrix and resisting force should be submitted to the geometric transformation class, where

they are transformed to the global domain, and assembled into the global stiffness and residual force, respectively. Then the linear equations are formed at the structural level:

$$\mathbf{K}_g^k \cdot \Delta\mathbf{p}^k = \Delta\mathbf{P}^k \tag{4.21}$$

In the above generalised expression, the $\Delta\mathbf{p}$ denotes the incremental displacement in the global system, while $\Delta\mathbf{P}$ represents the unbalanced load between the structural resisting force $\mathbf{P}$ and the external load $\mathbf{P}_r$.

$$\Delta\mathbf{P}^k = \mathbf{P}^k - \mathbf{P}_r^k \tag{4.22}$$

the general form of updating the nodal displacement for iteration i follows:

$$\mathbf{q}_i = \mathbf{q}_{i-1} + \Delta\mathbf{q}_i \tag{4.23}$$

4.2.2 Temperature gradients in beam elements considering localised fire action

For beams subjected to localised fire action, potentially there could be two elementary patterns of temperature gradient formed in the member. One elementary pattern may be the gradient along the member length, while the second can be the gradient across the member section. Whether the fire model defines uniform gas temperature (heat flux) or not, there is always a gradient across the depth because the member surface is heated When it comes to thermo-mechanical analysis, the across-section gradient shall lead to thermo-bowing,

whereas the non-uniform thermal expansion along the length may exist due to the longitudinal gradient.

4.2.2.1 Temperature gradient through the member section

The temperature gradient across the beam section could be implemented with **Beam2DThermalAction** or **Beam3DThermalAction**, as it is primarily developed to consider the thermal action due to the uniformly imposed fire action. In the case of 2D beam application, there are up to 8 temperature zones that can be defined across the beam section. 9 data points therefore are expected to be specified in terms of their temperature histories and the relative locations in the section, as plotted in Figure 4.6. During the period of fire action, the time-variant temperature for each fibre will be determined by linearly interpolating the data from the adjacent data points. For a fibre with the centroid local coordinates (x_i, y_i), its temperature is given by:

$$T_{fi} = \frac{y_{fi} - Y_n}{Y_{n1} - Y_n} T_{n-1} + \frac{y_{fi} - Y_{n-1}}{Y_n - Yn1} T_n \tag{4.24}$$

In the usage of 3D beam elements with I-shape section, **Beam3DThermalAction** provides capability to describe the temperature distribution with respect to its different parts, such as upper and lower flanges, and web. Correspondingly, 4 temperature zones may be used for each part as shown in Figure 4.6. If a fibre locates in the web, interpolation will be performed with respect to y coordinate similarly as defined in Equation 4.24. For fibres located in the flanges, interpolation shall be carried out along z axis.

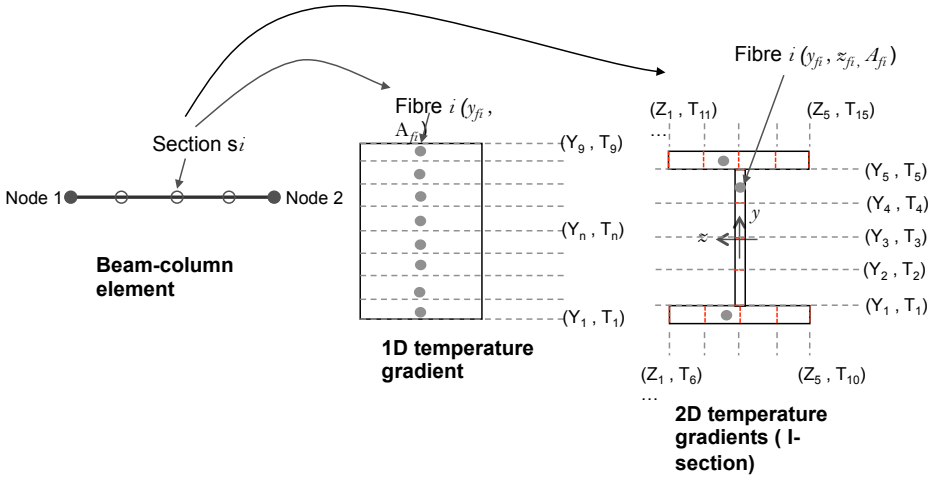

Figure 4.6: Implementation of BeamThermalAction for temperature gradient across section

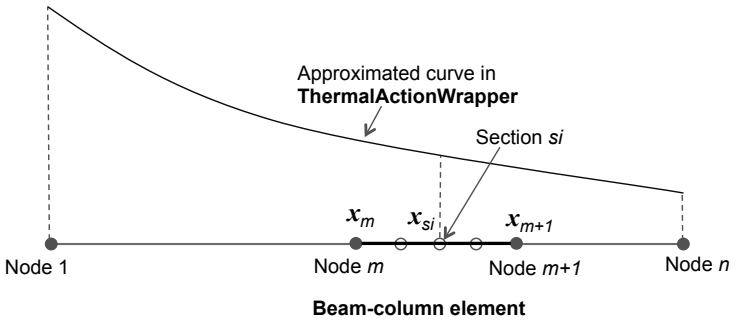

Figure 4.7: Implementation of ThermalActionWrapper for temperature gradient along member length

4.2.2.2 Temperature gradient along the member length

As explained earlier, the displacement based beam formulation was adopted to model the framed beams and columns, being incorporated with the mixed-order interpolation for thermal response. To do so, a **ThermalActionWrapper** class is introduced to describe the temperature variation along the member length, providing the fibre temperature at the integration points. Nodal Thermal Actions are wrapped up into the class, which enables a different form of interpolation to

be performed to determine the temperature profile at each section (integration point) of the beam element. For instance, assuming a beam as shown in Figure 4.7 has been discretised into n nodes and $n-1$ elements, an arbitrary beam element among them may be between node m and node $m+1$. The global coordinates of the integration point (Section si) $\mathbf{x}_{si}$ can be given as:

$$\mathbf{x}_{si} = w_{si} \cdot \mathbf{x}_m + w'_{si} \cdot \mathbf{x}_{m+1} \tag{4.25}$$

where w_{si} and w'_{si} are the weighting coefficients for section si with respect to the element connected node m and node $m+1$, which are of coordinates $\mathbf{x}_m$ and $\mathbf{x}_{m+1}$. The calculated $\mathbf{x}_{si}$ can be plugged into the interpolation scheme enabled by **ThermalActionWrapper**, with temperature profile approximated in accordance with discussion in Section 3.6.2.

4.3 Thermo-mechanical analysis for slabs subjected to localised fire

4.3.1 Thermo-mechanical shell elements

It has been accepted that the deflections of the composite slab system in fires are dominated by the effect of thermal expansion (Gillie et al., 2001a; Elghazouli and Izzuddin, 2000), and during the late stages of heating and higher temperatures membrane action is found beneficial in terms of load bearing resistance (Bailey et al., 2000; Gillie et al., 2004). For composite structure in fire, the performance is highly related to the behaviour of concrete floor slabs (Yu and Huang,

2008). Shell elements considering thermal action were introduced in OpenSees (Jiang et al., 2012; Jiang, 2012a), in order to achieve the computational capability for analysing reinforced concrete and composite steel framed structures. A **ShellMITC4Thermal** element was first created by modifying the existing linear shell element **ShellMITC4**, with geometric nonlinearity enabled using the Total Lagrangian(TL) formulation. A **MembranePlateFiberSectionThermal** had been brought into the definition of shell element on the basis of **MembranePlateFiberSection**, which simply defines a plate section with single material and specific thickness. A number of validation analyses were performed by Jiang (2012a) to test the performance of shell elements.

A new shell element **ShellDKNGThermal** for simulating slab under fire action is introduced in OpenSees. The element is modified from the **ShellDKNG** (Lu et al., 2015) which is based on the general **ShellMITC4** element and employs a multi-layer shell formulation by assuming no slip between each layer. The steel reinforcement can therefore be smeared as a layer and then assembled into the composite slab using **plateRebarThermal**. Updated Lagrangian (UL) description is used to address the geometric nonlinearity, with which the local coordinate system is to be updated during the analysis and corresponding to the current state of the system.

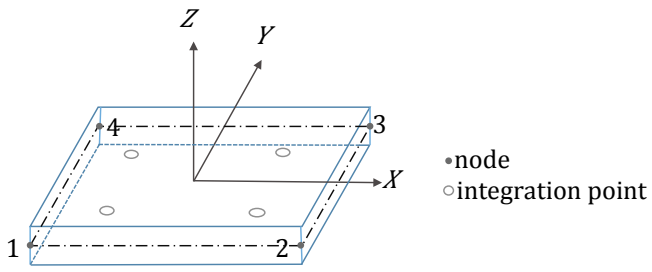

Figure 4.8: A typical four-node shell element

∘ *Multilayer shell formulation*

The proposed element comprises four nodes as the general **shellMITC4** element, and determines its state through the multilayer shell section **LayeredShellSectionThermal**, which discretises the shell section as an array of laminated layers. For each layer, a different biaxial material can be assigned as well as its unique thickness. Therefore the steel reinforcement layers inside the concrete slab can be represented by thin layers of steel in a smeared approach, whereas the rest of the layers can be defined as concrete material. The multilayer configuration is illustrated in Figure 4.9. During the section state determination, temperature for each layer is calculated in accordance with its location and interpolated with the temperature data transferred from the thermal action to the element. Furthermore, the trial strains (total strain) over a layer thickness are assumed to be identical and calculated as a sum of membrane strain in the mid-layer and bending strain induced by the rotating curvature, which follows the Discrete Kirchhoff Quadrilateral (DKQ) thin plate theory by ignoring the effect of shear strain (Jürgen Bathe et al., 1983).

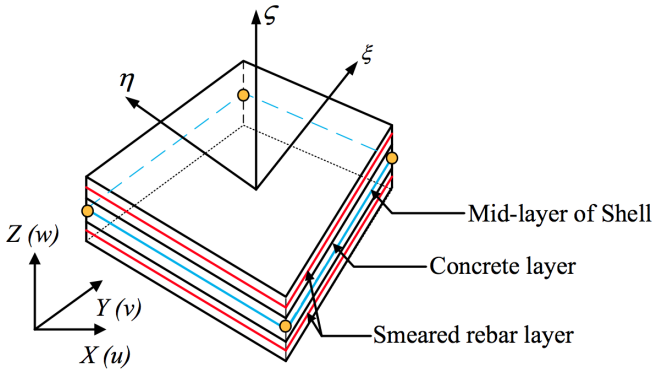

Figure 4.9: Configuration of multilayer shell section (Lu et al., 2015)

∘ ***Materials for Shell analysis***

A wide range of material models are available in OpenSees for defining material

behaviour considering multi-axial interaction at ambient temperature. Among these models, a few have been particularly developed for or can be used for concrete material, such as the Drucker Prager material, Damage2P model, and a user defined material provided by X.Z. Lu. A **DruckerPragerThermal** was modified by Jiang (2012a) based on the original **DruckerPrager** material and was used in modelling concrete slabs in fire (Jiang et al., 2014). The development is not only in terms of the damage estimation, but also in terms of the concrete material response to fire, which is currently considered with reduction factors and thermal expansion defined in accordance with the Eurocode 2 (EN-1992-1-2) (CEN, 2004). The modification was first delivered by Jiang (2012a), with a few benchmark analyses carried out (Jiang et al., 2014). As shown in Figure 4.10, a plane stress description based on the von Mises surface and Rankine criterion was used by the author to develop a stable material model for concrete at elevated temperatures. This **ConcretePlaneStressThermal** is currently modified from the existing **ConcreteS** class, which uses an incremental model to obtain the stress tensor. A full plastic description using return mapping algorithm (Feenstra and De Borst, 1996) is beyond the scope of this thesis, and is expected to be completed in the future. For simplified models only considering elastic behaviour, a **ElasticIstropicThermal** material is available to define a linear thermal expansion ratio α_t in addition to the elastic modulus E.

To include the contribution of steel reinforcement, a smeared reinforcement layer (Huang et al., 2003a; Jiang et al., 2014) is introduced into the multilayer shell section, which was modelled in OpenSees using the multi-dimensional material **DurckerPragerSteelThermal** (Von-Mises Criterion) in the work (Jiang et al., 2014). Such an isotropic material overestimates the resistance of steel rebars and

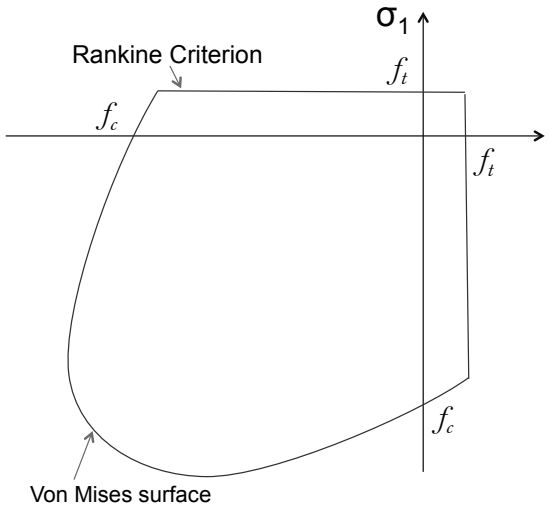

Figure 4.10: A plane stress model for concrete

does not take advantage of the existing uniaxial material library (specially developed models for reinforcing rebars). A new representation of steel reinforcement layer using **PlateRebarThermal** is developed based on the **PlateRebar** class (Lu et al., 2015) which employs uniaxial materials along different directions and can be easily plugged into the plate section. The thermally induced effect upon steel reinforcement layer properties can be implemented with **SteelECThermal**, in which the material degradation and thermal elongation are defined according to Eurocode 2(EN-1992-1-2) for hot rolled or cold formed steel reinforcement.

◦ ***Shell with Non-uniform thermal action***

Similar to the discussion for beam thermal action, it is appropriate to categorise the temperature gradients in slab as through-depth gradient and planar (along the slab plane) gradient. The former gradient is usually found in the slab subjected to the uniform fire action such as post-flashover fires. The latter gradient which always coexists with the temperature variation through the slab thickness, can

be observed in slabs subjected to localised fire action, which has been discussed in Chapter 3.

To account for the gradient through the depth, the **ShellThermalAction** class is adequate to represent the temperature variation, which offers eight temperature zones. In each zone, linear interpolation is performed for the fibre layer, similarly calculated as 4.24. Moreover, an approximation to the planar temperature gradient for the slab in localised fire is achieved with **ThermalActionWrapper**, as described in Section 3.6. The implementation of thermal action has been added into the codes for shell elements as a thermal type load, where the temperature profile is firstly updated to initialise a new load step, with data distributed to the corresponding Gauss integration points to invoke the thermo-mechanical response. An in-plane interpolation is performed to obtain the global coordinates of each Gaussian point:

$$x = \sum_{i=1}^{4} N_i \cdot x_i, \quad y = \sum_{i=1}^{4} N_i \cdot y_i \tag{4.26}$$

where N_i are the bilinear shape functions for the four-node shell element.

4.4 Conclusion

In this chapter, the strategies for modelling structural members subjected to localised fire action are presented. Beam-column elements and shell element are modified or developed to account for the non-uniform temperature distribution induced by localised fires. Conclusions are summarised as below:

- Beam-column elements using force based and displacement based formulations are developed to model the beams and columns subjected to longitudinally non-uniform heating, which incorporates the implementation of dimensionally reduced heat transfer analyses and the rapid estimation approach.

- Fibre based section is employed to describe the section state of framed beam-column element, for which modifiers are applied to consider the non-uniform total strain distribution led by different thermal expansions at various sections.

- Layered shell element using Updated Lagrangian formulation is modified for modelling concrete slabs in fire. A plane stress concrete material associated with layer representation of steel rebars is incorporated with the shell element.

Chapter 5

An OpenSees-based and integrated tool for modelling structures in fires

5.1 Introduction

The development of OpenSees was initiated in 2009 in Edinburgh towards adding a "structures in fire" modelling capability into the framework which will be consistent with the ethos of the other components of OpenSees in terms of being object-oriented and extendable potential. The early-stage work focused on the main topics as: (1) modelling of the fire action and analysis of the fire induced heat transfer to the structural components; (2) thermo-mechanical analysis for modelling structural response to the thermal actions produced by a fire. Based on this work, the concept of an integrated computational tool (SIFBuilder) was

proposed for automated modelling of structures in fire within the OpenSees framework as mentioned in previous chapters.

In this chapter, to differentiate between different terms, a class will be emphasised in bold as **Class**, while a C++ function will be written as **function**, and the variables inside a function will be written as variable. Additionally, there may be words written in *italic* which represent a term that is commonly accepted by the programming community.

This chapter begins with a review of the OpenSees framework, as well as its key features. It is followed by the development details in fire modelling, heat transfer analysis, and thermo-mechanical analysis. The SIFBuilder module for integrating all the different analyses is introduced in the last section.

5.2 OpenSees framework and its features

OpenSees is an object-oriented software framework for finite element analysis. It is implemented using C++ programming (Zienkiewicz et al., 2005) in a modular fashion and interpreted by Tool command language (Tcl) (Ousterhout and Jones, 2009). The framework allows further development by researchers in different areas to modify or implement specific modules with relatively little dependence on other modules.

•Object oriented programming

OpenSees is primarily written in C++ which is an objected oriented programming language (Stroustrup, 2000). Here the concept of *object* can be interpreted as an independent entity that is treated in isolation from all other objects, and

composed of data and functions that define the object's attributes and behaviours. The functions (or methods) associated with an object typically operates on the data that it contains, and can be invoked by a request from other functions. An object-oriented programming (OOP) language like C++ can be treated as a class-based language, since *class* is the key device that provides the blueprint of the objects and specifies the object's internal data structure and procedural functions.

As a class is instantiated to create objects, the internal structure of objects is encapsulated and invisible to the computational processes which have to manipulate them through the objects' interface. This property enables modular programming for a large software system and is usually referred to as *encapsulation*. The other property that makes C++ more exciting is *inheritance*, which produces families out of individual classes. A class (or sub class) derived from the base class (superclass) inherits data and functions from the base class and allows the addition of new internal components which saves a great deal of coding effort by avoiding repetitive work. It is also permitted to redefine the inherited methods with various input forms and different output specifications, which is termed as *polymorphism*. This literally means "many formed" and refers to an important property of OOP. Especially the *virtual* function as a form of dynamic polymorphism assures that the most-derived class (lowest sub-class)'s implementation of the inherited function is called, which could bypass the originally declared function in the base class.

In object-oriented programming, three types of relationships exist between the classes, which are referred to as association, generalisation, and aggregation. The classes and their relationships can be visualised as class diagrams using the Unified

Modelling Language (UML) (Fuentes-Fernández and Vallecillo-Moreno, 2004) as Figure 5.1 shows. Rectangular boxes represent the classes with their names in the top block, and the two blocks below list the class' attributes and operations respectively. When an object of class 1 uses or interacts with an object of class 2, the relationship between them is termed as *association* and is represented with a line linking the classes. When an object of a class consists of component objects as instances of other classes, the relationship between the assembly class and the components is denoted as *aggregation* and represented by a diamond at the assembly class and a line from the diamond to the component class. For a class derived from its base class, a triangle attached to the parent class and a line from the triangle is used to represent the relationship: *generalisation*.

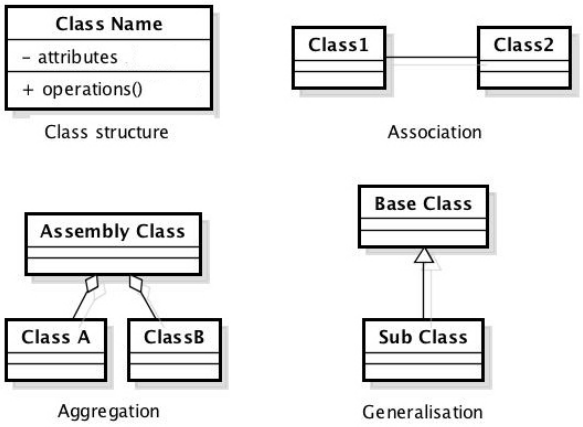

Figure 5.1: Class diagram notations

•Framework for finite element analysis

OpenSees was initially developed for simulating structural response to seismic loading, using finite element method (FEM). To complete an FE structural analysis, the following tasks should be sequentially accomplished : 1) Discretisation

of the structural domain into elements and nodes; 2) Formulation of stiffness matrices and residual forces in elements; 3) Assembling element stiffness matrices and force vectors to establish the global linear system of equations with the incorporation of the boundary conditions; 4) Solving the linear system of equations with a specific solver; 5) Updating each elemental state using the given solution from step 4 and checking for convergence.

To execute the above listed tasks, a comprehensive collection of classes were developed in OpenSees, which may be categorised into four fundamental modules(and base classes): **ModelBuilder**, **Domain**, **Analysis**, and **Recorder**(Figure 5.3). The **ModelBuilder** offers an entry for the user and can be manipulated to construct the FE model as a product of discretisation. The FE model objects are created and added to the **Domain**, which serves as a central storage object to hold the model information and to communicate with the other modules. The **Analysis** module is responsible for processing the global system of equations and providing a solution to advance the analysis. The successfully converged results are recorded and returned to the user through the **Recorder** module, which tracks the status of the selected FE objects and reports on them based on the user's request.

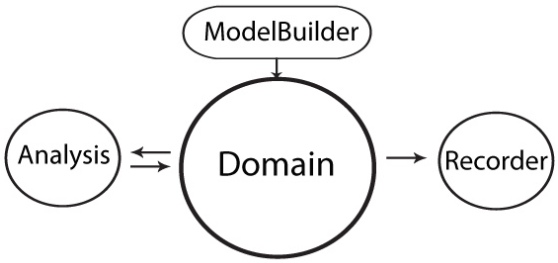

Figure 5.2: Architecture of OpenSees framework

The objects comprising an FE model stored in **Domain** are traditionally

described using abstractions such as **Node**, **Element**, **Load**, and **Constraint**(Dubois-Pèlerin et al., 1992; Dubois-Pe'lerin and Zimmermann, 1993). The boundary condition object **Constraint** can be realised as single point constraint **SP_Constraint** as well as multi point constraint **MP_Constraint**. An external load is applied through **LoadPattern** which may also have various derivations in order to impose different loads.

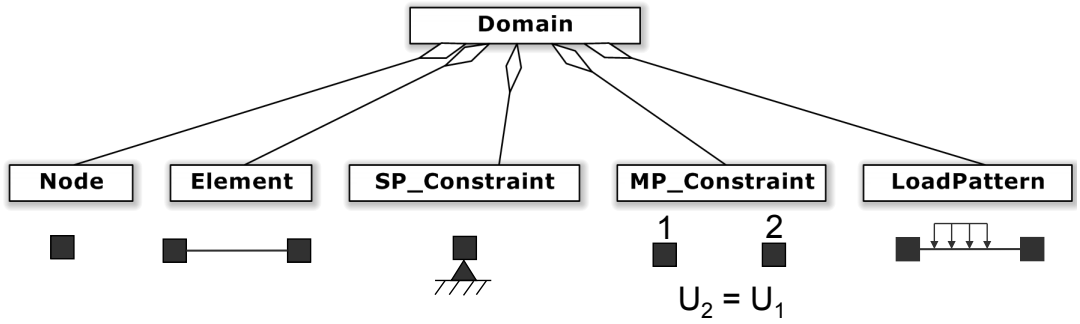

Figure 5.3: Classes abstractions of a finite element model in OpenSees, adapted from (McKenna et al., 2010)

•Tcl interpreter

A few users of OpenSees may be armed with specially developed tools with a graphical user interface (GUI), but most of the OpenSees users still rely upon Tcl commands as the main means of input to build models and conduct analyses. Tcl is a programmable scripting language aiming for a simple-syntax grammar and a standard programming structure. In addition to this, a developer-friendly interface embedded in Tcl permits extensions to the command library, which allows OpenSees developers to programme a standard Tcl entry to their codes rather than a resource file written in C++ format. Facilitated by the Tcl interpreter, OpenSees users are allowed to create their own powered FE analyses using Tcl commands (Scott et al., 2008b). Typical Tcl commands may have a format shown below, where a hashtag sign (#) indicates a sentence of comments,

and a dollar sign ($) represents *variable substitution* where the value of the variable is returned.

```
# Tcl built-in command:

set nodeCrdx 0;

# "set" assigns a value to the variable;

set nodeCrdy [expr $nodeCrdx+2];

#  "expr" evaluates its following expression, hence [expr 1+2]
   will return 3;

# OpenSees extended command:

Node 1 $nodeCrdx $nodeCrdy;

# A node tagged as 1 will be defined with coordinates (0, 2);
```

5.3 Fire modelling and heat transfer analysis in OpenSees

Fire modelling and heat transfer modules have been added into OpenSees through the work conducted by Jiang during his PhD study in Edinburgh University (Jiang et al., 2011). Further development has continued, carried out by the author such as to model the effect of localised fire action and dimensional reduction for rapid estimating heat transfer in structural members. Moreover, Tcl commands are enabled and facilitated by mesh tools, which are later adapted for the implementation of SIFBuilder, as an integrated tool to automate the whole analysis process.

The class diagrams presented in the following sections are based on the UML

notations. A few classes marked in orange are originally created by author, and classes highlighted in light yellow colour indicate that modifications are performed during this thesis work. These modified classes origin from the UoE development of OpenSees have been reported in detail (Jiang et al., 2011; Usmani et al., 2012), whereas the unmarked classes (in white) are the original OpenSees classes created by various developers.

5.3.1 The development of heat transfer module

•Class hierarchy of heat transfer module

While developing the heat transfer module, the class hierarchy is desired to be consistent with OpenSees practice. Figure 5.4 shows a class diagram to represent the classes developed for heat transfer analysis in OpenSees. Similar to the role of **Domain** for a structural model, the **HeatTransferDomain** serves as the central storage which receives the model input from **HTModelBuilder**, and communicates with HT analysis classes to obtain the solution. For each step with converged results, **HTRecorder** and its derived classes are responsible to write the requested data in specific files.

Components of a heat transfer model are corresponding to the structural components as presented earlier in Figure 5.3, and named as **HeatTransferNode**, **HeatTransferElement**, **SP_TemperatureBC**, **MP_TemperatureBC**, **HeatFluxBC** and **BoundaryPattern**. **HeatFluxBC** defines a Neumann type boundary condition, whereas a Dirichlet type boundary condition is specified by the class **TemperatureBC**. Both the boundary condition classes work with **BoundaryPattern** during the analysis. Heat transfer analysis is performed as

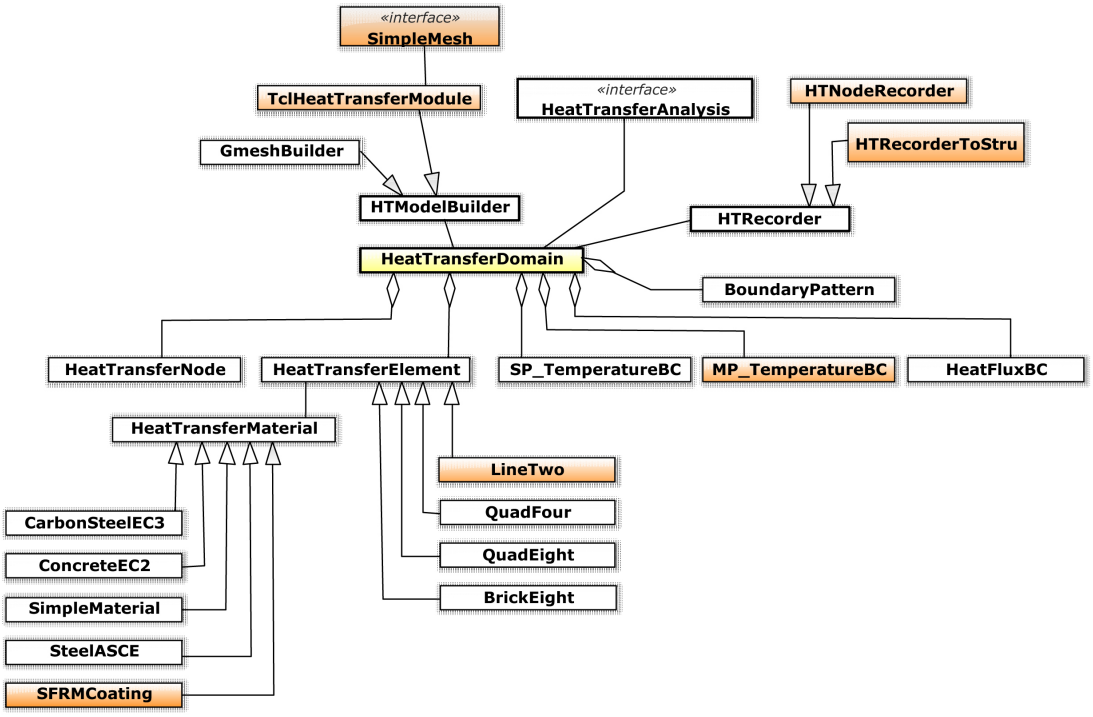

Figure 5.4: Class diagram of the heat transfer module

transient analysis, through the classes derived from **HeatTransferAnlysis** and OpenSees analysis classes. An insightful discussion about heat transfer classes can be found in the work (Jiang et al., 2011).

•Heat transfer materials

Currently the available heat transfer materials have covered the commonly used materials in most structures, which includes previously developed materials of steel and concrete, and the recently created **SFRMCoating** material for spray-applied fire-resistive material (SFRM). When performing heat transfer analysis, the material class must provide its temperature dependent conductivity and specific heat for all materials except for **SimpleMaterial**, where constant parameters are assigned.

•Heat transfer elements

As shown in Figure 5.4, a collection of the heat transfer elements have been developed for solving general problems. As presented in Chapter 3, the strategy of dimensional reduction for heat transfer analysis has been demonstrated, where the heat transfer analyses might be performed in different dimensional environment and the results have proven feasible for most realistic structural response simulations to fire.

A 1D **LineTwo** heat transfer element may be applied in the analyses modelling the heat transfer from fire to a concrete slab after dimensional reduction, whereas a 2D **QuadFour** element is likely to be used for heat transfer through a beam section. For analyses not involving dimensional reduction, 3D **BlockEight** elements ought to be used. Taking **LineTwo** for instance, the development is initialised as inheriting the architecture of its base class **HeatTransferElement**, with the interface returning tangent matrices and residual vectors to the global handler. These terms have been decomposed into four different parts accounting for the contributions from the transient component(heat absorption), conduction, convection and radiation. This approach has been discussed in Chapter 2 when reviewing the thermal analysis of structures in fire. The standard interface of **HeatTransferElement** class specified for **lineTwo** is shown in Figure 5.5. The performances of different elements are compared via modelling the heat transfer through a flat slab, which is assumed to subject 2 hours of fire exposure at the bottom surface defined by the standard fire curve (CEN, 2002a), and losing heat to ambient air at its top surface. Coefficients of convection for exposed and unexposed surfaces are 4 $W/m^2 \times K$ and 25 $W/m^2 \times K$, while emissivities(absorptivities) for radiation at both surfaces are assumed as 0.7. The thermal responses modelled with different types of element are illustrated

```
class LineTwo : public HeatTransferElement
{
 public:
 LineTwo(int tag, int nd1, int nd2, HeatTransferMaterial& m, bool
    phaseTransformation = false);
 // Constructor
 ~LineTwo();

 // methods dealing with nodes associated with element and face
 const ID& getExternalNodes(void);
 const ID& getNodesOnFace(int faceTag);
 int getNumNodesperFace(void) {return 1;};

 // methods dealing with converged and trial status
 int commitState(void);
 int revertToLastCommit(void);
 int revertToStart(void);
 int update(void);

 // methods to return the linearized tangent matrices and residual
    vectors
 const Matrix& getCapacityTangent(void); // K^{c_p}
 const Matrix& getConductionTangent(void); // K^{k}
 const Matrix& getRadiationTangent(void); // K^{r}
 const Matrix& getConvectionTangent(void); // K^{h_c}
 const Vector& get_Q_Transient();  // R^{c_p}
 const Vector& get_Q_Conduction(); // R^{k}
 const Vector& get_Q_Radiation();  // R^{r}
 const Vector& get_Q_Convection();  // R^{h_c}

   // methods to apply heat flux boundary conditions
 void zeroFlux(void);
 int addPrecribedSurfFlux(PrescribedSurfFlux* theFlux, double
    factor) = 0;
 void applyConvection(Convection* theConvection, double factor);
 void applyRadiation(Radiation* theRadiation, double factor);
};
```

Figure 5.5: Interface for heat transfer element **LineTwo** class

in Figure 5.6, which have shown identical temperature growths regardless the sampling depth or exposure duration.

•Thermal Boundary conditions

To complete a heat transfer model, boundary conditions must be specified,

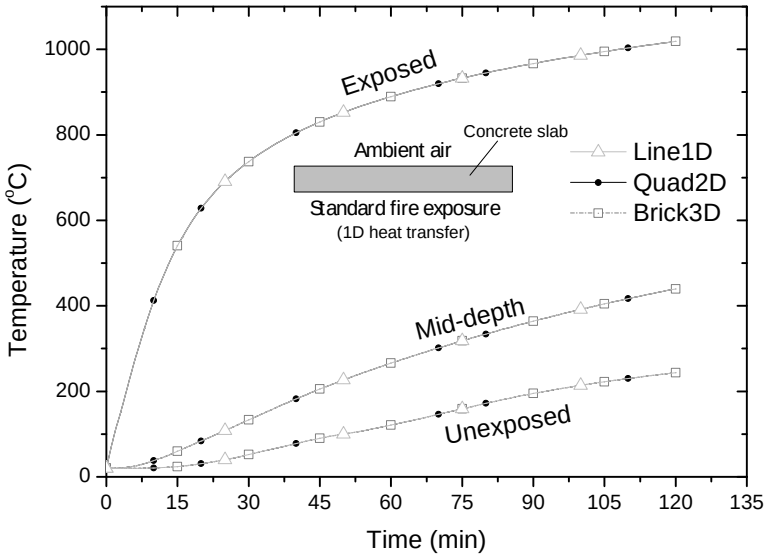

Figure 5.6: 1D heat transfer analysis of a concrete slab exposed to standard fire exposure

which may be represented by the fixed temperatures at one edge or surface, or prescribed heat fluxes, which are usually referred to as Neumann boundary conditions and implemented for localised fire exposure. The latest development is to enable the implementation of Multi-point boundary conditions in constructing a heat transfer model, a set of classes have been created, which include the main functional class **MP_ TemperatureBC**, and the assisting classes: **MP_ TempBCIter** and **PenaltyMP_ FE**. With the introduction of multi-point temperature boundary condition, thus gap conductance at the interface between different materials is enabled, e.g. the heat transfer through steel-concrete interface in a composite beam.

•Heat transfer recorders

Users receive the feedback from OpenSees via a variety of recorders, which is the same for structural analysis. New recorder classes were added to specify the request for the temperature history. As derived from the base class **HTRecorder**,

HTNodeRecorder and **HTRecorderToStru** shares a similar interface but use different procedures for processing specific requests. An object of **HTNodeRecorder** is deployed to handle the request upon a number of specified nodes, able to implicitly pass the data via the class **PathTimeSeriesThermal** (this class will be introduced later in this chapter) or explicitly write the data in a file. The constructor of **HTNodeRecorder** could be defined in multiple forms as shown as in Figure 5.7.

```
class HTNodeRecorder: public HTRecorder
{
  public:
  HTNodeRecorder(int tag);

  HTNodeRecorder(int tag, const ID* theNodes, HeatTransferDomain&
     theDomain);

  HTNodeRecorder(int tag, const ID* theNodes, HeatTransferDomain&
     theDomain, OPS_Stream &theOutputHandle);

  HTNodeRecorder(int tag, const ID* theNodes, HeatTransferDomain&
     theDomain, PathTimeSeriesThermal* thePathSeries);

  HTNodeRecorder(int tag, const ID* theNodes,HeatTransferDomain&
     theDomain, OPS_Stream &theOutputHandle,PathTimeSeriesThermal*
     thePathSeries);

  ~HTNodeRecorder();

  int record(double timeStamp);

  int setDomain(HeatTransferDomain &theDomain);
}
```

Figure 5.7: Interface for **HTNodeRecorder** class

Other than directly assigning nodes to the recorder, a vector of coordinates can be accepted by **HTRecorderToStru** to define the desired locations within the model (Figure 5.8). The local x coordinate is given as the first component in the vector and an array of y coordinates are defined as the rest of the component (for

```
HTRecorderToStru(int tag);

HTRecorderToStru(int tag, const Vector& theCrds,
         HeatTransferDomain& theDomain, double tolerance
            =0.00001);

HTRecorderToStru(int tag, const Vector& theCrds,
         HeatTransferDomain& theDomain, OPS_Stream &
            theOutputHandle,
        double tolerance=0.00001);
```

Figure 5.8: Constructors of **HTRecorderToStru** class

beam-column type elements). Once the recorder is constructed and initialised, the nearest nodes around the requested locations are found and the temperature data of these nodes is later recorded during the analysis. The final displayed data is linearly interpolated based on the distance to its neighbouring nodes.

5.3.2 Tcl application for heat transfer analysis

Tcl command library has been included to facilitate the script based usage of OpenSees. Since the fire and heat transfer modules were developed, it is desirable to have corresponding Tcl commands for performing heat transfer analyses in OpenSees. This will significantly reduce the complexity in constructing a heat transfer model without requiring knowledge of C++ programming as a user.

•A simple mesh tool

Heat transfer analysis in OpenSees is based on the finite element method to solve the transient governing equations. Therefore a mesh tool becomes necessary to discretise the model into nodes and elements. Despite there being tools such as **GmshBuilder** available for constructing FE models with the aid of *Gmsh* (an

open source finite element mesh generator), it was decided to develop a simple meshing class. This avoids the user manipulating *Gmsh* as an extra burden, especially as it is not necessary to use a comprehensive mesh tool since structural members are mostly of regular shapes. The final benefit is a built-in mesh tool that enables an efficient data transaction in the proposed integrated computational tool.

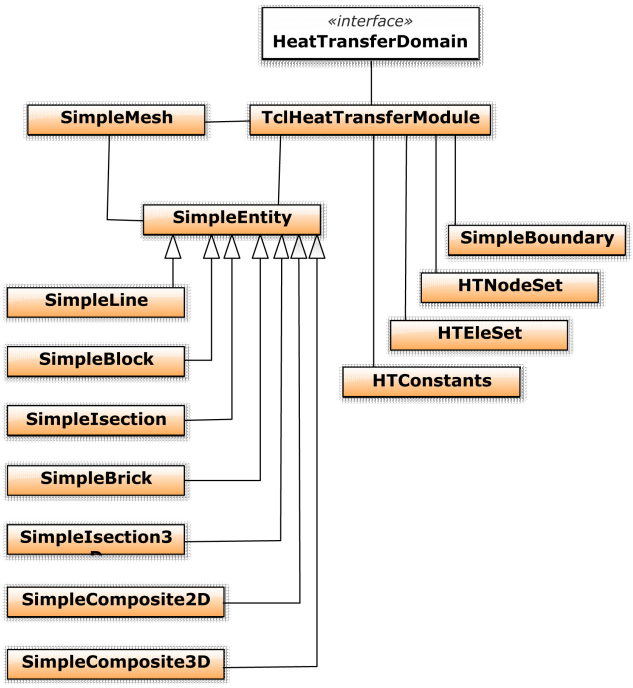

Figure 5.9: Class diagram of Tcl application for fire and heat transfer modules

A **SimpleMesh** as the principal class incorporates a few other supporting classes is developed to enhance the accessibility of Tcl commands for heat transfer analysis. A class diagram of the application has been shown in Figure A.1, where subclasses derived from **SimpleEntity**, e.g. **SimpleLine**, **SimpleBlock**, etc., are responsible to construct entities which represent the actual members or corresponding sections. Meshing schemes such as the seed distribution are stored in the class to initiate the mesh grid and can be refined along

the edge if requested. The standard interface of **SimpleEntity** is defined as shown in Figure 5.10, where the constructor of its derived class differs by the input data. Furthermore, classes such as **HTNodeSet** and **HTEleSet** are associated with **TclHeatTransferModule** to hold the tags (ID) of the selected nodes or elements, respectively. Boundary conditions are handled within **SimpleBoundary**, as the heat transfer constants (convective coefficient, absorptivity, emissivity) are given by **HTConstants** .

```
class SimpleEntity: public TaggedObject
{
  public:
  SimpleEntity(int tag, int EntityTypeTag);

  virtual ~SimpleEntity ();

  virtual int RefineSeeds(int SeedTag, const Vector&RefinedSeedsInfo
     );
  virtual int InitialMeshCtrl(Vector&);
  virtual bool InitialSeeds(void)=0;

  virtual int getEntityTypeTag(void);
  virtual void setMeshTag(int meshTag);
  virtual int getMeshTag(void);

  virtual const Vector& GetSeeds(int)=0 ;
  virtual int GetNumofNodes()=0;
  virtual int GetNumofEles()=0;
  virtual const ID& GetNumCtrlID()=0;
  virtual void  Print(OPS_Stream&, int = 0) {return;};
}
```

Figure 5.10: Interface for **SimpleEntity** class

The **SimpleMesh** class as shown in Figure A.1 is associated with **SimpleEntity** and **TclHeatTransferModule**. The latter contains the procedures defined for Tcl interpreter. As the main functional class, **SimpleMesh** receives model information such as seed distribution from **SimpleEntity** and parameters related to mesh control interpreted by **TclHeatTransferModule**. The actual mesh is

sought to be completed within two steps: **GeneratingNodes** and **GeneratingEles**, both as member functions of the class. During the generation of heat transfer nodes, a vector that contains the relative distance to the fire origin could be assigned to enable the heat transfer analysis to be performed at various sections. This is followed by the generation of heat transfer elements which can be specified as using the enthalpy method or direct heat capacity by defining the corresponding EleParameters. Various interfaces are made available to select the nodes or elements from the **SimpleMesh**, which can be used for defining boundary conditions or request data output.

•Tcl interface for adding HT commands in OpenSees

Tcl embedded in OpenSees not only makes the scripting job remarkably convenient, but also provides an excellent potential to extend the command collection. Based on the mesh tool, it becomes possible to create brief enough Tcl commands for heat transfer analysis and fire model definition in OpenSees. It is accomplished through the standard application interface provided by the Tcl library, e.g., the **Tcl_CreateCommand** for adding new commands. It can be implemented as presented in Figure 5.12.

•Tcl commands for heat transfer analysis in OpenSees

For users who want to conduct heat transfer analysis with OpenSees, it is necessary to follow the flowchart shown in Figure 5.13 when organising the Tcl commands and creating the script.

First and foremost, the module is activated by **HeatTransfer** to enable the application of the relevant commands and facilities. Notice that the argument following the **HeatTransfer** command shall define the number of dimensions that can be either 1D or 2D or 3D, which is useful in the cases that dimensional

```
class Simple_Mesh: public TaggedObject
{
  public:
  SimpleMesh(int tag, Simple_Entity* Entity,
        HeatTransferDomain* theDomain,
        HeatTransferMaterial* theHTMaterial,
        Vector& MeshCtrls,
        HeatTransferMaterial* theHTMateria1 = 0);
  SimpleMesh(int tag=0);
  ~SimpleMesh();

  int GetNumOfNodes();
  int GetNumOfEles();
  int SetOriginLocs(const Vector& originLocs);
  int SetEleParameters(const ID& eleParameters);

  int GeneratingNodes(const Vector& originLocs=0);
  int GeneratingEles(const ID& EleParameters=0);

  int SelectingNodes(ID& NodesRange, int crdTag, double MinValue,
     double MaxValue, double Tolerance=0.00001);
  int SelectingNodesbyFace(ID& NodesRange, int FaceTag=1);
  int SelectingEles(ID&ElesRange, const ID& NodesRange, int
     eleFaceTag=0);
  int SelectingElesbyFace(ID& ElesRange,int FaceTag,int &eleFaceID);

  int GetNodesForRecorder(ID& NodesRange, int dimTag,double PlaneLoc
     =0.0);
  int GetNodesForRecorder(ID& NodesRange, const Vector& MonitorLocX,
      double PlaneLoc=0.0);
  int GetNodesForRecorder(ID& NodesRange, double xLoc, double yLoc);

  const ID& getNumCtrlID();
  void  Print(OPS_Stream&, int = 0) {return;};
}
```

Figure 5.11: Interface for **SimpleMesh** class

reduction (this strategy has been introduced in Chapter 3) is applied. **HTMesh** shall be in association with **HTMaterial** and **HTEntity**, which accepts a wide range of entity types that are linked to the subclasses in the **SimpleEntity** family. The available types of entities and their usage can be found in detail from Appendix A. Seed distribution for the mesh can be refined if necessary by providing a vector containing element size and number. The final mesh is

```
//Head file included to enable implementation of Tcl library
#include <Tcl.h>

// Prototype of using Tcl_CreateCommand
Tcl_CreateCommand( (Tcl_Interp*) interp,
          (const char*) cmdName,
          (Tcl_CmdProc*) proc,
                    (ClientData) clientData,
          (Tcl_CmdDeleteProc*) deleteProc);

//Declaration of command procedure
int proc(ClientData clientData, Tcl_Interp *interp,
                   int argc, char *argv[]);
```

Figure 5.12: Interface for adding new Tcl command

completed once **HTMeshAll** is detected. This is followed by a few commands to declare the appropriate boundary conditions, as either fixed (**HTSetT**)or coupled (**HTcoupleT**) temperatures. Constants shall be defined before the heat flux boundary conditions are specified which list the coefficient of convection to or from ambient, ambient air temperature and the resultant emissivity of the fire plume. **HTPattern** is then used in association with *AmbientBC* for describing the heat loss to the ambient environment, while the keyword *FireExp* is to invoke fire exposure defined as a specified fire model ranging from uniform fire action to localised fire exposure. Before proceeding to heat transfer analysis definition, heat transfer results can be requested via **HTRecorder** command. Heat transfer analysis is finally completed after receiving **HTAnalyze** and thereafter the model can be wiped out using command **wipeHT**. An example demonstrating heat transfer analysis within OpenSees is presented in Appendix A.

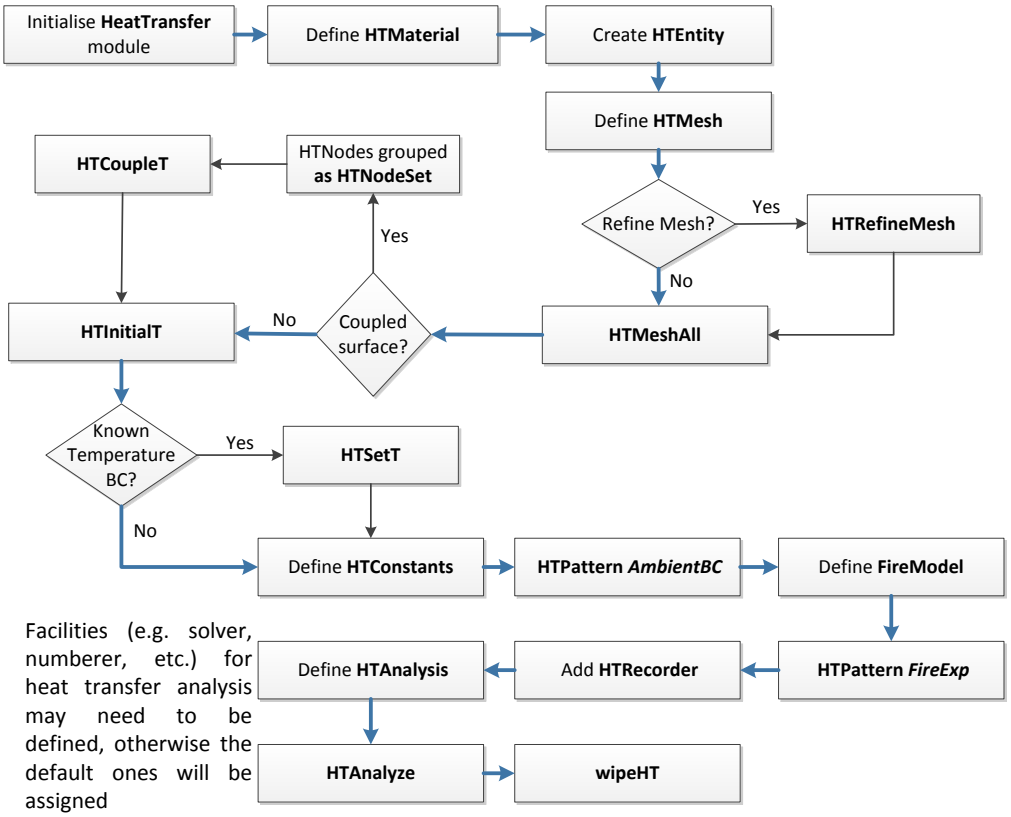

Figure 5.13: Configuration of HTEntities

5.3.3 Development of fire module

A number of fire models have been defined within an independent module, where a universal interface is provided to transform the fire action in the form of a heat flux distribution over structural surfaces. This can be realised through implementing the following classes, **Convection**, **Radiation**, and **PrescribedSurfFlux**, which are derived from the base class **HeatFluxBC**. For fire models with gas temperature given, the heat fluxes received by structural members are considered in the form of convection and radiation. However, localised fire models adopt an incident heat flux based on the measured test data, with compensation due

to the temperature difference between the heat flux gauge and member surface. The incident heat flux is the core output from the localised fire models, as a realisation of **PrescribedSurfFlux**. The heat flux compensation shall be defined using **Convection** and **Radiation** due to the temperature difference between heat flux gauge and structural surface. During the period of fire exposure, a **FireImposedPattern** similar to the **LoadPattern** in structural domain is required to handle the time-dependent factors. For the unexposed surfaces of a structural member, heat exchange with the ambient environment is in the form of convection and radiation, therefore the **BoundaryPattern** class becomes an aggregation of these **HeatFluxBC** subclasses.

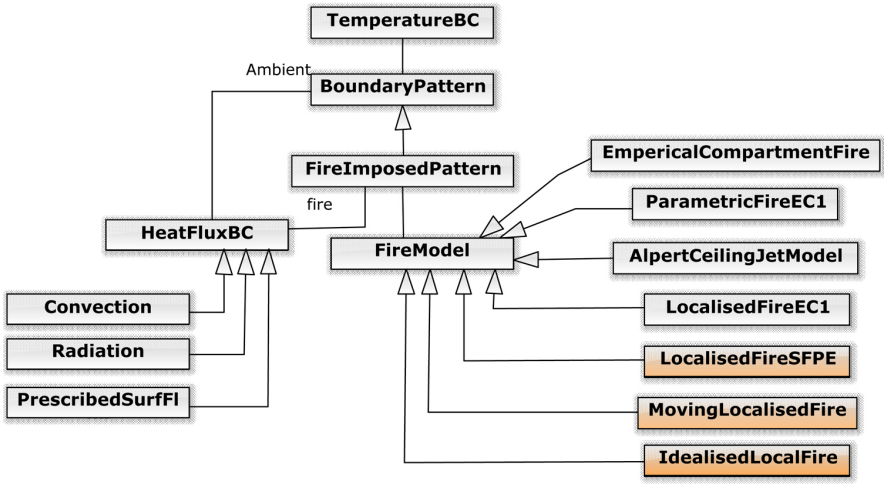

Figure 5.14: Class diagram representing time-dependent boundary conditions and the fire module

A diagram shown in Figure 5.14 is to illustrate the class hierarchy of fire module and its associated classes. Among them a number of classes containing fire models have been added for conducting analyses presented in Chapter 3. A typical localised fire model is defined as a form of time-variant heat flux, hence the interface only invokes updating and returning heat fluxes to the element. In the

```
class LocalizedFireSFPE : public FireModel
{
    public:
    LocalizedFireSFPE(int tag, double crd1, double crd2, double
       crd3, double D, double Q,
                  double HC, double HB, int centerLineTag = 3,
                     double qsquare = 0);

    virtual ~LocalizedFireSFPE();

    void applyFluxBC(HeatFluxBC* theFlux, double time);
    double getFlux(HeatTransferNode* the_node, double time,int
       FireType);
    private:
    double x1, x2, x3, d, ini_q, hc, hb;
    int centerLine, FireType;
    double Qsquare;
};
```

Figure 5.15: Class interface for **LocalizedFireSFPE**

LocalisedFireSFPE class, correlations between heat fluxes and radial distance to the fire source are defined according to SFPE handbook (Lattimer, 2002). The last added fire model class is **IdealisedLocalFire** with which it is possible to define incident heat flux with a linear, bilinear or quadratic distribution. The standard interface for localised fire model is seen from Figure 5.15.

With the above mentioned development, heat transfer to structural members is possible to be analysed in OpenSees with Tcl scripts. To demonstrate the usage, a Tcl script is written to perform heat transfer analysis in a steel beam underneath a concrete slab, which is assumed to be heated by a localised fire in accordance with SFPE correlations. The full version of the Tcl script for the example model is presented in Appendix A.

5.4 Thermo-mechanical analysis in OpenSees

The capability of performing thermo-mechanical analysis in OpenSees is enabled by implementing thermal action and thermo-mechanical elements, which include beam elements for modelling framed beams and columns and shell elements for slabs. In order to consider the comprehensive temperature dependent behaviour, thermo-mechanical materials and sections have been developed and are able to represent the material degradation and thermally induced expansion. With regard to the aforementioned integrated computational environment, a well designed middleware shall be provided to bridge the heat transfer and thermo-mechanical analyses.

5.4.1 Middleware design for linking heat transfer and thermo-mechanical analyses

The communication between the heat transfer module and thermo-mechanical analysis is the most important part of the integrated computational environment for structures in fire developed by the author (SIFBuilder). Temperature history captured by heat transfer recorder is readable by the thermo-mechanical module and follows a format that corresponds to different type of thermal action. The temperature history written into data files are accessible for users to edit if advanced thermal analyses are performed. The above method for transferring the temperature data is explicit and involves writing data files. An alternative approach is implicitly transferring the results with **PathTimeSeriesThermal**, which is directly attached to the definition of thermal action. Note that data

transaction in explicit (to report results) and implicit (to transfer results) patterns could take place at the same time using SIFBuilder.

PathTimeSeriesThermal is the key class that collects the vector of loading step and a matrix for temperature data. Assuming there are n steps in a heat transfer analysis, then the matrix of temperature data is of size (m, n), where m represents the number of data points received by thermal action (usually 9 or 15). This class is modified from **PathTimeSeries** by introducing a matrix for multipoint temperature data and a function for writing data into the the matrix, as shown in Figure 5.16. Applications of this class are mostly in specifying thermal actions with location based temperature histories.

```
  PathTimeSeriesThermal(int tag,
     const char *fileName,int DataNum =9, bool tempOut =true,
     double cfactor = 1.0);
  PathTimeSeriesThermal(int tag,
     int DataNum =9, bool tempOut =true,
     double cfactor = 1.0);

 int WriteResults(double currentTime, const Vector& newData);

 int numCols;
 int numRows;
 Matrix *thePath;
 int TempOut;
```

Figure 5.16: Class constructors and interfaces for **PathTimeSeriesThermal**

5.4.2 Implementation of thermal action

Thermal action class is responsible to handle heat transfer results and deliver the calculated temperature data to the structural elements. In the current implementation of OpenSees, there are various options to define thermal actions,

which could be user-defined, or imported from a text file, or implicitly transferred from the heat transfer module to the implementation of thermal loading in SIFBuilder. A class diagram illustrating thermal actions is shown in Figure 5.17. Here the development has been carried out in two steps: first the thermal actions for beam and shell elements to process temperature gradients only through the member sections (for uniform fire), and second the thermal actions extended to the longitudinal temperature gradients induced by localised fire action (Figure 5.18).

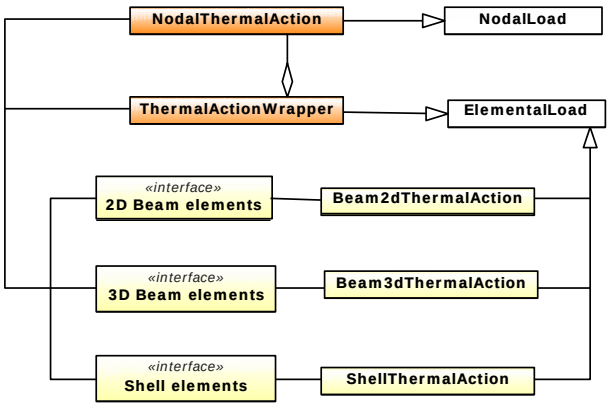

Figure 5.17: Class diagram of thermal action

As shown in Figure 5.17, the first step development includes the following classes: **Beam2dThermalAction**, **Beam3dThermalAction**, and **ShellThermalAction**. These classes are correspondingly used for beam and shell elements, having been enhanced by the incorporation of **PathTimeSeriesThermal** to receive the input for multi-point temperature history. The enhanced forms of classes are associated with new constructors, which could be represented by the implementation in **Beam2dThermalAction** (Figure 5.19).

Tcl commands for defining longitudinally uniform thermal action can be written in various forms to fulfil the different requirements, such as a 1D distribution along

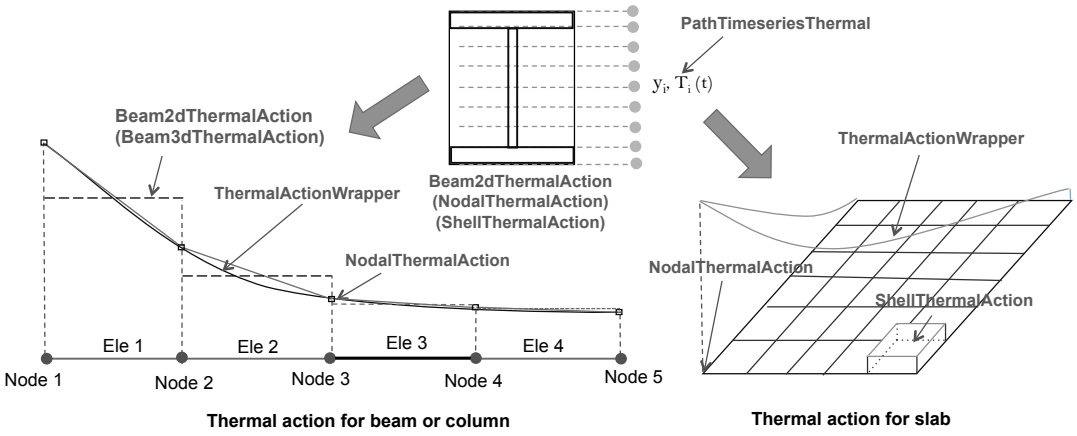

Figure 5.18: Implementation of thermal action for thermo-mechanical elements

```
Beam2dThermalAction(int tag,
         double locY1, double locY2,
         TimeSeries* theSeries, int theElementTag
         );

Beam2dThermalAction(int tag,
         const Vector& locs,
         TimeSeries* theSeries, int theElementTag
         );
Beam2dThermalAction(int tag, int theElementTag);
```

Figure 5.19: Class constructors of **Beam2dThermalAction**

the beam height (slab depth) with the maximum temperatures specified at up to 9 different locations. Additionally, for 3D beam section with I shape, 5 temperature slots for upper and lower flanges and web can be defined as a 2D profile. As mentioned earlier, the thermal action could be defined through reading an external text file that contains the time steps and temperature information. The time step is allocated in the first column, while the temperature data corresponding to each data point is listed in the other 9 (1D) or 15 (2D) columns.

It may be noticed in Figure 5.18 that **ThermalActionWrapper** and

NodalThermalAction are available for all the thermo-mechanical elements, which deal with the cases involving localised thermal action which is of major concern in this thesis. **ThermalActionWrapper** comprises of a limited number (2,3,or 5) of **NodalThermalAction** objects, between which a quadratic or cubic or mixed-order interpolation may be performed to approximate the temperature distribution along the beam length or shell plane. A quadratic interpolation constructor of **ThermalActionWrapper** is presented in Figure 5.20. The theory and its validation has been presented in Chapter 4.

```
ThermalActionWrapper(int tag, int EleTag,
          NodalThermalAction* theNodalTA1,  NodalThermalAction*
             theNodalTA2,
          NodalThermalAction* theNodalTA3
         );
```

Figure 5.20: Class constructor of **ThermalActionWrapper** with three **NodalThermalAction**s

As an alternative approach, **NodalThermalAction** could be applied independently at the nodes and therefore a linear interpolation could be employed to obtain the temperature inside the element. Although the temperature history is defined on the nodes, elemental thermal action must be declared to invoke the element to call the linked **ThermalActionWrapper** or **NodalThermalAction**. Tcl commands for the implementation of nodal thermal action could be written as follows:

```
#Definition of nodal thermal action
load $NodeID1 -nodalThermal -source $fileName1 $y1 $y2 $y3 $y4 $y5 $y6
    $y7 $y8 $y9;
load $NodeID2 -nodalThermal -source $fileName2 $y1 $y2 $y3 $y4 $y5 $y6
    $y7 $y8 $y9;
load $NodeID3 -nodalThermal -source $fileName1 $y1 $y2 $y3 $y4 $y5 $y6
    $y7 $y8 $y9;

#Thermal action for 2D or 3D beam section
eleLoad -ele $beamID -type -beamThermal -source -node;

#Thermal action for shell section
eleLoad -ele $shellID -type -shellThermal -source -node;

#Using ThermalActionWrapper
eleLoad -ele $eleID -type -ThermalWrapper -nodeLoc $NodeID1 0 $
   NodeID1 $factor $NodeID1 1;
#'-ele' could be replaced by '-range' for multiple elements as used
   elsewhere
```

5.4.3 Implementation of beam-column elements

For frame structures, beam-column elements (may be generally mentioned as beam elements later for convenience) have been extensively used to model beam and columns, which allow a great deal of computational efficiency particularly for large frame models. As discussed in Chapter 4, beam-column elements in the application of thermo-mechanical analyses can be formulated as displacement based or force based, showing a difference in terms of accuracy and mesh size. Considering that flexural deformation is the primary concern for beams and columns, the cross section is discretised into a number of fibres, through a variety of fibre based sections as reported in the works (Usmani et al., 2012; Jiang and Usmani, 2013). For each fibre that comprises the cross section, a variety of thermo-mechanical materials have been developed based on existing material models with the addition of temperature dependent properties defined according to Eurocodes (CEN, 2002a,

2004, 2005). The class hierarchy of beam implementation has been presented in

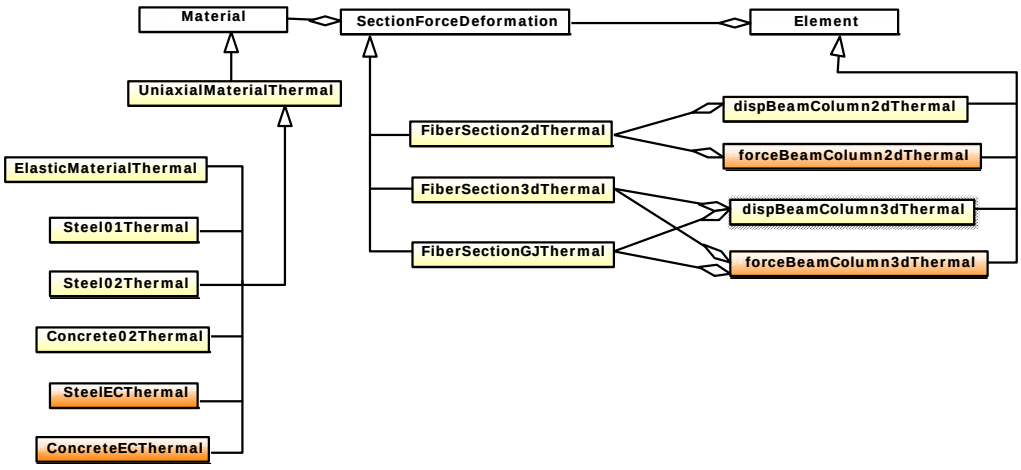

Figure 5.21: Class diagram for beam-column element implementation

Figure5.21, where **Material**, **SectionForceDeformation** and **Element** are abstract classes. As shown in the Figure, beam elements are derived from the base class **Element** and preserves the general interface and data structure of the original beam-column elements, such as the calculation of stiffness matrix and residual vectors, and so on. To enable thermo-mechanical analysis, the following code has been added into the beam element class: (1) Load implementation, to receive temperature data from the defined thermal action, which might be a temperature gradient with a uniform distribution along the beam length, or a localised distribution defined by **ThermalActionWrapper** or **NodalThermalAction**; (2) Consideration of non-uniform thermal elongation in the formulation of tangent stiffness matrix; (3) Optimisation of the residual calculation for the first iteration in each step of thermal action.

•Development for applying localised thermal action

The methodology for considering localised thermal action has been explained in

```
// if loadtype == LOAD_TAG_ThermalActionWrapper;
for (int i = 0; i < numSections; i++) {
    int order = theSections[i]->getOrder();
    const ID &code = theSections[i]->getType();
    double xi6 = 6.0*xi[i];
  int ndm = theNode0Crds.Size();
  Vector theIntCrds = Vector(ndm);
  for(int m = 0; m<ndm; m++){
  theIntCrds(m) =  theNode0Crds(m)+xi[i]*(theNode1Crds(m)-
     theNode0Crds(m));
  }
  //global coordinates of the Gauss integration point
  Vector dataMixV = ((ThermalActionWrapper*) theLoad)->getIntData(
     theIntCrds);
  //obtain the section thermal elongation
  if(theSections[i]->getClassTag()==SEC_TAG_FiberSection2dThermal)
   SectionThermalElong[i]= ((FiberSection2dThermal*)theSections[i
       ])->getThermalElong()(0);

  const Vector &s = theSections[i]->getTemperatureStress(dataMixV)
     ;
    double si;
  double ThermalEloni;
  //Calculation of thermal-induced force
  if(s!=0){
     for (int j = 0; j < order; j++) {
  si = s(j)*wt[i];
  ThermalEloni = SectionThermalElong[i]*wt[i];
  switch(code(j)) {
  case SECTION_RESPONSE_P:
  q0Temperature[0] += si;
  AverageThermalElong += ThermalEloni; break;
  case SECTION_RESPONSE_MZ:
  q0Temperature[1] += (xi6-4.0)*si;
  q0Temperature[2] += (xi6-2.0)*si; break;
  default:
  break;
  }
     }
  }
  }
```

Figure 5.22: Implementation of thermal action in displacement based beam element

Chapter 4 when discussing the formulation of the beam elements. The section classes at integration points receive the temperature data from its affiliated beam element, which may be interpolated in the global coordinate system if

ThermalActionWrapper is available. For thermal action only defined at the nodes with **NodalThermalAction**, a linear interpolation is performed to get the temperature data for sections. A distributive scheme is utilised for considering the non-uniform thermal elongation along the beam length for displacement based beam elements, to bypass the assumption that longitudinal strain is constant along the beam length in the two-node element formulation. However, non-uniform thermal elongation can be naturally considered when the beam element is based on flexibility, which is usually referred to as the force based beam element. The different formulations thus lead to slight differences in accounting for the localised thermal action when implementing the elements, which requires a calculation of distributive thermal elongations for displacement based elements and the optimisation for the internal iteration in force based beam elements. The implementation of thermal action for displacement based beam element is presented in Figure 5.22. The full version of the code developed for beam elements can be found in Appendix C.

```
for (int i = 0; i < numFibers; i++) {
    FiberForce = Fiber_Tangent[i]*fiberArea[i]*DeltaThermalElong[i
        ];
    SectionArea +=fiberArea[i];
    SectionMomofArea += (fiberArea[i]*(fiberLocs[i] - yBar)*(
        fiberLocs[i] - yBar));
    ThermalForce += Fiber_ElongP[i]*fiberArea[i];
    ThermalMoment += Fiber_ElongP[i]*fiberArea[i]*(fiberLocs[i] -
        yBar);
      sTData[0] += FiberForce;
      sTData[1] -= FiberForce*(fiberLocs[i] - yBar);
  }
  AverageThermalElong(0) = ThermalForce/SectionArea;
  AverageThermalElong(1) = ThermalMoment/SectionMomofArea;
```

Figure 5.23: Function in fibre section to return the average thermal elongation

•Development of fibre sections and uniaxial materials

With regard to the material nonlinearity, beam section is discretised into fibres as a fully validated approach for frame members where flextural deformation dominates. For 2D beam elements, **FiberBeamSection2dThermal** shall be defined at the integration points, whereas the **FiberBeamSection3dThermal** as well as **FiberBeamSectionGJThermal** are appropriate to be used for 3D beam elements. These classes are initially created based on the existing section classes (Scott et al., 2008a) which have no thermal effect considered. The preliminary development of section classes for thermo-mechanical analyses are referred to in the work (Usmani et al., 2012). As non-uniform thermal action is a major concern in this thesis, the code has been modified to evaluate the average thermal elongation (AverageThermalElong) for each section, as shown in Figure 5.23. Similar changes could be seen in 3D section classes.

Temperature dependent behaviour is eventually addressed with the thermo-mechanical material classes. For the beam section as an aggregation of fibres, uni-axial material model is employed to represent its contribution to the section resisting stiffness. Currently a handful of materials have been developed in OpenSees for concrete and steel, which include **Steel01Thermal**, **Steel02Thermal**, **Concrete02Thermal**, **SteelECThermal**, **ConcreteECThermal**. Among them, the first three materials are adapted from the original OpenSees classes which describe the material behaviour at the ambient temperature, with modifications to introduce stiffness and strength reductions with temperature and thermal strain calculation. The latter two are revised Steel and Concrete material models to the the full Eurocode version as defined in Eurocode 2 and Eurocode 3, respectively.

5.4.4 Implementation of shell elements

OpenSees, being a tool initially developed for earthquake engineering, lacks resources for modelling concrete slabs. This limited capability is due to the commonly accepted approach that treats floor slabs as a rigid diaphragm for most analyses. In case of structural behaviour in fire, modelling the concrete slab is extremely important because of its unique contributions to resisting fire action (Bailey et al., 2000; Gillie et al., 2001a). This contribution features both of bending and membrane actions which have been investigated in many published works (Gillie et al., 2004; Huang, 2010). To model concrete slabs in fire within OpenSees, an earlier effort was presented in (Jiang et al., 2014), which discussed the implementation of shell elements in the context of uniform thermal action. In this work, the continuing development for shell analysis focused on the implementation of localised fire based on exploring the use of new classes of multi-layer shell elements with geometric nonlinearity included.

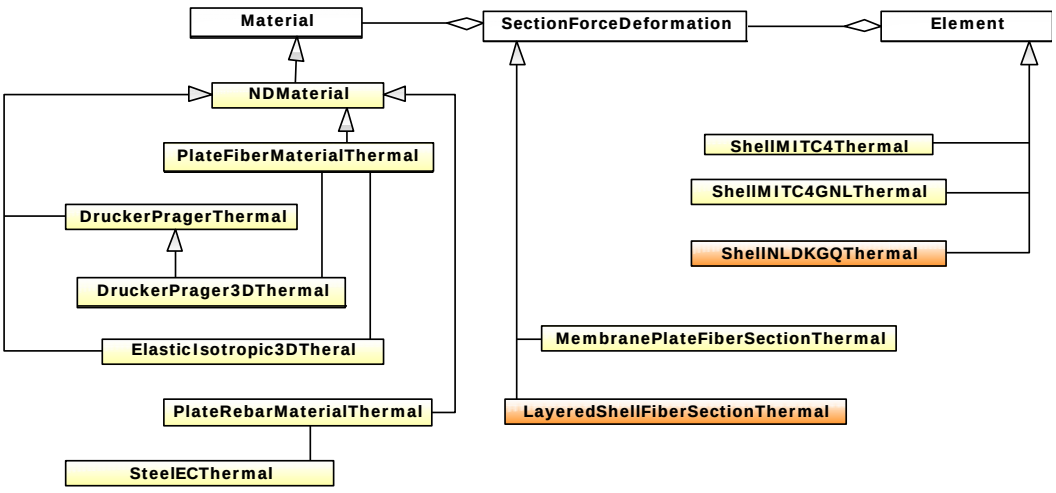

Figure 5.24: Class diagram of shell implementation

The class diagram shown in Figure 5.24 lists the currently available classes for

conducting shell analyses with fire action taken into account. Similar to the beam analysis, classes are derived from the following abstract classes: **Element**, **SectionForceDeformation**, and **Material**, which also implies its class hierarchy. With respect to the shell element classes, a **ShellNLDKGQThermal** is newly listed on OpenSees site and defines a geometrically nonlinear shell element based on an updated Lagrangian formulation. The ambient version of this class is originally modified from **ShellMITC4**, with geometrical stiffness included through Lu's work (Lu et al., 2015), and further updated by the author for thermo-mechanical analysis. An alternative option for geometrical nonlinearity is **ShellMITC4GNLThermal** which adopts a total Lagrangian description. If geometric nonlinearity is not of interest, **ShellMITC4Thermal** is adequate. In terms of the shell section class, it is allowed to define a five-layer plate section using **MembranePlateFiberSectionThermal**, for which only one material can be assigned. An advanced section class is developed as **LayeredShellFiberSectionThermal**, which is modified from Lu's work for a multi-layer shell section (Lu, 2013). Both section classes are applied with layer temperatures, for which a linear interpolation is performed in conjunction with the thermal action classes. Sequentially, the section classes are responsible for calculating thermally induced section forces to account for the effect of thermal expansion. The material state at each layer is updated following the request of shell section class. Currently one elastic material and two ideally elasticplastic materials are available to model the multi-axial behaviour for shell analysis. The elastic material **ElasticIsotropic3DThermal** is defined with constant elastic modulus and poisson ratio, as well as an invariant coefficient for thermal expansion. Plastic behaviour of concrete used to be modelled by **DruckerPragerThermal** and a plate fibre representation via **PlateFiberMaterialThermal** in Jiang's work,

and was recently redirected to using **ConcreteSThermal** which is a plane stress material with Mises Yield surface associated with Rankine criterion. A **PlateFromPalneStressThermal** transformation was developed to adapt the plane stress material to shell element implementation. A similar approach is applied to the smeared reinforcement layer, which is invoked by **PlateRebarThermal** to provide an orthogonal description derived from uniaxial materials.

•Development for applying localised thermal action

When fire action is imposed on the slab, the calculated temperature history is transferred through the **ShellThermalAction** (in-plane uniform distribution), **ThermalActionWrapper** and **NodalThermalAction** (in-plane non-uniform distribution). As a subclass derived from **ElementalLoad**, **ShellThermalAction** itself is able to define an in-plane uniform thermal action. After being enriched by **ThermalActionWrapper** and **NodalThermalAction**, it is possible to convey a localised temperature profile to the thermo-mechanical model in the case of localised fire. A typical process within the shell element class is presented in Figure 5.25, where the thermal action is received as **ThermalActionWrapper**. The coordinates of connected nodes are used to calculate the global coordinates of the corresponding Gauss integration points, which serves as input to obtain the interpolated temperature profile. This is followed by the calculation of thermally induced section force as a returned result from *getTemperatureStress*.

•Development of shell sections and n-dimensional (ND) materials

The current section classes for shell analysis are **MembranePlateFiberSectionThermal** and **LayeredShellFiberSectionThermal**. The former class was derived from **MembranePlateFiberSection** which defines a laminated section

```
counterTemperature = 1;          //indicator of thermal action
    step
  // Loop over the integration points
  Vector theNode1Crds = nodePointers[0]->getCrds();
Vector theNode2Crds = nodePointers[1]->getCrds();
Vector theNode3Crds = nodePointers[2]->getCrds();
Vector theNode4Crds = nodePointers[3]->getCrds();

int ndm = theNode1Crds.Size();
Vector theIntCrds = Vector(ndm);

for (int j=0; j<4; j++)  {
//Obtain interpolated temperature
 double xi = sg[j];
 double eta = tg[j];

 theIntCrds.Zero();
 for(int i=0;i<3;i++){
 theIntCrds(i) = shapefn2d(xi, eta, 1)*theNode1Crds(i)
                 + shapefn2d(xi, eta, 2)*theNode2Crds(i)
         + shapefn2d(xi, eta, 3)*theNode3Crds(i)
         + shapefn2d(xi, eta, 4)*theNode4Crds(i);
 }

Vector dataMixV = ((ThermalActionWrapper*) theLoad)->getIntData(
   theIntCrds);
  const Vector &s = materialPointers[j]->getTemperatureStress(
     dataMixV);
  residThermal[2*j] = s(0);
residThermal[2*j+1] = s(1);
```

Figure 5.25: Implementing **ThermalActionWrapper** in the shell element class

with 5 layers of the same material assigned. The recently developed class **LayeredShellFiberSectionThermal** was established from the work presented by Lu et al. (2015), which offers a multi-layer definition for a shell type section, and allowing various materials to be assigned to each layer. The major tasks of section class are: (1) to determine layer temperature; (2)to calculate thermally induced section forces; (3)and to update the material status of each layer fibre. Temperature is determined through linear interpolation between the specified temperature

zone boundaries, while the thermally induced force is obtained according to the discussion in section 4.3 as shown in Figure 5.26.

DruckerPrager material was first modified by Jiang et al. (2014) to model the behaviour of concrete slabs in fire. A new revision was completed by the author to implement the tension cut-off (Walker et al., 2002). This modified **DruckerPragerThermal** co-works with its 3D representation **DruckerPrager3DThermal** and its plate material wrapper **PlateFiberMaterialThermal**. A recent addition to the thermo-mechanical ND materials is the **CocreteSThermal**, which adopts a plane stress configuration and defines more suitable yielding surfaces for modelling concrete behaviour. A material wrapper **PlateFromPlaneStressThermal** modified from **PlateFromPlaneStress** (Lu et al., 2015) is responsible to adapt the plane stress material to the usage of shell section. As aforementioned, smeared steel rebar layer is modelled using PlateRebarThermal which interprets the uniaxial materials to multi-axial implementation.

5.5 A tool to perform integrated 'structure in fire' simulations

•The concept of SIFBuilder

Development of OpenSees Thermal is an ongoing project and is presently limited to only a few elements, material models and fire scenarios. This cannot fully exploit the great potential of the OpenSees framework. Furthermore, a single software to carry out the full set of analyses including realistic fire load modelling

```
const Vector&
LayeredShellFiberSectionThermal::getTemperatureStress(const Vector&
    dataMixed)
{
  this->countnGauss = 0;
  double* ThermalTangent = new double[nLayers];
  //reset variables
  for (int i = 0; i < nLayers; i++) {
          ThermalTangent[i]=0;
          ThermalElongation[i]=0;
  }
  double FiberTemperature = 0 ;
  double tangent, elongation;
  double averageThermalForce =0.0;
  double averageThermalMoment =0.0;
  //calculate section forces
  for (int i = 0; i < nLayers; i++) {
  double thickness = 0.5*h*wg[i];
    double yi = ( 0.5*h ) * sg[i]
  double tangent, elongation;
  FiberTemperature = this->determineFiberTemperature( dataMixed, yi)
      ;
  theFibers[i]->getThermalTangentAndElongation(FiberTemperature,
      tangent, elongation);

  ThermalTangent[i]=tangent;
  ThermalElongation[i]=elongation;
  averageThermalForce += elongation*thickness*tangent;
  averageThermalMoment+= yi*thickness*elongation*tangent;
  }
  (*sT)(0) = averageThermalForce - AverageThermalForceP;
  (*sT)(1) = averageThermalMoment - AverageThermalMomentP;
  AverageThermalForceP = averageThermalForce;
  AverageThermalMomentP = averageThermalMoment;
  return *sT;

}
```

Figure 5.26: Calculation of thermal induced force in Shell section class

(e.g. localised and travelling fires); heat transfer to structural components (by radiation, convection and conduction); and structural response, is still unavailable. In order to move towards a more comprehensive solution for a unified analysis, an OpenSees based research tool named SIFBuilder is proposed, which

aims to perform automated structural fire analyses for large structures under realistic fires. It is a comprehensive computational tool, which could enable structural engineers to obtain the structural response automatically with the application of the fire load on the structure in the same manner as any other form of load and so provide a performance-based structural fire engineering tool. It would potentially also become a testbed to foster a wide range of future developments, which may be new fire models featuring advanced characteristics in terms of fire science, or new thermo-mechanical constitutive models for materials, sections and elements to improve the accuracy and efficiency of integrated simulations.

A few third-party preprocessor tools have been developed for conducting analyses in OpenSeeS. One typical application is **BuildingTcl**, which includes a number of Tcl procedures within its library. A graphical interface provides a user friendly process for building the finite element model, and eventually generating a Tcl script to complete the analysis in OpenSees. Such a purely Tcl based tool is efficient in modelling structures against earthquake loading or other mechanical loadings. However, for modelling structures subjected to fire loading, the heat transfer analyses and the subsequent definitions of thermal actions presents a much greater level of complexity. C++ based process is thus adopted, taking advantage of its object-oriented property and the generalised application interfaces (APIs) to the OpenSees classes. As an individual project in OpenSees, SIFBuilder is designed to be a hub that communicates with different modules and controls the integrated analysis based on user instructions via the Tcl interpreter. Here new Tcl commands are specially developed for SIFBuilder, and have been kept simple in terms of the grammar and intuitive in terms of the architecture.

5.5.1 Framework design for SIFBuilder

• **Input for SIFBuilder**

Unlike commercial packages, neither OpenSees nor SIFBuilder have a graphical user interface (GUI). However, there is a script based user input capability based on Tcl, which provides considerable flexibility and scope due to its programmable nature. Similar to other commonly used FEM software, SIFBuilder requires the user to input basic structural information for generating the structural model. Procedural scripts are written to specify geometry, materials, loads, heat transfer parameters, fire type, analysis procedures, solution algorithm and output requirements using Tcl commands. A SIFModel is firstly created to store the building information, for which the typical user input script includes:

(1) model type definition for identifying the dimension of analysis (2D or 3D);
(2) geometry of the structure (bay lengths in each direction and storey heights in a Cartesian coordinate system);
(3) material type and cross section type for the structural members;
(4) boundary conditions for the structural model.

Following the SIFModel generation, a user may define:
(5) structural loading (point load at joints or uniformly distributed load on members);
(6) and thereafter the fire loading information.

The mechanical load and fire action are stored in the SIFModel, out of which a finite element model can be created as:
(7) building FE model with mesh control specified.

Data output after creating FE model can be requested as:

(8) a variety of SIFRecorders which captures the nodal displacement or elemental forces.

Finally the full set of loading can be set up and executed by:

(9) SIFAnalyze command followed by incremental step and number of steps that are defined for each corresponding analysis.

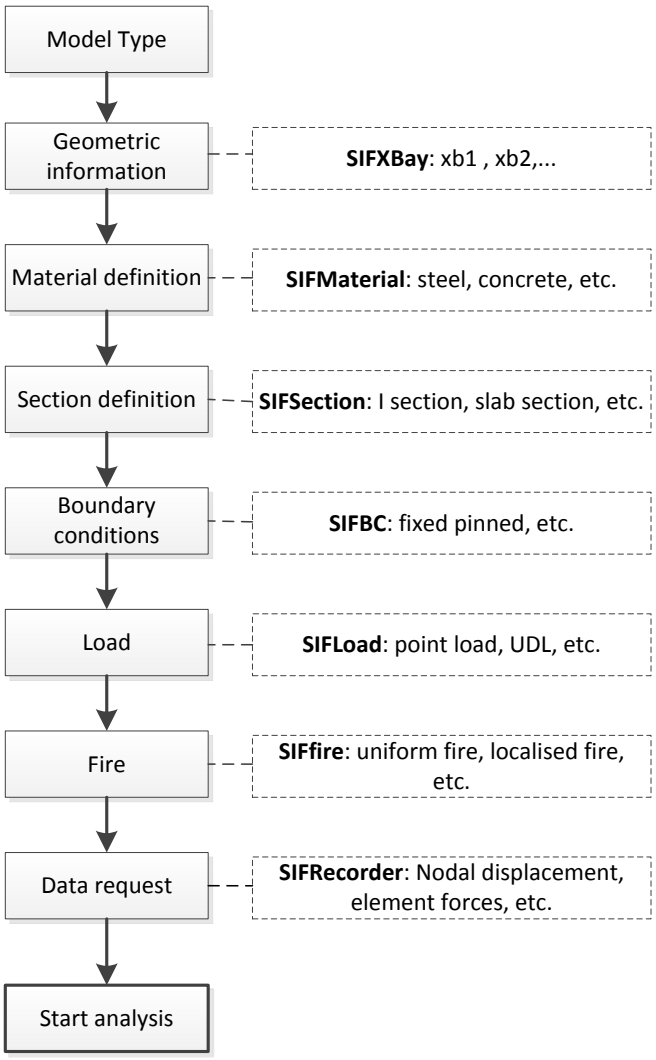

Figure 5.27: Class diagram of SIFBuilder Module

Figure 5.27 shows the work flow of writing the Tcl script for performing integrated

thermo-mechanical analysis in the project SIFBuilder. SIFBuilder is programmed to hold the building configuration throughout the structural analysis, allowing further operations over the SIFModel which may include removal of members to create variations of the building model, such as atrium spaces or large compartments. The heat transfer analysis module launches after the thermal action step is executed. Nodal temperature histories are calculated and automatically mapped onto the fibres of the corresponding elements. Following the heat transfer analysis, structural analysis is performed on the building, accounting for the thermally induced deformation and the degraded material properties.

•Developed classes in the SIFBuilder project

SIFBuilder is programmed in C++, constructed with the same hierarchy as used in the main framework. A **SIFBuilderDomain** has been created as the central storage to a variety of classes, which are responsible for holding all general information on materials, sections, members, and so on.

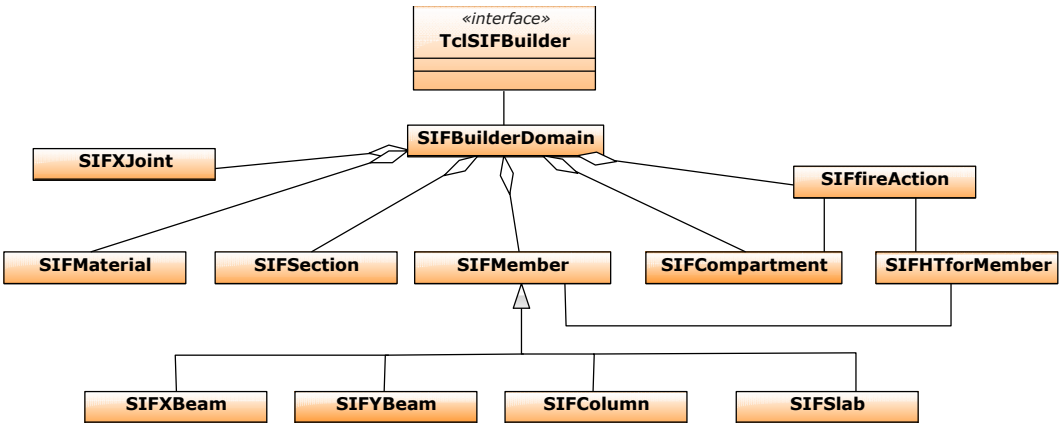

Figure 5.28: Input of SIFBuilder Module

As shown in Figure 5.28, **TclSIFBuilder** provides a command-based entry to the **SIFBuilderDomain**. Operations as shown in Figure 5.29 are programmed

to identify the input and then process the received information. One direct product of these procedures is a generalised SIFModel to hold the information of the building and loading details. Such as for a building constructed using a structural frame, the model recognises it as a composition of joints and members. A **SIFJoint** class therefore contains the joint coordinates in the global system, being instantiated at every joint including the foundation. Between these joints, a variety of classes derived from **SIFMember** are defined to represent the beams, columns and slab. Particularly for the beam representations along the x and z axes, **SIFXBeam** and **SIFZBeam** are respectively defined for the convenience of numbering. The additional and indispensable information for a **SIFMember** is of course its section description, which is linked to a **SIFSection** and accompanied by a **SIFMaterial**. During one complete analysis, material properties and section profiles always came from these classes and are supplied to the heat transfer and structural models. Another component of the SIFModel is the **SIFCompartment**, which literally refers to the compartments in the building being modelled. And it is usually associated with the **SIFfireAction**, as the main class to handle the imposed loading.

In SIFBuilder, fire impact is presumed to be compartment-based, which thereafter searches for all the heated members within the compartment, and then invokes **SIFHTforMember** to perform heat transfer analysis for each heated member. The heat transfer results are captured as **PathTimeSeriesThermal** and plugged into various thermal action classes corresponding to the heated structural members. In pursuit of an integrated modelling environment, most of the essential processes including heat flux impingement on the structural members, heat transfer and the implementation of thermal action are automatically carried

```
int TclSIFBuilderCommand_addMaterial(ClientData clientData,
    Tcl_Interp *interp, int argc, TCL_Char **argv);
int TclSIFBuilderCommand_addSection(ClientData clientData,
    Tcl_Interp *interp, int argc, TCL_Char **argv);
int TclSIFBuilderCommand_assignSection(ClientData clientData,
    Tcl_Interp *interp, int argc, TCL_Char **argv);
int TclSIFBuilderCommand_addXBay(ClientData clientData, Tcl_Interp *
    interp, int argc, TCL_Char **argv);
int TclSIFBuilderCommand_addYBay(ClientData clientData, Tcl_Interp *
    interp, int argc, TCL_Char **argv);
int TclSIFBuilderCommand_addStorey(ClientData clientData, Tcl_Interp
     *interp, int argc, TCL_Char **argv);

int TclSIFBuilderCommand_addFireAction(ClientData clientData,
    Tcl_Interp *interp, int argc, TCL_Char **argv);
int TclSIFBuilderCommand_applyAndanalyze(ClientData clientData,
    Tcl_Interp *interp, int argc, TCL_Char **argv);
int TclSIFBuilderCommand_addFirePars(ClientData clientData,
    Tcl_Interp *interp, int argc, TCL_Char **argv);
int TclSIFBuilderCommand_SetBC(ClientData clientData, Tcl_Interp *
    interp, int argc, TCL_Char **argv);
int TclSIFBuilderCommand_AddLoad(ClientData clientData, Tcl_Interp *
    interp, int argc, TCL_Char **argv);

int TclSIFBuilderCommand_AddSIFRecorder(ClientData clientData,
    Tcl_Interp *interp, int argc, TCL_Char **argv);
int TclSIFBuilderCommand_BuildSIFModel();
int TclSIFBuilderCommand_BuildModel(ClientData clientData,
    Tcl_Interp *interp, int argc, TCL_Char **argv);
```

Figure 5.29: Declaration of Procedures for **TclSIFBuilder**

out. As the development is ongoing for SIFBuilder, important benefits are noticed from using such an object-oriented approach. Different operations can be distributed into different classes, whereas each one of them has only a limited number of tasks, leading to a highly modular program structure.

•Construction of SIFModel

The so-called SIFModel is a higher-level term compared to the finite element description of the structure. It is constructed within the function (procedure) **TclSIFBuilderCommand_BuildSIFModel()**, once the geometry configuration is

determined with vectors specifying the dimension of bays and storeys. At first, a number of **SIFCompartment** instances are created as a looped operation over the structure, which always follows the order from X-axis (XBay) to Z-axis (ZBay), and then Y-axis (Storey), as illustrated in Figure 5.30. Then the **SIFJoint** is repeatedly defined at each frame joint with coordinates given in the global coordinate system. The third step is to create **SIFMember**s, which subsequently define instances corresponding to **SIFSlab**, **SIFXBeam**, **SIFZBeam**, and **SIFColumn**. During this step, the corresponding **SIFJoint**s are found and assigned to their connected members. Moreover, it is necessary to create links between the **SIFMember**s and the **SIFCompartment** that contains these members, which is useful for the later implementation of compartment based fire exposure. The available interface provided by **SIFCompartment** can be found in Figure 5.31, where the connected members are possible to be added and returned.

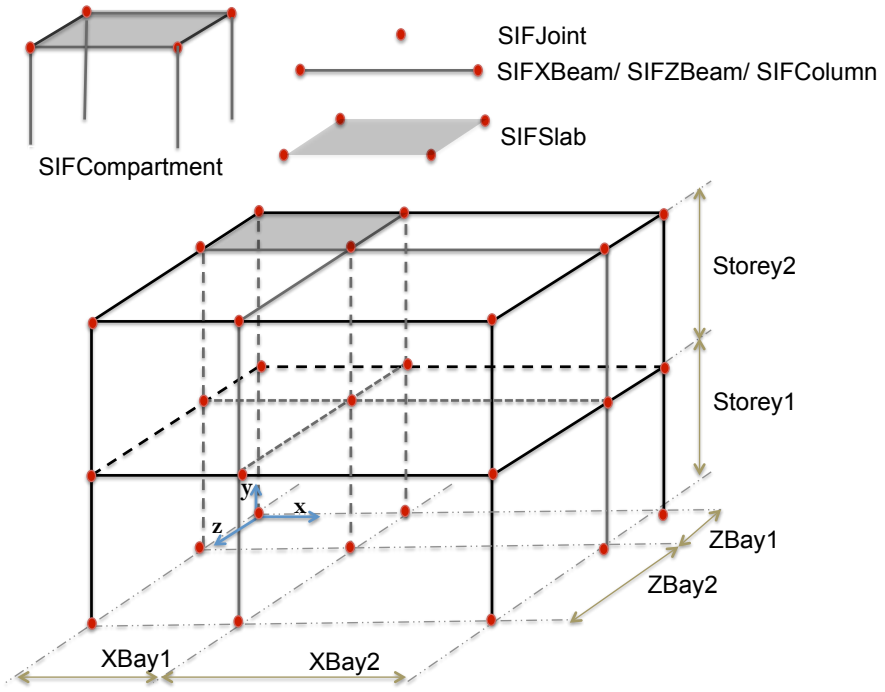

Figure 5.30: Class diagram of SIFBuilder Module

```
class SIFCompartment: public TaggedObject
{
public:
 SIFCompartment(int tag, const ID& Compinfo, const Vector&
     CompOrigin);

 //Add member tags, and return tags when being requested
 int AddXBeam(int MemberTag);
 const ID& getConnectedXBeams(void);
 int AddZBeam(int MemberTag);
 const ID& getConnectedYBeams(void);
 int AddColumn(int MemberTag);
 const ID& getConnectedColumns(void);
 int AddSlab(int MemberTag);
 const ID& getConnectedSlabs(void);

 const ID& getCompartmentInfo(void);
 const Vector& getCompartmentOrigin();
 virtual ~SIFCompartment ();
 virtual void  Print(OPS_Stream&, int = 0) {return;};
private:
   ID theCompInfo;
 Vector theCompOrigin;
 ID* theXBeamTags;
 ID* theYBeamTags;
 ID* theColumnTags;
 ID* theSlabTags;
};
```

Figure 5.31: Interface in the **SIFCompartment** class

When the Tcl interpreter receives definitions about the boundary conditions and loading cases, the SIFModel shall be established beforehand. While defining boundary conditions, restraints are attached to the relevant **SIFJoint** located by their tag or coordinates. Similarly for self weight or mechanical load, a load vector in each **SIFMember** is employed to specify the magnitude and direction. Slight difference is seen in adding fire action, where **SIFfireAction** as a class is instantiated with a specific fire model type and compartment tag, and is added to the **SIFBuilderDomain** for later implementation. The input may vary as it is dependent on the type of fire model, which may be standard fire that just requires

a duration, or parametric fire (CEN, 2002a) that asks for opening factor and boundary insulation properties, or localised fire models that require heat release rate, coordinates of fire origin, and so on. The above information is embedded into SIFModel, and can be read and extracted from the associated objects to create finite element based structural model for thermo-mechanical analysis.

•Construction of the finite element model of the structure

A finite element (FE) model should be ready prior to the thermo-mechanical analysis. A function **GenStructuralModel** in **SIFBuilderDomain** is invoked to build up the FE model, while the Nodes and elements are subsequently created by extracting model information from the SIFModel as stored in **SIFBuilderDomain**. There are two steps for node generation. The first step is to perform a full loop over all the joints with nodes created. Such a loop is realised through a **SIFJointIter**, which is like the other types of iterator classes that are defined for repeated operations over the instances of the same class type. Such an approach has been widely used elsewhere in OpenSees, which implicitly searches for the available instances with no need to specify a tag.

Following the node generation at each joint, the second step is to discretise the members with a certain level of mesh refinement, which is determined by the parameters received as MeshCtrlPars in **GenStructuralModel**. Node and element generation for beams and columns is performed within **MeshSIFMember** as the process is essentially identical. Nodes inside the member are distributed along the longitudinal direction with a uniform space. Between the nodes, element is defined with a 3D beam section given by the associated **SIFSection**, and the material model is obtained from the assigned **SIFMaterial**. A special situation for element definition occurs at each end of the member, where the node is given

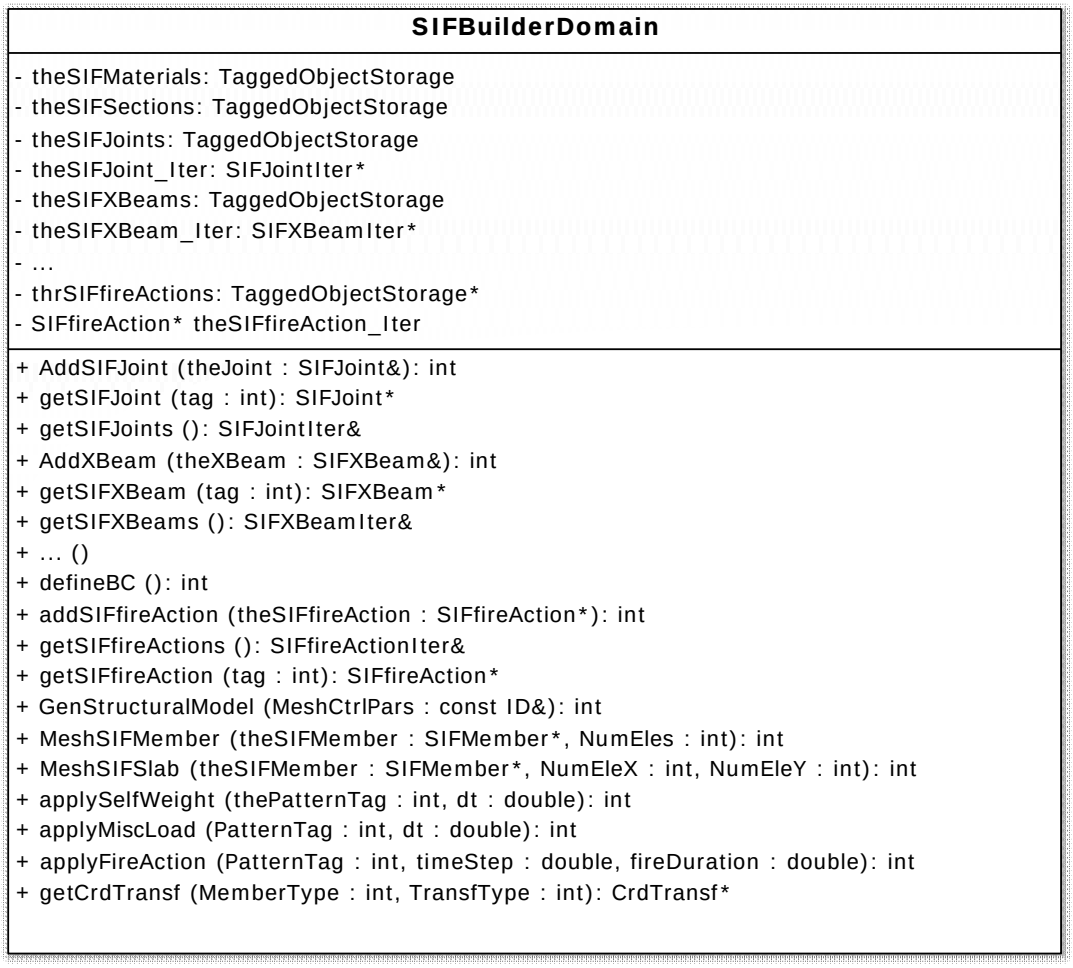

Figure 5.32: Member variables and functions of **SIFBuilderDomain**

by the connected **SIFJoint**. Unlike beams and columns, slabs are discretised using a different function **MeshSIFSlab**, as nodes are created all over the plane and shell elements are defined between the nodes. To take into account the offset of beam centroid from the slab plane additional nodes are needed. Between the nodes at the edge of the slab and along the beam, rigid links are defined as multi-point constraints to restrain the displacement appropriately and are added to the structural **Domain**, which also stores the nodes and elements after the model generation. A flowchart showing the generation of the structural model is presented in Figure 5.33.

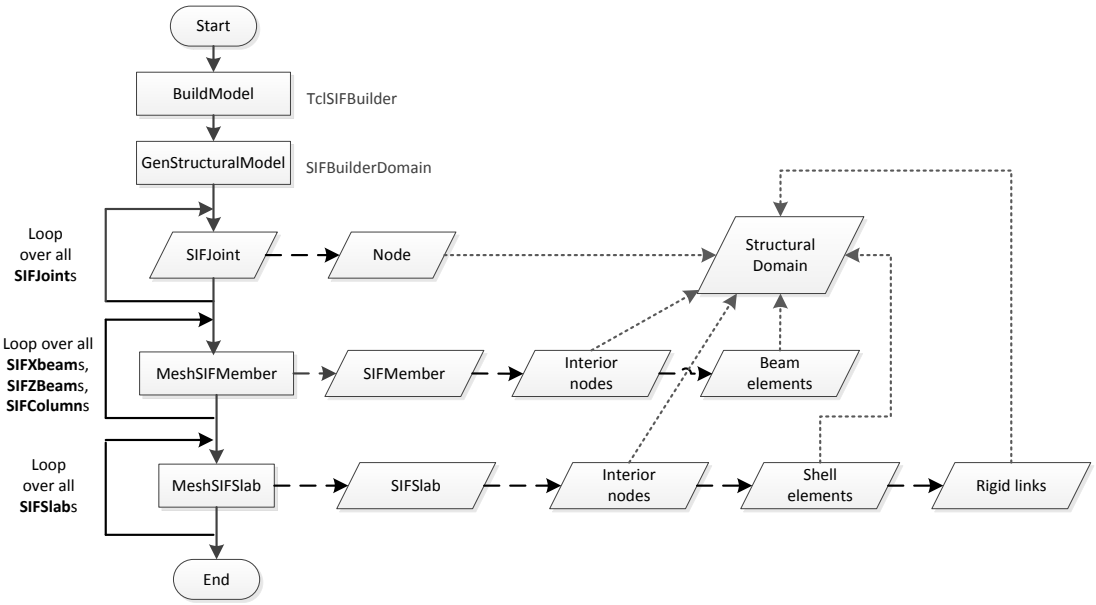

Figure 5.33: Flowchart showing the generation of structural model

•Performing coupled structural analysis with SIFBuilder

To automatically perform coupled thermo-mechanical analyses for structures in fire is a ultimate objective of SIFBuilder. The work flow of handling sequentially coupled analyses can be illustrated as shown in Figure 5.34. Having been addressed in the above discussion, the FE model is produced with a discretised representation which is comprised of nodes and elements. Boundary conditions are thereafter specified by searching for the valid constraint indicators in **SIFJoint**, which are converted to a number of **SP_Constraint**s at the nodes corresponding to the pinned or fixed conditions.

The loading cases for a structure are categorised as self weight, imposed loads (such as wind pressure or point loads), and fire action. When self weight is taken accounted, a uniformly distributed load shall be calculated with the density and dimensions given by **SIFMaterial** and **SIFSection**, respectively. Both the self weight and imposed loads can be applied on nodes or elements, the latter of which

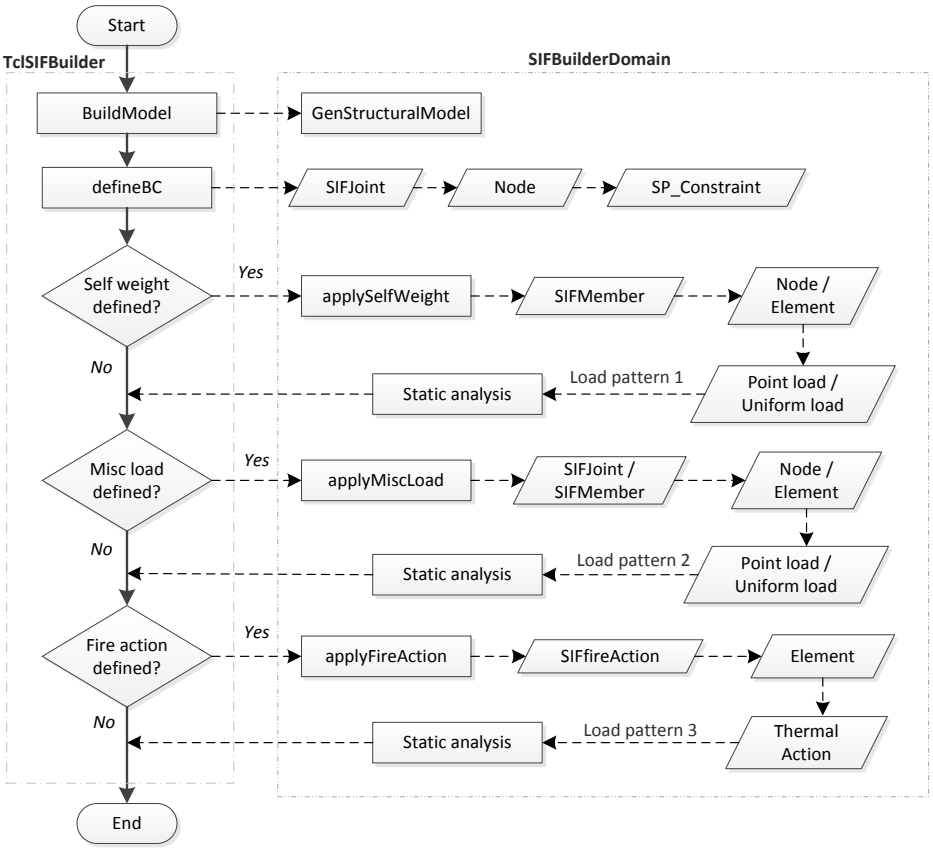

Figure 5.34: Flowchart showing the integrated analysis in SIFBuilder

may be dependent on the class interfaces (e.g., UDL can not be applied directly on shell elements). The effect of load is manipulated by the structural domain after each completed analysis and then treated as the initial state for the next one.

When the analysis is performed for fire action, as the flow chart shows **SIFfire-Action** is retrieved from the SIFModel and executed. As discussed earlier, the fire action is in association with a compartment, where the connected members are found and then analysed separately to obtain the corresponding temperature histories. A **SIFHTforMember** is created for each member and tasked to conduct the heat transfer analysis. Firstly it is necessary to initialise the fire model

which depends upon whether the fire is spatially uniform or localised. For uniform fire models, the initialisation is only to create a fire model object, whereas an additional transformation is needed for the origin of localised fire source. The reason for doing so is the fixed reference system used in heat transfer analyses for beams or columns, where the longitudinal axis is always the Z-axis. In addition to initialising a fire model, the unexposed surfaces must be allowed to lose heat to the ambient environment, while the exposed surfaces receive heat flux through convection and radiation. The typical exposure of a beam within a compartment is depicted in Figure 5.35, as parts of the beam are isolated from fire impact by the partition.

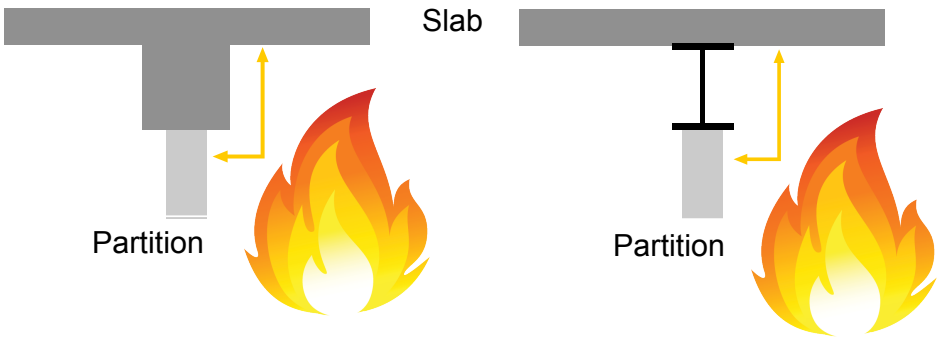

Figure 5.35: Typical exposure of a beam to compartment fire

Heat transfer analyses are carried out in the **SIFHTforMember**, which could perform 2D analyses over beam and column sections and 1D analyses over the depth of slabs. For localised fire exposure, dimensional reduction of heat transfer analysis is implemented to significantly cut the computing overhead. Recorders are defined during the analysis to capture the temperature evolution, which is stored with **PathTimeSeriesThermal** as the final product of the heat transfer analysis. Especially in the case of localised fire, an array of **PathTimeSeries-Thermal** rather than a simple instance is returned to **SIFfireAction** to define the thermal action, which is in the form of **ThermalActionWrapper** to describe

the spatial distribution of thermal response. Finally the solution algorithm and analysis facilities are reset to carry out the thermo-mechanical analysis.

5.5.2 Demonstration of using SIFBuilder

Presented here is an example to briefly demonstrate the Tcl usage with SIF-Builder. As shown in Figure 5.36, the building is assumed to be comprised of two bays along each direction corresponding to the global x and z axes, respectively. Storey height is set as 5m for the ground floor, above which a 4m high storey is located.

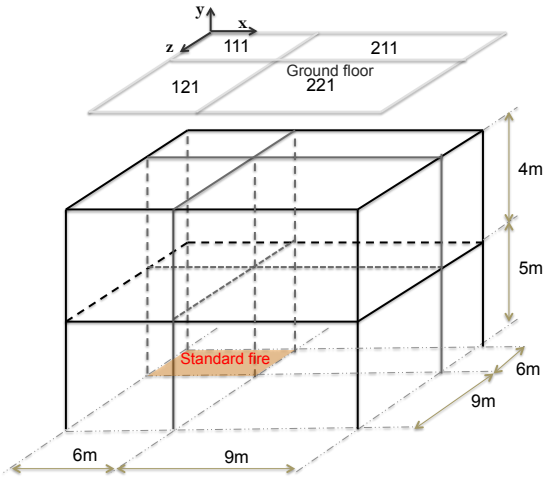

Figure 5.36: Typical exposure of a beam to compartment fire

```
source DisplayPlane.tcl;
source DisplayModel2D.tcl;
source DisplayModel3D.tcl
file mkdir HTData;
SIFBuilder;
```

Tcl script for constructing the building model begins with lines written in a simple fashion. A SIFModel will be created based on the above information and governs

the building configuration, using which the finite element (FE) models for heat transfer and thermo-mechanical analyses are built up.

```
#Geometry
SIFXBay 6 9 ;
SIFZBay 6 9;
SIFStorey 5 4;
```

The FE model requires the section definition in conjunction with a material library. Typical Tcl scripts responsible for material and section definitions are written as follows:

```
AddMaterial steel 1 -type EC3 3e8  2e11;
AddMaterial concrete 2 -type EC2 0 30;
AddSection ISection 1 1 0.203 0.102 0.0054 0.009;  #   UB203x102x23
AddSection ISection 2 1 0.203 0.203 0.007 0.011;   #   UC203*203*46
AddSection  SlabSection 3 2 0.1;
AssignSection beams 1;
AssignSection columns 2;
AssignSection slabs 3;
```

The first line of the code above defines a Eurocode 3 carbon steel material, which is associated with an I-section (UB 203x102x23). This section is later assigned to the beams, whereas for the columns another I section is defined as universal column section (UC 203x203x46) and assigned. Concrete slab of 100 mm thickness has also been included in this model. Columns at the ground floor are assumed to be fixed to the foundation. A uniformly distributed load (2kN/m^2) is applied to the slabs followed by the fire action. A uniform fire following the standard time-temperature curve is located in compartment 111 (as Figure 5.36 shows). The script written in Tcl is:

```
SetBC fixedJoint -locy 0;
```

```
AddLoad -member allslabs -load 0 -2000 0;
AddFire -compartment 111 -type standard;
```

The FE model can be generated now, with 6 elements used for discretising each single member along each direction. The following commands could be written to define recorders, such as the 3D display recorder, or recorders for joints and members. The script could ends with a SIFAnalyze command to invoke the combined loading cases. The commands are written as below:

```
BuildModel -MeshCtrl 6 6 6;
DisplayModel3D DeformedShape $ViewScale $xLoc1 $yLoc1 $xPixels $
    yPixels 0
SIFRecorder Joint -file Joint111.out -joint 111 disp;
SIFRecorder Member -file XBeam111.out -xBeam 111 Mideflect;
SIFRecorder Member -file Slab111.out -slab 111 Mideflect;

SIFAnalyze SelfWeight -dt 0.5 Load -dt 0.5 Fire -dt 30 -duration
    360 -output HTData;
```

A 3D plot of the structure by the display recorder is presented in Figure 5.37, while the results based on this generic model are discussed in next chapter.

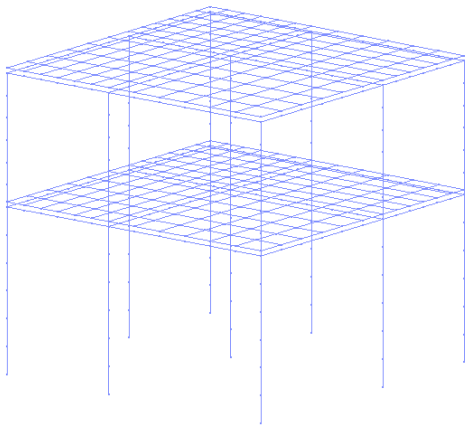

Figure 5.37: Typical exposure of a beam to compartment fire

5.6 Conclusion

Development work has been performed in OpenSees to advance the heat transfer and structural analyses for structures subjected to localised fire action. Based on this, an integrated computational tool is developed to model framed structures in fire. This tool incorporates the previously completed developments for heat transfer and thermo-mechanical analyses into an automated and integrated environment. The development work is hereby summarised:

- An idealised fire model is developed to implement heat fluxes with a linear, quadratic or exponential decay. A localised fire model is added to the fire model library, which adopts the SFPE correlations between incident heat fluxes and radial distance to the fire origin.

- Further development in the heat transfer module is conducted to analyse the localised fire action, and particularly for performing dimensionally reduced heat transfer analyses. Tcl application for heat transfer analysis associated with a simple mesh tool is enabled to allow for submitting Tcl script to perform heat transfer analysis within OpenSees.

- A comprehensive development is carried out in OpenSees for modelling beams and slabs in localised fire, which involves different thermal actions, beam elements, and shell elements.

- A framework is set up to integrate the modules for fire modelling, heat transfer analysis, and thermo-mechanical analysis. The tool creates a building model and invokes heat transfer analyses for each of the structural members involved in a fire event, in which partial fire exposure may also be

considered. A finite element model for the structure is also generated from the building model and heat transfer results are automatically implemented.

Chapter 6

Modelling beams and slabs subjected to localised fire action

6.1 Introduction

As discussed in previous chapters, displacement based and force based beam elements have been made available to analyse beams subjected to localised fires. In this chapter, a large amount of work conducted for performance checking and understanding the fundamental mechanisms of beam behaviour in connection with localised fire action. The numerical studies are based on a generic rectangular beam which is subjected to uniform distributed load and a quadratic or linear distribution of temperatures along longitudinal direction. Through the depth of beam section, a linear decay is applied from the bottom to the top surfaces. Different boundary conditions are also assumed for the generic beam, which include simply supported, pinned and fixed ends. Through the numerical studies,

both the developed beam elements are verified and validated against theoretical solution and results from ABAQUS. However, force based beam-column element has shown better performance than beam-column element of displacement based formulation. For both the linear and quadratic distributions, three to six elements are found enough and adequate to represent the localised response. An I-section steel beam is modelled with 1MW SFPE localised fire applied, which appears run-away collapse after 15 minutes in the case that half of loading capacity imposed.

For modelling concrete slabs in OpenSees, a four node shell element incorporating with layered shell sections was developed in OpenSees and has been presented in previous chapters. Following the beam-column element discussion, numerical studies are carried out to discuss the geometric and material nonlinearities in modelling concrete slabs subjected to localised heatting, which have also been compared with ABAQUS results. The layered shell element has been found valid and the need to a more efficient multi-dimensional model for concrete material is identified in OpenSees development. The FE solution is later implemented to model a square slab heated by localised fire, which is assumed with different boundary conditions and fire loads. The results suggest less deflections caused by localised fires than that caused by standard fire exposure, while more lateral (horizontal) restraints may lead to higher deformation induced by thermal expansion.

6.2 Implication of beam elements to model beams subjected to localised thermal action

6.2.1 Numerical studies for the beams subjected to localised thermal action

For steel beams subjected to localised fire beneath its mid-span, a simplified model as shown in Figure 6.1 could well represent the beam behaviour by taking advantage of the the symmetrical configuration, and with a 40mm wide and 80mm deep rectangular steel section. The 3m long beam (half model) is assumed to experience non-uniform temperature increases along length as well as through-depth gradients. The temperature increase along the element is idealised to be a linear distribution or a quadratic one which offers more intense localisation near the hot end. There are many aspects that raise the author's interest as listed in Table 6.1. As depicted in Figure 6.1, the boundary condition of this generic beam is primarily assumed as simply supported, whereas the pinned and fixed connections are alternatively defined as the comparative cases. A uniform distributed load (UDL) of 1kN/m is imposed on the beam to represent the mechanic loading. Longitudinal temperature distribution is defined as linear or quadratic decay, which begins with higher temperatures at left end (mid-span of the full beam model) of 800^oC at the bottom and 400^oC at the top, and ends with zero temperatures at the right-hand end of the beam model. The half-length temperature distribution of the quadratic case is 100^oC to 200^oC, which are a quarter of the highest temperatures.

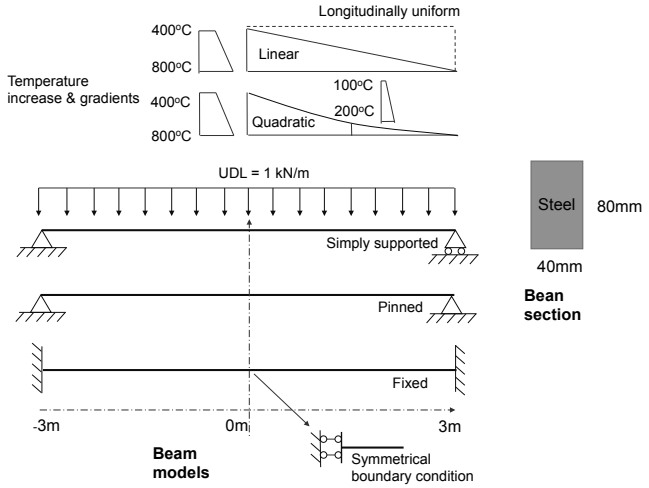

Figure 6.1: Beam benchmark test for non-uniform thermal action

Table 6.1: Various conditions for modelling the beams subjected to localised thermal action

Aspect	Options
Distribution of thermal action	*Linear, Quadratic, longitudinal uniform*
Element type	*Displacement based, force based beam element*
Material model	*Elastic material, Eurocode 3 steel*
Boundary condition	*Simply supported, pinned, fixed end*
Number of elements	*2, 3, 6, 12, 24*

6.2.1.1 Effect of mesh size

Here the boundary condition of this idealised beam is assumed to be simply supported. Finite element models are built using both of displacement based (abbreviated as DB) and force based (FB) beam elements, in order to illustrate the localised nonlinearity along the beam as the non-uniform thermal action is applied. A complex scenario has been defined, which includes longitudinal and through depth gradients. Prior to the thermal action, the applied UDL

leads to a 4.5 $kN \cdot m$ bending moment at the left end of the beam. A few graphs have been presented to visually compare the nonlinear solution by various means. Among them Figure 6.2 firstly shows the analyses performed using DB elements and linear elastic material, which is assigned with a coefficient of thermal expansion α of $1.2 \times 10^{-}5m/(m \cdot K)$ and elastic stiffness of $2{\times}10^5$ MPa. The results are validated against theoretical calculations, which are dedicated to the vertical deflection only and ignore the geometrically nonlinear effect caused by horizontal displacement. Based on this assumption, a linear elastic solution to beam deflection $\omega_0(x)$ induced by UDL (q) is given as:

$$\omega_0(x) = \frac{1}{EI_z}\big(-\frac{qx^4}{24} + \frac{qL^2x^2}{4} - \frac{5qL^4}{24}\big) \tag{6.1}$$

where L is the hal length of the beam, and the origin of x axis is at the beam centre. Similarly, the deflection shape as a result of temperature increase and gradients could be calculated based on the linearly elastic model. Here the calculation only accounts for the flexural deflection and ignores the elongation part. The classic relationship between the curvature θ and the beam deflection $\omega(x)$ could be adopted:

$$\theta = \frac{d^2\omega}{dx^2} \tag{6.2}$$

Where the curvature θ is obtained from the thermally induced strain (elongation), which is linearly correlated to the temperature gradient. The deflection curve can be given as a combined deflection induced by the UDL and the thermal action:

$$\omega_1(x) = \omega_0(x) + \frac{\theta_T}{EI_z}\big(-\frac{x^3}{6L} + \frac{x^2}{2} - \frac{L^2}{3}\big) \tag{6.3a}$$

$$\omega_2(x) = \omega_0(x) + \frac{\theta_T}{EI_z}\big(\frac{x^4}{12L^2} - \frac{x^3}{3L} + \frac{x^2}{2} - \frac{L^2}{4}\big) \tag{6.3b}$$

where $\omega_1(x)$, $\omega_2(x)$ are the deflections in linear and quadratic cases, respectively. θ_T is the maximum temperature gradient at the left end(mid-span of full model):

$$\theta_T = \alpha \cdot \frac{T_{bottom} - T_{top}}{2d} \tag{6.4}$$

in the above calculation, T_{bottom} and T_{top} are the temperatures at the bottom and top surface at the beam left end.

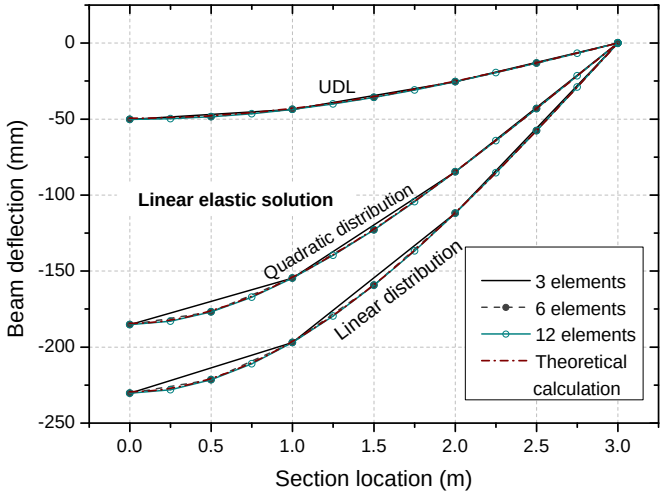

Figure 6.2: Beam deflection modelled by displacement based elements with elastic material

The comparison presented in Figure 6.2 not only demonstrates that the beam deflection can be precisely predicted for non-uniform thermal action, but also shows that the effect of mesh size is negligible when elastic material behaviour is assumed. The degree of deflection is highly dependant on the temperature gradients, whereas the uniform rise of temperature only leads to horizontal displacement. It seems reasonable to analyse beams with a few elements, even if highly localised temperature distribution appears along the beam. However, the material property of structural material may deteriorate as a consequence of elevated temperature, which means the elastic material assumption can only be

valid for very low temperature, i.e., 20 to 100^oC, for which the steel material is considered to retain full strength and stiffness.

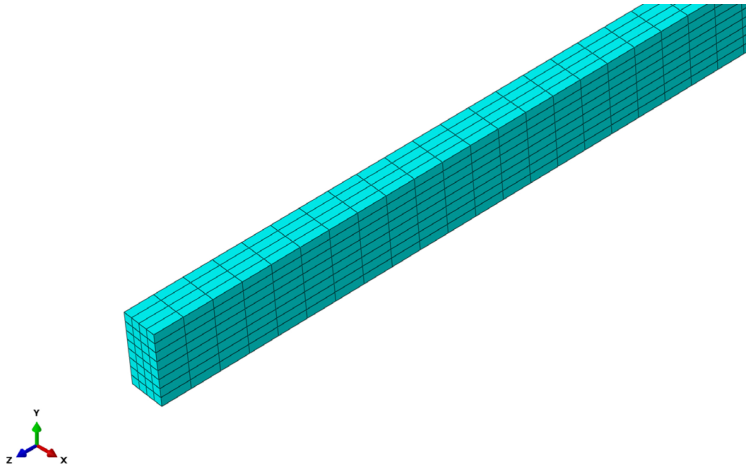

Figure 6.3: A 3D solid model of the beam in ABAQUS

[

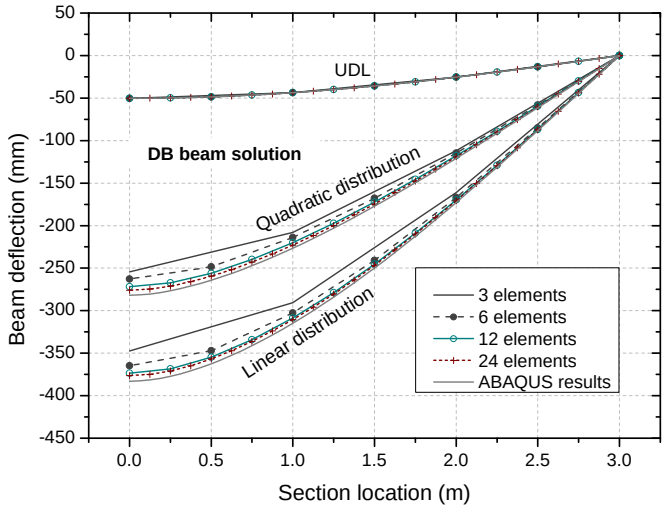

Figure 6.4: Beam deflection modelled by displacement based elements with Eurocode 3 steel material

If defining the material as Eurocode 3 carbon steel (CEN, 2005) (the yield strength is assumed as 300 MPa and the elastic stiffness remains as 2×10^5 MPa), localised material degradation occurs in the intensely heated part, causing a difference in

results for different number of DB elements used. The deflection curves have been shown in Figure 6.4, where the beam model is similar to the elastic one, but uses Eurocode 3 steel material model to address the material degradation. The OpenSees results have also been compared with numerically modelled results conducted within ABAQUS using a solid 3D model as presented in Figure 6.3, which subdivides the cross section as 4×8 elements, with 96 elements along the length. As observed from the plot, model using fewer beam elements leads to lower deflection, for both the quadratic and linear temperature distribution, which is attributed to the limitation of the displacement based beam element. Due to the linearly-interpolated-curvature scheme, the DB beam element distributes the plasticity formed at one section to the whole element. The process inside the element may be described as: (1) one section experiences a high temperature; (2) the softened section therefore requests more deformation to compensate the stress loss; (3) larger nodal displacements without rigid-body modes are updated to fulfil the section request; (4) linear interpolation scheme increases deformation for every section in the beam; (5) resisting forces of all sections are increased to share the unbalanced load. Due to this reason, the beam modelled with fewer DB elements tends to be a bit stiffer, resulting in smaller deflection. However, when more than 12 elements are used for the simply supported beam, the deflection curve begins to converge. Nearly identical results are produced by ABAQUS using the aforementioned 3D solid model, which hereby validates the implementation of non-uniform thermal action and Eurocode 3 steel material.

For beams analysed with force based elements and structural steel material, a better performance of convergence has been observed. The deflection curves are extracted and illustrated in Figure 6.4, where a different number of elements are assigned to the beam model. The result suggests that the nodal displacements

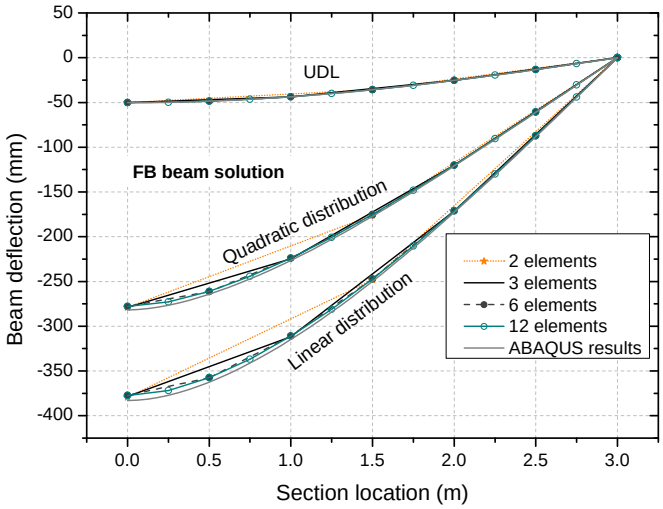

Figure 6.5: Beam deflection modelled by force based elements with Eurocode 3 steel material

are precisely predicted even by the model that is comprised of only two elements, and refining the mesh doesn't lead to a different and better result. Similarly, the beam has been investigated for the different distributions of temperature. In both cases, the beam model shows a stable performance despite the increase of element number. Such an excellent performance relies on the internal iteration inside the force based beam element, which is carried out to determine the section and element states, and not strictly following any linear or other interpolation, as the self adjustment occurs during iterations. Although, there is linear interpolation utilised for initialising the section forces, the committed section forces should have been slightly modified in conjunction with the refined section deformation. But what really enables such a better performance is the mechanism which individually evaluates section deformations, allowing localised discontinuity that can be taken into account during the numerical integration.

Considering the beam is free to displace at the right end, the horizontal translational displacement should also be dependant on the choice of element type

and mesh size. The comparison is made in Figure 6.6, where the usage of DB elements shows a larger deviation in terms of the element number, and the translational displacement tends to be stable when more than 3 force based elements are used. Even though, the discrepancy between two FB elements and 24 FB elements models is just 0.5mm, which is believed to be caused by the geometric transformation. The two element model does not seem capable of addressing the geometric nonlinearity, especially in the case when temperature distribution is quadratic.

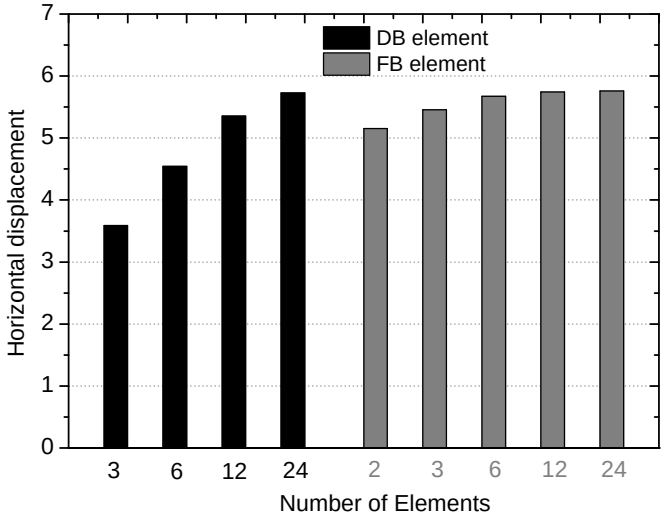

Figure 6.6: Horizontal displacement of simply supported beam

Besides the effect of element number, number of sections (integration points) in each element, the number of fibres in each section should be paid attention. For mechanical loading, the beam performance regarding number of integration points is presented by Neuenhofer and Filippou (1998). In the paper, the flexibility based approach is suggested to be more sensitive to the number of integration points than stiffness based method, which requires more elements to address the nonlinear behaviour. Nevertheless, the localised effect induced

by non-uniform thermal action is more complex. Theoretically speaking, both approaches would require a reasonable number of integration points to offer a more accurate approximation to the non-uniform thermal action when it is not linearly distributed. Additionally, the performance of beam elements may rely on the fineness of discretising beam section as fibres. There is no doubt that more fibres will lead to a more accurate description of section state, as the strain and stress are assumed to be constant in each fibre.

Table 6.2: Beam end displacement analysed with different number of fibres and integration points (Quadratic distribution)

No. of Elements	**No. of Sections**	**No. of Fibres**			
		4	8	16	32
3 DB Eles	3	254.58	251.35	250.28	250.17
	5	258.86	255.59	254.62	254.38
	7	258.93	255.59	254.49	254.32
	9	259.28	255.58	254.57	254.36
3 FB Eles	3	298.62	295.12	292.93	292.40
	5	283.14	278.86	277.20	276.78
	7	282.81	278.29	276.40	276.14
	9	283.23	277.81	276.67	276.29
6 DB Eles	5	268.67	264.61	263.42	263.15
12 DB Eles		279.09	273.77	272.63	272.21
6 FB Eles		282.54	278.23	276.38	276.09
12 FB Eles		282.84	277.72	276.53	276.14

Table 6.2 lists a number of analyses in which the left end displacement of the beam model is monitored, when different number of elements, sections(integration

points), and fibres are used and the temperature distribution along the beam length is selected as quadratic. An accurate estimate of the left end nodal displacement is 276.05 mm, as predicted by the beam model comprised of 48 force based beam elements, and 10 integration points for each element, as well as a 64-fibre section. Comparing with the reference solution, the results extracted from three DB element model turned out to be quite conservative, all around 254 mm. And it has been found that increasing the number of integration points does not improve the result adequately, but using less than five sections is not recommended. When the beam element is flexibility based, a three element model proves to be much more efficient in terms of reaching the reference result, and could be even better if at least five sections and 16 fibres per section are defined for the beam.

6.2.1.2 Material response

It may be summarised from the above discussion that the force based beam element provides a generally better solution than the displacement based beam element, and the discrepancy caused by mesh size should be related to the localised material degradation as a product of localised thermal action. For a simply supported beam, the midspan (left end in this section) bending moment is the largest at 4.5 $kN \cdot m$ when the previously defined $1kN/m$ UDL being applied. As the fibre temperature rises, both its stiffness and yield stress decline, and the most severe degradation should be found at the left hand end of the beam where the thermal action is the most intense. Figure 6.7, Figure 6.8, and Figure 6.9 show the material responses in the fibres at the left end section, which includes the distribution of fibre strain, stress, and tangent stiffness across the section in the

case of the quadratic thermal action, where the analyses are carried out using 6 FB elements and 12 DB elements. Notice the fibre strain is hereby referred to as the mechanical strain (total strain subtracted by thermal strain or elongation). The section comprises of 16 fibres, 8 of which are monitored. The centroid locations of sampled fibres are -35 mm, -25mm, -15 mm, -5 mm, 5 mm, 15 mm, 25mm, 35 mm as in a 2D section fibres along the local y axis are of interest.

Once the UDL is applied, a linearly distributed strain is first observed which obeys the assumption of plane section remains plane. The shape of strain distribution continues to be linear even after the thermal action is applied, and until the temperature exceeds 400^oC. According to the definition of Eurocode 3 carbon steel, the thermal strain is nonlinearly correlated to the temperature and becomes constant when the steel temperature exceeds 750 ^oC, which obviously results in the nonlinear distribution of mechanical strain as the temperature is considerably elevated. Regarding the difference caused by element types, a larger strain is seen at the bottom layer with the force based approach, which is due to the non-uniform distribution of total strains. Nonetheless, displacement based element implements a linear interpolation, which is inadequate to address the localised development of section deformations.

Unlike the strain propagation, an opposite development appears in the distribution of fibre stresses while the assumed maximum net temperature rises to 800 ^oC, or marked as 100% thermal action as shown in Figure 6.8. Stresses are seen to decrease near the downward face of the beam due to the plasticity developed in those fibres dominated by the fibre temperature propagation across the section. To balance the compression and resist the bending moment, the neutral axis of

the left end section is forced to move towards the upper layer which can be observed in Figure 6.7 and Figure 6.8. The propagation of neutral axis is different compared to the ordinary bending case at ambient temperature, in which the fibre stresses sequentially reach yield stress as the bending moment increases and exceed the first yield moment capacity. According to Figure 6.8, the early stress distribution is approximately linear as the material property has not encountered severe degradation for relatively low temperature rise (50% of thermal action). Moreover, Higher tensile stresses are found from the results of FB model, which are corresponding to the different strain developments shown in Figure 6.7.

The last variable which is highly dependant on the temperature is the tangent stiffness (Figure 6.9), as it is also correlated to the mechanical strain developed in the fibre. In the early period when no thermal action is imposed, tangent stiffnesses in the fibres remain 200000 MPa since materials remain elastic. When the thermal action is applied to 50% of the load, a linear distribution of the tangent stiffnesses is seen in both DB and FB models. It reveals that the initial stiffnesses of the fibres experienced reduction due to the elevated temperature, and the temperature is linearly distributed across the section. Despite the relatively high temperature, no plasticity has been observed in the fibres yet. Nevertheless, the elasticity is later bypassed in most of the fibres as a radical reduction of the yield strength and stiffness occurs. This plastic behaviour is not only found in the tensile area, but also in the edge fibres under compression, which is due to the upward movement of the neutral axis which reduces the area of compression and increases the stress level.

From the above discussion, material responses (being categorised as material degradation and thermal elongation), are the effects that govern the beam

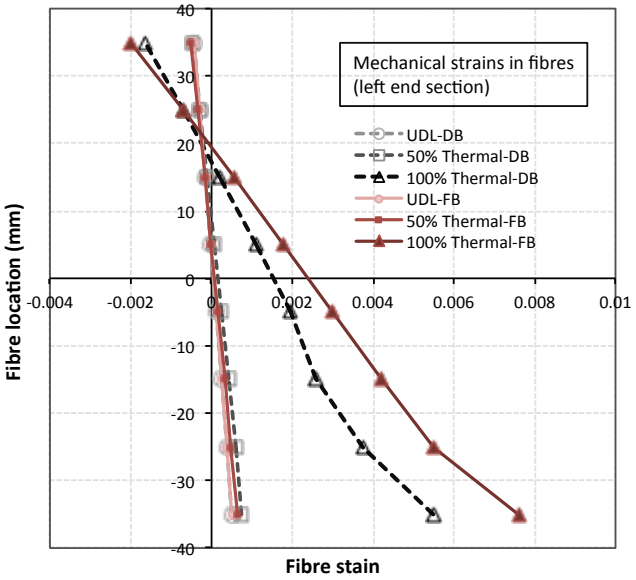

Figure 6.7: Fibre strains at the left end section of the simply supported beam for quadratic temperature distribution case

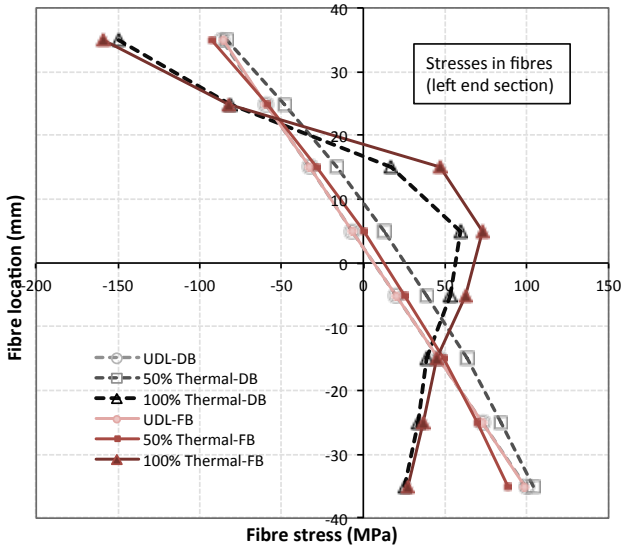

Figure 6.8: Fibre stresses at the left end section of the simply supported beam for quadratic temperature distribution case

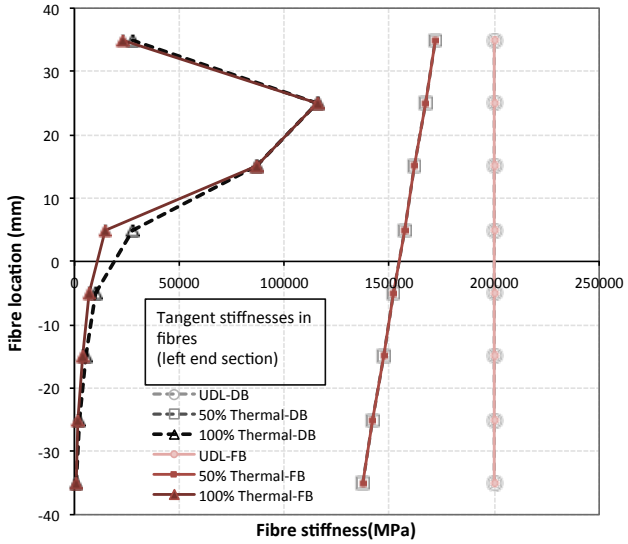

Figure 6.9: Fibre stiffnesses at the left end section of the simply supported beam for quadratic temperature distribution case

performance when subjected to localised thermal action. In Figures 6.10(a) and 6.10(b), attention is now drawn to the vertical displacement of the left end node, to evaluate the different beam approaches from the perspective of the material responses. Notice that the upper limit of temperature rise in Figure 6.10(a) is set to 400 ^oC, which represents 50% of thermal action after UDL as described in the earlier analyses. To individually investigate the material effects, analyses are conducted with the following hypothetical material behaviours: (1)All considered, (2) *material degradation* only, (3)*stiffness reduction only*, 4)*thermal elongation only*. Among these categories, the second of which takes account of the material degradation but no thermal elongation, which recalls the traditional understanding about the member failure (Usmani et al., 2001). The third material assumption ignores the strength reduction, and therefore only the softening behaviour is taken into consideration. For these two hypothetical models, reduction factors are defined as the Eurocode 3 carbon steel, whilst

the thermal elongation is manually eliminated. Conversely, the last model only accounts for the thermal elongation and has the material degradation removed.

When the temperature increase in the fibres is not higher then 400^oC, an overview of Figure 6.10(a) reveals that the vertical displacement of the left end node is nearly identical regardless of which element and how many of them are used. Along with this general finding, it is also understood that displacement resulting from the temperature gradient is the dominant component when comparing the *all considered*and *thermal elongation only* results. Little difference is found in the developed displacements due to *material degradation* and *stiffness reduction only*, because the temperature is not high enough for yield strength reduction.

When the 100% of thermal action is applied, considerable variation is firstly seen from the nodal displacements given by the analyses based on displacement oriented approach, which has been discussed earlier in conjunction with the better performance provided by force based formulation. As illustrated in Figure 6.10(b), while the material strength and stiffness are both reduced (*material degradation*) in responding to the elevated temperature, the displacements modelled with various number of DB beam elements produce the same discrepancies as the results obtained from the *All considered* analyses. If only stiffness reduction is considered, the overall displacements reduce very slightly but the difference between the different types of elements reduces considerably. On the other hand, it should be noted that the displacements obtained from the *thermal elongation only* cases present negligible differences between different analyses, but produce the greatest contribution to the development of beam end displacement as seen previously for the 50% thermal action case.

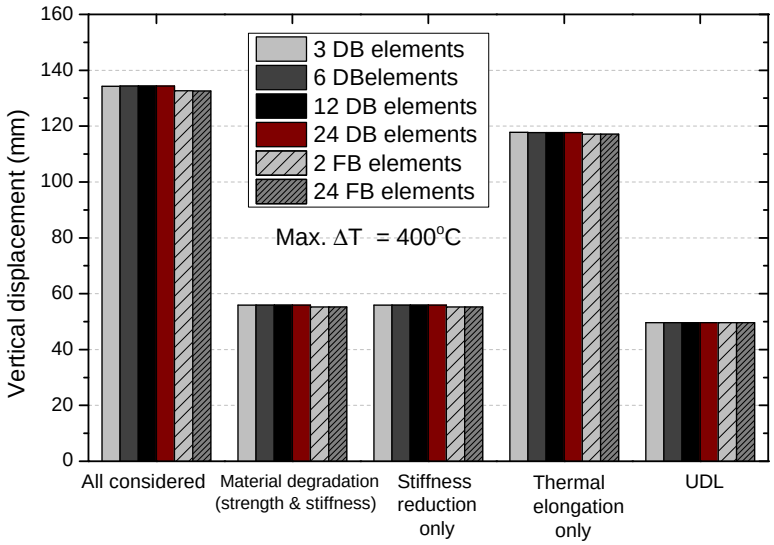

(a) Maximum temperature increase = 400^oC

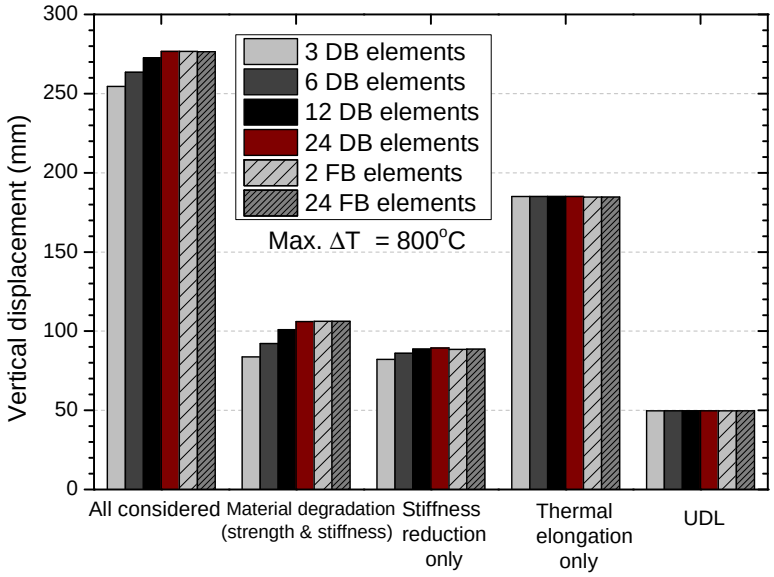

(b) Maximum temperature increase = 800 ^oC

Figure 6.10: Vertical displacement at the beam end analysed with different elements and material behaviour

6.2.1.3 Type of longitudinal gradient and boundary conditions

Concerns about the localised thermal action are recognised as the temperature gradients that may appear along the transverse section or longitudinal direction of the member or both. If a beam encounters transverse gradients such as a beam exposed to spatially uniform fire and shielded by the slab, the non-uniformly developed thermal elongation over the beam section would lead to the so-called thermal bowing which affects beam deflection much more than the uniform temperature over the section (Usmani et al., 2001). For example, a beam with very thin walled parts that may not experience significant temperature gradients because of efficient heat transfer through the section. A thermal gradient in such beams may only emerge when the beam is heated by localised fire action, where the temperature gradient is more likely to be seen along the length of the beam and dominated by the distribution of incident heat fluxes. For most practical cases, however, the combined effect of these two individual gradients may be important. Taking the previously used beam model as an example, the longitudinally uniform but transversely varying temperature distribution may lead to a uniform curvature along the length (there are no redundant constraints associated with the beam). Entirely different behaviour may be found for a beam only subjected to longitudinal gradient, as in this case it would reach runaway collapse solely due to material degradation and before the collapse, a low level of deflection takes place caused by the reduction in resistance to the applied bending moment. Such a phenomenon has been presented in Figure 6.11, which illustrates the history of vertical displacement against the pseudo computational time. The first period of loading (0 to 1) represents the impact of UDL, followed by thermal action which is applied in 100 steps. Three different curves are shown in the graph, representing three different scenarios of thermal action: (1) longitudinal

gradient only (800^oC at the left end, 200^o at the centre, and 0 at the right end); (2) transverse gradient only (800^oC at the bottom decreasing to 400^oC at the top); (3) dual gradient that combines the previous two types of gradient. The distributions of temperature gradients could be referred to in Figure 6.1.

If the beam is loaded with only the longitudinal gradient, the deflections induced by material softening are, as expected, much lower than the deflections in the other two cases, primarily due to the absence of thermal bowing. The runaway collapse of the beam occurs at 82%-84% of thermal load, resulting from the strength reduction across the whole section at the left end. For the beam applied with transverse gradients, the deflection gradually increases as the temperature gradient is uniform along the length and develops in proportion to the load factor (pseudo time). As seen from the figure, transverse gradient leads to the fast growing downward deflection with the beam collapse around load factor 0.85. However, collapse is not observed in the beam subjected to dual gradients even at the end of analysis, which is obviously due to the lowest average temperature in the beam. It is also observed that the beam model with flexibility based approach is numerically stable and follows the solution further into the post failure phase.

For a single beam, its boundary conditions can be simplified as aforementioned three general types: (1) simply supported, (2) pinned, (3) fixed, as shown in Figure 6.1. In the whole structural system, the beam-column connection behaves as a finite stiffness spring, for which the boundary restraint effect may be equivalent to something between these three simplified representations. By altering the boundary condition of the beam model, various deflection curves have been obtained as depicted in Figure 6.12, where dual gradients are applied as quadratic distribution along the length plus the linear gradient through the section. When

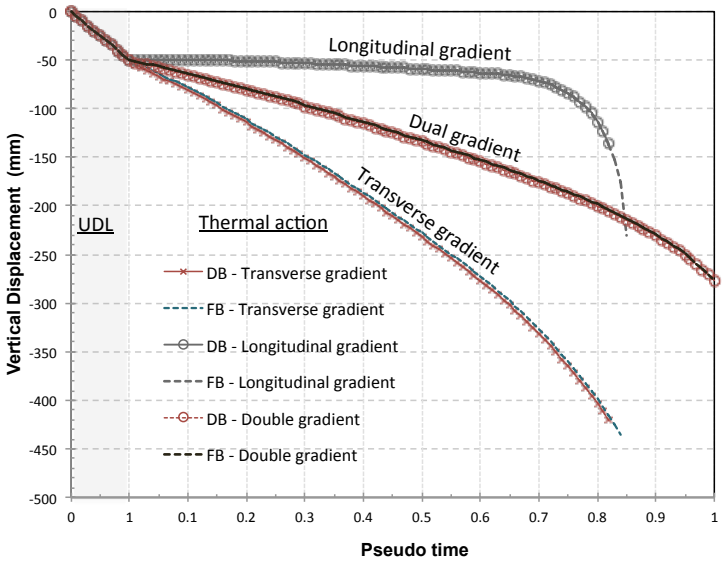

Figure 6.11: Vertical displacement of the beam end responding to different temperature gradients

the maximum temperature is lower than 400^{o}C, greater deflection appears in the pinned beam compared to simply supported case, which is due to the compressive second order effect induced by axial restraint. When the thermal action is fully applied, the greatest deflection takes place in the simply supported beam as a result of material softening (plastic hinge nearly forms at the left end) and lack of axial resistance. Throughout the analysis, the smallest deflection always occurs in the fixed beam as benefited from the rotational restraint.

6.2.1.4 2D and 3D beam elements

A framed structure could be modelled with a 2D plane frame under the assumption that ignores the interaction between individual planes. For studying the real behaviour of the structures in real fires, a 3D model should provide better solution rather than a 2D model. Within OpenSees, options for 3D

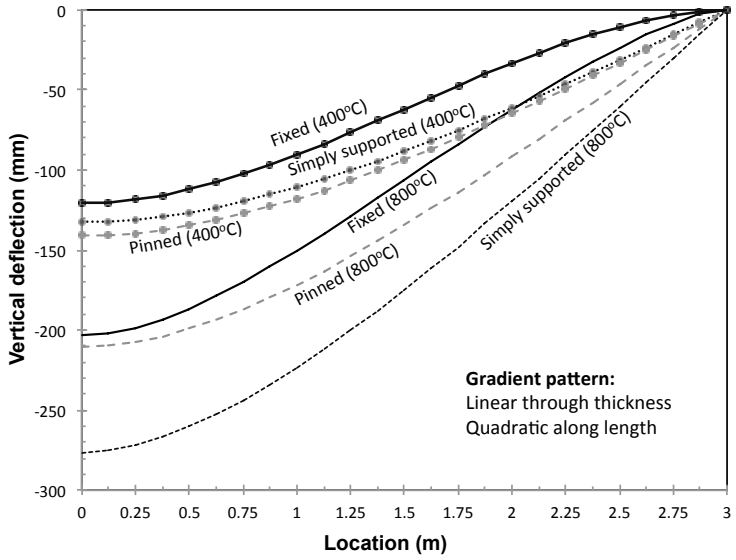

Figure 6.12: Deflection of beams with various boundary conditions

modelling are available, which involve the 3D version of thermal action, section definition, and elements. To define thermal action for 3D beam elements, **Beam3DThermalAction** is used to process temperature rise with uniform distribution along the length. Meanwhile, **ThermalActionWrapper** remains available for tackling the longitudinally non-uniform thermal action along with the corresponding **NodalThermalAction**. Fibre based section definition remains the basis for determining the element state in 3D cases, which are implemented with **FibreSection3DThermal** and **FibreSectionGJThermal**. The latter offers a predefined torsional stiffness to restrain the torsional degrees of freedom. In terms of the beam elements, 3D versions have been available for elements formulated with displacement and force based approaches, respectively. Figure 6.13 compares the beam end displacements that are modelled in 2D and 3D environments. Additionally, the displacement of beam end modelled using ABAQUS as

mentioned before is presented. The nearly identical results are seen from the figure, which suggests the reliability of the elements regardless of the dimensional context.

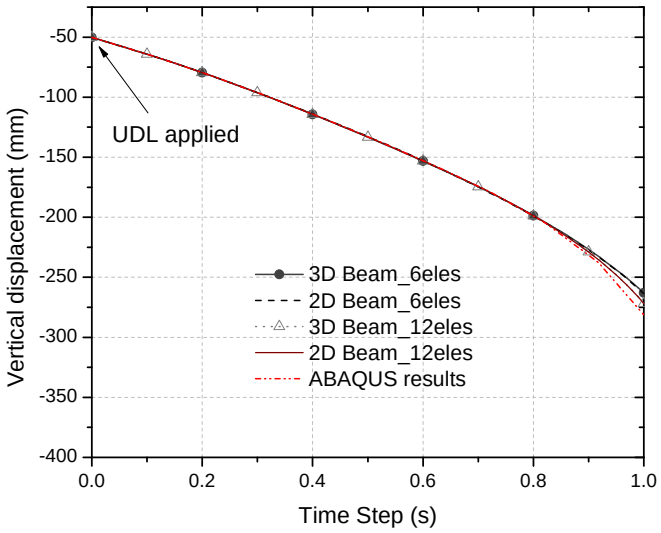

Figure 6.13: Beams subjected to non-uniform thermal action modelled with 2D and 3D Beam elements

6.2.2 Thermo-mechanical response of beam members subjected to localised fire

6.2.2.1 Configuration of the beam in localised fire

In this section, a steel beam is modelled with simply supported boundary conditions and subjected to localised fire action which locates horizontally at the mid-span, as shown in Figure 6.16. A universal beam section UB305 $\times$ 127 $\times$ 42 is chosen for the beam. Fire load is represented by an SFPE localised fire model, with the rate of heat release as 1 MW and the nominal diameter as 0.5m.

The top face of the upper flange is assumed to be attached with an perfectly insulated plate, which ignores the heat loss from the steel beam to the concrete slab in a composite slab system. Uniform distributed loads are assigned to the beam with loading ratios as 25% and 50% of the ultimate capacity, respectively. The yield strength of the beam is assumed to be 275MPa, while the elastic Modulus at the ambient temperature is 2.1×10^5 MPa. Temperature dependent properties of the steel are defined according to Eurocode 3 (CEN, 2005), as an embedded consideration in the material model *SteelECThermal* in OpenSees. Considering the symmetrical temperature distribution about the weak axis of the beam section, a 2D finite beam element model is adequate to represent the beam behaviour. The discussion in Section 6.2.1 has suggested that 48 displacement based beam elements should be enough to address the material and geometric nonlinearities. Whereas the number of elements may be appropriately decreased to 12 elements (9 integration points) as if the beam is formulated with force based description.

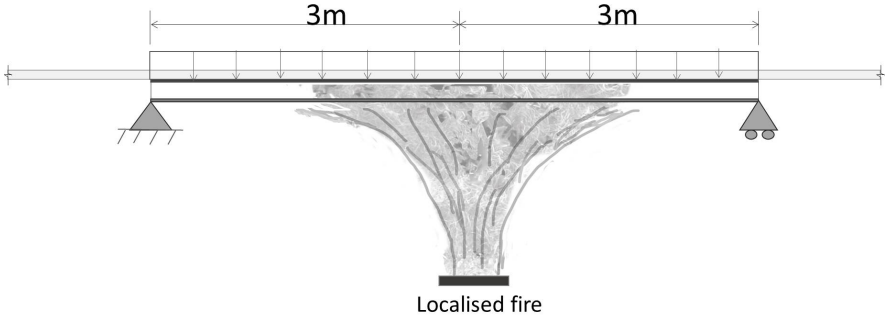

Figure 6.14: Single beam subjected to localised fire action

Moreover, the techniques developed for handling localised fire action are implemented in these analyses, with rapid estimation which have been discussed in Section 3.6. Here the fire load and the beam setup are intensionally chosen to be the same so the accuracy of interpolation could refer to the previous discussion.

Different schemes are applied to approximate the thermal response, which include a quadratic interpolation and a linear representation between the highest and the lowest temperature. Additionally, the full 3D heat transfer results are applied to the beam at all 49 nodes when the beam is meshed with 48 elements. Interpolation may be performed as illustrated in Figure 6.15, where the lower flange temperature of the beam is presented as an example.

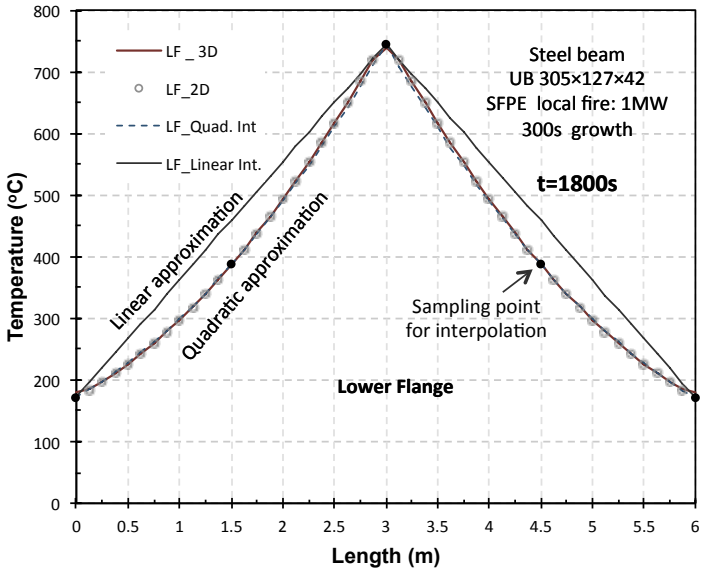

Figure 6.15: Implementation of longitudinally non-uniform thermal action for the beam exposed to a localised fire

6.2.2.2 Beam deflection upon exposure to a localised fire

When 25% of the loading capacity is imposed on the beam, collapse is not seen in the beam during the exposure to the localised fire. The beam deflection starts to develop from $t = 250s$, while the fire plume impinges on the beam. The subsequent development is primarily induced by the temperature gradient through the beam section, especially the temperature difference between the lower and

upper flanges. The additional deformation is attributed to the material softening resulting from the elevated temperature, as the maximum temperature exceeds 700^oC. However, the temperature evolution slows down significantly after 900s (15min) of heating, as a steady state of heat transfer has been reached. In the beam with the higher loading ratio of 50%, rapidly developing deflection is observed at $t = 835s$ which indicates the collapse of the beam. This is because of the substantial loss of strength at the mid-span section, which forces the neutral axis to move upward as shown from Figure 6.7 and Figure6.8, leading eventually to collapse when the sectional moment of resistance falls below the applied moment.

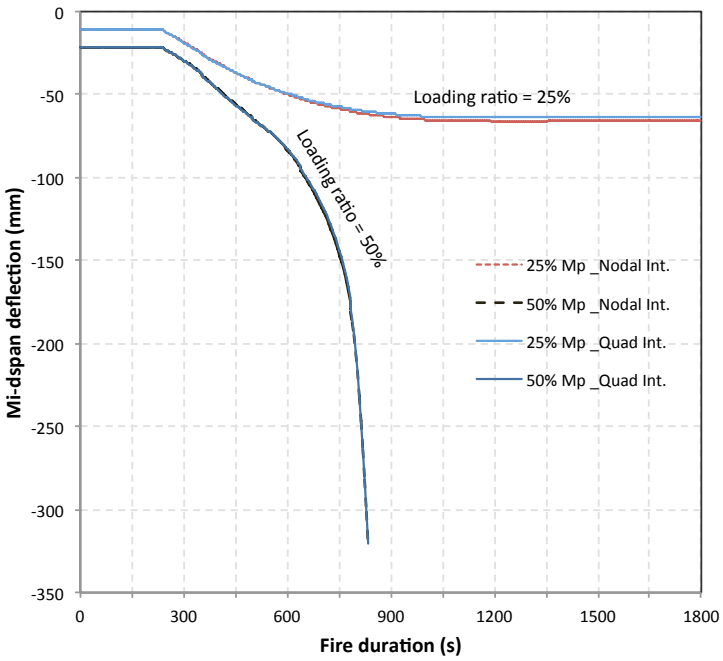

Figure 6.16: Beam deflection subjected to localised fire action

As presented in Figure 6.16, the deflection curves are extracted from the thermo-mechanical analyses conducted with the thermal action defined with nodal thermal action (Sectional results given by 3D heat transfer analysis) and quadratic

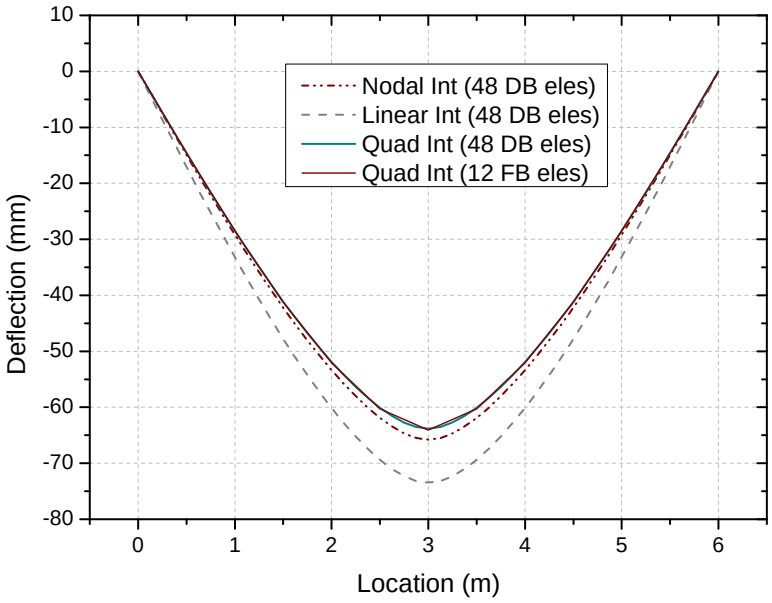

Figure 6.17: Beam deflection subjected to localised fire action

interpolation (2D analyses at sampling sections), respectively. Both the analyses have given nearly identical results, although a slight difference is seen in the deflection curves for loading ratio set as 25%, which is caused by the slightly underestimated temperature by quadratic interpolation in the adjacent area to the mid span. The along length deflection is further compared in Figure 6.17, where the temperature approximation schemes correspond to the curves shown in Figure 6.15. An over-estimated response is given by the linear interpolation, whereas the quadratic interpolation presents very close results, regardless of which type of element is used. A substantially decreased number of elements is required when the model uses the force based beam elements.

6.3 Implication of shell elements to model slabs subjected to localised thermal action

6.3.1 Shell element performance considering non-uniform thermal action

6.3.1.1 Geometric nonlinearity

A cantilever plate is introduced to evaluate the performance of the shell element and its associated section and materials, which will be presented later. As shown in Figure 6.18, the slender plate is fixed at the left end, and free at the other sides. This cantilever plate can be modelled as a line of beam elements, or a plate comprised of shell elements, or 3D continuum elements which is not presented here. A point load is assumed to be applied at the right hand end in the beam model, whereas in the shell model the load is equally distributed as a number of upward forces at the edge nodes.

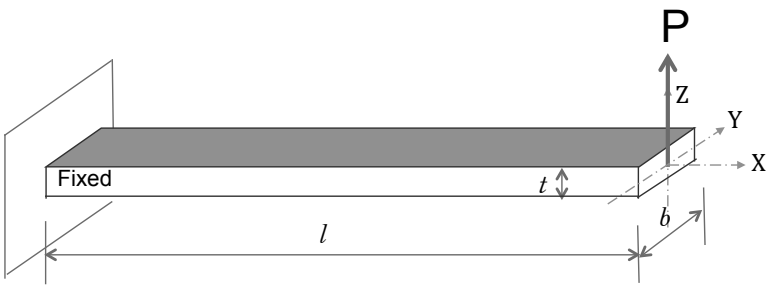

Figure 6.18: Configuration of cantilever slab

When large deflection occurs in the plate, geometric nonlinearity should be observed in the form of load/deflection interaction, as a result of updated l_1 which is the real horizontal distance between the fixed end and the load point.

The classic beam solution to this problem is governed by the following equation:

$$\frac{d\theta}{ds} = \frac{P}{EI}(l_1 - x), \quad \theta(0) = 0, \theta'(l) = 0, \tag{6.5}$$

where θ is the rotation of the centroid plane, s is the arc-coordinate along the neutral axis. And E is a common notation for elastic modulus, while I as a section parameter represents its second moment of area, and x for the horizontal distance to the fixed end.

An analytical solution to the vertical displacement of the free tip δ_B (Wang et al., 2008) is given as:

$$\frac{\delta_B}{l} = 1 - \frac{2}{\sqrt{\alpha}}[E(\mu) - E(\phi, \mu)] \tag{6.6}$$

in the above equation, $E(\mu)$ is the complete elliptic integral of the second kind, whilst $E(\phi, \mu)$ is the incomplete elliptic integral of the second kind. Parameters μ and ϕ are given as:

$$\mu = \sqrt{\frac{1 + \sin\theta_B}{2}}, \ \phi = \arcsin(\frac{1}{\sqrt{2}\mu}) \tag{6.7}$$

where θ_B denotes the rotation of the free tip. The final solution now relies on the exact value of θ_B, which has been estimated with a variety of expressions for different ranges of validity. An accurately converged solution is proposed by Wang et al. (2008) for α ranging from 0 to 5, which is expressed with the following equations:

$$\theta_B = \frac{\alpha}{2}\frac{f(\alpha)}{g\alpha} \tag{6.8}$$

$$\begin{aligned} f(\alpha) = 1 + 3.98575 \times 10^{-2}\alpha^2 - 5.41174 \times 10^{-2}\alpha^4 + 5.72575 \times 10^{-3}\alpha^6 \\ +3.79533 \times 10^{-4}\alpha^8 - 8.87896 \times 10^{-6}\alpha^10 + 2.63041 \times 10^{-8}\alpha^{12} \\ -1.51429 \times 10^{-11}\alpha^{14} - 2.29142 \times 10^{-15}\alpha^{16} - 3.45006 \times 10^{-21}\alpha^{18} \\ -7.00678 \times 10^{-28}\alpha^{20} \end{aligned} \tag{6.9}$$

$$\begin{aligned} g(\alpha) = 1 + 0.131524\alpha^2 - 5.99231 \times 10^{-2}\alpha^4 + 2.34466 \times 10^{-3}\alpha^6 \\ +9.90299 \times 10^{-4}\alpha^8 - 1.37001 \times 10^{-5}\alpha^10 + 3.44172 \times 10^{-8}\alpha^{12} \\ -1.45098 \times 10^{-11}\alpha^{14} - 2.26721 \times 10^{-15}\alpha^{16} - 3.50731 \times 10^{-21}\alpha^{18} \\ -7.00678 \times 10^{-28}\alpha^{20} \end{aligned} \tag{6.10}$$

Vertical deflection of the free tip has been plotted in Figure 6.19, where the FE results are gained from models using shell elements and beam elements respectively and compared to the above derived analytical solution. The generic plate model here is set as $L = 6m$, $B = 0.2m$, and $t = 0.05m$, with an elastic material assigned which has elastic modulus (E) as $2 \times 10^5 MPa$, Poisson's ratio (ν) as 0.3. A point load P is ramped to 50kN for capturing the nonlinear behaviour. Geometric nonlinearity appears significantly in the results when updated-Lagrangian geometric transformation is utilised, compared to the linear solution provided by **ShellMITC4Thermal** elements. The nonlinear behaviour observed from the shell approach shows nearly identical results as extracted from corotational beam model and the analytical solution.

A uniform thermal gradient is applied to the cantilever plate following the

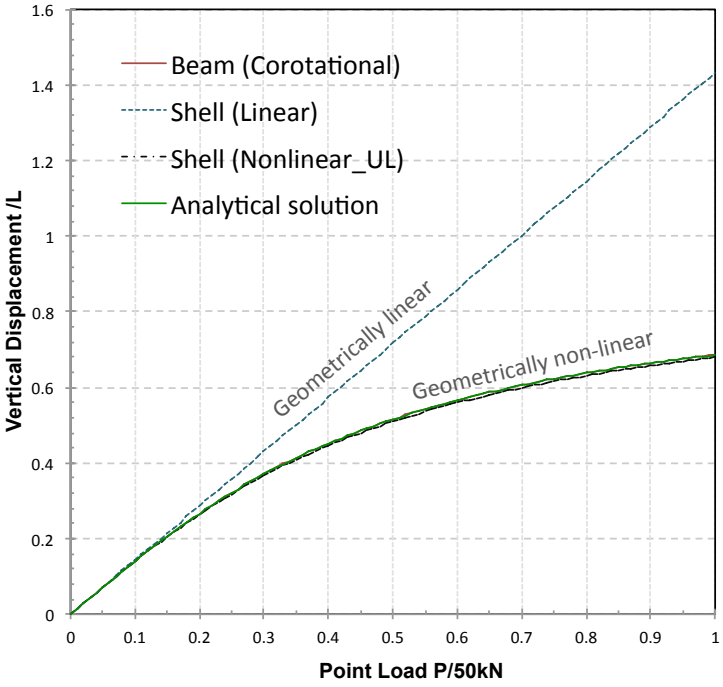

Figure 6.19: Free-tip displacement of a cantilever plate subjected to end load analysed using different models

implementation of 25kN end load. The maximum temperature at the bottom of the plate is assumed to be 1000^oC, whereas the top is at zero. Nonlinear increase is observed in additional deflection caused by the temperature gradient, which has been plotted with Figure 6.20. Identical results showing geometric nonlinearity have been presented from these analyses.

6.3.1.2 Material nonlinearity

Material nonlinearity involved in modelling a concrete slab is primarily induced by its complex material properties, and it is further complicated by thermal effect. A **ConcretePlaneStressThermal** material has been chosen to model

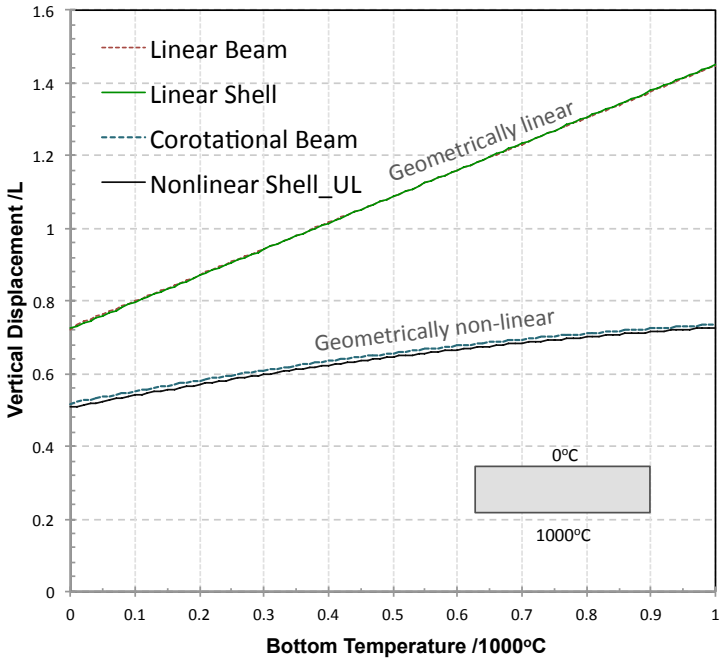

Figure 6.20: Free-tip displacement of a cantilever plate subjected to end load and thermal gradient analysed using different models

the concrete behaviour, while the plastic behaviour of reinforcement is achieved with **PlateRebarThermal** and **SteelECThermal**. To validate the numerical solution, the above presented cantilever plate are now modified to an RC plate with dimensions: $l = 3m$, $b = 0.4m$, $t = 0.1m$. The cross section has been illustrated in Figure 6.21, with reinforcement layers that are 0.393 mm thick (393mm^2/m reinforcement layer is equivalent to 10mm bars spaced 200mm) along longitudinal and lateral directions, with 20 mm concrete cover layers at the outer side. Material properties for concrete and steel reinforcement are listed in Table 6.3. The constitutive relationship for compression is defined according to Eurocode 2 (EN1992-1-2) (CEN, 2004) as normal weight concrete with siliceous aggregates. Geometric nonlinearity is included in all these conducted analyses.

The RC plate at first subjected to an increasing point load at the free tip until

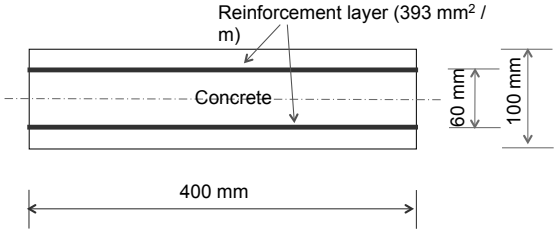

Figure 6.21: Reinforced concrete section of the slender plate

Table 6.3: Material properties for the RC section of the investigated plate

Material property	Value
Concrete compressive strength f_c	30 MPa
Concrete tensile strength f_t	3.0 MPa
Concrete cracking strain $epsilon_{cu1,\theta}$	0.005
Yield strength of steel reinforcement f_y	345 Mpa
Young's Modulus of steel reinforcement E_s	2.06×10^5 MPa

the beam collapse. This loading procedure is analysed with a beam model and a nonlinear shell model, respectively. Furthermore, a shell model has also been created in ABAQUS (ABAQUS, 2002) for comparison. Noticed that a **ConcreteECThermal** material is assigned to the beam with the parameters listed in Table 6.3, while a Concrete Damaged Plasticity material is defined for the model in ABAQUS. The load-deflection curves resulting from different models are plotted in Figure 6.22. A good agreement has been found from these results, despite the slightly different failure loads that suggest a conservative result in ABAQUS. The difference is likely to be caused by the multi-axial behaviour of the concrete, and due to the limitations of the plane stress concrete material.

The second loading case on this RC plate combines the point load and thermal action, which begins with a 500 N point load (roughly 20% of the load bearing

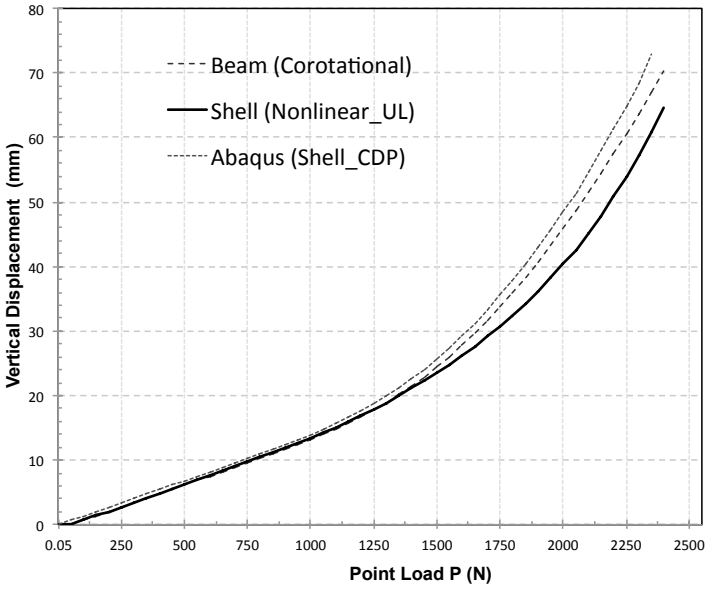

Figure 6.22: Free tip deflection of the RC slender plate

capacity) applied at the free tip, followed by a thermal gradient similar to the previous case. The temperature increase of the bottom surface gradually increases from zero until the beam collapses, while the top surface remains zero. Between these two surfaces, a linear distribution of temperature is assumed for the plate through its depth. The vertical displacement of free end according to the bottom temperature is plotted in Figure 6.23. Nearly identical deflection is found from the presented three models when the bottom surface temperature has not exceeded 700^{o}C. After 700^{o}C, a conservative prediction is given by the beam model, compared to the shell models in OpenSees and ABAQUS. With respect to the failure temperature, ABAQUS shell model (783^{o}C) predicts approximately 50^{o}C lower than the beam model (830^{o}C), and 80^{o}C than the OpenSees shell result (860^{o}C).

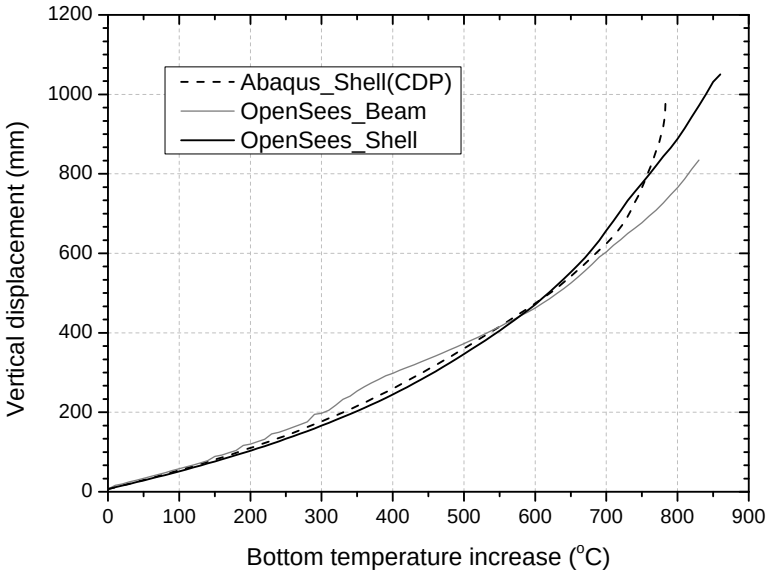

Figure 6.23: Free tip deflection of the RC slender plate

6.3.1.3 Shell element with non-uniform thermal action

A flat slab as shown in Figure 6.24 is adopted to to investigate the performance of the shell element under non-uniform thermal action. The dimensions of this flat slab are set as $l = 6$ m, $b = 6$ m, $t = 0.1$m. The slab is simply supported on four edges, with necessary constraints assigned to eliminate rigid body motions. The slab deflections along the sampling path of the slab are compared with respect to different distributions of temperature gradients across the plane, which include a quadratic decay, a linear decay and a uniform distribution. The maximum thermal gradient and temperature increase are assumed at the centre of the slab as 800^oC to 200^oC from the bottom to the top, whilst no temperature increase assigned to the corner. For quadratic decay, the temperature distribution at the half length of the radial path is defined as a quarter of the maximum values (200^oC to 50^oC). Such a spatially non-uniform distribution of temperatures is realised through **ThermalActionWrapper** as previously discussed.

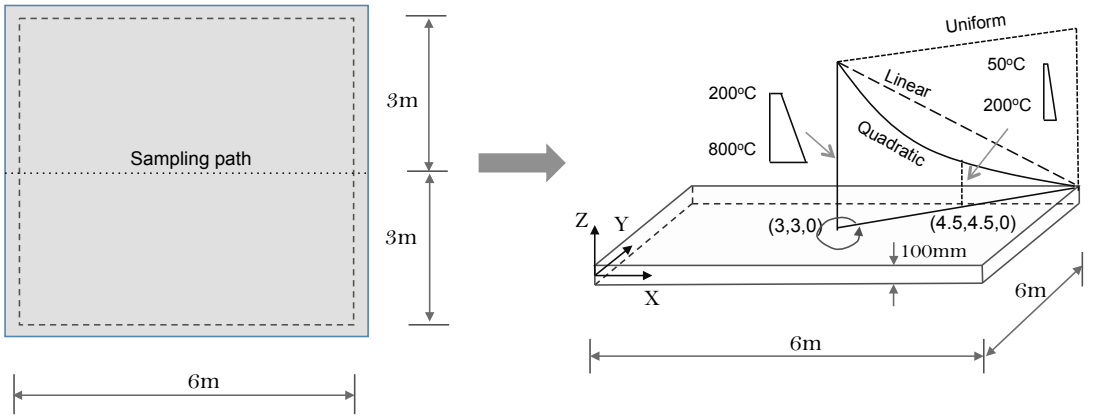

Figure 6.24: A generic slab with simply supported boundary conditions

The slab is first modelled with an elastic material, of elastic modulus 1.92×10^5 MPa, Poisson's ratio of 0.2, and the coefficient of thermal expansion of 1.0×10^{-5}. In OpenSees, the **LayeredShellFiberSectionThermal** class is used to formulate the section response for the geometricly linear shell element **ShellMITC4Thermal** as well as the nonlinear shell element **ShellNLDKGQThermal**. **ElasticIstropic3DThermal** associated with **PlateFiberMaterialThermal** are employed to represent the elastic behaviour with a constant coefficient of thermal expansion (1.0×10^{-5}). When geometric nonlinearity is not considered, the slab deflections along the sampling path are plotted in Figure 6.25, where the greatest deflection occurs in the uniform case as the most severe case. Deflections responding to a quadratic distribution of thermal gradients are found the smallest, while a medium level of deflection is produced by the linearly distributed thermal gradients around the slab centre.

However, the deflection shapes seem completely different when geometric nonlinearity is considered, which have been illustrated in Figure 6.26. More deformations are seen in the slab subjected to linear and quadratic distribution of thermal gradients compared to the geometrically linear analyses. Among these

two cases, quadratic distribution even causes larger deflection than the uniform case in the vicinity of slab centre, which is also due to the decrease of deflection in the uniform case after considering geometric nonlinearity. Around the slab centre, a linear distribution seems to be the most dangerous whereas the largest deflection remains in the slab applied with uniform distributed temperature gradients. Notice in Figure 6.25 and Figure 6.26, slab deflections modelled by ABAQUS are also presented as comparisons and validations regarding the performance of the geometrically nonlinear shell element under localised thermal action.

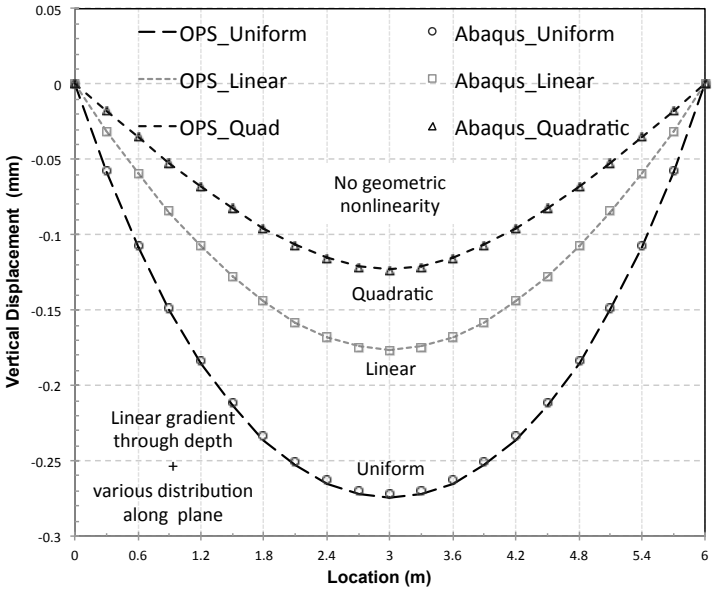

Figure 6.25: Slab deflections subjected to various types of localised thermal action modelled using geometrically linear elastic shell elements

When material nonlinearity (plasticity) and geometric nonlinearity are both taken into account, deflections of this generic slab (Figure 6.27) show similar shapes as found in the geometrically linear and elastic analyses. The largest deflection again occurs in the slab subjected to uniform distributed thermal gradients. This is due to the material softening in the bottom layers through the whole slab, which frees

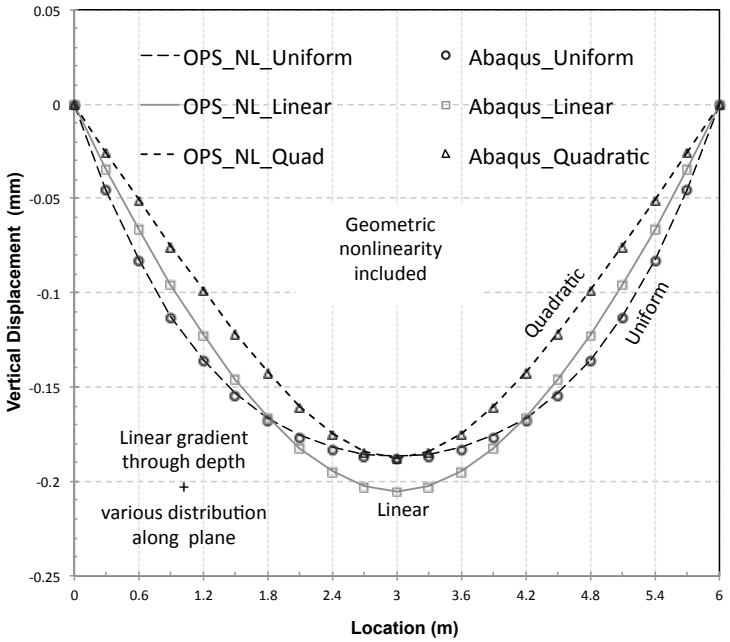

Figure 6.26: Slab deflection subjected to various types of localised thermal action modelled using geometrically nonlinear elastic shell elements

the corner resistance to bending and leads to the similar response as found in geometric linear analyses (much lower deflection-induced stresses). Not much difference is observed in the quadratic cases after the introduction of material nonlinearity, as a result of limited material softening near the slab edges due to lower temperatures. Moreover, the effect of material nonlinearity appearing in the linear case is between the quadratic and uniform distributions. ABAQUS analyses using *Concrete Damaged Plasticity* model (Yazdani and Schreyer, 1990) are also provided as a reference to the results. Different level of errors are observed between the predictions in the three cases, where the greatest discrepancy is in the uniform case at the slab centre. For slabs subjected to linear and quadratic distribution of thermal gradients, OpenSees predictions are generally acceptable but still remain necessary to the future development of advanced concrete models.

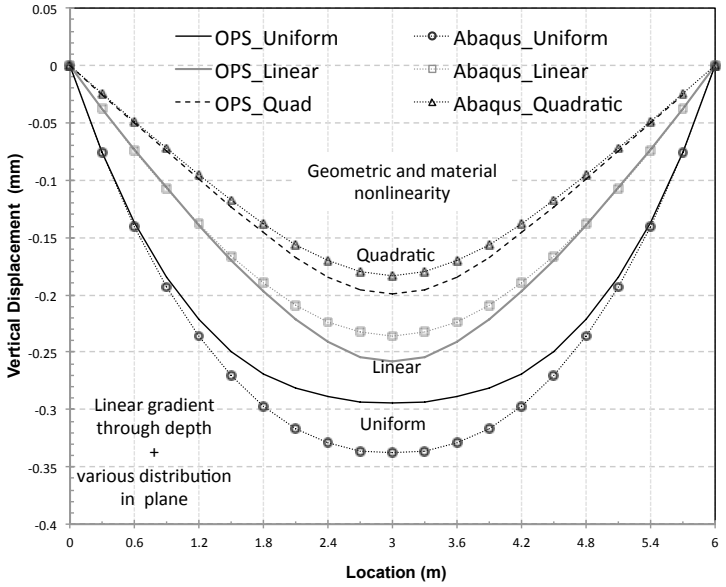

Figure 6.27: Slab deflection subjected to various types of localised thermal action modelled using geometrically nonlinear plastic shell elements

6.3.2 Thermo-mechanical response of concrete slab subjected to localised fire

6.3.2.1 Two-way bending of reinforced concrete slabs at ambient temperature

For reinforced concrete slabs loaded with a UDL at ambient temperature, a few tests were reported by (McGregor and G, 1994). One test tagged as B1 used a rectangular plate of dimensions 2745mm×1829mm in plan with a thickness of 68.2mm, as shown in Figure 6.28. The specimen was simply supported on four edges and loaded with a gradually increasing UDL. Reinforcing bars were placed in the slab as an orthogonal mesh in two ways at the bottom and the top with approximately 18mm thick concrete covers. The equivalent areas of steel

reinforcement along both directions were 260mm^2/m, while the nominal yield strength (0.2%) of steel rebars was 450 MPa. The compressive strength of the concrete was measured as 18.7MPa (tensile strength is assumed as 1.87MPa in numerical modelling).

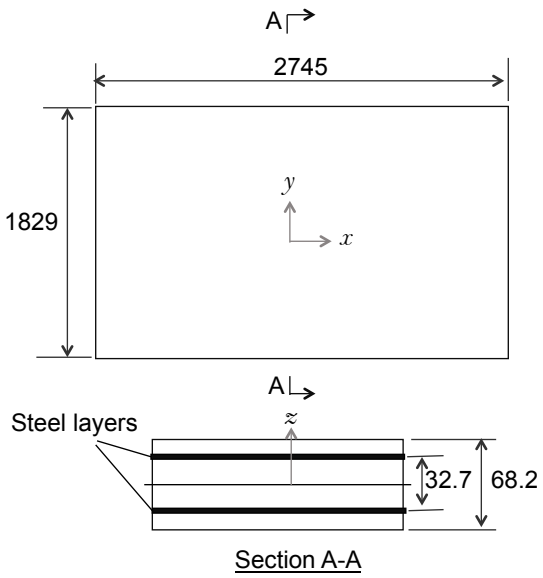

Figure 6.28: Configuration of Slab Test B1

The mechanical response of this RC slab is modelled in ABAQUS and OpenSees using the developments discussed in the last section. When geometric nonlinearity is not enabled, the central deflection rapidly develops around a UDL magnitude of 34.7MPa, which is the ultimate load calculated according to the yield-line calculation (Huang et al., 2003a). Both the ABAQUS and OpenSees models predict slightly less deformation at the early stage of the test. By including geometric nonlinearity, OpenSees is able to predict a similar load-deflection curve as observed in the test but a slightly higher ultimate load (51kN/m^2) corresponding to the collapse (46 kN/m^2 observed in the test). A much higher failure load is predicted by ABAQUS (58kN/m^2) which also reaches the highest

deflection (-0.147m) compared to the OpenSees result (which fails to converge at -0.098m as rebars reach yield strength) and the test data (approximately -0.103m) corresponding to the start of runaway.

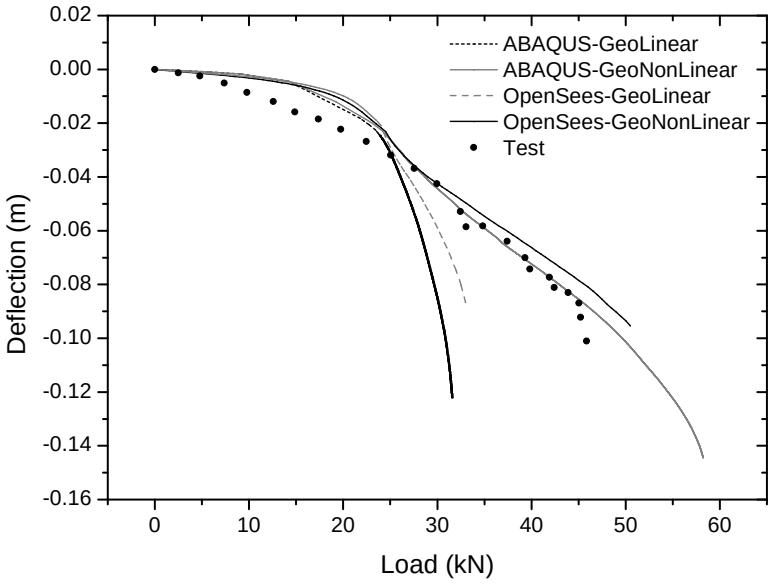

Figure 6.29: Central deflection of Slab B1 subjected to UDL

6.3.2.2 Two-way reinforced concrete slabs subjected to localised fire action

The small size RC slab B1 tested above is now assumed to be subjected to localised fire action. An SFPE type of localised fire is placed underneath the slab, with two different locations of the fire source as shown in Figure 6.30. Heat transfer analyses were performed for the first scenario in which the fire origin is exactly underneath the corner of the slab. The SFPE correlation for incident heat fluxes is adopted to estimate the influence of localised heating when the fire impinges on the ceiling slab. The rate of heat release from the fire source is prescribed to be 1MW, while the nominal diameter is assumed as 1m and the vertical distance from the fire

source to the ceiling is taken as 3m. The concrete is assumed to contain Silicious aggregate with 1.5% moisture content retained. Coefficients for convection and radiation for fire-slab and slab-ambient air interactions are defined according to Eurocodes (CEN, 2002a, 2004). The strategy of modelling heat transfer from the fire to the slab is consistent with the heat transfer analyses presented in Chapter 3.

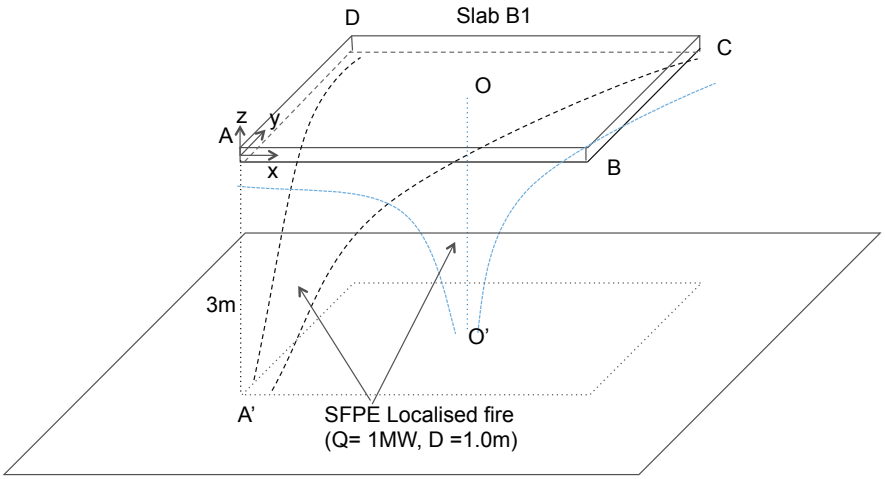

Figure 6.30: Slab B1 subjected to localised fires with origins at different locations

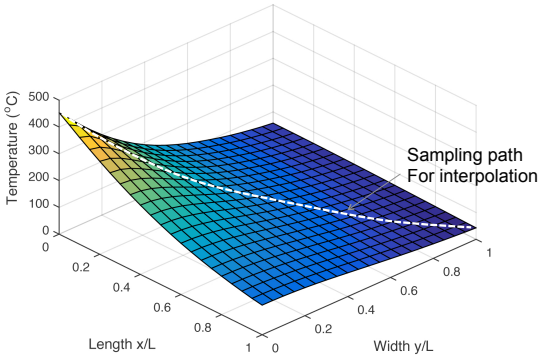

Figure 6.31: Temperature distribution in Slab B1 subjected to SFPE localised fire

The temperature distribution at the bottom surface of this concrete slab is illustrated in Figure 6.31, where the peak temperature reached 455.8 ^{o}C after 30mins of exposure to the steady-state SFPE localised fire (without consideration

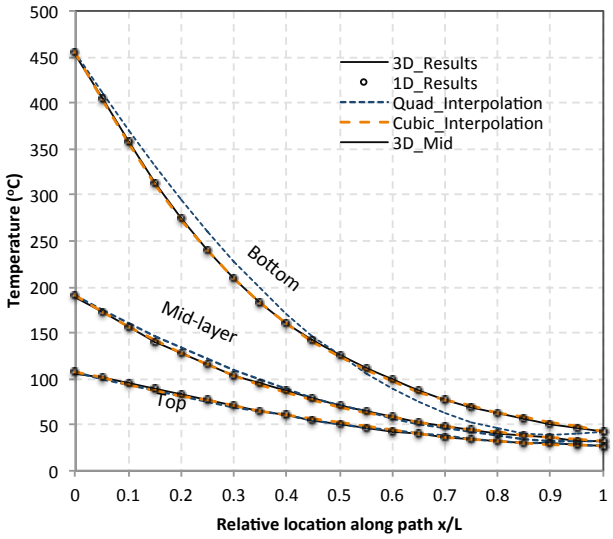

Figure 6.32: Along path temperature distribution and interpolation for Slab B1 subjected to SFPE localised fire

of fire development). Along the diagonal (longest) path, the temperature variation at different depths of slab is presented in Figure 6.32, including the distribution at the bottom surface (exposed to fire), the mid-depth layer and the top surface (unexposed). Higher temperature gradients are found in the lower layers due to the low thermal conductivity of concrete, which also leads to a low level of heat conduction horizontally as already found in Chapter 3. Quadratic and Cubic interpolations are performed to approximate the temperature distribution. Based on the previous discussion on the accuracy of polynomial interpolation, the cubic interpolation scheme is primarily used in approximating the thermal response of the concrete slab subjected to the SFPE localised fire. Good agreement is seen in Figure 6.32 between 3D results and cubic interpolated results when sampling points are chosen as (0, 0.3, 0.7, 1.0) of the slab length (width), whereas discrepancies are observed in quadratic interpolated over the whole length the

slab. The same methodology can be used for resolving temperature distributions resulting from the fire source located at any other point under the slab.

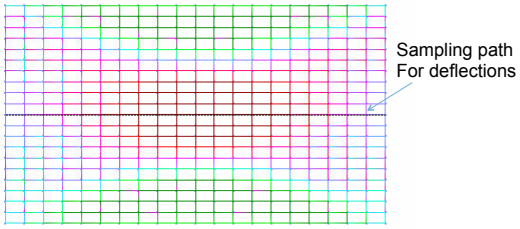

Figure 6.33: Finite element mesh of Slab B1 for thermo-mechanical analysis

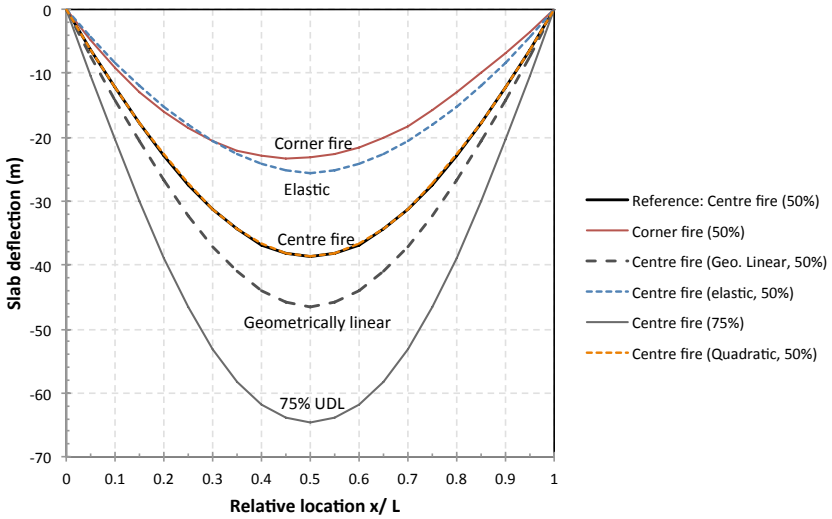

Figure 6.34: Central deflection of Slab B1 subjected to localised fire

Following the implementation of heat transfer results and the uniformly distributed loading (23kN/m^2 corresponding to 50% of loading capacity), thermo-mechanical analyses are sequentially performed to investigate the slab deflections in the slab B1 heated by the SFPE localised fire. The finite element mesh of the slab B1 is shown in Figure 6.33 (The colours represent a measure of stress intensity facilitated by DisplayModel facility in OpenSee but currently it does not have the capability of quantitatively describing the colour scheme). Deflections are investigated and plotted along a sampling path (shown in Figure 6.33).

As shown in Figure 6.34, the centre fire (reference case) causes greater deflections compared to the corner fire, as the centre fire heats a lot more of the slab to higher temperatures. It is observed that identical deflection shapes are produced from the analyses using quadratic and cubic interpolations. Material and geometric nonlinearities are separately disabled in the analyses to examine the differences in modelling. Significantly lower deflections are seen in the results obtained from elastic (only thermal expansion) but geometrically nonlinear analyses, which suggests that the material degradation has penetrated a significant depth of the slab. When modelling the slab deflections with plastic material but no geometric nonlinearity, larger deflections are predicted. Furthermore, when a larger loading ratio, 75% of ultimate load is applied before the centre fire, it generatres greater plastic deformations in the lower layers and leads to greater deflections in the slab.

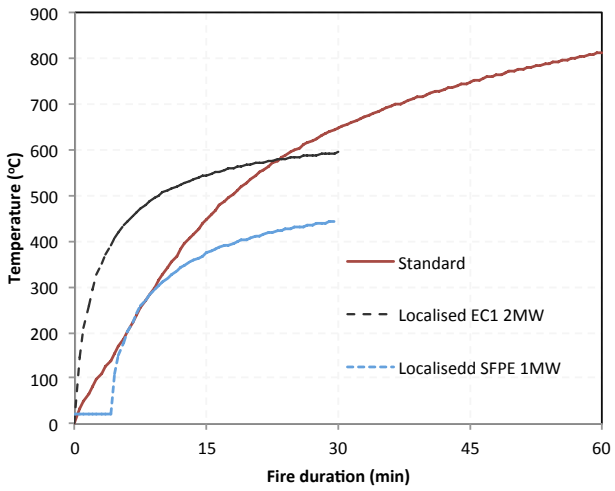

Figure 6.35: Histories of central peak temperatures at the generic slab bottom subjected to different fire exposure

Instead of the slab B1, a large size slab based on the 6m×6m generic plate is now used to model the slab behaviour under various fire exposure and boundary

conditions. The slab thickness and reinforcing bars are kept identical to the slab B1, and the material properties are also kept consistent with the previous models. The heat transfer solutions and approximations have been addressed in Chapter 3, which can now be implemented without any further checks. This generic slab is subjected to a standard fire, a 1MW SFPE localised fire and a 2MW EC1 localised fire, separately. The standard fire lasts for one hour while the durations of localised fires are assumed to be 30 minutes. A fire growth represented by a t-square fire (Drysdale, 2011b) with a growth constant k as 300s is associated with the SFPE localised fire exposure. The variation of peak temperatures over the fire duration are plotted in Figure 6.35. The temperature increases rapidly in the case of the 2MW EC1 fire at the early stages and then enters a slow growth period until the end of assumed 30 minutes of exposure. For 1MW SFPE localised fire considering fire growth, heat flux input is ignored until the fire impinges on the ceiling. Temperature at the bottom of the slab gradually increases in the case of Standard Fire and exceeds the maximum temperature in the localised cases after 25 minutes.

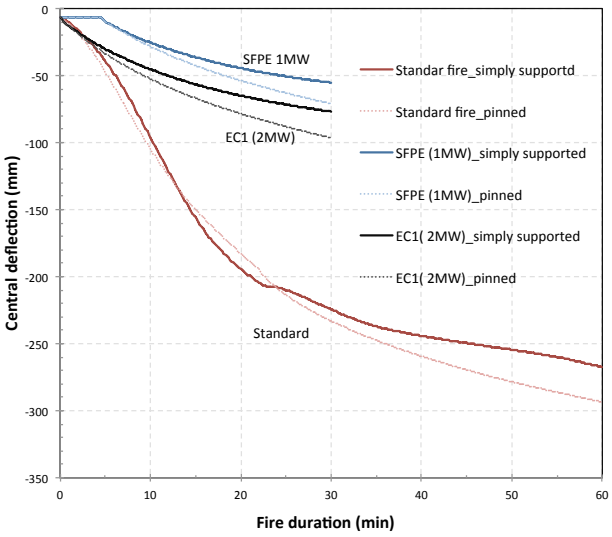

Figure 6.36: Central deflection of the generic slab subjected to localised fires

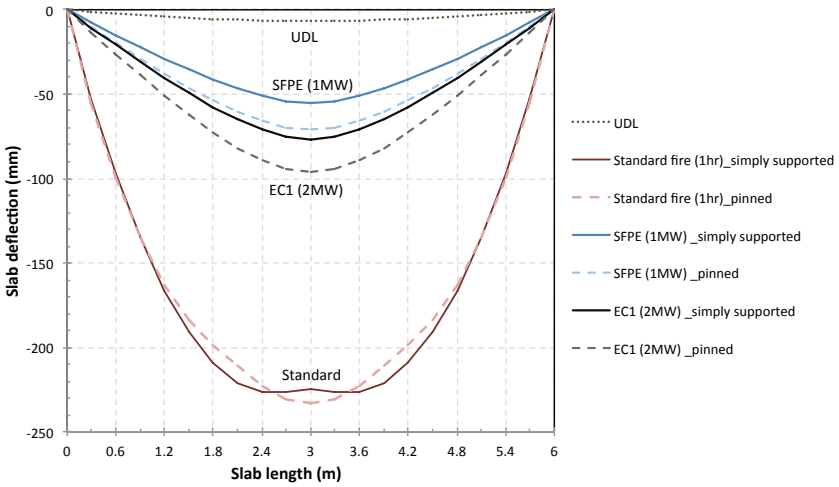

Figure 6.37: Deformed shape of generic slab subjected to localised fires

The corresponding central deflections are shown in Figure 6.36, with different boundary conditions assigned to the slab edges, which include simply supported and pinned boundaries (which imply rigid restraint to lateral translations). Generally the pinned slabs experience great deflections than the simply supported slabs, which are caused by the lateral restraints that prevent the thermal expansion of the slab. Significantly greater deflections are found in the case of the standard fire, as a result of uniform heating and high gas temperatures achieved by the end of the fire. For localised heating, the central deflection is small, with a slightly larger deflection developing in the case of the EC1 localised fire. The deflection shapes of these investigated generic slabs are summarised with reference to 30 mins exposure and plotted in Figure 6.37. Deflections caused by uniform heating are significantly higher, with a slight snap-back shown around the slab centre, which is caused by the material softening in lower layers and strength retained in cooler layers. From the plot, it may be concluded that localised fire exposure is not so detrimental to the slab and a low levels of deflections occur,

however it should be noted that the localised fires used here are of relatively low heat release rate and of shorter duration than the standard fire.

6.4 Conclusion

In this chapter, a large amount of analyses have been performed to study the performance of beam-column elements and shell element which are used to model beams and slabs subjected to localised fires. A number of conclusions can be summarised as below:

- Comprehensive numerical tests have been performed to evaluate the performance of beam elements using different formulations. It is found that the structural deflection induced by localised heating is dominated by thermal expansion and material softening, especially for relatively low temperatures ($\leqslant 400^o$C). For localised high temperatures, the accuracy of numerical prediction is controlled by the reduction of material strength.

- A simply supported steel beam subjected to SFPE type localised fire is modelled using different beam-column elements. Similar results can be achieved by using fewer force based beam-column elements and quadratic temperature interpolations. A higher UDL (50% of load carrying capacity) can lead to the beam collapse in 14 minutes of localised heating.

- Thermo-mechanical analyses are performed to examine the robustness of shell elements for ambient temperature and localised heating. These analyses are compared to the beam element prediction, ABAQUS simulations, and experimental tests, showing good agreement.

- A small slab is subjected to SFPE type localised fire action with a fire source placed at the corner and the centre of slab. A 6m$\times$6m slab with various boundary conditions is examined against different localised fires (EC1 Localised fire and SFPE Localised fire). It is found that higher loading ratio and centre fire could can relatively large deflections, but still much smaller than the deflection caused by Standard Fire exposure. Axial restraints to the slab can cause higher level of deflections compared to the slab with simply supported boundary conditions.

Chapter 7

Coupled analysis for evaluating structural performance considering localised heating effects

7.1 Introduction

In a prescriptive design approach regime, the global behaviour of structures is largely ignored. Traditional design strategy for structural fire safety was based on Standard Fire tests with respect to the performance of isolated members. Performance-based engineering or PBE approaches have gained enormous popularity in structural fire safety Engineering, which often requires a comprehensive simulation for fire action and fire induced structural behaviour. The proposed

'SIFBuilder' tool was developed for this purpose, and is capable of performing a highly integrated analysis of framed structures subjected to different design fires, which include both idealised uniform fires and idealised non-uniform fires. The former category of fire models are typically represented by the Standard Fire curve as widely adopted in traditional design, and the Parametric Fire curves which account for the fuel load and compartment configuration parameters. The latter category is typically referred to as the localised fire models, which may be extended to the Travelling Fires (Stern-Gottfried and Rein, 2012a,b). As discussed in Chapter 3, heat transfer analyses within OpenSees are automatically performed for each member by taking advantage of the dimensional reduction concept and fast estimation approaches developed as part of this research. The cross section of steel members can be either fire protected or unprotected, and in addition to these standard cases the tool also features the partially protected columns to consider the damaged or missing fire protection. This comprehensive analysis can be performed using a full-scale structural model in OpenSees, which is able to simulate the structural behaviour in fire, and also consider different types of local effects such as localised fire action or partial damage to fire protection as a result of a preceding extreme event, such as an earthquake, for instance.

This Chapter will present a few illustrative cases that are conducted on a generic $2 \times 2 \times 2$ frame building model using *SIFBuilder* as an integrated computational tool which has been introduced in Chapter 5. The usage of *SIFBuilder* shall be demonstrated, with an emphasis on the global behaviour of the simple frame structure and the effect of partial damage to the fire protection.

7.2 A generic frame structure

7.2.1 Model Configuration

A generic steel frame structure is modelled using *SIFBuilder*, while a schematic overview of this frame structure is shown in Figure 7.1. The configuration of this two-storey frame structure is similar to the small frame used by Lamont et al (Lamont et al., 2004), which was to investigate the behaviour of a small structure resulting from different design fires ('short hot' or 'long cool' fire). The y axis of the global coordinate system is set as the default along vertical direction (this is convenient to create a 2D model in the xy plane). The plan layout of this idealised building is shown in Figure 7.4, which consists of two bays(6m and 9m span) along each axis. A grid line system is used to describe the layout with tags ranging from 1 to 9, along both the x and z axes. Using this tag system, the compartment could be numbered in accordance with the left upper column as Figure 7.4 shows. Such a numbering system is only suitable for modelling small frames as the number of grid lines cannot exceed 9. For larger frames, the components of a building model are identified using its x (XBay), y(YStorey), z(ZBay) coordinates in *SIFBuilder*.

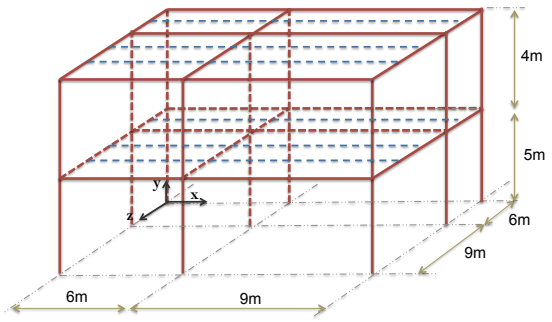

Figure 7.1: Configuration of the generic frame model

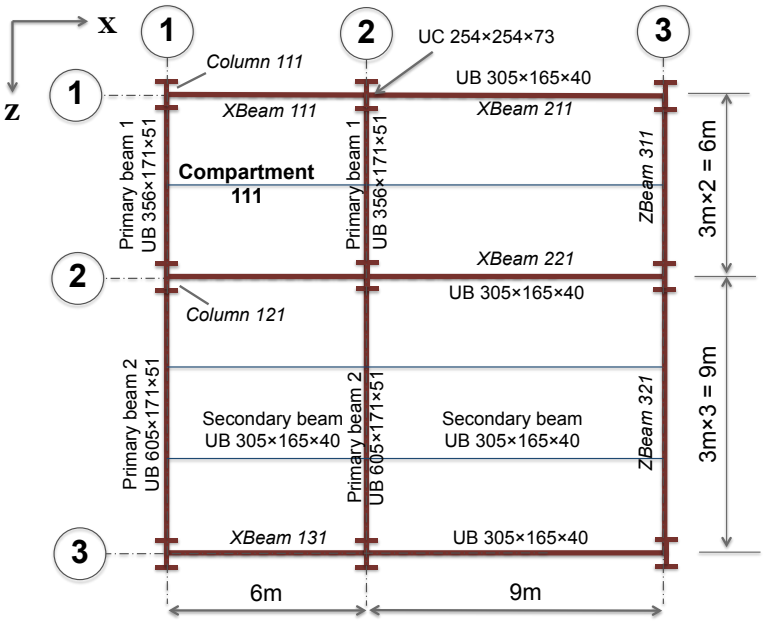

Figure 7.2: Configuration of the generic frame model

The structural design is similar to the Cardington test building (British Steel, 1998, 1999; Usmani, 2000; Lennon, 2003). Two different sizes of primary beams are used in the framing system, including a UB356×171×40 steel beam for the 6m span, and a UB610×228×101 for the 9m span. Secondary beams with a spacing of 3m are assigned to the floor system, using a UB305×165×40 section. All the steel section beams are assumed to be of yield strength 275 MPa. Instead of using the usual profiled decking, a flat slab is used for simplicity with double reinforcement layers and with a 20mm thick concrete cover. The reinforcement layers are assumed to be constructed of A142 standard mesh (141mm^2/m) of yield strength 600 MPa. Normal weight concrete for the slab of compressive strength 30MPa is adopted for the floor slab. All the beam and column joints are assumed to be rigidly connected, and no bracing members are included in this model.

All the steel beams and concrete components are left unprotected, whereas Spray-applied Fire Resistive Material (SFRM) is employed to protect the steel

Table 7.1: Cross sections and materials assigned to the structural members

Member Type	**Cross Section**	**Yield strength**(MPa)
Primary Beam 1	UB356×171×51	275
Primary Beam 2	UB610×228×101	275
Secondary Beam	UB305×165×40	275
Steel Column	UC254×254×73	275
Concrete Slab	100mm thick slab	35
Steel Reinforcement	A142 Mesh	600

columns. The contribution of SFRM coatings to the load bearing capacity is ignored because of its extremely low strength and modulus (Chen et al., 2010). Thermal properties of SFRM are considered constant during the fire, while the corresponding parameters can be adopted as discussed in Section 3.4 (Thermal conductivity $\lambda = 0.05W/m/K$, density $\rho = 350kg/m^3$, and specific heat $c_p = 1100J/k/kg$).

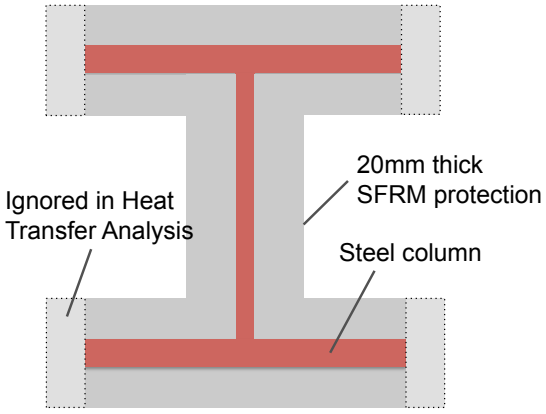

Figure 7.3: The cross section of SFRM insulated column

7.2.2 Loading cases

A uniform distributed load is applied to the slabs to represent the dead and imposed loading, which was adopted to be 4.95kN/m^2 as in the Cardington tests.

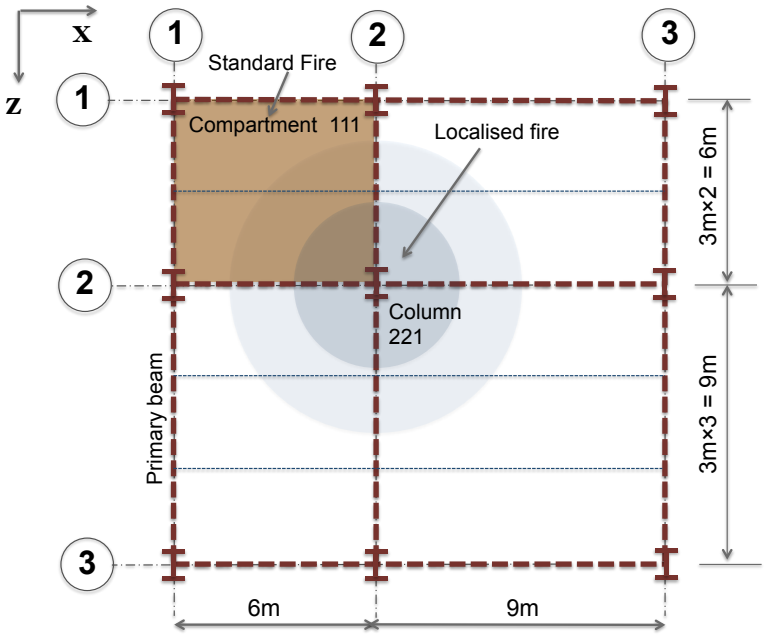

Figure 7.4: Fire Case 1: Standard Fire in Compartment 111, and Fire Case 2: Localised fire surrounding Column 221

Two different fire scenarios are examined for this steel framed structure, as illustrated in Figure 7.4. The first scenario is an idealised uniform fire occurring in the confined compartment (Compartment 111), where the time-temperature relationship is chosen to conform to the Standard Fire curve. It is assumed that during the fire, flames and smokes remain confined to the compartment by the wall partitions therefore structural members are only partially exposed, which shall result in a non-uniform temperature distribution across the section of the beams and columns, all of which is automatically accounted for by *SIFBuilder*. The second fire scenario is used to demonstrate the *SIFBuilder* tool for determining

the structural response to an idealised non-uniform fire. A localised fire defined according to the Eurocode 1 model is chosen to describe the non-uniform fire action, which is assumed to be a fire source surrounding the central column at the ground floor. Considering the 5m high ceiling and to simulate a relative large fire, the rate of heat release is chosen as 5MW, while the nominal diameter of the fire source is assumed to be 1m. In this fire scenario, the building may be considered as a car park which does not allow build-up of a smoke layer because of the open perimeter. It has to be pointed out that ignoring the effect of smoke layer usually underestimates the degree of incident heat flux and overestimates the non-uniformity of the fire action, especially for buildings with facades.

7.2.3 Finite element model

A finite element model as shown in Figure 7.5 is created in the structural domain to conduct the thermo-mechanical analyses for both fire scenarios. The model is comprised of beam-column elements that are employed to model the behaviour of primary and secondary beams (12 elements per beam) as well as the columns(6 elements per column), and with shell elements that represent the concrete slabs. An offset between beam elements and the shell elements has been considered in the model, and to model the composite action between them rigid links are used as multi-point constraints to represent the shear studs. Temperature dependent material properties are enabled via the thermo-mechanical materials as discussed in Chapter 4. Prior to the structural analysis, a number of heat transfer analyses are performed for structural members to obtain the member-based temperature evolution, which may be a single 1D or 2D analysis while the fire exposure is idealised as spatially uniform gas temperature for the Standard Fire scenario.

While in the case of localised fire exposure, a number of heat transfer analyses are performed at the selected sections of each member, by taking advantage of the dimensional reduction approaches for heat transfer analyses (Tcl script can be seen in Appendix C).

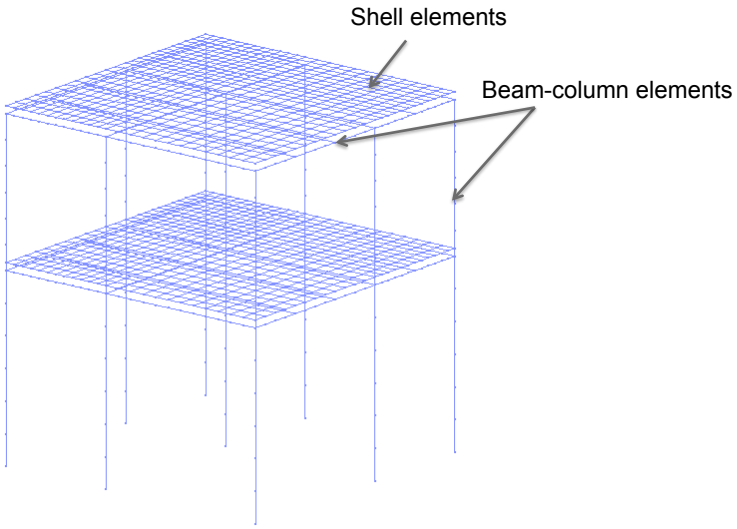

Figure 7.5: OpenSees model for the generic frame structure

7.2.4 Efficiency of SIFBuilder

The developed SIFBuilder is employed to model the generic building, which aims to significantly decrease the time consumption involved in fire modelling, thermal and structural analyses. A comparison has been presented in Table 7.2 regarding the complexity of the whole process in OpenSees and ABAQUS. The highly integrated environment provided by SIFBuilder enables automated implementation of fire action and data communication between thermal and structural models. Moreover, the rapid estimation scheme can further reduce the number of section analyses for modelling the heat transfer from fire to structural

members, while the dimensionally reduced scheme in ABAQUS may need section analyses performed for each node. No matter which computational strategy is adopted in ABAQUS, massive time consumption is unavoidable to transfer the data to the structural FE model if the user choose to do it manually, or extra effort is necessary to develop third party tools to extract the data from heat transfer model and apply it. As an integrated computational tool, SIFBuilder is more convenient in this procedure, which consists of built-in middle-ware to bridge the thermal and structural modules, and makes itself outstanding from the commercial FE packages and other computational tools.

Table 7.2: Modelling of generic building subjected to localised fire within OpenSees and ABAQUS

<table>
<tr><th rowspan="2">Step</th><th rowspan="2">OpenSees</th><th colspan="2">ABAQUS</th></tr>
<tr><th>Reduced HT</th><th>Full-3D HT</th></tr>
<tr><td>Fire modelling</td><td>Built-in model</td><td colspan="2">Specially developed routine</td></tr>
<tr><td rowspan="2">Thermal analysis</td><td colspan="3">12 primary beams, 6 secondary beams, 5 columns, 4 slabs</td></tr>
<tr><td>59× 2D
12× 1D</td><td>221× 2D
144× 1D</td><td>18× 3D for Beam
4× 3D for slab
5× 2D for column</td></tr>
<tr><td>Data transfer</td><td>Automatically
(no extra time cost)</td><td colspan="2">Manually or via developed code
(Extra time and effort)</td></tr>
<tr><td rowspan="2">Structural analysis</td><td>Self generated model</td><td colspan="2">Manually defined model</td></tr>
<tr><td colspan="3">540 beam-column elements & 2880 shell elements</td></tr>
</table>

7.3 Thermo-mechanical responses to idealised uniform and non-uniform fires

The aforementioned two fire scenarios are discussed based on the generic frame model. For each type of fire exposure, thermal responses of the structural members including beams, columns and slabs are examined in the form of temperature distribution and evolution. It is followed by the discussion on the structural responses, which are presented mainly as deformation shapes and loading deflection histories.

7.3.1 Idealised uniform fire action

As the fire exposure is idealised as a spatially uniform action on the structural members, thus the temperature distribution can be estimated using 1D over the depth(for the slab) or 2D sectional analyses (for beams and columns). For demonstration, a one hour Standard Fire curve is adopted here to describe the time-temperature relationship. Meanwhile, the partial exposure resulting from the confinement of the fire has also been considered in this case.

7.3.1.1 Thermal response to Standard Fire exposure

It is assumed that the hot gases are confined within the compartment (No.111 in this generic building), beams at the edge of the compartment and columns are subjected to partial exposure to the fire because of the finite thickness of insulating partition walls. The boundary conditions for heat transfer analyses

of these members subjected to fire action are depicted in Figure 7.6. The heat exchange between the SFRM insulated column and the fire is marked with red bold dashed lines (Figure 7.6(a)), and the rest of surfaces are assumed to lose heat to the ambient via convection and radiation. The exposed surfaces are correspondingly defined according to the exact location of the columns in the compartment. For beams that are located at the edges of the compartment, the steel section is also partially exposed to the hot gas, which result in the heat transfer boundary conditions assumed as shown in Figure 7.6(b). However, secondary beam is completely engulfed in fire (Figure 7.6(b)), where the steel section absorbs the heat through all the surfaces except the top surface that is shielded by the composite concrete slab as assumed in this model.

When subjected to Standard Fire exposure, the temperature evolution in member sections varies in accordance with the locations across the section. As marked in Figure 7.6, 15 temperature slots are monitored for I section members, and 9 temperature data points are collected for slabs. For columns that are insulated by SFRM coatings and heated through partial exposure to the fire, the highest temperature appears at C-1, and the lowest may be at C-3, and the web temperature can be represented by C-2. Similarly, temperature histories at typical points of the cross section of the beams and slab are recorded and plotted in Figure 7.7 and Figure 7.8.

As shown in Figure 7.7, a significant delay of temperature increase can be observed in the SFRM insulated columns. In the most intensely heated part, the steel temperature remains below 150^{o}C, whilst even lower temperature (up to 50^{o}C) can be found at the opposite side as the fire is not directly imposed. The single side exposure of the column web experiences temperatures at an intermediate

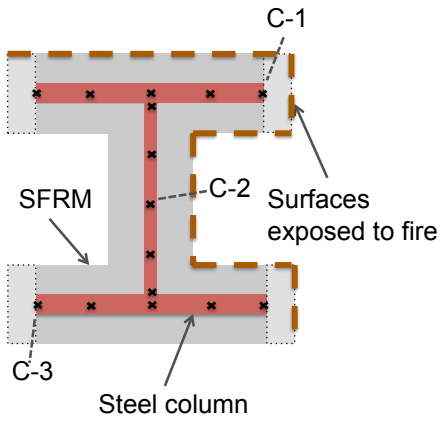

(a) SFRM insulated steel column

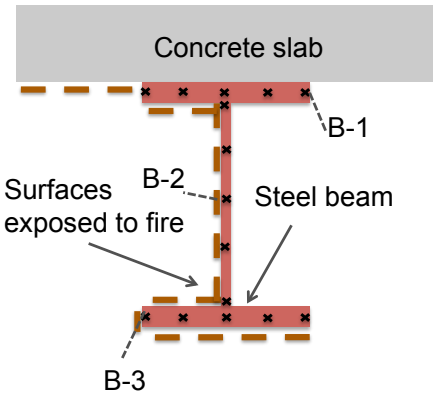

(b) Primary steel beam

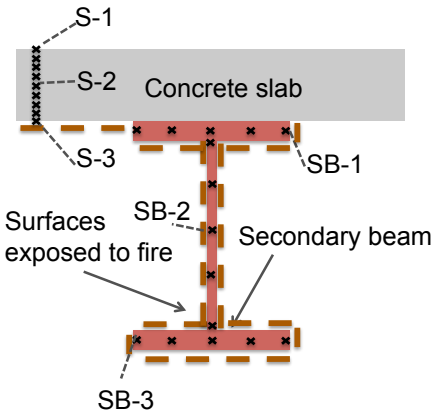

(c) Secondary steel beam

Figure 7.6: Partial exposure of structural members subjected to one hour Standard Fire

level, which did not exceed 100^{o}C. For unprotected edge beams that are located around the fire compartment, temperature increases are significantly higher than the observed response in the insulated columns. Non-uniform development of the temperatures are found as well due to the partial fire exposure. At the lower flange (left or right half of the flange) which is engulfed in the fire, temperature increases rapidly as curve B-3 shows and gradually converges to the gas temperature. In the web, lower temperature appears as a result of single face exposure. Meanwhile,

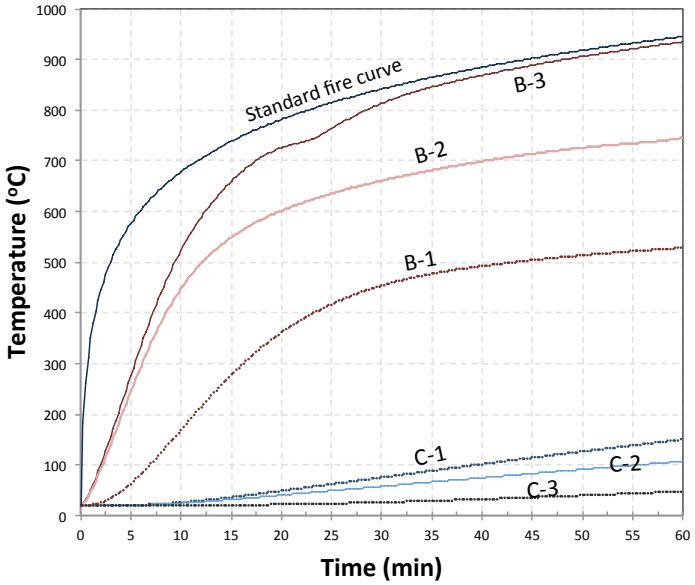

Figure 7.7: Temperature evolution of the beam and column in a compartment fire (one hour Standard Fire) considering partial exposure

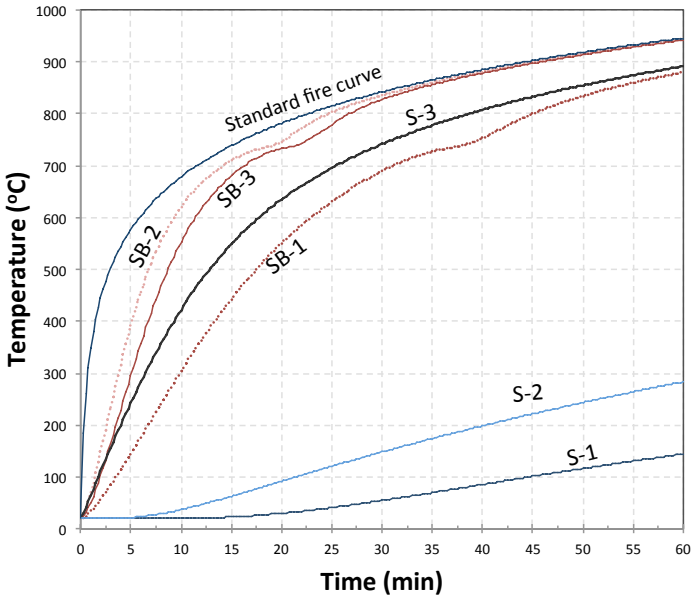

Figure 7.8: Temperature evolution of the secondary beam and slab in a compartment fire (one hour Standard Fire)

the lowest temperature can be always found at B-1, which absorbs heat through heat conduction from the directly exposed parts. The temperature difference between B-2 and B-3 is approximately 200^{o}C after 30 minute exposure, while another 200^{o}C temperature difference can be seen between B-1 and B-2.

Unlike the edge beams, the secondary beam involved in a compartment is completely engulfed in the fire except the top face of the upper flange. Different heating histories are seen in the web and flanges of the secondary beam, which shows the maximum temperatures in the web as it is thinner than the flange, and the lowest temperature appears in the upper flange as a result of heat loss to the concrete slab. The temperature distribution along the depth of the slab can be represented by the temperatures at the bottom, mid-depth and top layers, which are three points out of 9 recorded locations. The bottom surface of the concrete slab directly absorbs heat from the fire, which leads to the highest temperature (S-3) in the slab. However, a significant thermal gradient can be found in the vicinity of bottom layer, as the temperature drops rapidly from the bottom surface to mid-depth layer (S-2). The temperature difference between the mid-depth layer and the top surface is much lower, which reaches 140^{o}C at the end of the 1hr Standard Fire exposure. In the mean time, the maximum temperature at the exposed surface increases to 891.3^{o}C.

7.3.1.2 Thermo-mechanical response to Standard Fire exposure

The deformed shape of the generic building after 1hr Standard Fire exposure is presented in Figure 7.9, where the deformation is factorised by 10. Large deflections are seen in the Slab 111 especially at the centre, which is a combined action of thermal bowing and material degradation. As the edge beams are

concurrently heated, the neighbouring slab system is affected by the confined compartment fire. However, the deflections of adjacent slabs are relatively small. The deflection history of slab and beams are presented in Figure 7.10. The largest deflection occurs at the slab centre which reaches 0.31m at the end of the fire exposure, whereas the different degrees of deflection are shown at the mid-span of the edge beams (XBeam111, XBeam121, ZBeam 111, and ZBeam 211). Among them, the beams connected to adjacent slabs experienced higher deflections compared to the outer beams, which is caused by the higher slab loads as shared with other supporting beams. ZBeam 211 as a primary beam takes the most load, which leads to the largest mid-span deflection in beams.

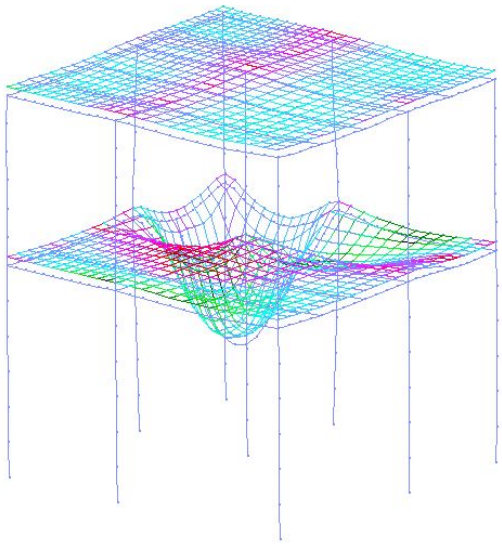

Figure 7.9: Deformed shape of the generic building subjected to one hour Standard Fire exposure

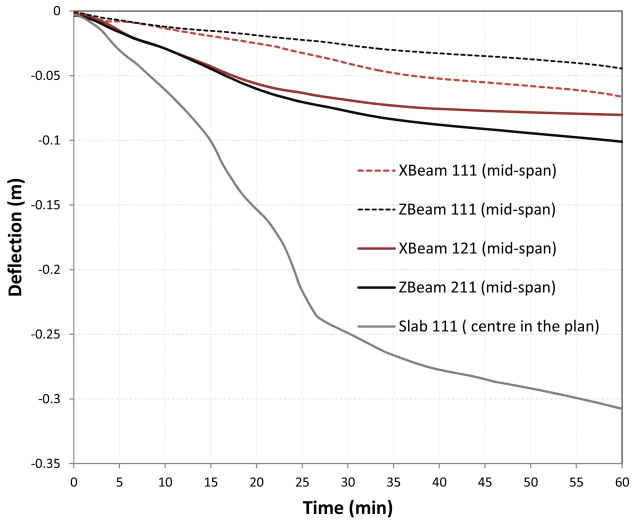

Figure 7.10: Beam and slab deflections for the one hour Standard Fire exposure

7.3.2 Idealised non-uniform fire action

Unlike the idealised uniform fires, spatial non-uniformity is seen in the localised fires (Pchelintsev et al., 1997; CEN, 2002a). In this case, the generic frame structure is assumed to be subjected to a fire surrounding the central column and remains localised while no partitions exist in the building. The EC1 localised fire model is used to describe the spatial distribution of incident heat fluxes with respect to the radial distance to the fire origin, which is virtually at the centre of the central column. Dimensionally reduced heat transfer analyses are used to approximate the thermal response of the structural members under the localised fire action. The fire lasts for 30mins without the consideration of fire growth, although it can be assumed as a t-squared fire model (Buchanan, 2001) as discussed in Chapter 4.

7.3.2.1 Thermal response to EC1 localised fire exposure

As previously mentioned, the fire source is hypothetically placed surrounding the central column (Column 221) at the ground floor, with a relatively high fire load (HRR = 5MW, D = 1m). During the fire, steel beams are assumed to be completely engulfed in the fire flames. Thus the boundary conditions for the heat transfer analyses should be defined without consider partial fire exposure similar to the secondary beam as shown in Figure 7.6(c). In addition to the convection and radiation defined for heat exchange between fire and member surfaces, incident heat fluxes are applied to represent the localised impact by the fire. The calculation methodology and corresponding parameters are adopted in consistency with the analyses completed in Chapter 3. Dimensional reduction is carried out during the heat transfer analysis and the rapid approximation approach is used to define the non-uniform thermal action. Heat transfer analyses are performed at different sections of the members, which produce different temperature profiles depending on the spatial location. In this example, 3-point quadratic interpolation for demonstration purpose is employed to approximate the horizontally non-uniform distribution of temperatures in beams and slabs, although a high level of accuracy is not strictly achieved. Moreover, for columns heated by the localised fire, the vertical non-uniformity of incident heat fluxes is ignored, which is taken as the maximum heat flux corresponding to the column top engulfed in fire.

Taking the XBeam 121 for instance, temperatures in different parts of the beam section are plotted in Figure 7.11 with respect to different locations, which include the section exactly above the fire origin and the mid-span section (note the temperature distributions are approximately uniform along the flanges and web).

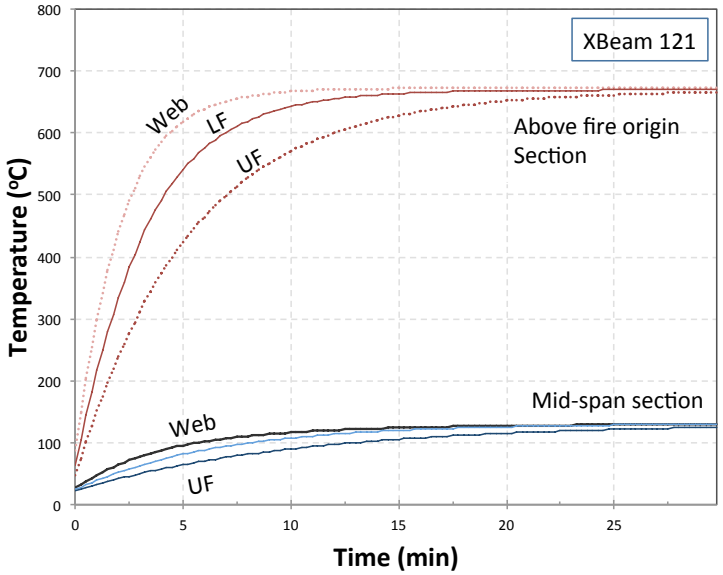

Figure 7.11: Temperature evolution of XBeam 121 above the fire origin and at the mid-span

A thinner web experiences rapid temperature increase compared to the other parts, which eventually reach a similar temperature as the heat input is uniformly applied (this is based on the consideration that the incident heat fluxes received by different parts of the beam section are treated as identical in relatively large localised fires (Lattimer, 2002)). The maximum temperature of the beam sections reaches 672.7^{o}C at the section above the fire source, whereas a lower level of thermal response is seen in the section at the mid-span of the beam which is horizontally 3m away from the fire origin. The maximum temperature of the beam at this location is 129.7^{o}C.

Similarly, a significantly non-uniform distribution of temperatures along the plane is seen in the slabs. The non-uniformity is of course induced by localised fire action, and can be approximately treated as correlated to the radial distance from the slab section to the fire origin. For concrete slabs subjected to localised fire

action, the in-plane distribution of temperatures at different layers of concrete slabs has been extensively discussed in Chapter 3, which incorporates the approximation scheme that was developed for localised fire exposure. For example, the temperature profile in the 6m × 6m slab 111 can be estimated using the polynomial interpolations over a number of selected 1D section analyses. The temperature evolution of different layers and locations in the slab are shown in Figure 7.12, from which it is observed that the maximum temperature always appears at the bottom surface of the slab above the fire origin. It rapidly increases after the fire is imposed and reaches 577.5^{o}C at the end of the 30 minutes exposure. By contrast, the mid-depth to top layers undergo experience much lower temperatures through out the fire. A simliar low-level of thermal response can be found at the centre of the slab in the plan for all layers thorough the thickness, not exceeding 50^{o}C.

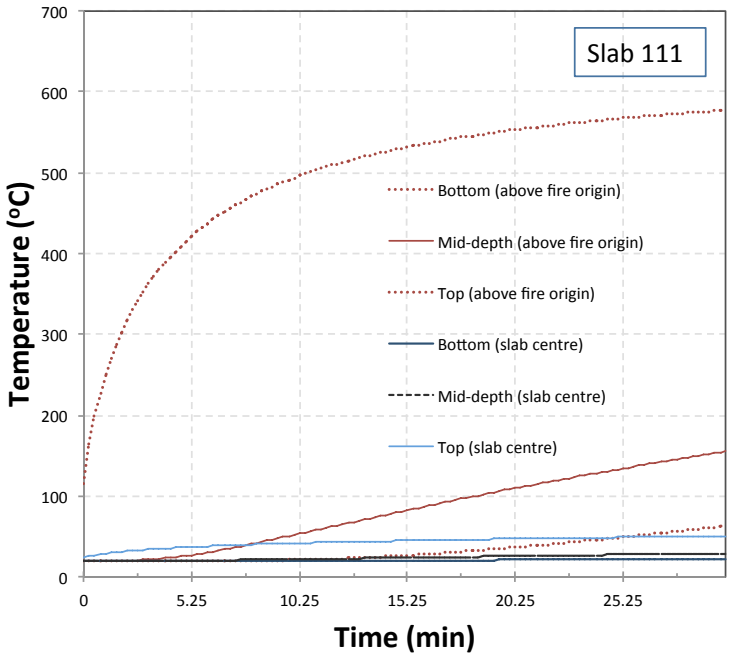

Figure 7.12: Temperature evolution of Slab 111 above the fire origin and at the mid-span for the localised fire scenario

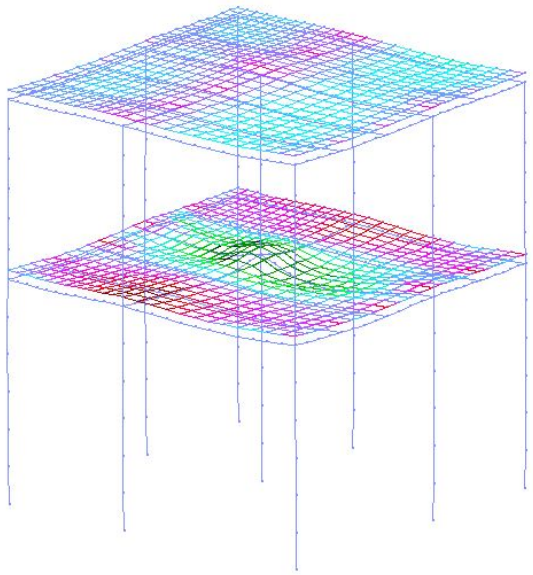

Figure 7.13: Deformed shape of the generic building subjected to a 30 minute EC1 Localised fire

7.3.2.2 Thermo-mechanical response to EC1 Localised Fire exposure

The deformed shape of the generic building subjected to 30 minutes Localised Fire exposure is shown in Figure 7.13, which has also been magnified by a factor of 10. Much smaller deflections are seen in the members, and the deflections are limited to the area surrounding the central column. Deflections at the slab centres and mid-spans of the beams are monitored and the results have been presented in Figure 7.14. The average magnitude of deflections in the Slab 111 is significantly lower compared to the Standard Fire case, whilst a slightly larger deflection can be seen in Slab 221 (9m×9m). Very slight increases are observed in the deflection histories of the beams connected to the central column, which may be caused by the thermal expansion of the central column as it is gradually heated to 90^oC. Through the studies conducted in Chapter 4, it is

understood that the central slab deflection is difficult to develop in the event of a corner fire. The largest deflection is found in the ZBeam 211, which is connected to the two large span compartments and as a primary beam bears the load transferred from the slab and secondary beams. A maximum deflection of 0.035m is observed at 20 minutes of fire exposure. Meanwhile, no significant deflections are developed in the other beams. However, the locally heated beams and slabs may redistribute the load to the columns. The variation of axial force in each column at ground floor are plotted in Figure 7.15. It is found that the axial force in central column keeps increasing because of its thermal elongation. Meanwhile the axial forces in adjacent columns (Column 121, 211, 231, 321) decrease as the softening of secondary beams around the central column decreases the load carried by the middle primary beams (XBeam 121,XBeam 221, ZBeam 211, ZBeam 221). Meanwhile, the axial forces in corner columns (Column 111, 131,311,331) all increase as some of the load is redistributed to them.

7.4 The effect of partially damaged fire protection

This section is concerned with fire protection using SFRM coatings to protect the steel columns. As a widely used passive fire resistive material, the coating is expected to remain effective for many years even though its actual condition is unknown, given that is is usually hidden behind architectural decoration and finishes because of its aesthetically undesirable appearance. During its lifetime, a building structure may be exposed to significant deformation from several loadings, such as high winds or seismic action. If there are minimal external

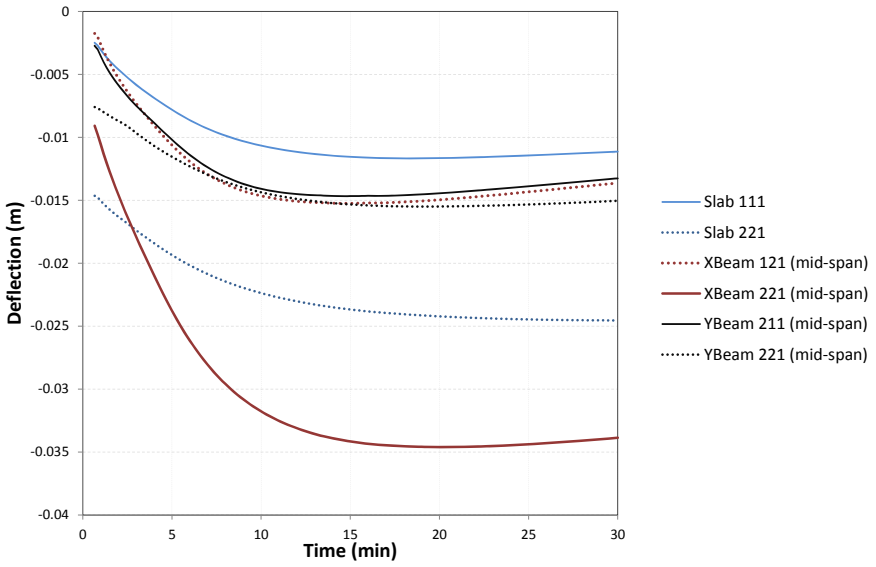

Figure 7.14: Beam and slab deflections subjected to a 30 minute EC1 Localised fire

signs of damage, as is possible in a well-designed structure, it would normally be assumed that the fireproof coating is also in good condition. Furthermore, an invasive and comprehensive inspection in a functioning building would be inconvenient and expensive. However, cementitious fireproof coating has very low strength and ductility, and is therefore prone to damage (Chen et al., 2010; Leo Braxtan and Pessiki, 2011), potentially leading to significant reduction in fire resistance of the protected member (Keller and Pessiki, 2012; Wang, 1998). To determine the actual level of passive fire protection in a building in the aftermath of a high magnitude of loading (or after a relatively long period of moderate magnitudes of repeated non-monotonic loading), it is very important to understand the performance and damage mechanisms of SFRM coatings and to develop methodologies to determine the in situ condition of cementitious coatings

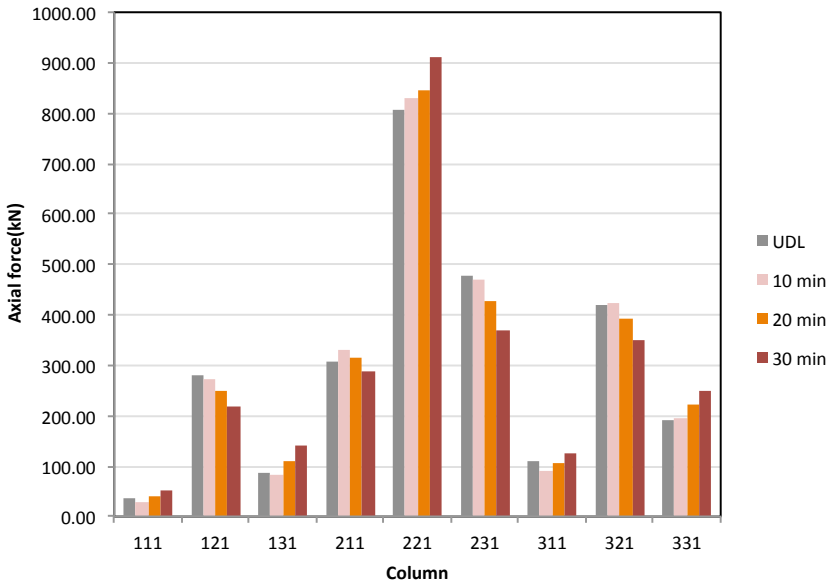

Figure 7.15: Axial forces in the columns when subjected to a 30 minute EC1 Localised fire

under such loadings. Such quantitative studies could be used to estimate the damage to the SFRM coatings as a result of structural deformation from static or dynamic loading (such as earthquake excitation). In this section, the loading induced damage to the fire protection is not calculated directly in accordance with the actual deformation of the structure. For demonstrating the capability of the *SIFBuilder* tool artificial removal of coatings of different lengths along the column members is assumed. A sequential quantitative computation of damaged fire protections in the context of multi-hazard scenarios and based upon this author's studies of damage mechanisms (Chen and Jiang, 2015; Chen et al., 2015) would be carried out in the future, as this is out of the scope of this thesis. This section summarises the numerical studies on SFRM damages and modells the structural response after removal of partial fire protection using the generic building model by taking advantage of the developed *SIFBuilder* tool.

7.4.1 Damage mechanism of SFRM coatings

Comprehensive experimental studies (Chen et al., 2010; Chen and Jiang, 2015; Chen et al., 2015) were carried out in Tongji University to observe the damage pattern and to investigate the damage mechanisms in SFRM coatings. Small scale tests were performed mostly on steel plates for tension and bending tests and on steel mini-columns for compression tests (to prevent local buckling) that were partially insulated by SFRM coatings and subjected only to monotonic loadings. These test specimens are schematically shown in Figure 7.16. Following the test programme, a significant amount of modelling work was carried out by the author to understand the damage propagation in the coatings attached to the deformed steel members. The damage simulation for various type of loading cases was completed in ANSYS and features the implementation of Cohesive Zone Material(CZM) (de Borst et al., 2004a) model to describe the steel-SFRM interfacial behaviour. This finite element model has been extensively used by the author to model the SFRM damage evolution, which is found reliable for predicting damage patterns when compared against the experimental work.

Based on the experimental and numerical studies conducted with various dimensions of coatings and steel plates (Figure 7.16), the damage mechanisms of SFRM coatings on steel plates can be categorised as interfacial failure, tensile cracks, and shear fractures that are usually found on the compression side of the bending tests. A simulated damage propagation is depicted in Figure 7.17, which shows the locations of different crack types in the tension and compression sides of the reference bending test (Chen and Jiang, 2015). In the pure bending case, interfacial cracks at the tension side first appear at both ends of the SFRM-Steel interface when the curvature (at neutral axis) reaches 0.39×10^{-3}, which are followed by the first pair

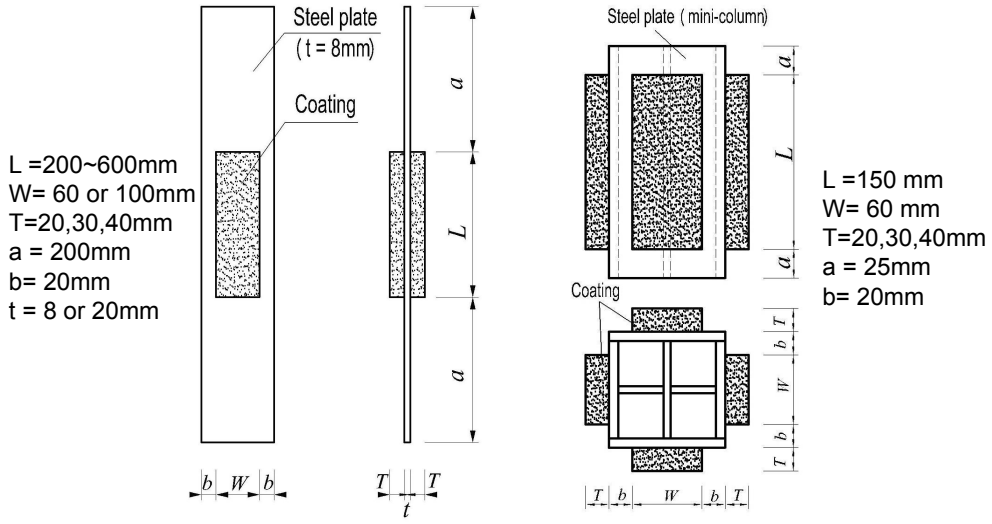

(a) Specimen for tension and bending tests (b) Minicolumn for compression test

Figure 7.16: Steel specimens tested for damage mechanisms under monotonic loadings (Chen and Jiang, 2015; Chen et al., 2015)

of transverse cracks at the curvature of 0.42×10^{-3}. The second pair of transverse cracks occurs when the plate is loaded to reach the curvature of 0.45×10^{-3}. As one crack develops through the thickness of the SFRM coatings, tensile stresses are released in the vicinity of the crack, which leads to the accumulation of stresses in the remaining continuous coatings and could eventually develop to a series of transverse cracks and interfacial cracks. The combination of transverse cracks and interfacial cracks is harmful to the integrity of SFRM protections and could lead to severe reduction of structural fire performance. Meanwhile, at the compression side of the bending specimen, no transverse cracks can be found. Interfacial cracks initiate as the curvature reaches 1.063×10^{-3} and then propagate towards the centre. The sagging deformation would later cause shear fractures in the coatings as pointed out in Figure 7.17(b). For thicker coatings or strengthened coatings, the damage at the compression side may be dominated by the interfacial cracks as

the shear fractures can not occur. This is to some extent even more dangerous, since the complete divison of coating bulk peels off and leaves a bare surface of steel plate.

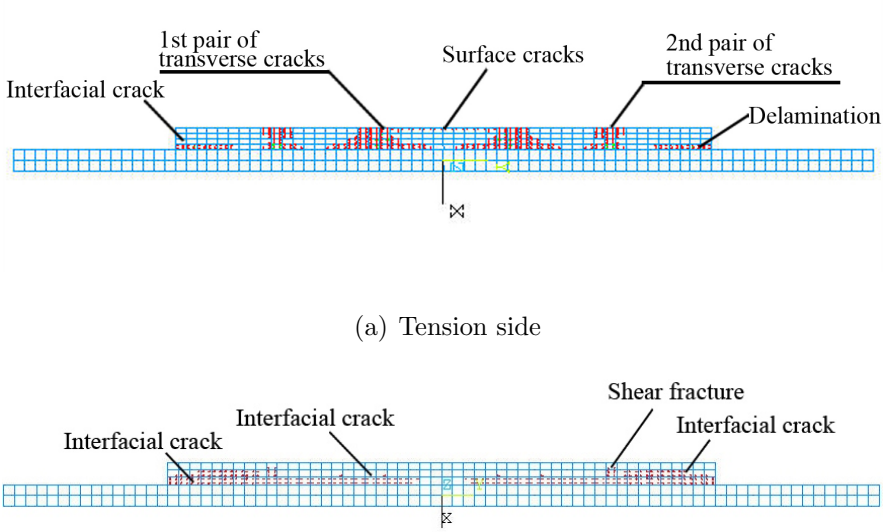

(a) Tension side

(b) Compression side

Figure 7.17: Damage mechanism under monotonic loadings (Chen and Jiang, 2015; Chen et al., 2015)

When the steel plates are loaded with monotonic axial loadings such as tension, a similar cracking mechanism is identified. As the axial strain of the steel plate reaches 0.89×10^{-3}, interfacial cracks are observed in the 200mm long coatings. The first pair of transverse cracks appears at the axial strain of 1.19×10^{-3}, later the second pair occurs at $1.55\times10^{(}-3)$. When steel plates are subjected to axial compression, the incompatibly developed axial deformation(because of the difference in moduli of the coating and substrate) leads to interfacial cracking, which is the only damage pattern that can be found in the compression tests. The bonding contact between SFRM coating and steel plate is gradually destroyed as the compressive load is increased. When the axial strain reaches -2.30$\times10^{-3}$,

approximately 60% of the interfacial contact becomes debonded. The SFRM coatings eventually drops off from the steel plate if the compressive load is sufficiently high (axial strain $\varepsilon = 3.62 \times 10^{-3}$).

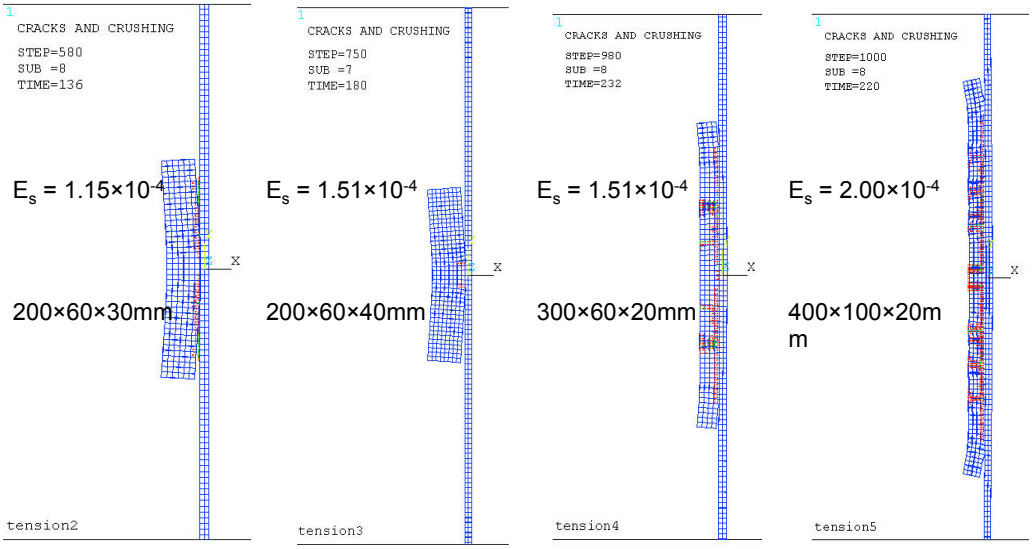

Figure 7.18: Damage mechanism of SFRM coatings of various dimensions

The monotonic loading tests, along with the previous work that it builds on, provides a basis for developing an assessment method to determine the condition of SFRM coatings in real structures under a variety of loading conditions. However, the aim of this research has so far been to understand and quantify the nature of the failures under relatively simple monotonic and quasi-static loading leading to simple stress states (axial compression, axial tension and flexural). The fundamental damage mechanisms have bee understood and one of the key findings is that the SFRM coating may be fragmented into different parts when the steel members experiences large deformations. As Figure 7.18 shows, different sets of transverse cracks sequentially develop in the coatings, which is accompanied by the interfacial cracks as a result of transferring shear stress. When the fully developed transverse cracks meet with interfacial cracks,

the associated bulk of coating is prone to peel off. This is even more evident in the case of flexture deformation, interfacial cracks propagate and meet with the subsequently developing transverse cracks (tension side) or shear fractures (compression side) which lead to partial loss of SFRM coatings near the ends. As these small scale tests may not represent realistic deformation conditions in a real building, further work needs to be done to establish how the basic failure mechanisms in cementitious coatings identified so far manifest themselves when the coatings are subjected to cyclic and dynamic loading with possible torsional components and correspondingly complex stress states.

7.4.2 Column in fire with partial damage to fire protection

Partial damage to SFRM coatings is artificially assigned in the work presented in this section, as it is expected that analyses in the future will evaluate the damage based on the degree of structural deformation or impact damage, which may be caused by extreme loadings such as earthquake or explosion. Using the generic building model, a part of the fire protection is removed from the central column 221 as shown in Figure 7.19, where h is adopted as 0.5m in this section. Thermal response in the unprotected part of the column is obviously higher than the response in the protected part. Therefore a linear transition between the hot section and cool section is applied to approximate the temperature decay as observed in Chapter 3, where the results of heat transfer analyses suggest that a 0.5m transition region is appropriate (a linear decay is hereby adopted for convenience, although the shape of transition maybe similar to a cubic curve as found in the previous studies). The generic frame, now the partially-damaged fireproofing on the central column is subjected to two previously examined fire

scenarios: the confined one hour Standard Fire and the open-plan EC1 Localised Fire. Considering that the central Column 221 is not heavily loaded (the load ratio is around 21%), an extra squash load of 700 kN is also imposed at the Joint 222 (top of the central columns) to examine the column behaviour under a higher stress level. The thermal and structural analyses are also performed within OpenSees using *SIFBuilder* and all the developed facilites.

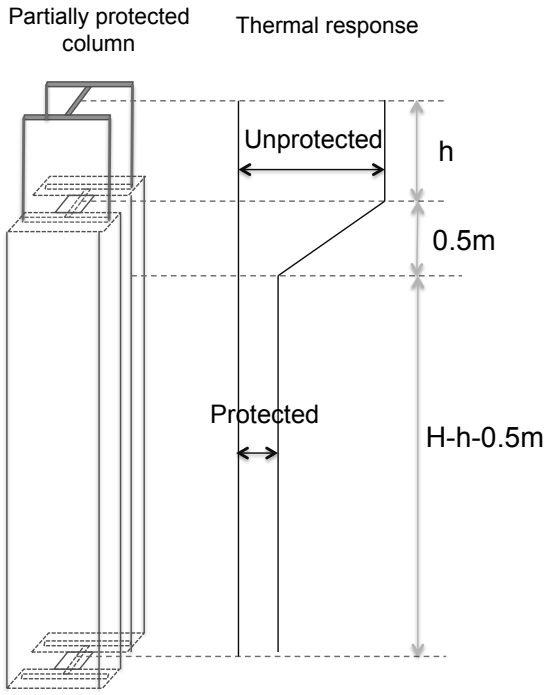

Figure 7.19: Partially protected Column 221

Thermal response of the column sections can be obtained using the above mentioned the scheme (Figure 7.19). For the upper part of the column without fire protection, temperatures increase rapidly in both fire scenarios. As illustrated in Figure 7.20, thermal response represented by flange (C-1 for Standard Fire exposure) temperature quickly reaches 600^oC within 12 minutes for the localised fire. The temperature goes up to 828^oC for the Standard Fire scenario. For the unprotected section, the temperatures are much lower. The maximum

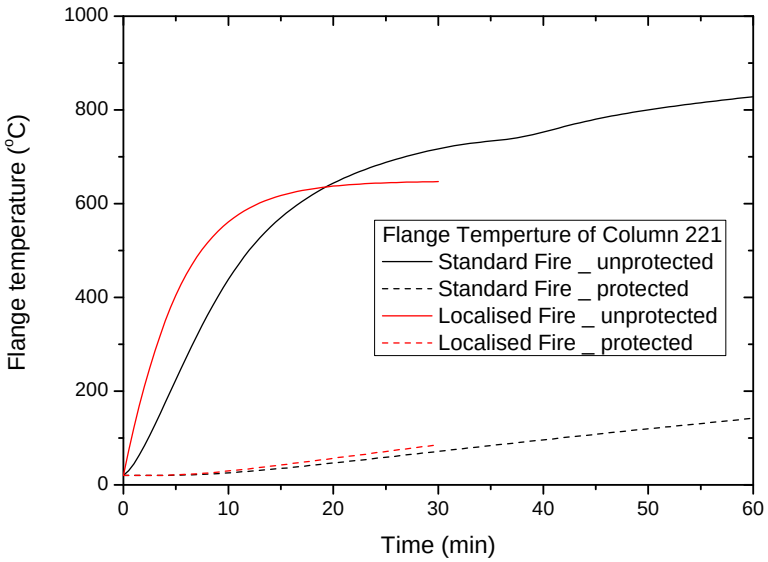

Figure 7.20: Thermal response of the column sections with partially damaged fire protection

temperature in the protected web could only reach 85^oC after 30 minutes of localised fire exposure, whereas a maximum of 142^oC can be found in the protected column section when subjected to Standard Fire exposure (even lower temperatures could exist in the flanges as the column is not fully exposed to the fire).

The structural deflections are essentially similar to the cases considering no fire protection damage, regardless of the different fire scenario and column loading ratio. The mid-span deflections of XBeam 121 with respect to different loading cases are plotted in Figure 7.21. Deflections caused by the Standard Fire exposure on average larger than the deflections observed in the Localised Fire case. Moreover, a slightly larger deflection (6mm) is seen in the case of no fire protection damage, which is likely to have been caused by the column expansion because the central column experiences much higher temperatures compared to the case with no damage to fire protection. This difference is not seen in the Standard Fire case

because of partial fire exposure which leads to a large part of the column section remaining relatively cool. An additional effect is the non-uniform heating that could cause thermal bowing which may decrease the deflection level of adjacent members. By increasing the load ratio in the central column, it is seen that the deflection of the XBeam 111 correspondingly increases (Figure 7.21). Especially in the case of Localised Fire exposure, the deflection of the XBeam 111 for high column load ratio exceeds the deflections at normal (low) load ratio. This suggests that greater column softening occurs due to the full exposure to fire and thus the connected members also experience greater downward displacement.

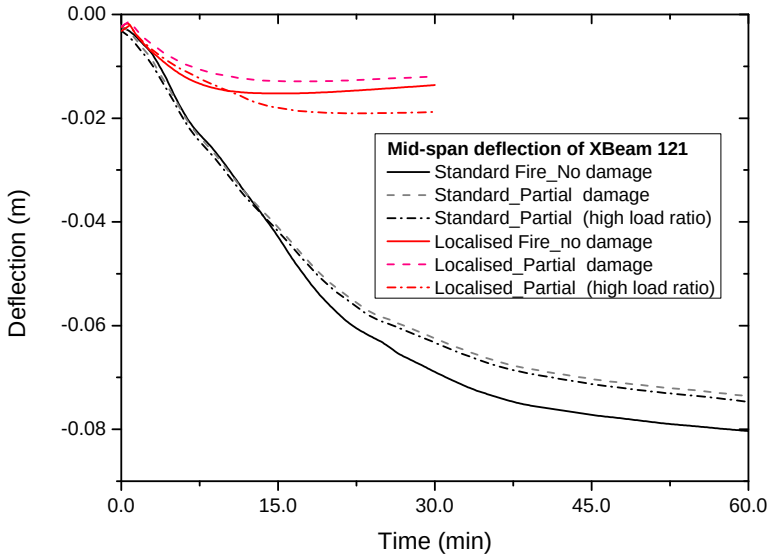

Figure 7.21: Mid-span deflections of XBeam 121 for different loading cases involving partially damaged fire protection

The axial forces in the central column captured from the top element have been presented in Figure 7.22. When the column with the lower load ratio is subjected to the Standard Fire exposure, the axial force begins with 808kN and nearly remains at the same level during the fire. When exposed to Localised Fire, it also reaches a similar value after 15 minutes. A short and rapid increase

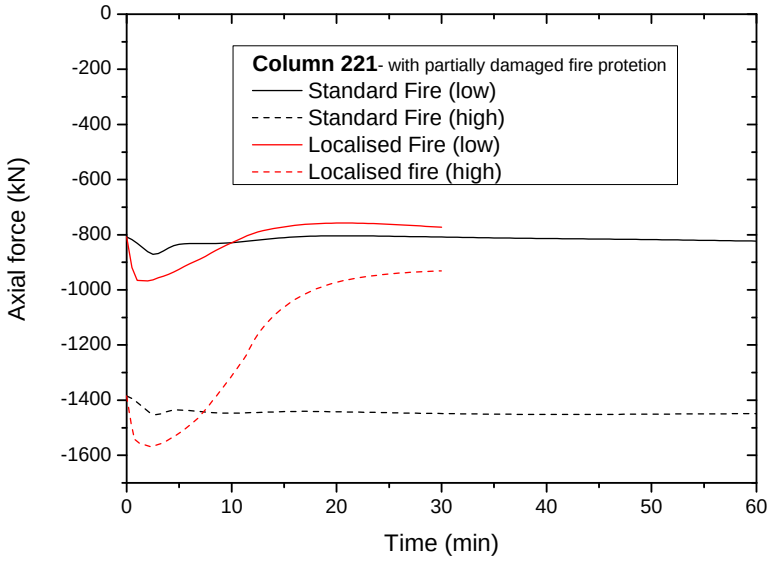

Figure 7.22: Axial forces in the upper part of Column 221 for different loading cases involving partially damaged fire protection

is seen in both fire scenarios which indicates the developed axial force due to the restrained thermal expansion. This is followed by the material softening due to the elevated temperature which releases the additional force caused by expansion. When the central column is heavily loaded (the load carrying capacity is approximately 2560kN), a similar response is seen in the case of Standard Fire exposure. However, a rapid decay can be observed in the central column exposed to localised fire, which indicates that plasticity rapidly develops in the column sections not protected against fire action. Notice that for the fibre on the unexposed side of the column section without fire protection, the maximum temperature could reaches only to 379.2^oC at the end of one hour Standard Fire exposure. However, for the EC1 Localised Fire, the maximum temperature of the fibre at the same location is 631.7^oC. Therefore partial loss of fire protection, whether resulting from the long term deterioration or because of some extreme event, can potentially be a major source of concern for the fire safety of buildings,

especially for fire scenarios where the partial exposure cannot be relied upon. Locally developed high temperatures may lead to the material failure or local buckling of the columns, and may cause severe damage to the structure, especially if progressive collapse is triggered.

7.5 Conclusion

Based a generic framed building model, analyses using *SIFBuilder* are performed to investigate the global behaviour of a frame structure in two fires. The building is separately subjected to a confined compartment fire based on the Standard Fire curve and a localised fire defined as an EC1 Localised Fire with the fire origin placed at bottom of the central column assuming an open plan building. Partial damage to fire protection at the central column is also considered.

- The usage of *SIFBuilder* is demonstrated by modelling a generic building under two different fire scenarios.

- Large deflections are observed from the slab directly exposed to Standard Fire, which affects the neighbouring slabs with small deflections developed. Non-uniform temperature distribution can be found in the beams and columns which are partially exposed to the fire confined within the compartment. Structural deformation caused by localised fire is not significant, which only causes deflections in the vicinity of the central column.

- Damage mechanisms of SFRM coatings on steel plates are identified as a combination of interfacial cracks, transverse cracks, and shear fractures.

Large surface strains or bending curvature could lead to the peeling off of SFRM coatings.

- After artificially removing a 500mm length of fire protection, the central column experiences a significantly higher temperatures in the upper sections. The localised heating due to the partial loss of fire protection does not influence the structural deformation significantly, but it could potentially lead to column failure when the loading ratio is relatively high.

Chapter 8

Conclusions and future work

8.1 Conclusions

8.1.1 Introduction

The aim of this thesis project has been to develop an integrated computational tool for modelling 'structures in fire', with particular emphasis on the thermal and structural behaviours under localised fire action. The recent development in modelling structural behaviours in fires has been reviewed. A strategy of using dimensionally reduced heat transfer analyses to approximate the localised thermal response has been established. This is followed by a quantitative investigation of the temperature differences between dimensionally reduced and full 3D heat transfer results from the analyses carried out for idealised non-uniform fires. Thermo-mechanical modelling of structural response using beam-column elements

and shell elements has been further developed in OpenSees to enable the consideration of non-uniform heating. The recent software development in OpenSees for modelling structures subjected to localised fire exposure has been described, along with the original development of *SIFBuilder* as a computational tool integrating all the developments so far for Structural fire modelling in OpenSees. The usage of *SIFBuilder* was demonstrated with a few analyses specially designed to simulate the global behaviour of framed structures subjected to different types of fire action including partial damage to passive fire protection. This chapter summarises the work presented in this thesis and provides recommendations for further work desirable for OpenSees development.

8.1.2 Summary and conclusions

In this thesis, a set of comprehensive analyses have been carried out to determine the feasibility of dimensional reduction in heat transfer analysis for structural members subjected to localised fire action, which is accompanied with a rapid estimation scheme for thermal response to localised fire action. Beam-column elements and slab element have been modified or developed to account for the non-uniform temperature distributions in beams and slabs subjected to localised fires. An integrated computational tool is developed to model framed structures in fire, which incorporates the previously completed developments for heat transfer and thermo-mechanical analyses into an automated environment. Simple input in Tcl is requested to initiate an analysis using *SIFBuilder* within OpenSees, which bridges the fields of fire modelling and structural engineering, and should help facilitate future research on new materials and elements for modelling structures in fire, in addition to enabling the simulation of structural response under a range

of complex fire scenarios without a prohibitive level of analyst effort. Extensive numerical studies have been conducted to test the computational performance of newly developed beam-column and shell elements, and followed by example cases demonstrating the usage of the proposed integrate computational tool, which are based on a generic framed composite structure with partial damage to passive fire protection included. The key conclusions are listed as below:

- It is justifiable to use dimensional reduction in all practical heat transfer analyses for structural members under all practical cases of realistic fire exposures, whether spatially uniform, localised or travelling fires.

- For protected steel plates, dimensionally reduced heat transfer analyses are able to predict the real thermal response. Nevertheless, it is not appropriate to employ dimensional reduction when partial damage of fire protection occurs.

- The rapid estimation scheme is implemented for beams and slabs subjected to localised fire action which can further reduce the computational cost.

- Beam-column elements using force based and displacement based formulations are developed to model the beams and columns subjected to longitudinally non-uniform heating, which incorporates the implementation of dimensionally reduced heat transfer analyses and the rapid estimation approach.

- It is found that the structural deflection induced by localised heating is dominated by thermal expansion and material softening, especially for relatively low temperatures ($\leqslant 400^o$C). For localised high temperatures, the

accuracy of numerical prediction is controlled by the reduction of material strength.

- Fewer force based beam-column elements can produce the similar results for a beam subjected to localised fire compared to beam model with displacement based formulation. A higher UDL (50% of load carrying capacity) can lead to the beam collapse in 14 minutes of localised heating.

- Shell element has been proved to be robust through analyses of slabs at ambient temperature or subjected to localised heating, which are compared to the beam element prediction, ABAQUS simulations, and experimental tests, showing good agreement.

- Higher loading ratio and centre fire could cause relatively large deflections, but still much smaller than the deflection caused by Standard Fire exposure. Axial restraints to the slab can cause higher level of deflections compared to the slab with simply supported boundary conditions.

- A comprehensive development is carried out in OpenSees for implementing localised fire models and modelling beams and slabs subjected to localised heating, which involves different thermal actions, beam-column elements, and shell elements.

- A framework is set up to integrate the modules for fire modelling, heat transfer analysis, and thermo-mechanical analysis. The tool creates a building model and invokes heat transfer analyses for each of the structural members involved in a fire event, in which partial fire exposure may also be considered. Coupled finite element analyses can be performed using this OpenSees based integrated computational tool.

- Large deflections are observed from the slab directly exposed to Standard Fire, which affects the neighbouring slabs with small deflections developed. Structural deformation caused by localised fire is not significant, which only causes deflections in the vicinity of the central column.

- Damage mechanisms of SFRM coatings on steel plates are identified as a combination of interfacial cracks, transverse cracks, and shear fractures. Large surface strains or bending curvature could lead to the peeling off of SFRM coatings.

- The central column engulfed by localised fire experiences significantly higher temperatures in the upper sections after removal of passive fire protection. However, this does not influence the structural deformation significantly, but could potentially lead to column failure when the loading ratio is relatively high.

8.2 Future work

This thesis has been primarily concerned with the development of an integrated computational tool within the OpenSees framework, which can quickly estimate the thermal response of structures subjected to localised fire acton and efficiently simulate structural performance in different fires. The programming development for the integrated tool in OpenSees is still ongoing and is expected to be a bug-free tool in the future, which requires more validation work and code refinement. Meanwhile, investigation of the localised effects induced by fire action and partial loss of fire protection require further work, which could be: experimental tests to further understand the fire behaviour and the damage mechanisms of passive fire

protection in real buildings; numerical modelling to establish better mathematical descriptions of localised fire action; and to more accurately and comprehensively predict the damage to fire protection. The most desirable future improvements may be summarised as follows:

- Travelling fires could be brought into the fire model library in a more realistic way, which may require new approaches to approximate the thermal response induced by travelling fire. Localised burning may incorporate the smoke layer into the heat flux calculation, as the unconfined ceiling is not realistic. Fire modelling driven by CFD analyses would be the ultimate solution to the fire behaviour in realistic buildings.

- The middle-ware components for transferring heat transfer results to the structural model may be developed as databases, which provide a higher efficiency in storing and requesting data especially for large models such as 3D heat transfer analysis.

- Uniaxial materials for steel and concrete should be further examined with respects to the unloading period, and the cooling phase. A more realistic concrete material model for analysing concrete slabs using shell elements needs to be developed with better performance in convergence.

- Finite element solution to the behaviour of composite floor systems in fire should be improved. The concrete ribs and the corresponding heat transfer issues should be properly accounted for.

- It is necessary to develop a quantitative estimation of SFRM damage based on appropriate measures of structural deformation. The damage to fire

protection is expected to be automatically calculated if the structural response is known. Such measures can be implemented within the earthquake response simulations which is the key strength of OpenSees.

- Further development for *SIFBuilder* may be to improve its capability for modelling complex structures. Graphic User Interfaces (GUI) can allow for a more user-friendly tool to create the models and defined the analysis cases. GUI based preprocessor and postprocessor could bridge the gap between general users and professional developers.

References

ABAQUS, 2002. ABAQUS/CAE User's Manual. Hibbitt, Karlsson & Sorensen, Incorporated.

Alemdar, B. N., White, D. W., 2005. Displacement, Flexibility, and Mixed BeamColumn Finite Element Formulations for Distributed Plasticity Analysis. Journal of Structural Engineering 131 (December), 1811–1819.

Alos-Moya, J., Paya-Zaforteza, I., Garlock, M., Loma-Ossorio, E., Schiffner, D., Hospitaler, a., 2014. Analysis of a bridge failure due to fire using computational fluid dynamics and finite element models. Engineering Structures 68, 96–110.

ANSYS, 2009. Release 12.0. ANSYS.

Bailey, C., 1998. Computer modelling of the corner compartment fire test on the large-scale Cardington test frame. Journal of Constructional Steel Research 48 (1), 27–45.

Bailey, C., oct 2004. Membrane action of slab/beam composite floor systems in fire. Engineering Structures 26 (12), 1691–1703.

Bailey, C., Burgess, I., Plank, R., 1996a. Analyses of the Effects of Cooling and Fire Spread on Steel-framed Buildings. Fire Safety Journal 26, 273–293.

Bailey, C., Moore, D. B., 2000a. The Structural behaviour of steel frames with composite floor slabs subject to fire: Part 1: Theory. The Structural Engineer 78 (7), 19–27.

Bailey, C., White, D., Moore, D., 2000. The tensile membrane action of unrestrained composite slabs simulated under fire conditions. Engineering Structures 22 (12), 1583–1595.

Bailey, C. G., 1995. Simulation of the structural behaviour of steel-framed buildings in fire. Ph.D. thesis, University of Sheffield.

Bailey, C. G., 1999. Buildings Subjected To Compartment Fires. The Structural Engineer 77 (8), 15–21.

Bailey, C. G., 2001. Membrane action of unrestrained lightly reinforced concrete slabs at large displacements. Engineering Structures 23 (5), 470–483.

Bailey, C. G., 2003. Efficient arrangement of reinforcement for membrane behaviour of composite floor slabs in fire conditions. Journal of Constructional Steel Research 59 (7), 931–949.

Bailey, C. G., Burgess, I. W., Plank, R. J., 1996b. Computer simulation of a full-scale structural fire test. Structural Engineer 74, 93–100.

Bailey, C. G., Moore, D. B., 2000b. The structural behaviour of steel frames with composite floorslabs subject to fire: Part 2: Design. Structural Engineer 78 (11), 28–33.

Bailey, C. G., Toh, W. S., 2007a. Behaviour of concrete floor slabs at ambient and elevated temperatures. Fire Safety Journal 42 (6-7), 425–436.

Bailey, C. G., Toh, W. S., 2007b. Small-scale concrete slab tests at ambient and elevated temperatures. Engineering Structures 29 (10), 2775–2791.

Bathe, K.-j., Bolourchi, S., 1980. A geometric and material nonlinear plate and shell element. Computers & Structures 11, 23–48.

Battini, J. M., 2002. Co-rotational beam elements in instability problems. Tech. rep., Royal Institute of Technology Department of Mechanics, Stockholm.

Bažant, Z. P., 2001. Prediction of concrete creep and shrinkage: Past, present and future. Nuclear Engineering and Design 203 (1), 27–38.

BRE, 2005. The integrity of compartmentation in buildings during fire. A review of part B of the building regulations, 174.

British Steel, 1998. The Behaviour of a Multi-Storey Steel Framed Building Subjected to Fire Attack.

British Steel, 1999. The Behavior Of Multi Storey Steel Framed Buildings In Fire.

BSI, 1990. BS 5950 Part 8: code of practice for fire resitant design. British Standards Institution.

Bucalem, M., Bathe, K., 1997. Finite element analysis of shell structures. Archives of Computational Methods in ....

Buchanan, A. H., 2001. Structural Design for Fire Safety. Wiley.

Cadorin, J.-F., Franssen, J.-M., sep 2003. A tool to design steel elements submitted to compartment firesOZone V2. Part 1: pre- and post-flashover compartment fire model. Fire Safety Journal 38 (5), 395–427.

Cadorin, J.-F., Pintea, D., Dotreppe, J.-C., Franssen, J.-M., sep 2003. A tool to design steel elements submitted to compartment firesOZone V2. Part 2: Methodology and application. Fire Safety Journal 38 (5), 429–451.

Cameron, N. J. K., Usmani, A., 2005a. New design method to determine the membrane capacity of laterally restrained composite floor slabs in fire Part 2 : Validation. Structural Engineer 83 (19), 28–33.

Cameron, N. J. K., Usmani, A. S., 2005b. New design method to determine the membrane capacity of laterally restrained composite floor slabs in fire Part 1 : Theory and method. Structural Engineer 83 (19), 28–33.

CEN, 1999. Development of design rules for steel structures subjected to natural fires in large compartments. No. 7210.

CEN, 2002a. BS EN 1991-1-2:2002: Eurocode1: Actions on Structures. General actions-actions on structures exposed to fire.

CEN, 2002b. Eurocode - Basis of structural design. En 3 (1), 89.

CEN, 2004. BS EN 1992-1-2:2004: Eurocode 2: Design of concrete structures. Generic rules-structural fire.

CEN, 2005. BS EN1993-1-2:2005: Eurocode 3: Desgin of Steel structures. General rules-structural fire design.

Ceresa, P., Petrini, L., Pinho, R., 2007. Flexure-Shear Fiber Beam-Column Elements for Modeling Frame Structures Under Seismic Loading State of the Art. Vol. 11.

Chen, S., Chu, J., Li, G., jul 2010. A study on damage mechanism of thick fire-proof coating for steel member subjected to monotonic loading. In: Structures in Fire: Proceedings of the Sixth International Conference. Vol. 206. p. 130.

Chen, S., Jiang, L., 2015. Damage mechanisms in cementitious coatings on steel members in bending. Proceedings of the ICE - Structures and Buildings 168 (Volume 168, Issue 5), 351–369(18).

Chen, S. W., Jiang, L. M., Li, G. Q., Usmani, A., 2015. Damage mechanisms in cementitious coatings on steel members under axial loading. Construction & Building Materials.

Coleman, J., Spacone, E., 2001. Localization Issues in Force-Based Frame Elements.

Couto, C., Vila Real, P., Lopes, N., Zhao, B., 2014. Effective width method to account for the local buckling of steel thin plates at elevated temperatures. Thin-Walled Structures 84, 134–149.

Crisfield, M., 1991. Non-linear finite element analysis of solids and structures, Volume 1. East, 360.

Dai, X. H., Wang, Y. C., Bailey, C. G., 2009. Effects of partial fire protection on temperature developments in steel joints protected by intumescent coating. Fire Safety Journal 44 (3), 376–386.

de Borst, R., Gutiérrez, M. a., Wells, G. N., Remmers, J. J. C., Askes, H., may 2004a. Cohesive-zone models, higher-order continuum theories and reliability methods for computational failure analysis. International Journal for Numerical Methods in Engineering 60 (1), 289–315.

de Borst, R., Remmers, J. J. C., Needleman, A., Abellan, M. A., 2004b. Discrete vs smeared crack models for concrete fracture: Bridging the gap. International Journal for Numerical and Analytical Methods in Geomechanics 28 (7-8), 583–607.

Drysdale, D., 2011a. Heat transfer. In: An introduction to fire dynamics, 3rd Edition. John Wiley&Sons Ltd., Edinburgh, Ch. 9, pp. 349–386.

Drysdale, D., 2011b. The pre-flashover compartment fire. In: An introduction to fire dynamics, 3rd Edition. John Wiley&Sons Ltd., Edinburgh, Ch. 9, pp. 349–386.

Dubois-Pe'lerin, Y., Zimmermann, T., 1993. Object-oriented finite element programming: III. An efficient implementation in C++. Computer Methods in Applied Mechanics and Engineering 108 (1-2), 165–183.

Dubois-Pèlerin, Y., Zimmermann, T., Bomme, P., 1992. Object-oriented finite element programming: II. A prototype program in smalltalk. Computer Methods in Applied Mechanics and Engineering 98 (3), 361–397.

Dwaikat, M., Kodur, V., 2011. Modeling Fracture and Delamination of Spray-Applied Fire-Resisting Materials under Static and Impact Loads. Journal of Engineering Mechanics 137 (12), 901–910.

Dwaikat, M., Kodur, V., Quiel, S., Garlock, M., jan 2011. Experimental behavior of steel beamcolumns subjected to fire-induced thermal gradients. Journal of Constructional Steel Research 67 (1), 30–38.

El-Zanaty, M. H., Murray, D. W., Bjorhovde, R., 1980. Inelastic behavior of multistory steel frames. Department of Civil Engineering, University of Alberta.

Elghazouli, A., Izzuddin, B., dec 2000. Response of idealised composite beamslab systems under fire conditions. Journal of Constructional Steel Research 56 (3), 199–224.

Ellobody, E., Bailey, C. G., 2011. Structural performance of a post-tensioned concrete floor during horizontally travelling fires. Engineering Structures 33 (6), 1908–1917.

Evans, D. D., 1995. Ceiling jet flows. SFPE handbook of fire protection engineering 2, 2–32.

Fang, C., Izzuddin, B., a.Y. Elghazouli, Nethercot, D., aug 2011. Robustness of steel-composite building structures subject to localised fire. Fire Safety Journal 46 (6), 348–363.

Feenstra, P. H., De Borst, R., 1996. A composite plasticity model for concrete. International Journal of Solids and Structures 33 (5), 707–730.

Felippa, C., 2000. A systematic approach to the element-independent corotational dynamics of finite elements. Tech. Rep. January.

Flint, G., 2005. Fire induced collapse of tall buildings.

Flint, G., Usmani, A., Lamont, S., Lane, B., Torero, J., 2007. Structural Response of Tall Buildings to Multiple Floor Fires (December), 1719–1732.

Foster, S. J., Bailey, C. G., Burgess, I. W., Plank, R. J., 2004. Experimental behaviour of concrete floor slabs at large displacements. Engineering Structures 26 (9), 1231–1247.

Franssen, J., 2005. SAFIR: A thermal/structural program for modelling structures under fire. Engineering Journal-American Institute of Steel ....

Franssen, J.-M., Pintea, D., Dotreppe, J.-C., sep 2007. Considering the effects of localised fires in the numerical analysis of a building structure. Fire Safety Journal 42 (6-7), 473–481.

Fuentes-Fernández, L., Vallecillo-Moreno, A., 2004. An Introduction to UML Profiles. European Journal for the Informatics Professional V, 6–13.

Garlock, M., Paya-Zaforteza, I., Kodur, V., Gu, L., 2012. Fire hazard in bridges: Review, assessment and repair strategies. Engineering Structures 35, 89–98.

Gibson, E. J., 1982. Working with the performance approach in building. Rotterdam: CIB Report Publication.

Gillie, M., a.S Usmani, Rotter, J., jun 2001a. A structural analysis of the first Cardington test. Journal of Constructional Steel Research 57 (6), 581–601.

Gillie, M., Usmani, A., Rotter, M., mar 2004. Bending and membrane action in concrete slabs. Fire and Materials 28 (24), 139–157.

Gillie, M., Usmani, A., Rotter, M., O'Connor, M., 2001b. Modelling of heated composite floor slabs with reference to the Cardington experiments. Fire Safety Journal 36 (8), 745–767.

Gillie, M., Usmani, A. S., Rotter, J. M., 2002. A structural analysis of the Cardington British steel corner test. Journal of Constructional Steel Research 58 (4), 427–442.

Han, L. H., Yang, Y. F., Yang, H., Huo, J. S., 2002. Residual strength of concrete-filled RHS columns after exposure to the ISO-834 standard fire. Thin-Walled Structures 40 (12), 991–1012.

Hasemi, Y., Yokobayashi, Y., Wakamatsu, T., Ptchelintsev, A. V., 1996. Modelling of heating mechanism and thermal response of structural components exposed to localised fires. In: Thirteenth meeting of the UJNR planel on fire research and safety.

Hasemi, Y., Yoshida, M., Yokobayashi, Y., Wakamatsu, T., 1997. Flame Heat Transfer And Concurrent Flame Spread In A Ceiling Fire. Fire Safety Science 5, 379–390.

Hillerborg, A., Modéer, M., Petersson, P.-E., nov 1976. Analysis of crack formation and crack growth in concrete by means of fracture mechanics and finite elements. Cement and Concrete Research 6 (6), 773–781.

Hinkley, P., jan 1986. Rates of production of hot gases in roof venting experiments. Fire Safety Journal 10 (1), 57–65.

Huang, H., Usmani, A. S., 1994. Finite element analysis for heat transfer. Springer-Verlag New York, NY.

Huang, Z., aug 2010. The behaviour of reinforced concrete slabs in fire. Fire Safety Journal 45 (5), 271–282.

Huang, Z., Burgess, I. W., J. Plank, R., 2000a. Effective stiffness modelling of composite concrete slabs in fire. Engineering Structures 22 (9), 1133–1144.

Huang, Z., Burgess, I. W., Plank, R. J., 1999. Nonlinear analysis of reinforced concrete slabs subjected to fire. ACI Structural Journal 96 (1).

Huang, Z., Burgess, I. W., Plank, R. J., mar 2000b. Three-Dimensional Analysis of Composite Steel-Framed Buildings in Fire. Journal of Structural Engineering 126 (3), 389–397.

Huang, Z., Burgess, I. W., Plank, R. J., 2003a. Modeling Membrane Action of Concrete Slabs in Composite Buildings in Fire. II: Validations. Journal of Structural Engineering 129 (8), 1103–1112.

Huang, Z., Burgess, I. W., Plank, R. J., 2003b. Modeling Membrane Action of Concrete Slabs in Composite Buildings in Fire.I:Theroretical development. Journal of Structural Engineering 129 (8), 1103–1112.

Huang, Z. F., Tan, K. H., 2003. Analytical Fire Resistance of Axially Restrained Steel Columns. Journal of Structural Engineering 129 (11), 1531–1537.

Huang, Z. F., Tan, K. H., 2007. Structural response of restrained steel columns at elevated temperatures. Part 2: FE simulation with focus on experimental secondary effects. Engineering Structures 29 (9), 2036–2047.

Ibrahimbegovic, A., 2009. Nonlinear Solid Mechanics : Theoretical Formulations and Finite Element Solution Methods.

Iding, R., Nizamuddin, Z., Bresler, B., 1977. FIRES-T3: A Computer Program for the FIre REsponse of Structures-Thermal Three-Dimensional Version. University of California, Fire Research Group.

IFSD, 1987. TEMPCALC User Manual. Institue of Fire Safety Design, Lund, Sweden.

Izzuddin, B., Song, L., a.S Elnashai, Dowling, P., 2000. An integrated adaptive environment for fire and explosion analysis of steel frames Part II:. Journal of Constructional Steel Research 53 (1), 87–111.

Izzuddin, B. A., 1990. Nonlinear dynamic analysis of framed structures. Ph.D. thesis, Imperial College London (University of London).

Izzuddin, B. A., Moore, D. B., 2002. Lessons from a full-scale fire test.

Jeffers, A. E., 2013. Heat transfer element for modeling the thermal response of non-uniformly heated plates. Finite Elements in Analysis and Design 63, 62–68.

Jeffers, A. E., Sotelino, E. D., 2009. Fiber heat transfer element for modelling the thermal reponse of structures in fire. Journal of Structural Engineering 135 (10), 1191–1200.

Jeffers, A. E., Sotelino, E. D., 2012. Analysis of Steel Structures in Fire with Force-Based Frame Elements 3 (4), 287–300.

Jiang, J., 2012a. PhD Thesis: Nonlinear thermomechanical analysis of structures using OpenSees. Ph.D. thesis, University of Edinburgh.

Jiang, J., Jiang, L. M., Kotsovinos, P., Zhang, J., Usmani, A., 2015. OpenSees Software Architecture for the Analysis of Structures in Fire. Journal of Computing in Civil Engineering 29 (1), 1–13.

Jiang, J., Khazaeinejad, P., Usmani, A., 2012. Nonlinear analysis of shell structures in fire using OpenSees. In: Proceedings of the 20th UK Conference of the Association for Computational Mechanics in Enginnering. No. March. pp. 127–130.

Jiang, J., Usmani, A., mar 2013. Modeling of steel frame structures in fire using OpenSees. Computers & Structures 118, 90–99.

Jiang, J., Usmani, A., Li, G.-q., 2014. Modelling of Steel-Concrete Composite Structures in Fire Using OpenSees. Advance in Structural Engineering 17 (2), 249–264.

Jiang, Y., 2012b. PhD Thesis: Development and application of a thermal analysis framework in OpenSees for structures in fire. Phd thesis, The Univeristy of Edinburgh.

Jiang, Y., Usmani, A., Welch, S., 2011. Development of heat transfer modelling capability in OpenSees for strctures in fire. In: Applications of Structural Fire Design. No. April.

Johansen, K. W., 1962. Yield-line theory. Cement and Concrete Association.

Jürgen Bathe, K., Dvorkin, E., Ho, L. W., 1983. Our discrete-Kirchhoff and isoparametric shell elements for nonlinear analysisAn assessment.

Keller, W. J., Pessiki, S., sep 2012. Effect of earthquake-induced damage to spray-applied fire-resistive insulation on the response of steel moment-frame beam-column connections during fire exposure. Journal of Fire Protection Engineering 22 (4), 271–299.

Kodur, V. K. R., Dwaikat, M. M. S., 2009. Response of steel beam-columns exposed to fire. Engineering Structures 31 (2), 369–379.

Kodur, V. K. R., Shakya, a. M., 2013. Effect of temperature on thermal properties of spray applied fire resistive materials. Fire Safety Journal 61, 314–323.

Kokkala, M., 1991. Experimental Study Of Heat Transfer To Ceiling From An Impinging Diffusion Flame. Fire Safety Science 3, 261–270.

Kotsovinos, P., Kotsovinos, P., Jiang, Y., Usmani, A., 2013. Effect of vertically travelling fires on the collapse of tall buildings. International Journal of High-Rise Buidings 2 (1), 49–62.

Kotsovinos, P., Usmani, A., 2013. The World Trade Center 9/11 Disaster and Progressive Collapse of Tall Buildings. Fire Technology 49 (3), 741–765.

Lamont, S., Usmani, A., Drysdale, D., nov 2001. Heat transfer analysis of the composite slab in the Cardington frame fire tests. Fire Safety Journal 36 (8), 815–839.

Lamont, S., Usmani, A. S., Gillie, M., 2004. Behaviour of a small composite steel frame structure in a "long-cool" and a "short-hot" fire. Fire Safety Journal 39 (5), 327–357.

Lange, D., Röben, C., Usmani, A., 2012. Tall building collapse mechanisms initiated by fire: Mechanisms and design methodology. Engineering Structures 36, 90–103.

Lattimer, B., 2002. Heat fluxes from fires to surfaces. In: SFPE Handbook of Fire Protection Engineering. pp. 269–294.

Lennon, T., 2003. Results and Observations from Full-Scale Fire Test at BRE Cardington. Building Research Establishment (215), 63.

Leo Braxtan, N., Pessiki, S., 2011. Bond performance of SFRM on steel plates subjected to tensile yielding. Journal of Fire Protection Engineering 21, 37–55.

Lie, T. T., Others, 1992. Structural fire protection. Vol. 78.

Liew, J., Tang, L., Holmaas, T., Choo, Y., aug 1998. Advanced analysis for the assessment of steel frames in fire. Journal of Constructional Steel Research 47 (1-2), 19–45.

Lim, L., Buchanan, A., Moss, P., Franssen, J.-M., 2004. Numerical modelling of

two-way reinforced concrete slabs in fire. Engineering Structures 26 (8), 1081–1091.

Lim, L., Wade, C., 2002. Experimental Fire Tests of Two-Way Concrete Slabs Experimental.

Liu, T., jan 1996. Finite element modelling of behaviours of steel beams and connections in fire. Journal of Constructional Steel Research 36 (3), 181–199.

Liu, T. C. H., Davies, J. M., 2001. Performance of steel beams at elevated temperatures under the effect of axial restraints. Steel and Composite Structures 1 (4), 427–440.

Liu, T. C. H., Fahad, M. K., Davies, J. M., 2002. Experimental investigation of behaviour of axially restrained steel beams in fire. Journal of Constructional Steel Research 58 (9), 1211–1230.

Loret, B., Prevost, J. H., 1986. Accurate numerical solutions for drucker-prager elastic-plastic models. Computer Methods in Applied Mechanics and Engineering 54 (3), 259–277.

Lu, X., 2013. Collapse simulation ofreinforced concrete high-rise buidling induced by extreme eathquakes. Earthquake Engineering & Structural Dynamics 42, 705–723.

Lu, X., Xie, L., Guan, H., Huang, Y., Lu, X., 2015. A shear wall element for nonlinear seismic analysis of super-tall buildings using OpenSees. Finite Elements in Analysis and Design 98, 14–25.

Lubliner, J., Oliver, J., Oller, S., Oñate, E., 1989. A plastic-damage model for concrete. International Journal of Solids and Structures 25 (3), 299–326.

Mason, J., 1999. Heat Transfer Programs for the Design of Structures Exposed to Fire.

McGregor, M. G. G., G, J., 1994. Tests of Reinforced Concrete Plates Under Combined Inplane and Lateral Loads. Structural Journal 91 (1).

McKenna, F., Scott, M. H., Fenves, G. L., 2010. Nonlinear Finite-Element Analysis Software Architecture Using Object Composition. Journal of Computing in Civil Engineering 24 (1), 95–107.

McKenna, F. T., 1997. Object-oriented finite element programming: frameworks for analysis, algorithms and parallel computing. Ph.D. thesis, University of California, Berkeley.

Mindeguia, J. C., Pimienta, P., Noumowé, A., Kanema, M., 2010. Temperature, pore pressure and mass variation of concrete subjected to high temperature - Experimental and numerical discussion on spalling risk. Cement and Concrete Research 40 (3), 477–487.

Moes, N., Dolbow, J., Belytschko, T., 1999. A finite element method for crack growth without remeshing 150 (February), 131–150.

Monti, G., Spacone, E., 2000. Reinforced Concrete Fiber Beam Element with Bond-Slip.

Nadjai, A., Vassart, O., Ali, F., Talamona, D., Allam, A., Hawes, M., 2007. Performance of cellular composite floor beams at elevated temperatures. Fire Safety Journal 42 (6-7), 489–497.

Najjar, S., Burgess, I., jan 1996. A nonlinear analysis for three-dimensional steel frames in fire conditions. Engineering Structures 18 (1), 77–89.

Neuenhofer, A., Filippou, F. C., 1997. Evaluation of Nonlinear Frame Finite-Element Models. Journal of Structural Engineering 123, 958–966.

Neuenhofer, A., Filippou, F. C., 1998. Geometrically Nonlinear Flexibility-Based Frame Finite Element. Journal of Structural Engineering 124 (x), 704–711.

Newman, G. M., 1991. Structural fire engineering investigation of Broadgate phase 8 fire. Steel Construction Institute, Ascot.

Ousterhout, J. K., Jones, K., 2009. Tcl and the Tk toolkit. Pearson Education.

Pchelintsev, A., Hasemi, Y., Wakamatsu, T., Yokobayashi, Y., 1997. Experimental and numerical study on the behaviout of a steel beam under ceiling exposed to a localized fire. In: Fire Safety Science 5. pp. 1153–1164.

Pilato, M., 2004. Version Control With Subversion. O'Reilly & Associates, Inc., Sebastopol, CA, USA.

Powell, G. H., Chen, P. F., 1986. 3D BeamColumn Element with Generalized Plastic Hinges. Journal of Engineering Mechanics 112 (7), 627–641.

Röben, C., Gillie, M., Torero, J., 2010. Structural behaviour during a vertically travelling fire. Journal of Constructional Steel Research 66 (2), 191–197.

Saab, H. A., 1990. Non-linear finite element analysis of steel frames in fire conditions. Ph.D. thesis.

Sanad, A., Lamont, S., Usmani, A., Rotter, J., 2000a. Structural behaviour in fire compartment under different heating regimes-Part 1 (slab thermal gradients). Fire Safety Journal 35, 99–116.

Sanad, A. M., Lamont, S., Usmani, A. S., Rotter, J. M., 2000b. Structural behaviour in fire compartment under different heating regimes- part 2 : (slab mean temperatures) 35, 117–130.

Sanad, A. M., Rotter, J. M., Usmani, A. S., O'Connor, M. A., 2000c. Composite beams in large buildings under fire-numerical modelling and structural behaviour. Fire Safety Journal 35, 165–188.

Scott, M. H., Fenves, G. L., 2006. Plastic Hinge Integration Methods for Force-Based BeamColumn Elements. Journal of Structural Engineering 132 (2), 244–252.

Scott, M. H., Fenves, G. L., McKenna, F., Filippou, F. C., 2008a. Software Patterns for Nonlinear Beam-Column Models. Journal of Structural Engineering 134 (April), 562–571.

Scott, M. H., Filippou, F. C., 2007. Response Gradients for Nonlinear Beam-Column Elements under Large Displacements (February), 155–165.

Scott, M. H., Franchin, P., Fenves, G. L., Filippou, F. C., 2004. Response Sensitivity for Nonlinear BeamColumn Elements. Journal of Structural Engineering 130 (September), 1281–1288.

Scott, M. H., Kidarsa, A., Higgins, C., 2008b. Development of Bridge Rating Applications Using OpenSees and Tcl. Journal of Computing in Civil Engineering 22 (August), 264–271.

Shepherd, P. G., Burgess, I. W., 2011. On the buckling of axially restrained steel columns in fire. Engineering Structures 33 (10), 2832–2838.

Sivaraj, S.-S., 2005. Collapse of the World Trade Center Towers. Final Report.

Sjöström, J., Byström, A., Lange, D., Wickström, U., 2012. Thermal exposure to a steel column from localized fires. Tech. rep.

Song, L., Izzuddin, B., Elnashai, A., Dowling, P., jan 2000. An integrated adaptive environment for fire and explosion analysis of steel frames Part I:. Journal of Constructional Steel Research 53 (1), 63–85.

Spacone, E., 1996. Fiber Beam-Column Model for Non-linear analysis of R/C Frames.Part II: Application. Earthquake Engineering & Structural Dynamics 25 (January), 727–742.

Spacone, E., Ciampi, V., Filippout, F. C., 1996a. Mixed Formulation Of Nonlinear Finite Element. Computers & Structures 58 (I), 71–83.

Spacone, E., Filippou, F. C., Taucer, F. F., jul 1996b. Fibre Beam-Column Model for Non-Linear Analysis of R/C Frames: Part I. Formulation. Earthquake Engineering & Structural Dynamics 25 (7), 711–725.

Stern-Gottfried, J., 2011. Travelling Fires for Structural Design. Philosophy.

Stern-Gottfried, J., Law, A., Rein, G., Gillie, M., Torero, J. L., 2010a. A Performance Based Methodology Using Travelling Fires for Structural Analysis. In: 8th International Conference on Performance-Based Codes and Fire Safety Design Methods. Lund, Sweden.

Stern-Gottfried, J., Rein, G., 2012a. Travelling fires for structural design-Part II: Design methodology. Fire Safety Journal 54, 96–112.

Stern-Gottfried, J., Rein, G., 2012b. Travelling fires for structural designPart I: Literature review. Fire Safety Journal 54, 74–85.

Stern-Gottfried, J., Rein, G., Bisby, L. a., Torero, J. L., 2010b. Experimental review of the homogeneous temperature assumption in post-flashover compartment fires. Fire Safety Journal 45 (4), 249–261.

Stroustrup, B., 2000. The C++ Programming Language, 3rd Edition. Addison-Wesley Longman Publishing Co., Inc., Boston, MA, USA.

Talamona, D., 2005. A Quadrangular Shell Finite Element for Concrete and Steel Structures Subjected to Fire.

Tan, K. H., Toh, W. S., Huang, Z. F., Phng, G. H., 2007. Structural responses of restrained steel columns at elevated temperatures. Part 1: Experiments. Engineering Structures 29 (8), 1641–1652.

Taucer, F. F., Spacone, E., Filippou, F. C., 1991. a Fiber Beam-Column Element for Seismic Response Analysis. Engineering (December 1991), 138.

Thomas, P. H., 1963. Investigations Into the Flow of Hot Gases in Roof Venting. Fire research technical paper. London : H.M.S.O.

TNO, 2011. Diana: Finite Element Analysis User's Manual-Release 9.4.4. TNO DIANA.

Toh, W. S., Tan, K. H., Fung, T. C., 2000. Compressive Resistance of Steel Columns in Fire: Rankine Approach. Journal of Structural Engineering 126 (3), 398–405.

Tondini, N., Vassart, O., Franssen, J.-m., 2012. Development of an Interface Between Cfd and Fe Software.

Usmani, A., 2000. PIT Project: Behaviour of steel framed structures under fire conditions MAIN REPORT (Cardington) (June).

Usmani, A., Cameron, N. J. K., 2004. Limit capacity of laterally restrained reinforced concrete floor slabs in fire. Cement and Concrete Composites 26 (2), 127–140.

Usmani, A., Röben, C., Al-Remal, A., 2009. A very simple method for assessing tall building safety in major fires. International Journal of Steel Structures (9), 17–28.

Usmani, A., Rotter, J. M., Lamont, S., Sanad, A., Gillie, M., 2001. Fundamental principles of structural behaviour under thermal effects. Fire Safety Journal 36 (8), 721–744.

Usmani, A., Zhang, J., Jiang, J., Jiang, Y., May, I., mar 2012. Using Opensees for Structures in Fire. Journal of Structural Fire Engineering 3 (1), 57–70.

Usmani, A. S., Chung, Y. C., Torero, J. L., 2003. How did the WTC towers collapse: A new theory. Fire Safety Journal 38 (6), 501–533.

Wakamatsu, T., Hasemi, Y., 1988. Heating Mechanism of Building Components Exposed to a Localized Fire -FDM Thermal Analysis of a Steel Beam under Ceiling-. In: AOFST 3. pp. 335–346.

Wakamatsu, T., Hesami, Y., Kagiya, K., Kamikawa, D., 2003. Heating Mechanism of Unprotected Steel Beam Installed Beneath Ceiling and Exposed to a Localized Fire : Verification using the real-scale experiment and effects of the smoke layer. In: Fire Safety Science–Proceedings of the Seventh International Symposium. International Association for Fire Safety Science, pp. 1099–1110.

Walker, J. D., Jr, C. E. A., Walker, J. D., Anderson, C. E., 2002. An analytic penetration model for a Drucker-Prager yield surface with cutoff 897 (1998).

Wang, J., Chen, J. K., Liao, S., 2008. An explicit solution of the large deformation of a cantilever beam under point load at the free tip. Journal of Computational and Applied Mathematics 212 (2), 320–330.

Wang, W. Y., Li, G. Q., 2009. Behavior of steel columns in a fire with partial damage to fire protection. Journal of Constructional Steel Research 65 (6), 1392–1400.

Wang, Y., 1997. Tensile Membrane Action And The Fire Resistance Of Steel Framed Buildings. Fire Safety Science 5, 1117–1128.

Wang, Y., 1998. Composite beams with partial fire protection. Fire Safety Journal 30 (4), 315–332.

Wang, Y., 2000. An analysis of the global structural behaviour of the Cardington steel-framed building during the two BRE fire tests. Engineering Structures 22 (5), 401–412.

Wang, Y., Moore, D., jul 1995. Steel frames in fire: analysis. Engineering Structures 17 (6), 462–472.

Wang, Y. C., 2003. Steel and Composite Structures: Behaviour and Design for Fire Safety. Taylor & Francis.

Wang, Y. C., Kodur, V. K. R., dec 2000. Research Toward Use of Unprotected Steel Structures. Journal of Structural Engineering 126 (12), 1442–1450.

Welch, S., Miles, S., Kumar, S., Lemaire, T., Chan, A., 2008. FIRESTRUC - Integrating advanced three-dimensional modelling methodologies for predicting thermo-mechanical behaviour of steel and composite structures subjected to natural fires. Fire Safety Science, 1315–1326.

Wickström, U., 1980. Tasef-2 - a computer program for temperature analysis of structures exposed to fire. Tech. Rep. 79, Lund Institute of Technology.

Wickström, U., 1985. Temperature analysis of heavily-insulated steel structures exposed to fire. Fire Safety Journal 9 (3), 281–285.

Wriggers, P., 2008. Nonlinear finite element methods. Springer.

Yazdani, S., Schreyer, H. L., 1990. Combined Plasticity and Damage Mechanics Model for Plain Concrete.

Yin, Y., Wang, Y., aug 2003. Numerical simulations of the effects of non-uniform temperature distributions on lateral torsional buckling resistance of steel I-beams. Journal of Constructional Steel Research 59 (8), 1009–1033.

Yin, Y., Wang, Y., feb 2005a. Analysis of catenary action in steel beams using a simplified hand calculation method, Part 2: validation for non-uniform temperature distribution. Journal of Constructional Steel Research 61 (2), 213–234.

Yin, Y. Z., Wang, Y. C., 2004. A numerical study of large deflection behaviour of restrained steel beams at elevated temperatures. Journal of Constructional Steel Research 60 (7), 1029–1047.

Yin, Y. Z., Wang, Y. C., 2005b. Analysis of catenary action in steel beams using a simplified hand calculation method, Part 1: Theory and validation for uniform temperature distribution. Journal of Constructional Steel Research 61 (2), 183–211.

You, H. Z., Faeth, G. M., 1979. Ceiling heat transfer during fire plume and fire impingement. Fire and Materials 3 (3), 140–147.

Yu, X., Huang, Z., 2008. An embedded FE model for modelling reinforced concrete slabs in fire. Engineering Structures 30 (11), 3228–3238.

Zhang, C., Li, G.-Q., Usmani, A., apr 2013. Simulating the behavior of restrained steel beams to flame impingement from localized-fires. Journal of Constructional Steel Research 83, 156–165.

Zhao, B., Desanghere, S., Darche, J., 2007. CFD and FEM coupling with computer programs FDS and ANSYS for fire resistence assement. In: INTERFLAM 11. pp. 1461–1466.

Zhao, B., Kruppa, J., 2002. Structural Behaviour of an Open Car Park Under Real Fire Scenarios. Second International Workshop "Structures in Fire" 280 (March), 337–350.

Zienkiewicz, O. C., Taylor, R. L., Zhu, J. Z., may 2005. The Finite Element Method: Its Basis and Fundamentals, Sixth Edition, 6th Edition. Butterworth-Heinemann.

Appendix A

Tcl scripts for heat transfer analysis

A.1 Available HTEntities

Table A.1: Commands for creating a heat transfer entity

Type	**HTEntity**	**Centroid**	**Dimension**
1D	Line	x_c	l
	Block	x_c, y_c	b, d
2D	Isection	x_c, y_c	b_f, h_b, t_w, t_f
	IsectionPro	x_c, y_c	b_f, h_b, t_w, t_f,$coat$
	Composite	x_c, y_c	b_f, h_b, t_w, t_f, b_s, h_s
	Brick	x_c, y_c	b,d ,
3D	Isection3D	x_c, y_c, z_c	b_f, h_b, t_w, t_f
	Composite3D	x_c, y_c, z_c	b_f, h_b, t_w, t_f

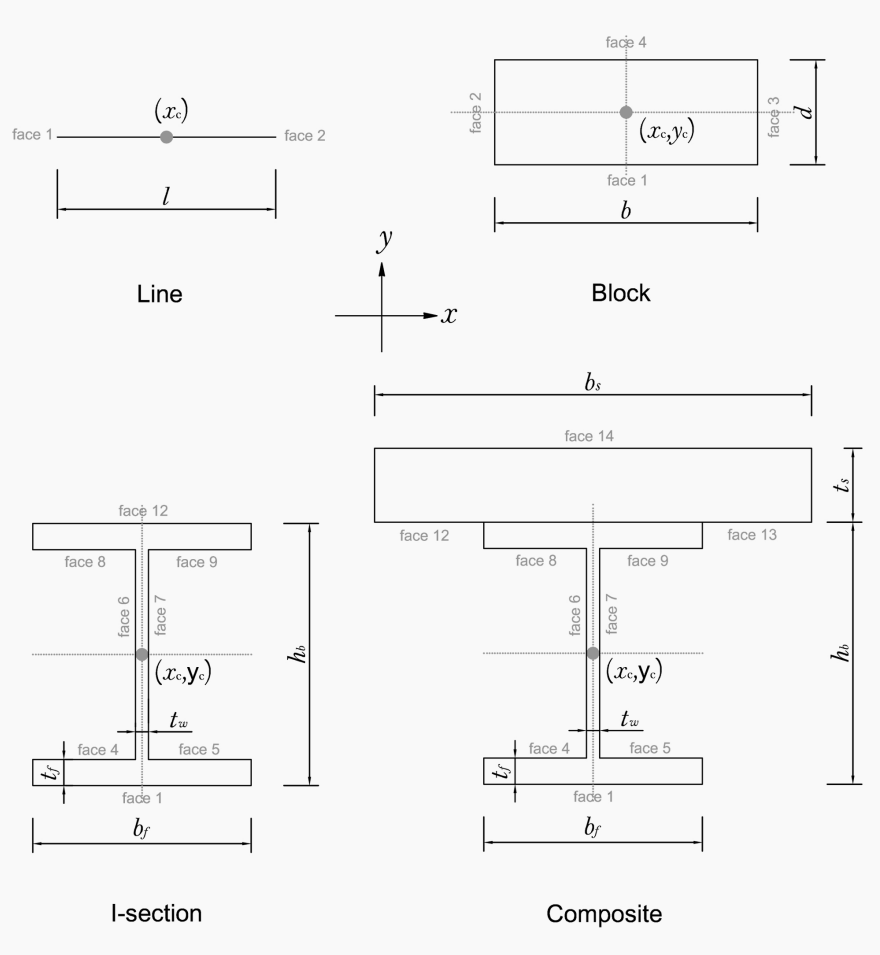

Figure A.1: Configuration of HTEntities

A.2 Tcl commands for defining fire models

```
FireModel standard $FireTag;
FireModel hydroCarbon $FireTag;
FireModel localised $FireTag -loc $locx $locy $locz -firePars $Q
    $D $square;
FireModel SFPElocalised $FireTag -loc $locx $locy $locz -firePars
     $Q $D $square;
FireModel Idealised $FireTag -loc $locx $locy $locz -firePars $d1
     $d2 $q1 q2isQuad;
```

A.3 Tcl Script for performing heat transfer analysis in OpenSees

../Appendix/HeatTransferofIsection.tcl

```
#Demostrating tcl commands for Heat Transfer module in OpenSees

HeatTransfer 2D;         #HeatTransfer activates the HTModule. 2D
   ,or 2d, or 3D or 3d indicate the model dimension.

#Defining HeatTransfer Materials
HTMaterial CarbonSteelEC3 1;
HTMaterial ConcreteEC2 2 0.015;
#HTMaterial GenericMaterial 2 350 1100 0.05

set d 0.3034; # depth
set bf 0.165; # flange width
set tf 0.0102;  # flange thickness
set tw 0.006; # web thickness
set coat 0.02;
set SlabW [expr 0.6+$bf];
set SlabT 0.1;

set halfD [expr $d/2];
#set halfB [expr $bf/2]

#HTEntity Block 1 0.2 0.2 0.4 0.4;
# Tag, $ x-coord of section centre, $ y-coord of section centre,
   $width of block, $ height of block
# surface definition of block: 1,2,3 and 4 is lower, left, right and
    upper surface respectively.
HTEntity Composite2D  2 0.0 0.0 $bf $d $tw $tf $SlabW $SlabT;
#HTEntity ProtectedIsection 2 0.0 0 $bf $d $tw $tf $coat ;

set elex [expr 0.6/20];
set eley [expr ($tf)/4];
set elewx [expr ($tw)/4];
set elewy [expr ($d-2*$tf-2*$coat)/20];
#set elewy [expr ($d-2*$tf)/40];
set eleCoat [expr $coat/5];
set eleSlabx [expr $SlabW/20];
set eleSlaby [expr $SlabT/16];

#HTMesh $MeshTag $EntityTag  $MaterialTag, -SecondMat
   $secondmaterialTag, -phaseChange, SecondMaterial,-origin
#HTMesh 1 1 1 -phaseChange 0 -MeshCtrls 0.02 0.02;   #-origin 0.02
#HTMesh 2 2 1 -SecondMat 2 -phaseChange 0 0 -MeshCtrls $elex $eley
   $elewx $elewy $eleCoat;
HTMesh 2 2 1 -SecondMat 2 -phaseChange 0 1 -MeshCtrls $elex $eley
   $elewx $elewy $eleSlabx $eleSlaby;

HTMeshAll;  #do the mesh
```

```
puts "Mesh"

SetInitialT 293.15;

# HTconstants tag, convection coefficient,ambient
    temp.,emissity,boltzman,absorptivity, irradiation
HTConstants 3 4.0 293.15 0.7 5.67e-8 0.7 418.738; # concrete
HTConstants 4 25.0 293.15 0.7 5.67e-8 0.7 418.738; # standard fire
    exposure

HTPattern AmbientBC 1 {
  #HeatFluxBC eleset 1 -faceTag 3 -type -ConvecAndRad -HTConstants
      1;
  HeatFluxBC -HTEntity 2 -face 16 -type -ConvecAndRad -HTConstants
      3;
  # 16 represents the top face of concrete
}

FireModel Standard 1;

#HTEleSet 2 -HTEntity 1 -face 1;
HTPattern fire 2 model 1 {
  #HeatFluxBC eleset 2 -faceTag 1 -type -ConvecAndRad -HTConstants
      2;
  HeatFluxBC -HTEntity 2  -face 1 4 5 6 7 8 9 12 13 -type
      -ConvecAndRad -HTConstants 4;
}

puts "fire2"

#HTRecorder -file temp.out -xloc 0.0 -yloc [an arrary of ylocs]

HTNodeSet  12 -HTEntity 2 -Locx [expr -$bf/2]  [expr $bf/2] -Locy [
    expr $d/2-$tf/2];
HTRecorder -file TempUF.out  -nodeSet 12;
HTRecorder -file Temp3d.out  -HTEntity 2 -dim 3;
HTNodeSet  13 -HTEntity 2 -Locx [expr -$bf/2]  [expr $bf/2] -Locy [
    expr -$d/2+$tf/2];
HTRecorder -file TempLF.out  -nodeSet 13;

HTAnalysis HeatTransfer
#HTAnalyze $numSteps $timeStep;
HTAnalyze 120 30;

wipeHT;
```

Appendix B

Tcl Scripts for

Thermo-mechanical analysis

B.1 Tcl commands for defining thermal action

```
#Thermal action for 2D beam section
eleLoad -ele $eleTag -type -beamThermal $T1 $y1 $T2 $y2;

#Thermal action for 2D or 3D beam section
eleLoad -ele $eleTag -type -beamThermal -source $fileName $y1 $
    y2 $y3 $y4 $y5 $y6 $y7 $y8 $y9;

#Thermal action for 3D I-section
eleLoad -ele $eleTag -type -beamThermal -source $fileName $y1 $
    y2 $z1 $z2;

#Thermal action for shell section
eleLoad -ele $eleTag -type -shellThermal -source $fileName $y1
    $y2 $y3 $y4 $y5 $y6 $y7 $y8 $y9;
```

B.2 Tcl script for analysing beam in localised fire

../Appendix/SteelBeaminLocalisedFire.tcl

```
# Modelling steel beams subjected to localised fire or non-uniform
   heating
set ANALYSIS "HasThermo";
wipe;
file mkdir BeamLF;

model BasicBuilder -ndm 2 -ndf 3;
source DisplayPlane.tcl;
source DisplayModel2D.tcl;
source DisplayModel3D.tcl

# define NODAL COORDINATES FOR BEAM
#define node
set NumEles 48;
set BeamLen 6000.0;
set EleLen [expr $BeamLen/$NumEles]
for {set NodeID 0} {$NodeID <= $NumEles} {incr NodeID} {
set locX [expr $NodeID*$EleLen];
set NodeTag [expr $NodeID+1];
node $NodeTag $locX 0 ;
}

set StaNodeTag [expr $NumEles/2+1];
set MidNodeTag [expr 3*$NumEles/4+1];
set EndNodeTag [expr $NumEles+1];

#define boundary condition;
fix 1 1 1 0 ;
fix $EndNodeTag 0  1 0 ;


uniaxialMaterial SteelECThermal 1 275 2.1e5;
uniaxialMaterial SteelECThermal 3 EC2NH 475 2.1e5;

set fpc -30
set epsc0 -0.003
set fpcu [expr $fpc*0.05];
set epsU -0.02
set lambda 0.1
set ft 0
set Ets [expr $ft/0.002];

uniaxialMaterial Concrete02Thermal 2 $fpc $epsc0 $fpcu $epsU $lambda
    $ft $Ets
```

```
#
    ##########################################################################

proc Wsection { secID matID d bf tf tw nfdw nftw nfbf nftf} {
  #
     ########################################################################

  # Wsection  $secID $matID $d $bf $tf $tw $nfdw $nftw $nfbf $nftf
  #
     ########################################################################

  # create a standard W section given the nominal section properties
  # written: Remo M. de Souza
  # date: 06/99
  # modified: 08/99  (according to the new general modelbuilder)
  # input parameters
  # secID - section ID number
  # matID - material ID number
  # d  = nominal depth
  # tw = web thickness
  # bf = flange width
  # tf = flange thickness
  # nfdw = number of fibers along web depth
  # nftw = number of fibers along web thickness
  # nfbf = number of fibers along flange width
  # nftf = number of fibers along flange thickness

  set dw [expr $d - 2 * $tf]
  set y1 [expr -$d/2]
  set y2 [expr -$dw/2]
  set y3 [expr  $dw/2]
  set y4 [expr  $d/2]

  set z1 [expr -$bf/2]
  set z2 [expr -$tw/2]
  set z3 [expr  $tw/2]
  set z4 [expr  $bf/2]

  section fiberSecThermal  $secID   {
      #                     nfIJ  nfJK    yI  zI    yJ  zJ    yK  zK
             yL  zL
      patch quadr  $matID  $nfbf $nftf   $y1 $z4   $y1 $z1   $y2 $z1
            $y2 $z4
      patch quadr  $matID  $nftw $nfdw   $y2 $z3   $y2 $z2   $y3 $z2
            $y3 $z3
      patch quadr  $matID  $nfbf $nftf   $y3 $z4   $y3 $z1   $y4 $z1
            $y4 $z4
  }
}
#
    ##########################################################################


# beam sections:
set d 307.2;  # depth
```

```
set bf 124.3; # flange width
set tf 8; # flange thickness
set tw 12.1;  # web thickness
set nfdw 8;   # number of fibers along dw
set nftw 4;   # number of fibers along tw
set nfbf 8;   # number of fibers along bf
set nftf 4;     # number of fibers along tf
set hw [expr $d-2*$tf];
Wsection  1 1 $d $bf $tf $tw $nfdw $nftw $nfbf $nftf

#Concrete section
section fiberSecThermal 2   {
  patch quad 2 8 8 -50 1500 -50 -1500 50 -1500 50 1500;
  layer straight 3 13 28.275 -25 -1450 -25 1450
    }

geomTransf Corotational 1;#
#geomTransf PDelta 1

#choose the section for the beam eles

#ELES FOR BEAMS
for {set eleID 1} {$eleID<= $NumEles} {incr eleID} {
  set NodeTag0 $eleID;
  set NodeTag1 [expr $eleID+1];
  #element forceBeamColumnThermal $eleID $NodeTag0 $NodeTag1 9 1 1;
  element dispBeamColumnThermal $eleID $NodeTag0 $NodeTag1 5 1 1;
}


#define beam element: dispBeamColumnThermal $eleTag $iNode $jNode
    $numIntgrPts $secTag $TransfTag;
#"numIntgrPts" is the number of integration points along the element
    ;
#"TransfTag" is pre-defined coordinate-transformation;


#define output
recorder Node -file WrapperData/N_MidSpan_DOF.out -time -nodeRange 1
     1 -dof 2 disp;
recorder Node -file WrapperData/N_NodeDeflect_DOF.out -time
    -nodeRange 1 $EndNodeTag -dof 2 disp;
recorder Element -file WrapperData/N_ElementGF.out -time -ele 1
    globalForce;
recorder Element -file WrapperData/N_ElementDef.out -time -ele1
    basicDeformation;

recorder Element -file WrapperData/Element1SecTemp1B.out -time
    -eleRange 1  $NumEles section 1  fiber [expr -$d/2] 0 TempElong;
recorder Element -file WrapperData/EleSec1SSB.out -time -eleRange 1
     $NumEles section 1  fiber [expr -$d/2] 0 stressStrainTangent;
recorder Element -file WrapperData/EleForceSec1.out -time -eleRange
    1  $NumEles section 1 forces;
```

```
# Define DISPLAY
    ------------------------------------------------------------
  set  xPixels 900; # height of graphical window in pixels
  set  yPixels 400; # height of graphical window in pixels
  set  xLoc1 10;      # horizontal location of graphical window (0
     =upper left-most corner)
  set  yLoc1 100;     # vertical location of graphical window (0
     =upper left-most corner)
  set ViewScale 0.000002; # scaling factor for viewing deformed
     shape, it depends on the dimensions of the model

#display 2D deformation shape
DisplayModel2D DeformedShape $ViewScale;
#define Uniform load
puts "Now applying uniform load"

pattern Plain 1 Linear {
#CREATE UNIFORM LOADS FOR BEAMS
set  UDL -9.38;
for {set level 1} {$level <= $NumEles} {incr level 1} {
  set eleID $level
  eleLoad -ele $eleID -type -beamUniform $UDL 0 0;
}
}

constraints Plain;
numberer Plain;
system BandGeneral;
test NormUnbalance 1.0e-3 100 0;
algorithm Newton;
integrator LoadControl 0.05;
analysis Static;
analyze 20;
loadConst -time 0.0

#define Thermal Action
if {$ANALYSIS == "HasThermo"} {
puts "Thermal action to beam"
set HalfNumEles [expr $NumEles/2]
# Define Thermal Load
pattern Plain 2 Linear {
set y1 [expr -$d/2];
set y2 [expr -$d/2+$tf];
set y3 [expr -$d/2+$tf+$hw/6];
set y4 [expr -$d/2+$tf+$hw/3];
set y5 [expr -$d/2+$tf+$hw/2];
set y6 [expr -$d/2+$tf+4*$hw/6];
set y7 [expr -$d/2+$tf+5*$hw/6];
set y8 [expr $d/2-$tf];
set y9 [expr $d/2];

#eleLoad -range 1 $NumEles -type -beamThermal 1000 $y1 800 $y2;

#load 1 -nodalThermal 100 $y1 20 $y2;
#load 4 -nodalThermal 200 $y1 100 $y2
```

```
#load 7 -nodalThermal 800 $y1 400 $y2
#load 10 -nodalThermal 200 $y1 100 $y2
#load 13 -nodalThermal 100 $y1 20 $y2
#set MidEles [expr $NumEles/2]
#load $StaNodeTag -nodalThermal -source BeamLF6M/
   HTNodeRecorder5024.dat  $y1 $y2 $y3 $y4 $y5 $y6 $y7 $y8 $y9;
#load $MidNodeTag -nodalThermal -source BeamLF6M/
   HTNodeRecorder5036.dat  $y1 $y2 $y3 $y4 $y5 $y6 $y7 $y8 $y9;
#load $EndNodeTag -nodalThermal -source BeamLF6M/
   HTNodeRecorder5048.dat  $y1 $y2 $y3 $y4 $y5 $y6 $y7 $y8 $y9;
#eleLoad -range 1 $NumEles -type -beamThermal -source -node
#eleLoad -range 1 $MidEles -type -ThermalWrapper -nodeLoc
   $StaNodeTag 0 $MidNodeTag 0.5 $EndNodeTag 1;
#eleLoad -range $MidEles $NumEles -type -ThermalWrapper -nodeLoc
   $StaNodeTag 0 $MidNodeTag 0.5 $EndNodeTag 1;

#eleLoad -range 1 $NumEles -type -ThermalWrapper -nodeLoc 1 0
   $EndNodeTag 1;
#eleLoad -range 1 $NumEles -type -beamThermal  -source
   HTNodeRecorder5024.dat  $y1 $y2 $y3 $y4 $y5 $y6 $y7 $y8 $y9;


eleLoad -range 1 $NumEles -type -beamThermal -source -node;
for {set NodeID 1} {$NodeID<=$EndNodeTag} {incr NodeID} {
    set NodeLoadID [expr 5000+$NodeID-1]
    set filepath "BeamLF6M/HTNodeRecorder";
    set fileType ".dat";
    append filepath $NodeLoadID $fileType;
  puts $filepath;
    load $NodeID -nodalThermal -source $filepath $y1 $y2 $y3 $y4 $y5
        $y6 $y7 $y8 $y9;
}
}



test NormDispIncr 1e-3 30 1;
algorithm Newton;
integrator LoadControl 5;
analysis Static;
analyze 360;
}


wipe;
```

B.3 Tcl script for analysing beam in localised fire

../Appendix/SlabB1inFireUsingShell.tcl

```
# units: m,N
wipe;


set ANALYSIS "HasPoint";
set TANALYSIS "Has0Thermo";

model BasicBuilder -ndm 3 -ndf 6;

file mkdir ShellData;

#source DisplayPlane.tcl
#source DisplayModel2D.tcl
#source DisplayModel3D.tcl

#8.72
#Concrete model
#these should both be even, number of elements per edge
set nx 16;
set ny 16;
set slabT 0.0678;
set slabB 1.829;
set slabL 2.745;
set UDL 1E3;

nDMaterial ElasticIsotropic3DThermal 2 1.92e9 0.2 0 1.4e-5;
#nDMaterial DruckerPragerThermal 2 $k $G $sigY $rho $rhoBar $Kinf
    $K0 $delta1 $delta2 $H $theta $mDen;
nDMaterial PlateFiberThermal 14 2;
# $secTag $matTag $thickness

nDMaterial ConcreteSThermal 7  1.12e10 0.2 18.7e6  1.87e6  1.12e9
nDMaterial   PlateFromPlaneStressThermal    4   7    12.77e9

set Bar_k 1.67e11; set Bar_G 0.77e11;  set Bar_sigY 3.45e8; set
    Bar_rho 0;
set Bar_rhoBar 0; set Bar_Kinf 0.0; set Bar_K0 0.0; set Bar_delta1 0
    .0 ; set Bar_H [expr 2e9/2.8]; set Bar_theta 1.0; set Bar_delta2
    0.0; set Bar_mDen 7850;
nDMaterial DruckerPragerSteelThermal 23 $Bar_k $Bar_G $Bar_sigY
    $Bar_rho $Bar_rhoBar $Bar_Kinf $Bar_K0 $Bar_delta1 $Bar_delta2
    $Bar_H $Bar_theta $Bar_mDen;
nDMaterial PlateFiberThermal 24 23;

uniaxialMaterial SteelECThermal 1 EC2NH 4.50e8 2e11;
#uniaxialMaterial ElasticThermal 1 2e11 1.2e-5;
```

```
nDMaterial PlateRebarThermal 3 1 0;
nDMaterial PlateRebarThermal 5 1 90;
# $secTag $matTag $thickness
#section PlateFiberThermal 2 4 $slabT;
#FOR NONLINEAR

section LayeredShellThermal  2  13  4 0.008875  4 0.008615 3 0.00026
    5 0.00026 4 0.00628 4 0.00654  4 0.00654 4 0.00654 4 0.00628 5 0
   .00026 3 0.00026 4 0.008615 4 0.008875 ;

#section LayeredShellThermal  2  10  4  0.01 4 0.01  4 0.01  4  0.01
     4 0.01 4  0.01  4  0.01 4  0.01 4  0.01 4  0.01 ;
#block2D $nx $ny 1 1 ShellNLDKGQThermal 2  ShellMITC4Thermal
   ShellMITC4GNLThermal
block2D $nx $ny 1 1 ShellNLDKGQThermal  2 {
    1   0. 0. 0.
    2   2.745 0. 0.
    3  2.745 1.829 0.
    4   0. 1.829 0.
}

#fully simply supported
fixX 0  0 0 1 0 0 0 ;
fixX 2.745  0 0 1 0 0 0 ;
fixY 0  0 0 1 0 0 0 ;
fixY 1.829  0 0 1 0 0 0 ;
fix 1  1 1 1 0 0 1 ;

puts "here";

set midSlabsb [expr $nx/2+($nx+1)*$ny/2];
#display 3D deformation shape
set  xPixels 1200;
# height of graphical window in pixels
set  yPixels 800;
# height of graphical window in pixels
set  xLoc1 10;
# horizontal location of graphical window (0=upper left-most corner)
set  yLoc1 10;
# vertical location of graphical window (0=upper left-most corner)
set ViewScale 0.001;
# scaling factor for viewing deformed shape, it depends on the
   dimensions of the model
#DisplayModel3D  DeformedShape $ViewScale $xLoc1 $yLoc1  $xPixels
   $yPixels

set CorEle 1;
set MidEle [expr 1+($nx)*$ny/2+$nx/2];
set SideEle [expr 1+($nx)*$ny/2];
recorder Node -file ShellData/DFreeSlabxT.out -time -nodeRange [expr
    1+($nx+1)*$ny/2] [expr ($ny/2+1)*($nx+1)] -dof 1  disp;
recorder Node -file ShellData/DFreeSlabyT.out -time -nodeRange [expr
    1+($nx+1)*$ny/2] [expr ($ny/2+1)*($nx+1)] -dof 2 disp;
recorder Node -file ShellData/DFreeSlabzT.out -time -nodeRange [expr
    1+($nx+1)*$ny/2] [expr ($ny/2+1)*($nx+1)] -dof 3 disp;
```

```
recorder Node -file ShellData/DFreeCentrezT.out -time -node [expr
   $nx/2+($nx+1)*$ny/2] -dof 3 disp;
recorder Node -file ShellData/DFreeSlabzTUP.out -time -nodeRange 1 [
   expr ($nx+1)] -dof 3 disp;
recorder Node -file ShellData/DFreeSlabzTDo.out -time -nodeRange [
   expr 1+($nx+1)*$ny] [expr ($ny+1)*($nx+1)] -dof 3 disp;
recorder Node -file ShellData/DfreeAllDispz.out -time -dT 0.99
   -nodeRange 1 [expr ($ny+1)*($nx+1)] -dof 3 disp;


recorder Element -file ShellData/CornerEleForceSec1sigma.out -time
   -ele $CorEle  material 1 fiber 1 stress;
recorder Element -file ShellData/CornerEleForceSec1Eps.out -time
   -ele $CorEle  material 1 fiber 1 strain;
recorder Element -file ShellData/CornerEleForceSec1Temp.out -time
   -ele $CorEle   material 1 fiber 1 TempAndElong;



if {$ANALYSIS == "HasPoint"} {
set UDLP [expr -$UDL*$slabB*$slabL/$nx/$ny];

pattern Plain 1 Linear {
   set NumNodes [expr ($nx+1)*($ny+1)]
  for {set nodeID 1} {$nodeID<=$NumNodes} {incr nodeID} {
    load $nodeID 0 0 $UDLP 0 0 0 ;
    }
    #set Load 100;
  #for {set ID 0} {$ID<=$ny} {incr ID} {
    #set nodeID [expr ($nx+1)*($ID+1)];
    #load $nodeID  0 0 [expr $Load/($ny+1)] 0 0 0 ;
  #}

}

constraints Plain;
numberer Plain;
system BandGeneral;
test NormDispIncr 1e-4  300 1;
algorithm Newton;
integrator LoadControl 0.5;
analysis Static;
analyze 200;
loadConst -time 0.0
}


if {$TANALYSIS == "HasThermo"} {

puts "Thermal action to slab"

set NumEles [expr $nx*$ny];

set StartNodeTag [expr ($nx+1)*($ny/2)+$nx/2+1]
```

```
set MidNodeTag [expr ($nx+1)*($ny*3/4)+1+$nx*3/4]
set EndNodeTag [expr ($nx+1)*($ny+1)]

set minusHalfD [expr -$slabT/2];
set HalfD [expr $slabT/2];

pattern Plain 3 Linear {
#set shellEndID [expr 100+$nx*$ny]
#for {set m 1} {$m<=$ny} {incr m} {
 # for {set n 1} {$n<=$nx} {incr n} {
   # set shellLoadID [expr 10000+($n-1)*100+$m-1];
  #set shellID [expr 1+($m-1)*$nx+$n-1];
    #set filepath "SlabTA/HTNodeRecorder";
    #set fileType ".dat";
    #append filepath $shellLoadID $fileType;
    #eleLoad -ele $shellID -type -shellThermal -source $filepath -50
        50;
  #eleLoad -range 1 $NumEles -type -shellThermal 800 [expr -$slabT
     /2] 400 [expr $slabT/2];
  load $StartNodeTag -nodalThermal 800 $minusHalfD 200 $HalfD;
  load $MidNodeTag -nodalThermal 200 $minusHalfD 50 $HalfD
  load $EndNodeTag -nodalThermal 0 $minusHalfD 0 $HalfD

  eleLoad -range 1 $NumEles -type -ThermalWrapper -nodeLoc
     $StartNodeTag 0 $MidNodeTag 0.5 $EndNodeTag 1;
  #eleLoad -range 1 $NumEles -type -shellThermal 400 [expr -$slabT
     /2] 100 [expr $slabT/2];

#}
#}
#eleLoad -ele 1 -type -beamThermal 600 -$HalfD 600 $HalfD;
}

#wipe;
constraints Plain;
numberer Plain;
system BandGeneral;
#test NormUnbalance 1.0e-4 10 1;
test NormDispIncr 1e-4  300 1;
algorithm Newton;
integrator LoadControl 0.005;
analysis Static;
analyze 200;

}
wipe;
```

Appendix C

Tcl Scripts for integrated analysis using SIFBuilder

../Appendix/FrameModelUsigSIFBuilder.tcl

```
#Modelling generic frame using SIFBuilder in OpenSees
source DisplayPlane.tcl;
source DisplayModel2D.tcl;
source DisplayModel3D.tcl
wipe;
file mkdir HTData;

SIFBuilder;

#AssignSection
SIFXBay 6 9 ;
SIFZBay 6 9;
SIFStorey 5 4  ;

AddMaterial steel 1 -type EC3 2.75e8  2e11;
AddMaterial concrete 2 -type EC2 0 30;

AddSection ISection 1 1 0.355 0.1715 0.0074 0.0115;
# $d $bf $tw $tf  UB356x171x51
AddSection ISection 2 1 0.6026 0.2276 0.0105 0.0148;
# $d $bf $tw $tf   UB610*229*101
AddSection ISection 3 1 0.3034 0.165 0.006 0.0102;
# $d $bf $tw $tf   UC305*165*40

AddSection ISection 4 1 0.254 0.254 0.0086 0.0142 -protected 0.02;;
# $d $bf $tw $tf   UC254*254*73
```

```
#AddSection Rect 2 1 0.1 0.1;  # $d $bf $tw $tf
AddSection  SlabSection 5 2 0.1;
AssignSection Xbeams 3 ;
AssignSection Zbeams 1 ;
AssignSection Zbeams 1 -ZBay 1;
AssignSection Zbeams 2 -ZBay 2;
AssignSection columns 4;
AssignSection slabs 5;

AddSecBeam  XBeam 3 Compartment 111 -numBeams 1;
AddSecBeam  XBeam 3 Compartment 211 -numBeams 1;
AddSecBeam  XBeam 3 Compartment 121 -numBeams 2;
AddSecBeam  XBeam 3 Compartment 221 -numBeams 2;
AddSecBeam  XBeam 3 Compartment 112 -numBeams 1;
AddSecBeam  XBeam 3 Compartment 212 -numBeams 1;
AddSecBeam  XBeam 3 Compartment 122 -numBeams 2;
AddSecBeam  XBeam 3 Compartment 222 -numBeams 2;
SetBC fixedJoint -Locy 0;
 #set boundary condition
AddLoad -joint 222 -load 0 600000 0;
AddLoad -member allslabs -load 0 -4950 0;
#AddLoad -liveLoad 2.0;
#AddFire -compartment 111 -type standard;
AddFire -compartment 111 121 211 221 -type EC1Local -origin 6 0 6
   -HRR 5e6 -Dia 1.0;
#BuildModel elastic;
BuildModel -MeshCtrl 12 10 12;

# Define DISPLAY
   ------------------------------------------------------------
  set  xPixels 1600;  # height of graphical window in pixels
  set  yPixels 1600;  # height of graphical window in pixels
  set  xLoc1 -800;      # horizontal location of graphical window (0
     =upper left-most corner)
  set  yLoc1 -800;      # vertical location of graphical window (0
     =upper left-most corner)
  set ViewScale 10; # scaling factor for viewing deformed shape, it
     depends on the dimensions of the model

  ####################################################
  ##DisplayModel2D $ShapeType $dAmp $xLoc $yLoc $xPixels $yPixels
     $nEigen

  ## display Node Numbers, Deformed or Mode Shape in 2D problem
  ##      Silvia Mazzoni & Frank McKenna, 2006
  ##
  ##  ShapeType :   type of shape to display. # options: ModeShape ,
      NodeNumbers , DeformedShape
  ##  dAmp :    relative amplification factor for deformations
  ##  xLoc,yLoc  :  horizontal & vertical location in pixels of
     graphical window (0,0=upper left-most corner)
  ##  xPixels,yPixels : width & height of graphical window in pixels
  ##  nEigen :    if nEigen not=0, show mode shape for nEigen
     eigenvalue
```

```
  ##
  ###################################################

DisplayModel3D DeformedShape $ViewScale $xLoc1 $yLoc1 $xPixels
   $yPixels 0

#SIFApply gravity
#SIFApply
#SIFApply Fire
#SIFApply load
SIFRecorder Joint -file Joint111.out -joint 111 disp;
SIFRecorder Member -file XBeam111.out -xBeam 111 Mideflect;
SIFRecorder Member -file XBeam121.out -xBeam 121 Mideflect;
SIFRecorder Member -file SecXBeam111.out -SecXBeam 111 Mideflect;
SIFRecorder Member -file Slab111.out -slab 111 Mideflect;
SIFRecorder Member -file Slab111all.out -slab 111 deflect;
recorder Element -file ElementColTopGForces.out -time -ele 330
   globalForce;
time {
#SIFAnalyze SelfWeight -dt 0.5 Load -dt 0.5 Fire -dt 30 -duration
   360 -output HTData;
SIFAnalyze Load -dt 0.1 Fire -dt 30 -duration 1800 -output HTData;
#SIFAnalyze Load -dt 0.02;
}
#SIFAnalyze SelfWeight -dt 0.2
print domain.out
```